Université de Montréal

# Propriétés supramoléculaires des cations diimidazolium disubstitués :

## des complexes d'inclusion en solution aux interactions à l'état cristallin et cristal liquide

par

Nadim Noujeim

Département de chimie

Faculté des arts et sciences

Thèse présentée à la Faculté des études supérieures
en vue de l'obtention du grade de Philosophiæ Doctor
en chimie

Août 2010

Université de Montréal
Faculté des études supérieures

Cette thèse intitulée :

# Propriétés supramoléculaires des cations diimidazoliums disubstitués : des complexes d'inclusion en solution aux interactions à l'état cristallin et cristal liquide

Présentée par :
Nadim Noujeim

A été évaluée par un jury composé des personnes suivantes :

Dr Jeffrey W. Keillor, président-rapporteur
Dr Andreea R. Schmitzer, directeur de recherche
Dr James D. Wuest, membre du jury
Dr Anne Petitjean, examinateur externe
Dr Rikard Blunck, représentant du doyen de la FES

# Résumé

Les sels d'imidazolium ont un rôle important dans certaines protéines et acides nucléiques et ont été utilisés à de nombreuses reprises dans des assemblages supramoléculaires en raison de leurs propriétés uniques. Les sels de diimidazolium dérivés sont toutefois moins connus. Ils ont pour l'instant uniquement été utilisés comme des précurseurs de carbènes *N*-hétérocycliques. Ils sont donc à la base de plusieurs catalyseurs utilisés pour des réactions de couplage croisés mais leurs propriétés sont toutefois méconnues dans le cadre de la chimie supramoléculaire. Cette classe de composés a nottament attiré notre attention en raison de la facilité de modification de leurs propriétés physico-chimiques par modification de leur structure chimique. L'objectif général des travaux présentés dans cette thèse est l'étude des propriétés supramoléculaires des sels de diimidazolium disubstitués en solution (aqueuse ou organique), ainsi qu'en phase solide ou cristal-liquide. L'influence de l'espaceur entre les deux noyaux imidazolium ainsi que l'influence des substituants latéraux et des contre-ions a été étudiée.

Dans un premier temps, les propriétés de complexation des sels de diimidazolium à des macrocycles sont étudiées. Les sels bromure sont étudiés en solution aqueuse avec plusieurs cyclodextrines et le cucurbit[7]uril, et les sels hexafluorophosphate sont étudiés en solution organique pour leur complexation avec l'éther couronne DB24C8 et un calix[4]arène. Cette nouvelle classe de composés a montré de très bonnes propriétés de complexation à ces différents macrocycles en solution et a également permis de contrôler différents assemblages supramoléculaires à l'interface air-eau.

Dans un deuxième temps, l'étude des sels de phénylènediimidazolium a permis de modifier les propriétés de complexation en solution pour obtenir la formation de complexes multiples avec le cucurbit[7]util en solution aqueuse. Cette même famille de composés a également permis la formation de cristaux liquides ioniques lorsque les substituants sont des chaînes alkyles plus longues.

La résolution de plusieurs structures cristallines de différents sels de diimidazolium a finalement permis de comprendre la nature des interactions intermoléculaires à l'état cristallin. La recherche présentée dans cette thèse a donc permis une étude détaillée des propriétés supramoléculaires des sels de diimidazolium dans tous les états de la matière qui leur sont accessibles.

**Mots-clés** : chimie supramoléculaire, chimie hôte-invité, complexes, cristaux liquides, génie cristallin, imidazolium, auto-assemblage, cyclodextrine, cucurbituril, éther-couronne, calixarène

# Abstract

Imidazolium salts play an important role in different proteins and nucleic acids and have been used many times in supramolecular assemblies due to their unique properties. Diimidazolium salts derived from imidazolium salts are less known. To date, they have only been used as precursors for *N*-heterocyclic carbenes, which are used to catalyze various cross-coupling reactions. Their properties are not well known in supramolecular chemistry. This class of compounds attracted our attention because of the ease of tuning their properties by modifying their chemical structure. The main goal of the research presented in this thesis was to study the supramolecular properties of disubstituted diimidazolium salts in solution (aqueous or organic solution), in the solid state and in the liquid-crystalline state. The role of the spacer between the two imidazolium moieties, of the sidechains and of the counterions was studied.

Firstly, the complexation between diimidazolium salts and various macrocycles was studied. Bromide salts were studied in aqueous solution with cyclodextrins and cucurbit[7]uril, while hexafluorophosphate salts were studied in organic solution with a DB24C8 crown ether and a calix[4]arene. This novel class of compounds showed very promising complexation properties with these macrocycles in solution and also allowed us to control the formation of various supramolecular assemblies at the air-water interface.

Secondly, phenylenediimidazolium salts were studied and allowed the modification of the complexation properties in aqueous solution. Multiple complexes can be formed simultaneously with cucurbit[7]uril in aqueous solution. The same class of compounds also has the ability to yield ionic liquid crystals when the alkyl sidechains are long.

The resolution of the crystalline structures of some synthesized diimidazolium salts allowed us to understand the nature of the intermolecular interactions in the solid state. The research presented in this thesis is a complete study of the supramolecular properties of diimidazolium salts in every accessible state of matter.

**Keywords** : supramolecular chemistry, host-guest chemistry, complexes, liquid crystals, crystal engineering, imidazolium, self-assembly, cyclodextrin, cucurbituril, crown ether, calixarene

# Table des matières

# Liste des tableaux

# Liste des Figures

# Liste des Schémas

# Liste des abréviations

| | |
|---|---|
| A | accepteur |
| Å | Angström |
| ADN | acide déoxyribonucléique |
| AM 1 | Austin model 1 |
| Asp | acide aspartique |
| ATP | adenosine triphosphate |
| BINOL | 1,1'-bi-2-naphtol |
| *t*Boc | *tert*-butyloxycarbonyl |
| C[4]P | tétrapropoxycalix[4]arène |
| C[n] | calix[n]arène |
| CAC | *critical aggregation concentration* |
| Calc. | *calculated* |
| CB | cucurbituril |
| CB[5] | cucurbit[5]uril |
| CB[6] | cucurbit[6]uril |
| CB[7] | cucurbit[7]uril |
| CB[8] | cucurbit[8]uril |
| CD | cyclodextrine |
| CE | *crown ether* |
| cmc | *critical micelle concentration* |
| Conv. | *conversion* |
| COSY | *correlation spectroscopy* |
| CP/MAS NMR | *cross polarized magic angle spinning nuclear magnetic resonance* |
| Cr | *crystalline phase* |

| | |
|---|---|
| d | doublet |
| D | donneur |
| DB24C8 | dibenzo-24-crown-8 |
| Dec. | *decomposition* |
| DMSO | diméthyl sulfoxyde |
| DNA | *deoxyribonucleic acid* |
| DSC | *differential scanning calorimetry* |
| ee | *enantiomeric excess* |
| Eq | *equivalents* |
| ESI | *electrospray ionization high resolution mass spectrometry* |
| Et | éthyle |
| His | histidine |
| HRMS | *high resolution mass spectrometry* |
| I | *isotropic* |
| IL | *ionic liquid* |
| ILC | *ionic liquid crystal* |
| ITC | *isothermal titration calorimetry* |
| LC | *liquid crystal* |
| m | multiplet |
| MD | *molecular dynamics* |
| Me | méthyle |
| Mp | *melting point* |
| MS | *mass spectrometry* |
| N | nématique |
| *n*Bu | *n*-butyle |

| | |
|---|---|
| *n*Hex | *n*-hexyle |
| NMR | *nuclear magnetic resonance* |
| *n*Oct | *n*-octyle |
| NOE | *nuclear Overhauser effect* |
| NOESY | *nuclear Overhauser effect spectroscopy* |
| *n*Pr | *n*-propyle |
| P | coefficient de partage eau/octanol |
| PEI | polyéthylènimine |
| PM3 | *parametrized model number 3* |
| POM | *polarizing optical microscopy* |
| ppm | *parts per million* |
| q | quadruplet |
| quint | quintuplet |
| r.t. | *room temperature* |
| Ref | *reference* |
| RNA | *ribonucleic acid* |
| RNase | *ribonuclease* |
| ROESY | *rotating Overhauser effect spectroscopy* |
| s | singulet |
| Ser | sérine |
| sext | sextuplet |
| SmA | *smectic A* |
| SmC | *smectic C* |
| SmT | *smectic T* |
| $S_N2$ | *bimolecular nucleophilic substitution* |

| | |
|---|---|
| t | triplet |
| *t*Bu | *tert*-butyle |
| UV | ultraviolet |
| XRD | X-ray powder diffractometry |
| α-CD | α-cyclodextrine |
| β-CD | β-cyclodextrine |
| β-DIME | 2,6-diméthyl-β-cyclodextrine |
| γ-CD | γ-cyclodextrine |

*À la mémoire de Philippe El-Hage*

# Remerciements

Ces quelques années passées au Département de chimie de l'Université de Montréal ont été parmi les plus belles de ma vie. Pendant tout ce temps, j'ai pu m'épanouir autant d'un point de vue scientifique que d'un point de vue personnel. Bien que la recherche ait été très difficile pendant les deux premières années après mon arrivée au laboratoire, j'ai pu apprendre que la persévérance et la curiosité scientifique permettaient toujours de trouver des solutions aux problèmes rencontrés. Tout ce que j'ai accompli pendant ces cinq années dans le groupe d'Andreea Schmitzer n'aurait pas été possible sans la contribution d'un grand nombre de personnes que j'aimerais remercier chaleureusement.

J'aimerais tout d'abord remercier ma directrice de recherche, Andreea Schmitzer, pour m'avoir accueilli dans son groupe de recherche il y a cinq ans, mais aussi et surtout pour m'avoir guidé dans mon apprentissage de la recherche scientifique. Merci également pour avoir toujours été aussi disponible et pour m'avoir laissé autant de liberté dans l'orientation des différents sujets de recherche sur lesquels j'ai travaillé. Merci aussi pour tout ce temps que tu as consacré pour m'aider à préparer les différentes demandes de bourses et les nombreuses présentations aux conférences. Finalement, merci de ton soutien pendant une période très difficile il y a quelques mois.

J'aimerais aussi remercier tous les membres passés et présents du groupe de recherche d'Andreea. Vous avez tous contribué à rendre très agréables ces années de recherches et à créer cette très belle ambiance caractéristique de l'aile V-300. Je voudrais particulièrement remercier tous les collaborateurs et stagiaires d'été avec qui j'ai eu l'occasion de travailler sur mes projets de recherche pendant ces cinq ans. Merci à Aline Bichouti, Marie Savonnet, Kevin Appert, Benjamin Jouvelet, Samantha Sanon, Ludovic Eberlin, Vaizanne Huynh et Claude-Rosny Elie pour vos contributions et votre persévérance. Merci également à Dr Loïc Leclercq pour toutes ces discussions scientifiques de qualité et pour ta contribution essentielle. Je tiens à remercier spécialement mes collègues actuels avec qui j'ai passé la plus grande partie de mon temps au laboratoire ces

deux dernières années : merci à Christine Chhun, Marc Vidal, Salim Samsam, Vincent Gauchot et Mathieu Branca. Il me sera probablement très difficile de trouver un environnement de travail aussi agréable par la suite.

Je voudrais également remercier Alain Grandbois et Nicolas Levaray. Nous avons vécu ensemble toutes les étapes importantes de nos études de doctorat et je garderai entre-autres, un excellent souvenir de nos pauses matinales au café de médecine !

Pendant mes études à l'Université de Montréal, plusieurs professeurs et personnels des laboratoires d'analyses du Département de chimie ont grandement contribué à mon épanouissement scientifique et à l'avancée de mes projets de recherche. J'aimerais remercier tout particulièrement les Professeurs Jeffrey Keillor et James Wuest pour leur enseignement de qualité et leur disponibilité pour la rédaction de lettres de recommandation pour des demandes de bourses. Merci également aux professeurs Shawn Collins, Joelle Pelletier et Géraldine Bazuin pour les relectures de manuscrits et pour les discussions très appréciées sur mes sujets de recherche. Je tiens enfin à remercier Sylvie Bilodeau, Michel Simard, Francine Bélanger, Pierre Ménard-Tremblay, Sylvain Essiembre et Huguette Dinel pour leur disponibilité et l'aide précieuse qu'ils m'ont apportée dans leurs différents domaines d'expertise.

J'aimerais remercier spécialement Dr Marie-Gabrielle LePironnec pour m'avoir transmis sa passion pour la chimie alors que je n'avais que treize ans ainsi que Dr Damien Belotti qui m'a initié à la recherche en chimie au début de mes études universitaires.

Cette thèse est pour moi plus que l'aboutissement de cinq années de recherches. Elle est l'aboutissement de nombreuses années d'études que je n'aurais jamais pu mener à bien sans l'aide et le très grand soutien que m'ont apportés ma famille. J'aimerais donc remercier mes parents, Chahine et Danielle, ainsi que mes sœurs, Dominique et Stéphanie, pour leur aide et leur amour. Ils ont toujours été présents dans les moments difficiles et m'ont toujours soutenu lorsque j'en avais besoin.

Je voudrais finalement remercier le Fonds québécois de la recherche sur la nature et les technologies, Boehringer-Ingelheim, la Faculté des études supérieures ainsi que le Département de chimie de l'Université de Montréal pour l'aide financière dont j'ai bénéficié.

# Chapitre 1 : Introduction

# 1.1 La chimie supramoléculaire

## 1.1.1 Bases de la chimie supramoléculaire

### 1.1.1.1 Définition

Contrairement à la chimie moléculaire qui est fondée sur la maîtrise des interactions covalentes, l'objectif de la chimie supramoléculaire est l'étude et l'utilisation des liaisons intermoléculaires (ou non covalentes). La chimie supramoléculaire a été définie comme « la chimie au-delà de la molécule, la chimie des assemblages moléculaires et de la liaison intermoléculaire » par Jean-Marie Lehn [1]. Elle se base sur les interactions intermoléculaires non covalentes utilisées pour auto-associer différentes molécules ou composantes ioniques, en structures hautement ordonnées [2, 3]. Plusieurs termes sont utilisés en chimie supramoléculaire selon la nature des phénomènes impliqués et des interactions présentes. Ces termes comprennent entre-autres : la chimie hôte-invité, la reconnaissance moléculaire, l'auto-assemblage, les machines moléculaires *etc*. Les fondements de la chimie supramoléculaire et des assemblages supramoléculaires ont été posés grâce aux travaux de Pedersen [4], Lehn [5] et Cram [6], ce qui leur a valu le prix Nobel de chimie en 1987 (Figure 1.1).

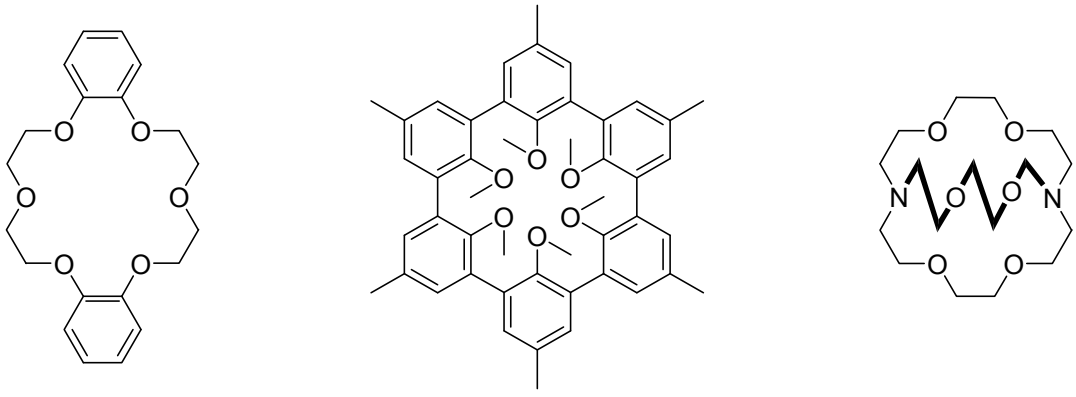


**Figure 1.1.** Quelques exemples des travaux de Pedersen, Cram et Lehn.

### 1.1.1.2 Classification des assemblages supramoléculaires hôte-invité

La chimie supramoléculaire est historiquement associée à la chimie hôte-invité (ou récepteur/substrat) et peut être sous-divisée selon la nature des forces entre les différentes composantes moléculaires d'une structure supramoléculaire. Si l'aggrégat hôte-invité est principalement formé grâce à des interactions électrostatiques, alors le terme de « complexe » est utilisé [1]. Si les espèces sont associées par des interactions moins spécifiques et non directionelles, comme des interactions hydrophobes, de van der Waals ou des effets d'empilement cristallins, alors le terme de « clathrate » [7] est utilisé (Figure 1.2).

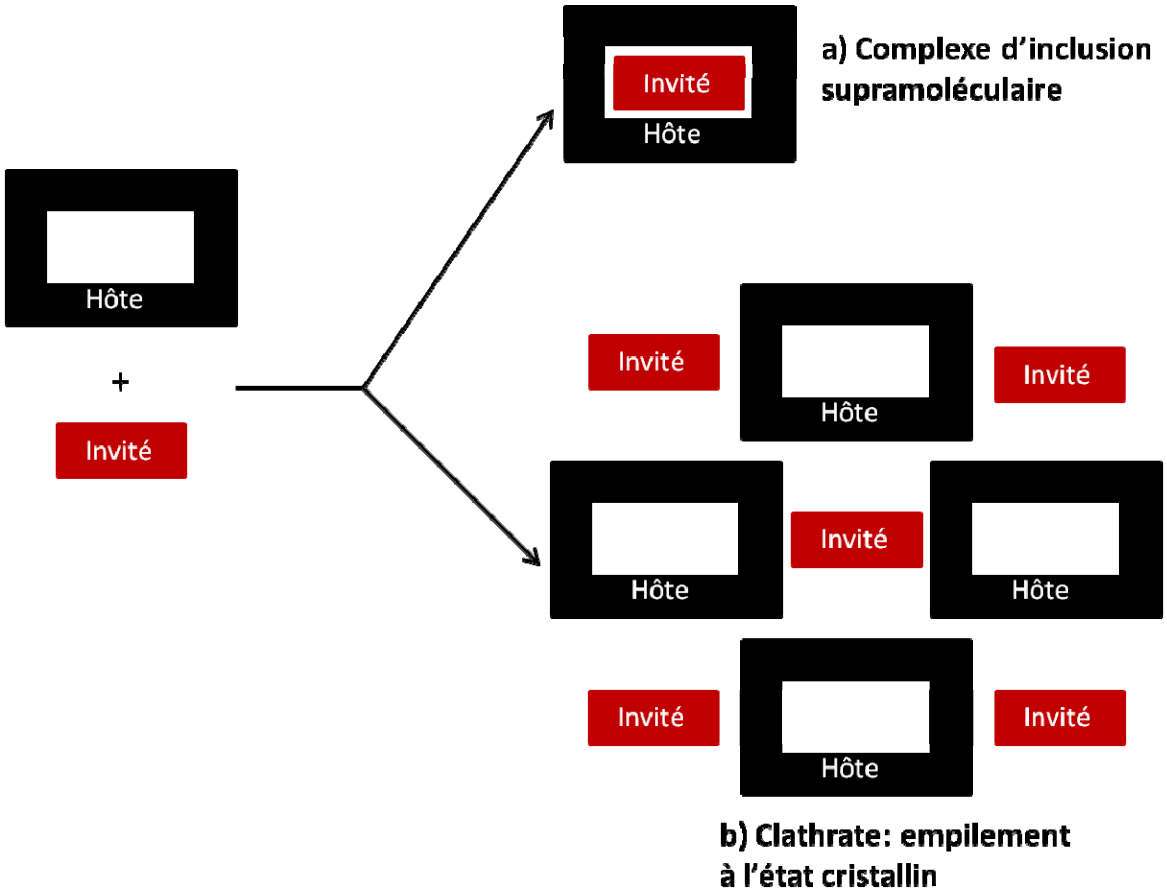


**Figure 1.2.** Représentation schématique illustrant la différence entre un complexe d'inclusion et un clathrate.

La chimie hôte-invité est basée sur quelques concepts historiques : pour pouvoir se lier au substrat, un récepteur doit posséder un ou des sites de liaison ayant un caractère électronique complémentaire à celui du substrat. Les sites de liaisons doivent être espacés sur le récepteur de telle manière à ce qu'ils puissent interagir avec le substrat. C'est le principe de la « clé et serrure » [8] qui indique que la taille, la forme et la position des sites de liaison sur un récepteur (par exemple une enzyme) doivent être idéales pour une reconnaissance spécifique du substrat.

#### 1.1.1.3 Sélectivité des systèmes supramoléculaires

Le but à atteindre lors de la conception de récepteurs supramoléculaires, que ce soit pour les systèmes naturels (telles les enzymes ou les protéines de transport) ou les systèmes synthétiques, est la sélectivité. Le récepteur doit pouvoir discriminer deux composés et mieux lier un substrat/une famille de substrats en particulier. Il est possible de mesurer l'affinité d'un récepteur envers un substrat en mesurant la constante d'association *K* qui représente la constante de l'équilibre thermodynamique de la formation du complexe Hôte•Invité [9]. Plus cette constante d'association *K* est élevée, plus le substrat considéré a une grande affinité envers l'hôte. Ce concept est la sélectivité thermodynamique.

$$K = \frac{[Hôte•Invité]}{[Hôte][Invité]} \qquad (1)$$

Un autre type de sélectivité est la sélectivité cinétique qui consiste en la comparaison de la vitesse de complexation de deux substrats sur un récepteur. Ce type de sélectivité est à la base de la catalyse supramoléculaire et enzymatique [10].

### 1.1.2 Interactions intermoléculaires

Plusieurs types d'interactions non covalentes permettent la cohésion des assemblages supramoléculaires. Alors que la chimie moléculaire traditionelle se base sur des interactions covalentes dont la force est comprise entre 200-400 kJ/mol, la chimie

supramoléculaire se base sur des interactions non covalentes, dont les forces et propriétés sont différentes, entre deux ou plusieurs molécules. Des exemples de forces non covalentes avec leurs forces moyennes peuvent être consultés en Figure 1.3. La force de chaque interaction individuelle peut donc varier et est parfois faible, mais c'est l'addition et la coopération de toutes les interactions non-covalentes d'un assemblage supramoléculaire qu'il faut prendre en compte pour expliquer sa stabilité [11, 12, 13, 14, 15 et 16].

Les interactions de type liaison hydrogène sont entre autres à la base de la structure en double hélice de l'ADN [17]. La liaison hydrogène est un type particulier d'interaction électrostatique qui est forte et directionnelle. Elle résulte généralement d'une interaction entre un atome d'hydrogène lié à un atome très électronégatif (donneur) et un autre atome très électronégatif porteur d'un doublet libre (accepteur). Il existe des liaisons hydrogène neutres (D-H···A) et des liaisons hydrogène chargées ($D^+$-H···A ; D-H···$A^-$ ou $D^+$-H···$A^-$) [18]. Les interactions par liaison hydrogène sont souvent considérées comme les interactions les plus importantes et utiles pour concevoir et synthétiser des systèmes supramoléculaires.

Les interactions entre noyaux aromatiques, comme les empilements $\pi$ et empilements T, sont des interactions électrostatiques mutuelles et réciproques entre le nuage d'électrons $\pi$ négativement chargé d'une molécule avec le réseau $\sigma$ de l'autre molécule [19]. Ces interactions ont notamment une influence importante sur l'organisation dans le cristal des composés aromatiques.

Parmi les interactions non covalentes existantes en chimie supramoléculaire, il est aussi important de considérer les interactions de van der Waals [20] qui sont des interactions non spécifiques et non directionnelles provenant de la polarisation du nuage électronique par un noyau adjacent, ce qui crée une attraction électrostatique faible de la molécule voisine. Ces interactions sont la source principale de l'attraction entre espèces polarisables et décroît rapidement (dépendance en $r^{-6}$) avec la distance. Bien qu'elles soient individuellement faibles (environ 5 kJ/mol), elles sont additives sur la totalité de la

molécule. Les interactions ion-dipôle proviennent des interactions électrostatiques entre un ion et une paire d'électrons libres d'une molécule polaire.

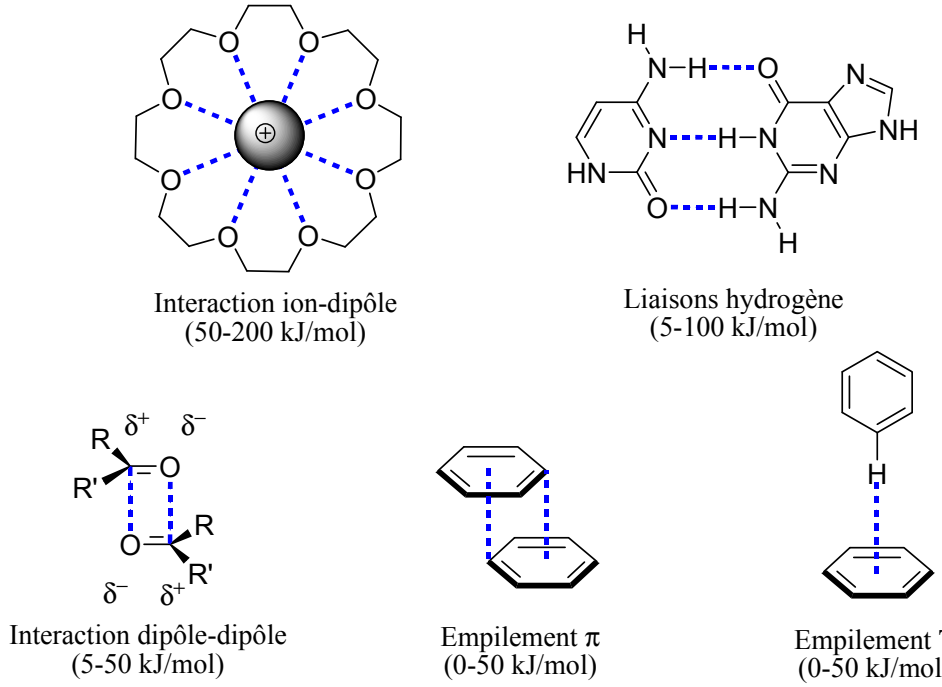


**Figure 1.3.** Différentes interactions non covalentes et ordre de grandeur de leurs forces.

L'interaction ion-dipôle est la force motrice de la solvatation des ions par des molécules polaires [1]. Les interactions dipôle-dipôle proviennent de l'attraction significative de deux dipôles alignés et les exemples classiques pour illustrer la force de ces interactions sont les points d'ébullition élevés des aldéhydes et cétones par rapport à leurs homologues hydrocarbonés. Les interactions ion-ion ont aussi un rôle important et leur force est comparable à celle des liens covalents. Il s'agit également d'interactions non directionnelles et non spécifiques [1].

Les effets hydrophobes sont également à prendre en considération [21]. Souvent considérés à tort comme une force, les effets hydrophobes sont en fait la manifestation de l'exclusion des grosses molécules ou particules des solvants polaires (souvent l'eau). Ces

effets ont un rôle très important dans la complexation de molécules organiques par des hôtes macrocycliques dans l'eau et peuvent être divisés en deux composantes : entropique et enthalpique. L'effet hydrophobe enthalpique consiste en la stabilisation des molécules d'eau qui ne solvatent plus l'hôte après la complexation avec le substrat. L'effet hydrophobe entropique consiste en la plus grande continuité dans la structure du solvant après complexation entre la molécule hôte et la molécule invitée (Figure 1.4).

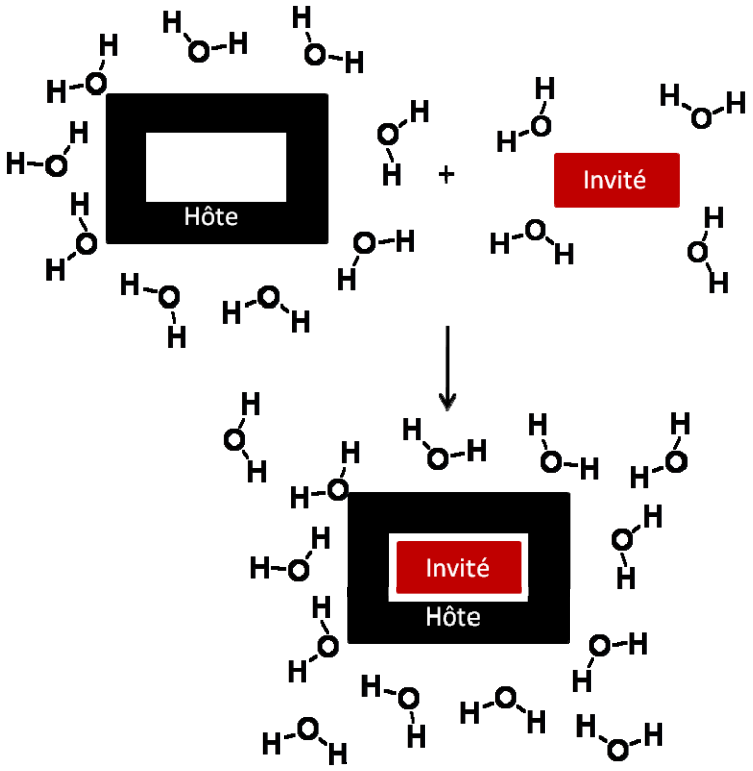


**Figure 1.4.** Illustration des effets hydrophobes en solution aqueuse.

### 1.1.3 Bases de la chimie hôte-invité en solution

Certains des complexes supramoléculaires les plus intriguants sont formés en solution à partir d'un substrat qui est complexé dans, ou à travers la cavité d'un récepteur macrocyclique. Une très grande attention a été portée envers ce type de composé en tenant compte du très grand nombre d'applications potentielles : il est envisageable de synthétiser

des machines moléculaires sophistiquées, de développer des matériaux possédant des propriétés physico-chimiques nouvelles ou encore d'obtenir des composés catalytiques activés par oxydo-réduction ou par photochimie, sans avoir besoin de les modifier chimiquement. Ce type de chimie supramoléculaire s'est particulièrement développée au cours des 15 dernières années et est en pleine expansion aujourd'hui. Parmi les exemples notables, il est possible de citer les « muscles moléculaires » du groupe de J. P. Sauvage [22, 23] et les machines moléculaires de J. F. Stoddart [24, 25, 26, 27 et 28]. Ces composés et machines supramoléculaires sont basés sur des molécules macrocycliques comme les cyclodextrines, cucurbiturils, éther-couronnes ou calixarènes ainsi que sur des molécules linéaires possédant des sites de reconnaissance souvent ioniques ayant une grande affinité pour ces macrocycles. Les macrocycles les plus couramment utilisés pour former des complexes en chimie supramoléculaire sont présentés dans les paragraphes suivants.

### 1.1.3.1 Macrocycles utilisés en chimie supramoléculaire

#### *1.1.3.1.1 Les éther-couronnes*

Les éther-couronnes comptent parmi les ligands macrocycliques les plus simples et sont omniprésents en chimie supramoléculaire, aussi bien en tant que récepteurs de cations, que de molécules neutres [29]. Ils consistent en une famille d'éthers cycliques, où les fonctions éther sont liées par des espaceurs organiques, souvent des groupements -$CH_2CH_2$-. Ces composés ont été découverts en 1967 par Charles Pedersen [30] et la synthèse du premier éther-couronne, le dibenzo-18-crown-6, était accidentelle. Il a rapidement été remarqué que ces éther-couronnes ont des propriétés de complexation de différents cations alcalins et organiques hors du commun (Figure 1.5).

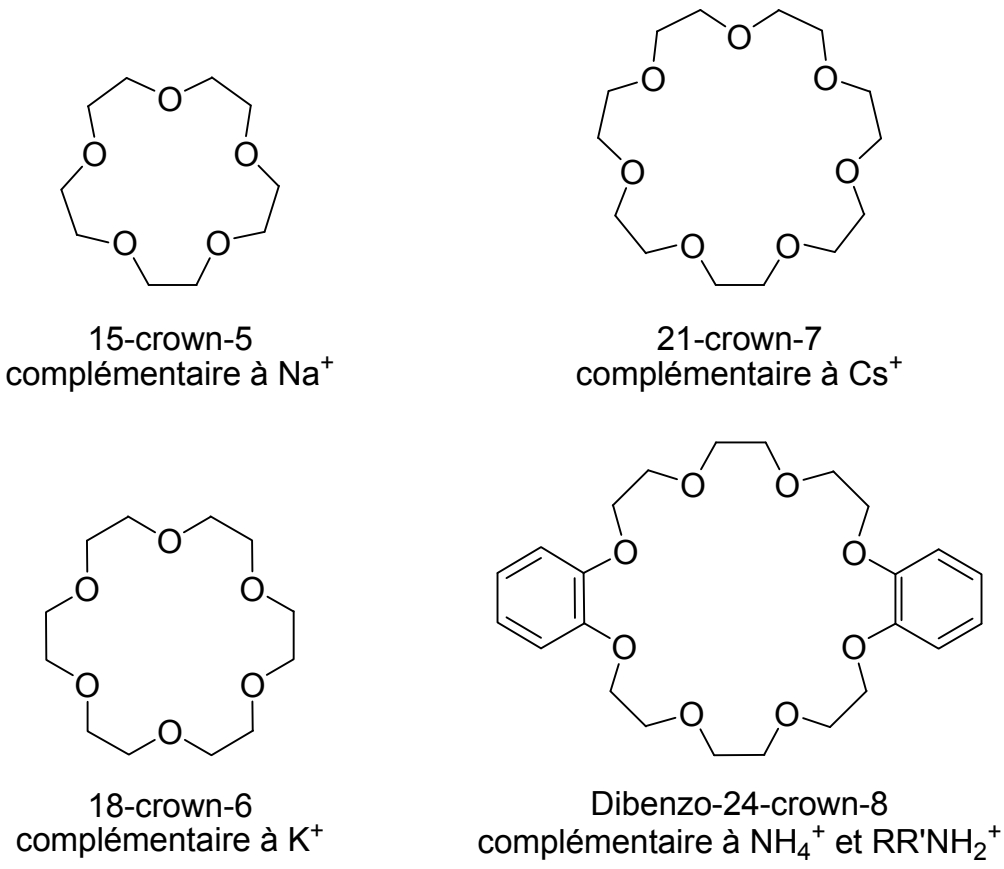


**Figure 1.5.** Quelques éther-couronnes communs.

En absence de molécule à complexer, les éther-couronnes sont généralement solubles dans une grande variété de solvants, allant de l'eau à l'hexane. Le 18-crown-6 a par exemple une valeur de log P = 0, indiquant un équilibre parfait entre son hydrophilie et sa lypophilie [31]. Ces propriétés de solubilité ont permis le développement d'applications majeures pour certains éther-couronnes : la catalyse par transfert de phase et l'activation d'anions. La catalyse par transfert de phase implique le transport de l'invité d'une phase à l'autre [32]. Les deux phases utilisées sont deux liquides non miscibles et la molécule d'intérêt à transporter (un composé ionique possédant un anion permettant de catalyser une réaction par exemple) est insoluble en phase organique en l'absence d'éther-couronne. À

l'ajout de macrocycle, la formation du complexe supramoléculaire permet le passage de l'espèce chargée en milieu organique. Pour respecter la neutralité électronique dans chaque phase, le contre-anion passe donc également en phase organique et la catalyse est ainsi possible.

*1.1.3.1.2 Les calixarènes*

Les calixarènes sont des macrocycles formés par la condensation de phenols parasubstitués avec du formaldéhyde [33] (Figure 1.6). Ils contiennent des cycles aromatiques liés entre eux et font donc partie de la famille des cyclophanes. Ils ont été développés dans les années 1980-90 par Gutsche [34]. Ils ont connu jusqu'à aujourd'hui un développement très poussé et sont toujours très utilisés en chimie supramoléculaire. Selon les conditions de synthèse, il est possible d'obtenir un nombre différent d'unités aromatiques dans le macrocycle [35]. Les calixarènes les plus couramment utilisés en chimie supramoléculaire sont les dérivés du *p-tert*-butylcalix[4]arène montré ci-dessous.

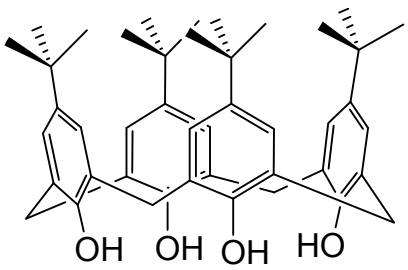


**Figure 1.6.** *p-tert*-Butylcalix[4]arène.

Ils sont considérés comme des molecules hôtes très polyvalentes en raison des très nombreuses possibilités de fonctionnalisation. En effet, selon les modifications apportées au squelette de base d'un calixarène, ils peuvent complexer aussi bien des cations, des anions ou des molécules neutres : la zone contenant les oxygènes phénoliques peut être modifiée pour complexer des cations, la cavité centrale hydrophobe est connue pour complexer fortement des molécules aromatiques comme le toluène [35] et la zone

supérieure peut, quant à elle, être modifiée et une grande panoplie de groupements chimiques peuvent y être attachés pour modifier à souhait les propriétés de complexation [36].

*1.1.3.1.3 Les cyclodextrines*

Cette classe de composés macrocycliques est sans aucun doute la plus utilisée en chimie supramoléculaire. En effet, les cyclodextrines sont utilisées en très grande quantité pour des applications industrielles dans les domaines agro-alimentaire, cosmétique et pharmaceutique, souvent en tant que transporteur d'un composé actif [37]. Ces composés sont également très utilisés en tant que base pour la conception et la synthèse de mîmes d'enzymes [38]. Ils ont l'avantage d'être non toxiques sur une grande plage de concentrations [39].

Les cyclodextrines sont des oligosaccharides cycliques constituées d'unités D-glucopyranose liées par un lien 1,4-glycosidique. Les trois composés les plus importants de cette famille sont l'$\alpha$-cyclodextrine ($\alpha$-CD), la $\beta$-cyclodextrine ($\beta$-CD) et la $\gamma$-cyclodextrine ($\gamma$-CD) qui possèdent respectivement six, sept et huit unités glucopyranose (Figure 1.7). La forme des cyclodextrines est souvent représentée par un cone sectionné et possédant une face primaire plus étroite, comprenant des groupements alcools primaires et une face secondaire plus large contenant les alcools secondaires. Ces deux faces possèdent des propriétés de complexation différentes [38]. L'inclusion des substrats dans les cyclodextrines est largement étudiée dans la littérature. Généralement, les cyclodextrines interagissent avec une molécule invitée apolaire dans l'eau, résultant en la formation de complexes d'inclusion 1:1. La molécule invitée est souvent positionnée (selon sa taille) dans la cavité hydrophobe de la cyclodextrine [38].

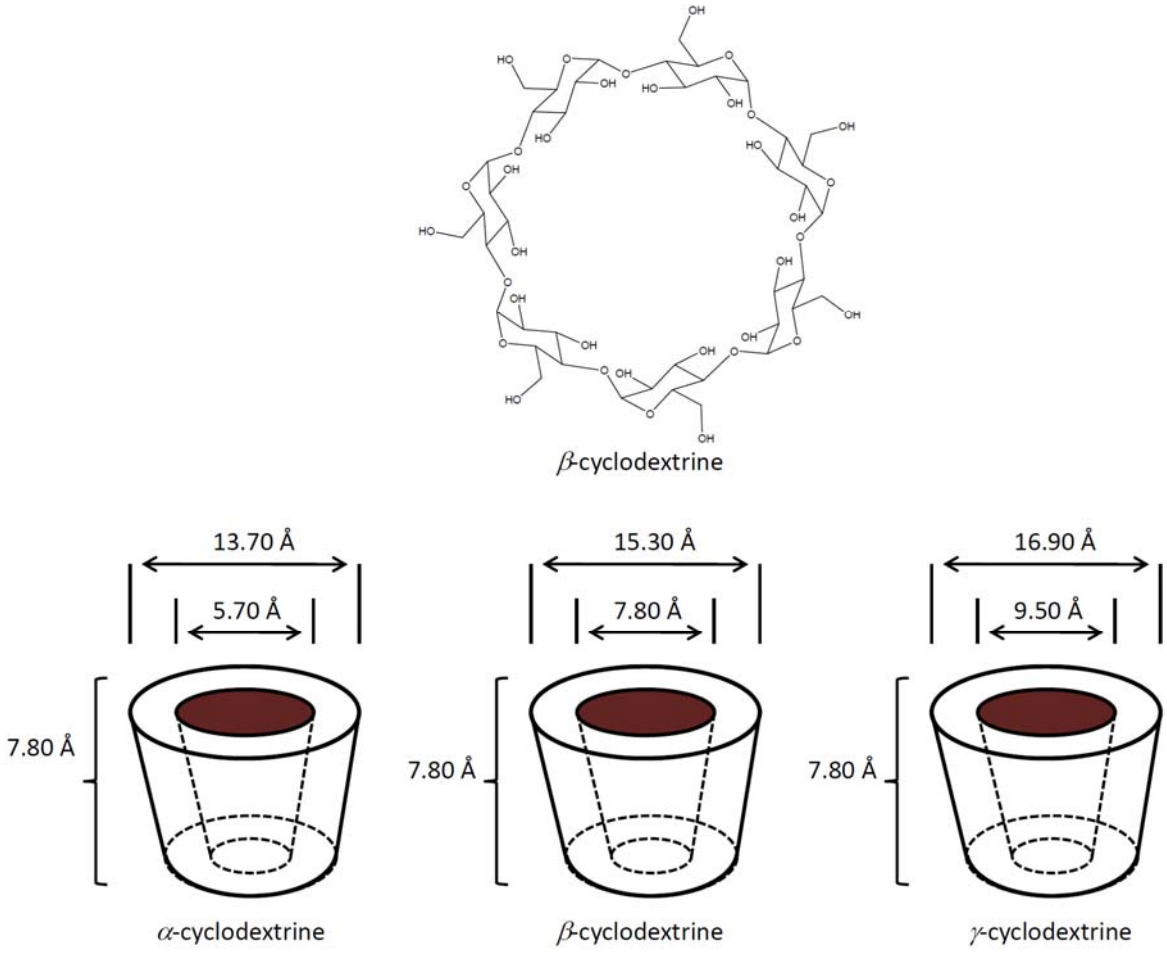


**Figure 1.7.** Les cyclodextrines communes et leurs dimensions.

*1.1.3.1.4 Les cucurbiturils*

Les cucurbit[n]urils (CB[n]) sont des oligomères cycliques de glycoluril pontés par des groupements méthylènes (où n représente le nombre d'unités glycoluril) [40]. Ils sont souvent comparés aux cyclodextrines en raison de leur profondeur comparable (9.1 Å) et de la largeur comparable de leurs cavités. Les CB[5] à CB[8] possèdent deux portails équivalents constitués de fonctions urées dans lesquelles les groupements carbonyles sont tous alignés à l'entrée de la cavité hydrophobe. La largeur de ces portails est d'environ 7.1

Å, et sont donc plus étroits que la largeur de la cavité hydrophobe interne. La structure des cucurbiturils les plus communs est illustrée en Figure 1.8 [40].

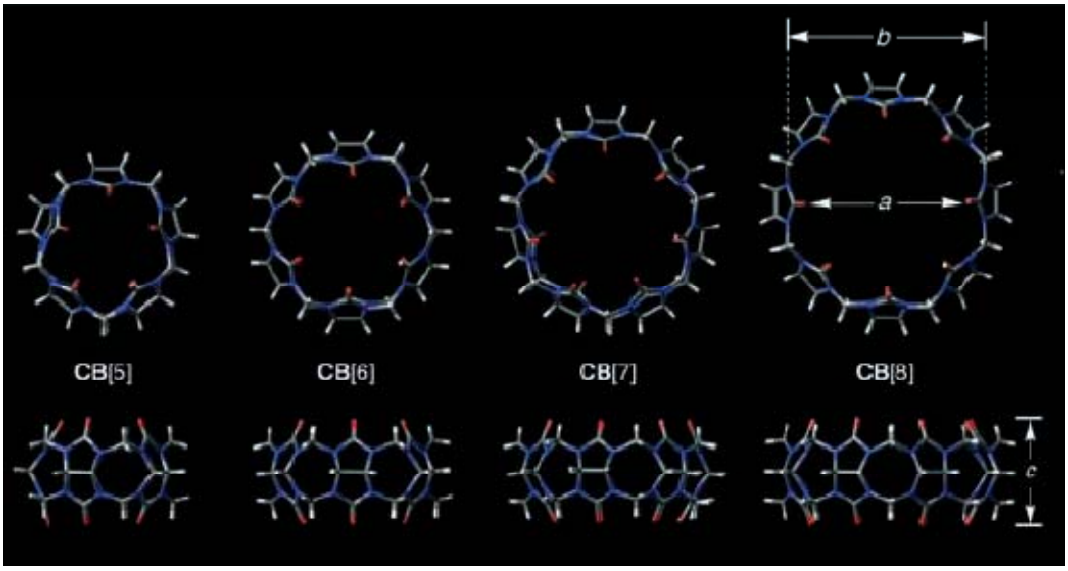


**Figure 1.8.** Vue de dessus et de côté des structures cristallines des CB[n].

Une des limitations possibles des CB[n] est leur solubilité dans l'eau, bien moins grande que celle des cyclodextrines. La solubilité de ces composés est néanmoins grandement augmentée en milieu très acide et il est souvent possible d'obtenir des complexes supramoléculaires très intéressants avec ce type de macrocycle. Vu la géométrie des cucurbiturils, ils sont souvent utilisés pour complexer des dications organiques possédant un espaceur hydrophobe [40]. La partie hydrophobe centrale de la cavité lie fortement des groupements alkyles et aromatiques alors que les deux portails peuvent interagir avec des cations par l'intermédiaire de liaisons hydrogène ou des interactions ion-dipôles (Figure 1.9). Ce type d'interaction est typique de ce que nous allons rencontrer dans les travaux présentés dans cette thèse.

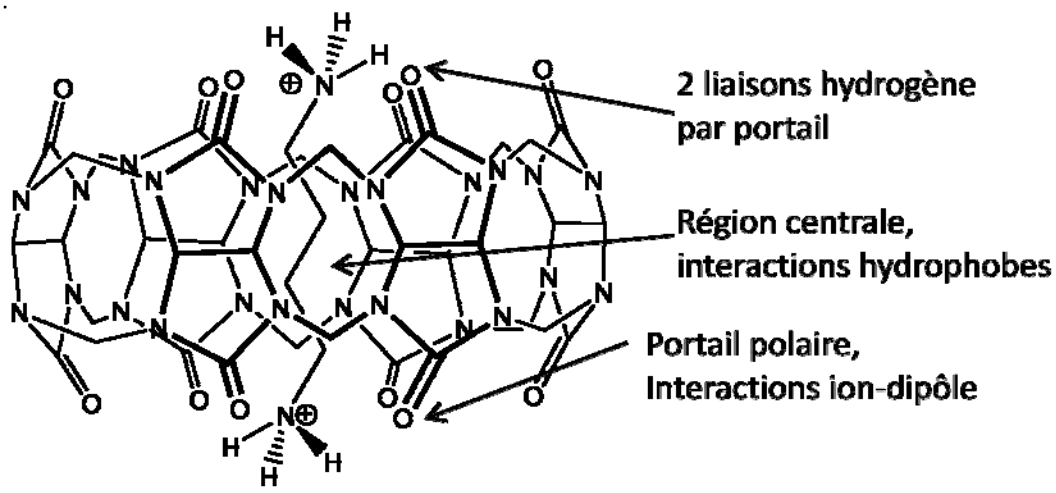


**Figure 1.9.** Mode de liaison entre le CB[6] et le dication butanediammonium.

### 1.1.3.2 Complexation et auto-assemblage en solution

*1.1.3.2.1 Effets thermodynamiques*

Les mécanismes de complexation en solution se basent souvent sur la complémentarité des différentes composantes moléculaires de l'assemblage supramoléculaire, ainsi que de leur préorganisation [41]. Le concept général de la préorganisation est la construction d'un hôte qui sera parfaitement complémentaire, aussi bien d'un point de vue stérique qu'électronique, de l'invité. Une complémentarité stérique implique que l'hôte doit pouvoir accommoder l'invité sans être trop gros ou trop petit. La complémentarité électronique vise, quant à elle, à apparier des charges négatives avec des charges positives, des donneurs de ponts hydrogène avec des accepteurs, des acides de Lewis avec des bases de Lewis, *etc.* Ce principe a très bien été expliqué par Cram dans les années 1980 [42]. La constante d'association est alors dans ce contexte une mesure quantitative de la complémentarité des composants du système supramoléculaire. Ce concept implique un rôle déterminant pour le solvant. Les interactions entre le solvant et l'hôte ou l'invité sont souvent de la même nature que les interactions entre l'hôte et l'invité.

Il faut donc prendre en considération les variations d'enthalpie et d'entropie dues à la réorganisation de l'hôte pour pouvoir accommoder l'invité, ainsi que l'augmentation nette du nombre de particules libres en solution. Le processus général de complexation en solution est résumé à la Figure 1.10 [3]. Généralement, la complexation est d'autant plus favorable que l'hôte est préorganisé, si l'on assume une bonne complémentarité avec l'invité.

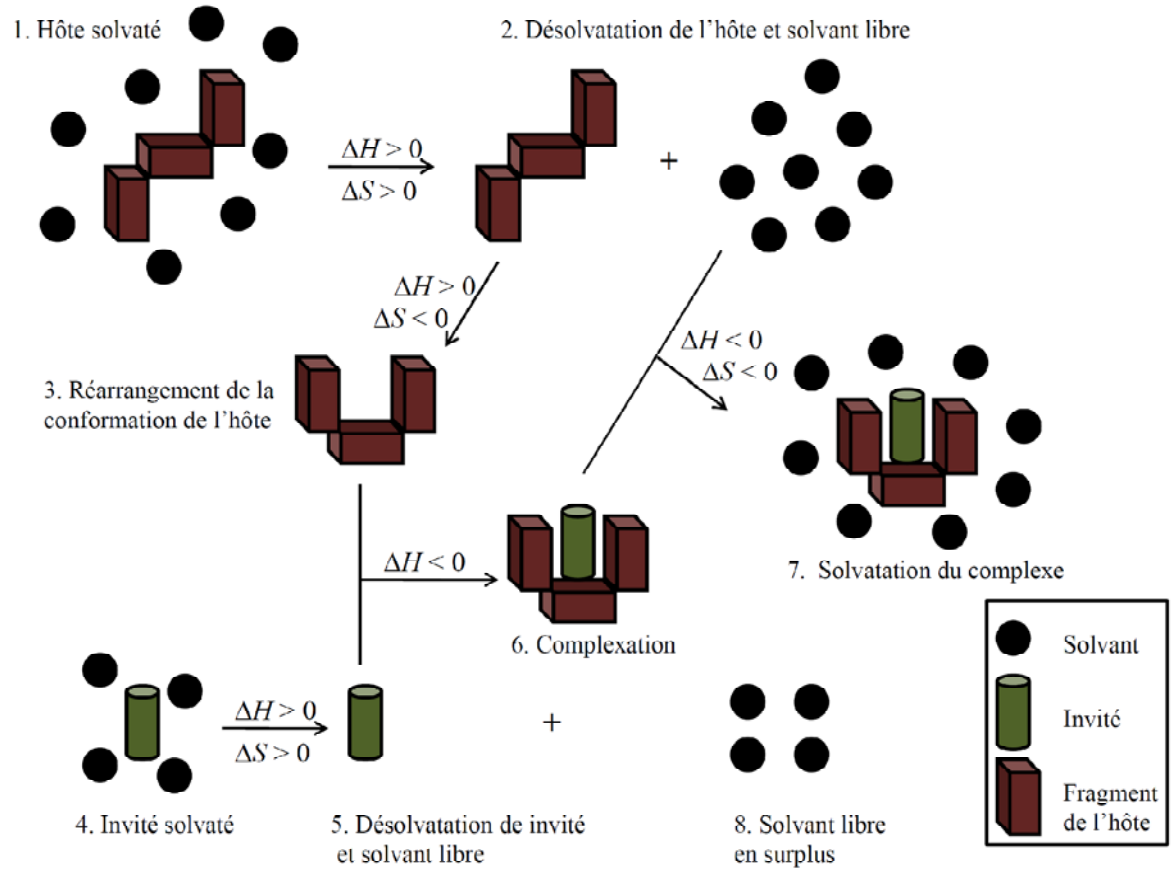


**Figure 1.10.** Processus de complexation en solution.

*1.1.3.2.2 Effets cinétiques et dynamiques*

Le degré de préorganisation d'un hôte pour pouvoir accommoder une molécule invitée a également un effet direct sur la cinétique de complexation, donc sur la vitesse des réactions de complexation et de décomplexation. La constante d'équilibre thermodynamique *K* peut aussi s'écrire comme étant le rapport $K = k_1/k_{-1}$ entre la vitesse de complexation ($k_1$) et la vitesse de décomplexation ($k_{-1}$) [3]. De manière générale, les vitesses de complexation et de décomplexation diminuent avec l'augmentation du degré d'encapsulation de la molecule invitée dans l'hôte. Entre autres, la cinétique de complexation peut permettre de distinguer différentes classes d'assemblages supramoléculaires. Par exemple, un *récepteur de cation* aura une cinétique de complexation lente et une constante d'association élevée, alors qu'un *transporteur de cation* aura une cinétique de complexation rapide et une moins bonne stabilité.

Un très bon exemple de contrôle thermodynamique et cinétique de complexation supramoléculaire est la synthèse de pseudorotaxanes et rotaxanes [43]. Notamment, le travail des groupes de Stoddart et Loeb sur les rotaxanes basés sur les éther-couronnes a été d'une grande inspiration pour toute la partie des complexes en solution présentée dans cette thèse.

*1.1.3.2.3 Exemple des rotaxanes basés sur les éther-couronnes*

La définition des pseudorotaxanes et rotaxanes a été donnée en 1969 par Schill et Justus [44] : un pseudorotaxane est un composé constitué d'une ou plusieurs molécules linéaires (axes) sur lesquelles sont complexés un ou plusieurs macrocycles (roues). Lorsque la complexation du macrocycle est cinétiquement bloquée sur l'axe par des groupements stériquement encombrés, on obtient un rotaxane. Ce n'est qu'à partir des années 1990 que des méthodes de synthèse efficaces des rotaxanes sont proposées [45]. Depuis, plusieurs substrats cationiques et dicationiques ont été développés pour la formation de pseudorotaxane et de rotaxanes avec l'éther-couronne dibenzo-24-crown-8 (DB24C8). L'autoassemblage en solution organique polaire entre l'éther-couronne et le cation

organique est rapide et les constantes d'association sont souvent assez élevées pour permettre la synthèse de rotaxanes et même de machines moléculaires plus complexes basées sur l'architecture des rotaxanes [46].

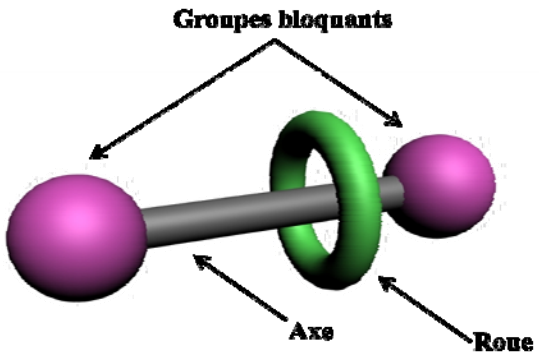


**Figure 1.11.** Représentation schématique d'un rotaxane

Les principaux cations organiques se liant au DB24C8 sont les dérivés des dibenzylammonium, du *bis*(pyridinium)éthane, du paraquat et de diverses amines secondaires (Figure 1.12) [47, 48, 49].

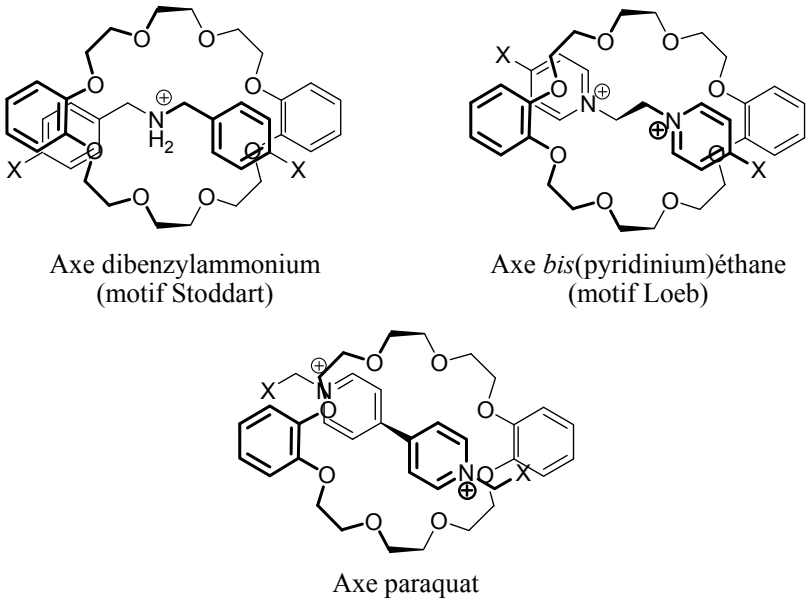


**Figure 1.12.** Pseudorotaxanes formés par la complexation de cations organiques linéaires avec DB24C8.

Comme nous l'avons souligné jusqu'à présent, les cations organiques sont des entités très utilisées pour l'assemblage de diverses architectures supramoléculaires, possédant des propriétés de complexation et de reconnaissance des anions. Malgré le grand nombre de cations organiques connus et utilisés en chimie supramoléculaire, le développement et l'étude de nouveaux motifs et systèmes auto-organisés restent d'un grand intérêt.

## 1.2 Les sels d'imidazolium en chimie supramoléculaire

L'imidazole et le cation imidazolium ont une importance considérable au niveau des sites actifs de plusieurs enzymes et acides nucléiques, notamment à travers l'histidine, un des vingt acides aminés naturels [50, 51]. Ils ont en conséquence été largement utilisés dans le domaine des mimes d'enzymes [52]. De plus, ses propriétés physico-chimiques en font un très bon choix comme motif de base pour concevoir et construire des assemblages supramoléculaires complexes comme nous allons le montrer dans cette section.

### 1.2.1 Propriétés physico-chimiques des sels d'imidazolium

Les sels d'imidazolium sont synthétisés par alkylation de l'azote $\pi$ d'un imidazole *N*-substitué (Figure 1.13) [53]. L'imidazole est un amphotère : le proton de l'azote $\sigma$ est légèrement plus acide qu'un alcool et a un pKa de 14,5, alors que l'azote $\pi$ est basique et peut capter facilement un proton (pKa proche de 7) [54]. Après alkylation, les cations imidazolium obtenus possèdent différentes propriétés acido-basiques : l'hydrogène H(2) situé sur le carbone *sp2* entre les deux atomes d'azote a un pKa compris entre 21 et 24 selon les substituants [51]. Les carbènes pouvant être obtenus par déprotonation de l'hydrogène H(2) sont à la base de plusieurs catalyseurs couramment utilisés en synthèse organique [55]. Les sels d'imidazolium sont toutefois peu connus en chimie supramoléculaire et ont attiré notre attention en raison de la facilité de modification de leurs propriétés de solubilité, que ce soit en milieu aqueux ou organique.

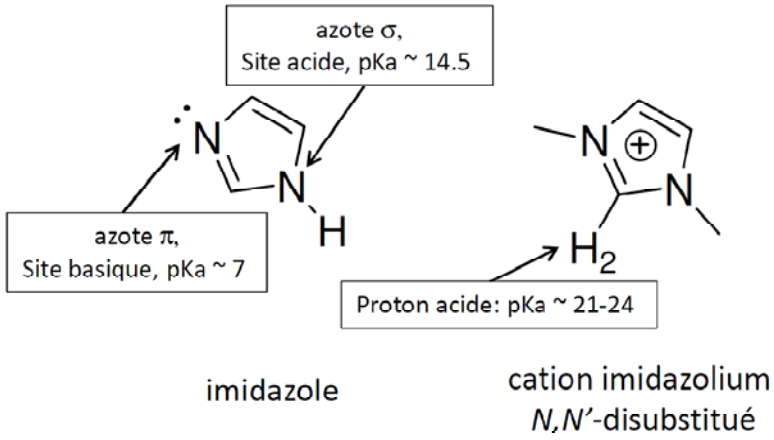


**Figure 1.13.** Propriétés acido-basiques de l'imidazole et des cations imidazolium *N,N'*-disubstitués.

Les sels d'imidazolium *N,N'*-disubstitués suscitent surtout un très grand intérêt en raison de la possibilité d'obtenir des liquides ioniques ; c'est-à-dire des composés ioniques dont la température de fusion est inférieure à 100 °C [56]. De plus, leurs propriétés physico-chimiques peuvent facilement être modulées, soit par modification des chaînes latérales, soit par modification du contre-ion. Parmi les propriétés recherchées, on peut citer, par exemple, une grande stabilité thermique, une conductivité élevée, une viscosité faible ou des solubilités différentes [57]. Il est possible de classer les sels d'imidazolium en quatre groupes selon le contre-ion utilisé : 1) les sels d'imidazolium possédant des anions halogènes qui sont hygroscopiques ; 2) des systèmes basés sur des anions pouvant réagir avec l'eau (anions hexafluorophosphate ou tétrafluoroborate) pour libérer de l'acide fluorhydrique ; 3) des composés stables basés sur des anions fluorés souvent hydrophobes, comme le triflate [$CF_3SO_3^-$] ou *bis*(trifluorométhanesulfonyl)imide [$(CF_3SO_2)_2N^-$] ; 4) enfin, des sels d'imidazolium alkylsulfonate ou alkylsulfate, dont l'hydrophobie va dépendre grandement de la longueur de la chaîne alkyle de l'anion [58, 59]. Ces propriétés remarquables des sels d'imidazolium peuvent en grande partie être expliquées par l'étude de leur auto-assemblage.

### 1.2.2 Auto-assemblage des sels d'imidazolium en phase liquide ionique et en solution

Le cation imidazolium possède un noyau aromatique pauvre en électrons ayant la possibilité de réaliser facilement un empilement π avec d'autres unités aromatiques, de préférence plus riches en électrons. De plus, le proton H(2) acide permet de réaliser des interactions de type empilement T avec d'autres systèmes π ou liaison hydrogène avec des anions ou paires d'électrons libres sur des atomes électronégatifs [60]. Les protons H(4) et H(5) sont également connus pour pouvoir réaliser des liaisons hydrogène de plus faible intensité avec des anions comme les halogénures (Figure 1.15).

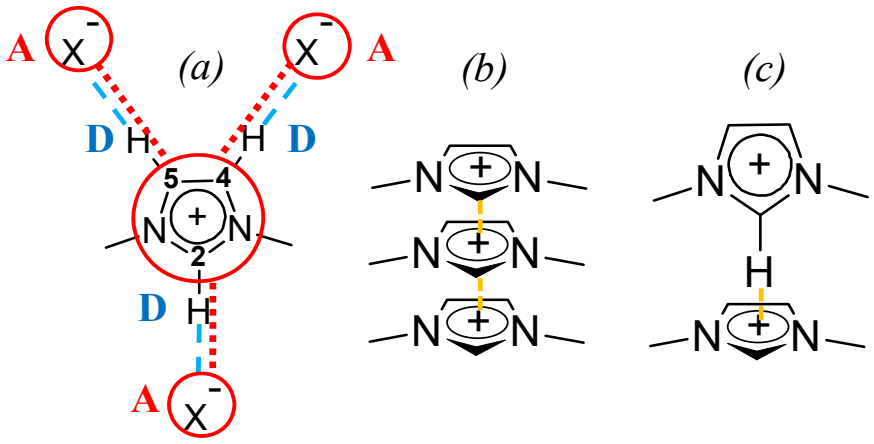


**Figure 1.14.** (a) Les trois liaisons hydrogène entre l'imidazolium (D: donneur) et un anion (A: accepteur); (b) empilement-π, (c) empilement-T (Figure tirée de [60]).

Les cations imidazolium possèdent une organisation supramoléculaire caractéristique, aussi bien en phase solide qu'en phase liquide. Ils s'associent principalement à travers les liaisons hydrogène possibles dans trois directions, qui permettent de former un réseau plan pouvant s'apparenter à une structure polymérique [61, 62, 63]. Ce type d'organisation est en contraste direct avec les composés ioniques classiques dont les aggrégats vont principalement se former à travers des interactions ioniques [64]. En plus de cet arrangement bidimensionnel vient s'ajouter une organisation

spatiale à trois dimensions grâce aux empilements π possibles entre les cycles aromatiques [65].

On peut se baser sur cette organisation supramoléculaire en phase liquide ionique pour décrire l'organisation en solution (Figure 1.16), où la dilution va progressivement briser le réseau des liaisons hydrogène, en engendrant des aggrégats supramoléculaires dont la taille varie selon la concentration. Ces aggrégats sont de type $\{[(I)_x(X)_{x-n}]^{n+},[(I)_{x-n}(X)_x]^{n-}\}$ (I : cation imidazolium, X : anion) [51]. Dans l'eau, l'existence d'une concentration critique d'aggrégation a été démontrée par différentes techniques comme la RMN, la spectroscopie UV-visible, ou la spectrométrie de masse [66, 67, 68, 69, 70]. Le phénomène d'aggrégation passe dans un premier temps par la formation d'un réseau de liaisons hydrogène entre les cations imidazolium et les molécules d'eau. Les interactions entre les anions et les cations imidazolium sont ensuites observées et ce sont finalement les interactions de type empilement π qui, à forte concentration, permettent de former une structure proche de celle d'un solide [53].

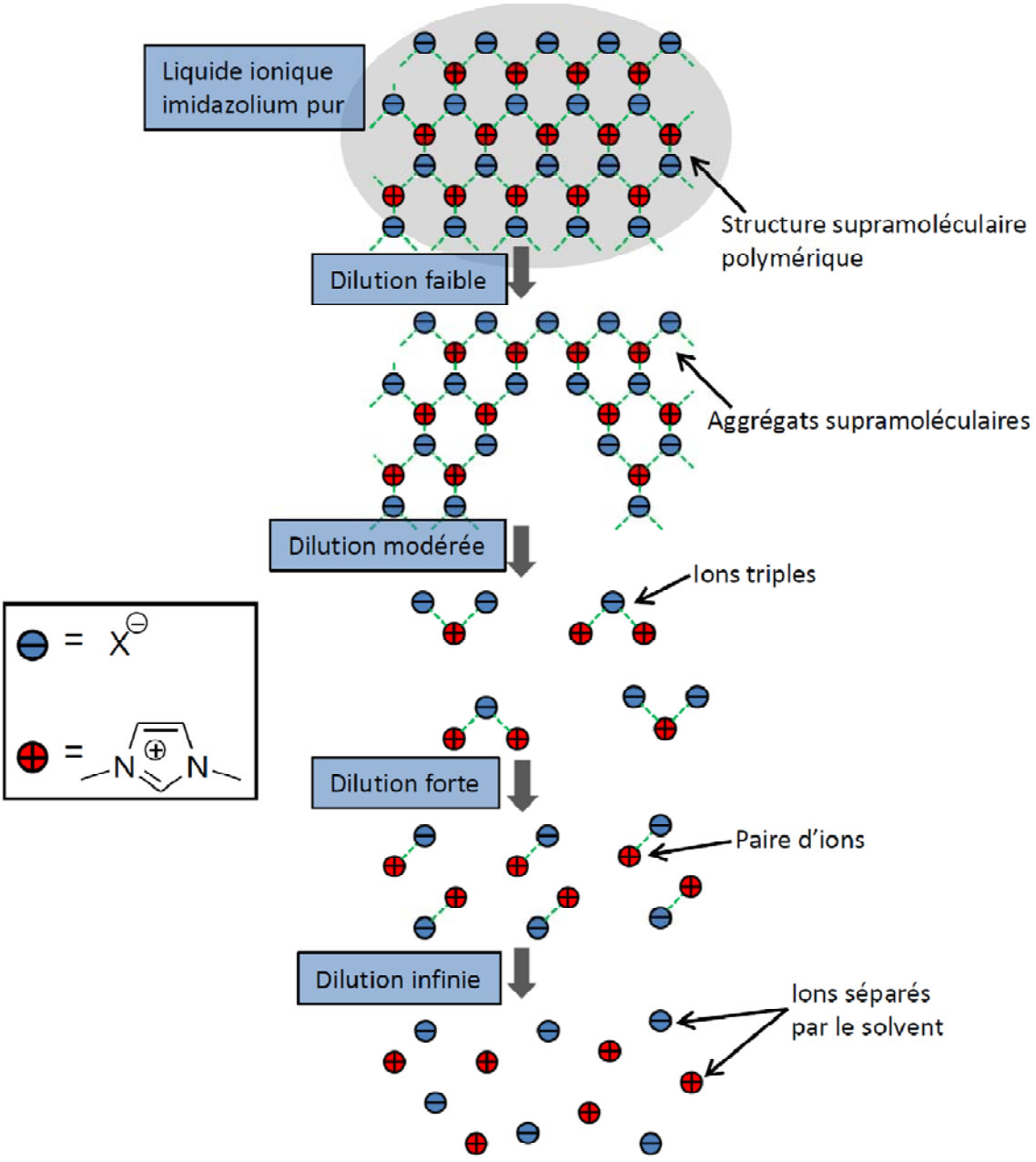


**Figure 1.15.** Modèle 2D simplifié de l'organisation des sels d'imidazolium selon la dilution ou en phase liquide.

## 1.2.3 Auto-assemblage des sels d'imidazolium en phase solide

### 1.2.3.1 Introduction

Le processus de cristallisation [71] est par essence même un processus d'auto-assemblage, dans le sens où les molécules doivent se reconnaître mutuellement en solution et trouver une orientation optimale dans le temps imparti. Les aggrégats qui en résultent doivent alors se lier à toujours plus de molécules pour former ultimement un noyau ordonné qui pourra cristalliser. La différence principale avec l'auto-assemblage en solution est le fait que l'auto-association cristalline est un phénomène hors équilibre dans lequel les aspects thermodynamiques et cinétiques contribuent à la structure finale. En effet, la structure finale du cristal est souvent fonction des conditions de cristallisation (température, nature et quantité de solvant) et les structures polymorphes sont communes. Souvent, des structures moins stables mais qui cristallisent plus vites prédominent par rapport aux structures plus stables mais qui ont une cinétique de cristallisation lente [3].

Dans les structures cristallines, il y a souvent coexistence de plusieurs interactions supramoléculaires de forces comparables et il est donc très difficile de prédire à l'avance laquelle va gouverner la formation du cristal. Pour évaluer la force des interactions intermoléculaires à l'état cristallin, il faut évaluer la distance et les angles entre les atomes. Les interactions de van der Waals sont, dans le cas des cristaux, des interactions qui définissent la structure moléculaire et qui contribuent favorablement à la stabilité générale du cristal. Ces interactions constituent la force motrice vers l'empilement compact de la structure. Les forces agissant à plus grande distance comme les liaisons hydrogène sont directionelles et peuvent même acquérir un certain caractère covalent [72].

En examinant une structure cristalline, il est important de ne pas uniquement prendre en compte les forces intermoléculaires qui stabilisent la structure cristalline : le mécanisme de formation du cristal n'est pas à négliger. Le processus par lequel les cristaux sont formés implique la formation de noyaux composés de molécules de soluté supersaturés

en solution (nucléation) [3]. Cette étape est suivie par une étape de croissance lorsque l'assemblage atteint une taille critique :

1. Formation d'aggrégats à partir du synthon S

   $S + S = S_2$

   $S_2 + S = S_3$

   …

2. Coalescence en aggrégats

   $S_n + S = S_{n+1}$

   $S_n + S_m = S_{n+m}$

   …

3. Formation d'un noyau critique Sn* et croissance

   $S_n^* + S = S_{n+1}*$

   $S_{n+1}* + S = S_{n+2}$

   …

4. Agglomération moléculaire au niveau macroscopique (Ω)

   $\Omega + S = \Omega S$

**1.2.3.2 Les sels d'imidazolium en phase solide**

L'organisation des sels de diimidazolium en phase solide est très proche de l'organisation en phase liquide ionique : les unités imidazolium sont généralement entourées de trois anions qui forment des liaisons hydrogène avec les trois protons disponibles [60]. De même les anions sont eux même entourés de trois cations imidazolium. Les interactions aromatiques entre les unités imidazolium permettent alors la formation de canaux dans lesquels les contre-anions sont accommodés. Ces interactions

peuvent être mises en évidence en compilant par exemple, des données cristallographiques pour les halogénures de 1-méthyl-3-alkylimidazolium (Tableau 1.1) [60, 73, 74, 75] : on remarque que toutes les distances H-X sont inférieures au rayon de Van der Waals, montrant ainsi la formation de liaisons hydrogène fortes à l'état solide.

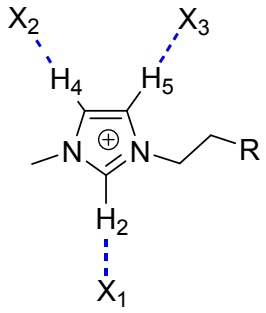


| X | R | Rayon de VdW pour H-X (Å) | $H_2$-$X_1$ | $H_4$-$X_2$ | $H_5$-$X_3$ |
|---|---|---|---|---|---|
| $F^-$ | $CH_3$ | 2.67 | 1.965 | 2.312 | 2.067 |
| $Cl^-$ | $CH_3$ | 3.09 | 2.517 | 2.882 | 2.995 |
| $Br^-$ | H | 3.48 | 2.775 | 2.886 | 2.967 |
| $I^-$ | H | 3.86 | 2.928 | 3.132 | 3.169 |

**Tableau 1.1.** Distances H-X dans différentes structures cristallines d'halogénures de dialkylimidazolium.

## 1.2.4 Auto-assemblage des sels d'imidazolium en phase cristal liquide

### 1.2.4.1 Introduction

Les cristaux liquides sont des fluides anisotropes partiellement ordonnés qui sont dans un état thermodynamique intermédiaire entre le solide ordonné dans les trois dimensions et le liquide isotrope. Dans ces phases, l'ordre de l'état cristallin est seulement partiellement perdu et les molécules individuelles ont un certain degré de mobilité. En

raison de la possibilité d'acquérir un ordre à une ou deux dimensions, elles peuvent posséder des propriétés cristallines comme la biréfringence [76, 77]. Les cristaux liquides sont souvent divisés en deux catégories : les mésophases lyotropes et thermotropes. Les cristaux liquides thermotropes sont obtenus par changement de température alors que les cristaux liquides lyotropes sont obtenus en présence d'un solvant approprié et selon la concentration utilisée.

Le mésomorphisme thermotrope est facilement atteignable par conception de molécules adéquates. Les molécules thermotropes sont souvent constituées d'un cœur rigide et d'extrémités composées de longues chaines alkyles. Les interactions intermoléculaires telles les interactions dipôle-dipôle jouent un rôle clé dans l'induction du mésomorphisme. Un cristal solide possède un ordre à longue distance par rapport aux positions des molécules dans les trois dimensions. Lorsque le solide est chauffé vers la phase liquide isotrope, il peut y avoir passage par plusieurs mésophases intermédiaires où plusieurs degrés d'ordre du cristal initial sont brisés pour former des cristaux liquides. Une séquence typique de transitions de phases pour un composé thermotrope est illustrée à la Figure 1.16.

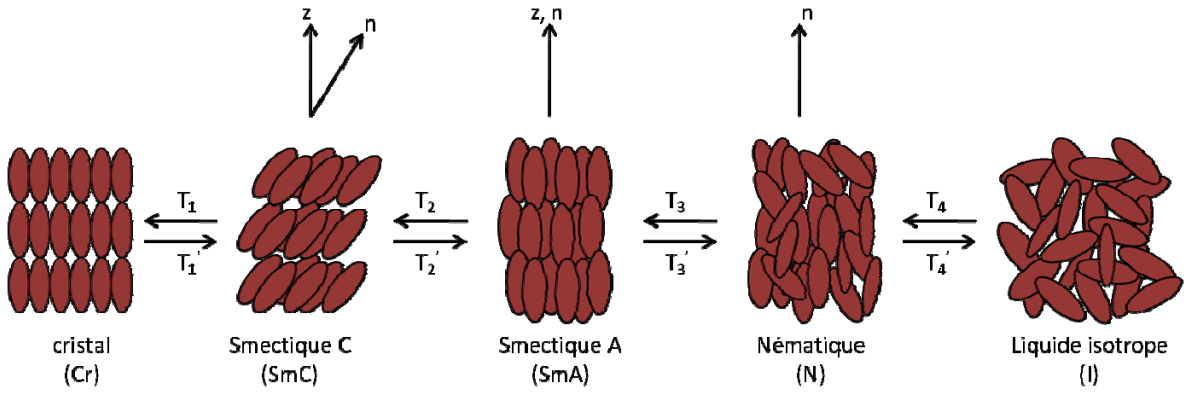


**Figure 1.16.** Illustration hypotétique des phases cristalline (Cr), smectique C (SmC), smectique A (SmA), nématique (N) et liquide isotrope (I).

La phase nématique est la phase la moins ordonnée. L'ordre de position de chaque molécule est perdu et seul un ordre à une dimension à longue distance est conservé. Les longs axes moléculaires sont distribués autour d'une direction particulière, notée **n**. Les centres de gravité de toutes les molécules d'une phase nématique sont distribués isotropiquement dans les trois dimensions. L'alignement de l'axe moléculaire le long de l'axe directeur **n** est uniquement approximatif. En raison de l'absence d'ordre, les phases nématiques ont souvent une viscosité approchant celle d'un liquide isotrope (**z** représente la normale à la couche de cristal-liquide).

Dans la phase smectique A (SmA), la rotation des molécules est libre selon leur axe principal. Elles possèdent un ordre dans leur orientation ainsi qu'un ordre à longue distance sur une dimension. Ces phases forment donc des couches qui ne sont pas clairement définies. Si l'axe directeur **n** dévie d'un angle θ par rapport à la couche, on parle de phase smectique C (SmC). Cette déviation est la seule différence entre les phases SmA et SmC. Les SmC sont favorisées par des molécules à cœur aromatique polaire mais non symétrique [78, 79]. D'autres mésophases avec une plus grande organisation à deux ou trois dimensions peuvent également être observées, comme des phases columnaire ou cubique [80].

#### 1.2.4.2 Les sels d'imidazolium en phase cristal liquide

Des cristaux liquides ioniques peuvent facilement être obtenus si au moins un des deux substituants latéraux des sels d'imidazolium est une longue chaîne alkyle. Pour mieux comprendre les applications potentielles des cristaux liquides ioniques basés sur le cation imidazolium, il est important de connaître la relation entre les propriétés des mésophases et la structure moléculaire. Les cristaux liquides basés sur les sels d'imidazolium peuvent généralement être séparés en quatre classes : 1) tout d'abord, les composés possédant une ou deux chaînes alkyles [81, 82, 83, 84] et pouvant également contenir un cycle aromatique. Ce type de composés permet souvent d'obtenir des mésophases smectiques ; 2)

des sels d'imidazolium possédant plus que deux chaînes alkyles [85, 86, 87], et ayant des proprieties fortement reliées à leur caractère amphiphile ; 3) des composés de géométrie globale cylindrique dont les cations imidazolium sont interconnectés par de longs espaceur flexibles. Des phases columnaires ou smectiques sont obtenues avec cette classe de composés [87, 88] ; 4) finalement, on trouve également des sels d'imidazolium dans lesquels l'hétérocycle est partie intégrante d'une unité rigide plus grande. Cette dernière classe est la moins étudiée des cristaux liquides ioniques basés sur les cations imidazolium [89].

Les composés de types 1-méthyl-3-alkylimidazolium sont les composés qui ont été le plus souvent étudiés pour leurs propriétés mésomorphes [90]. Plusieurs organisations supramoléculaires ont été proposées selon le contre-ion et la longueur de la chaîne alkyle à l'état cristal liquide (Figure 1.17) [89] :

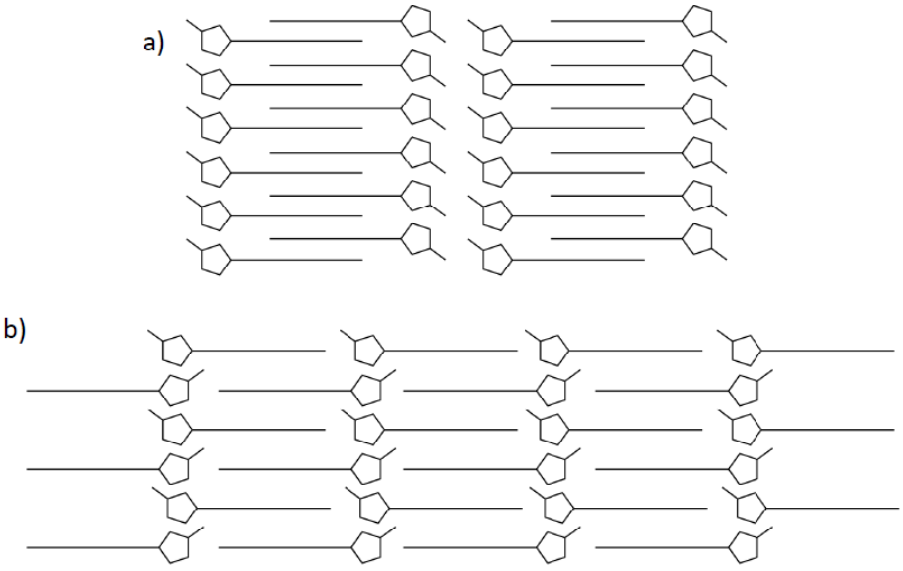


**Figure 1.17.** Organisations possibles des mésophases pour les cations 1-méthyl-3-alkylimidazolium. a) organisation parallèle ; b) organisation anti-parallèle.

A part leur auto-organisation, les cations imidazolium ont aussi été utilisés pour la construction d'échafaudages plus complexes, capables de reconnaître et de complexer des anions en solution.

## 1.2.5 Récepteurs d'anions basés sur les sels d'imidazolium

Les anions ont un rôle très important dans la majorité des systèmes biologiques, des canaux anioniques [91] à la molécule d'ATP, en passant par le squelette phosphaté de l'ADN. En conséquence, un grand intérêt s'est développé ces deux dernières décénies envers les composés synthétiques qui ont la propriété de reconnaître ou de se lier aux anions pour mimer les systèmes naturels [92]. En raison de leur structure et des liaisons hydrogène possibles, les cations imidazolium sont un motif de choix pour la conception de tels systèmes. Dépendament des anions, et de la structure des sels d'imidazolium des complexes 1:1 ou 2:1 peuvent être envisagés, ce qui laisse penser qu'une certaine sélectivité est envisageable.

Les sels d'imidazolium sont utilisés en tant que récepteurs d'anions depuis les années 1990, avec la synthèse de macrocycles contenant deux unités imidazolium et une série de différentes unités aromatiques [93, 94]. La synthèse de ces récepteurs macrocycliques (Figure 1.18) a conduit à la formation de liaisons hydrogène C-H···$Cl^-$ non conventionnelles. La difficulté principale dans la conception de récepteurs anioniques basés sur des cations est la sélectivité et il est nécessaire de pouvoir effectivement différencier la formation d'un complexe d'un simple changement de contre-ion.

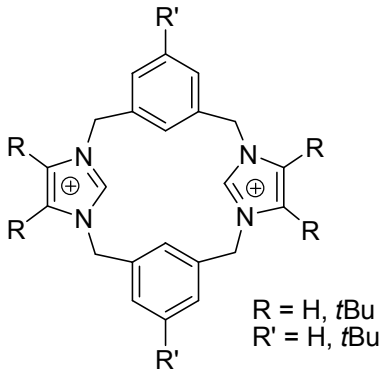


**Figure 1.18.** Imidazoliophane dicationique : premier récepteur d'anions basé sur le cation imidazolium.

Plusieurs types de récepteurs d'anions basés sur les cations imidazolium on ensuite été rapportés dans la littérature depuis et ils peuvent être classés en plusieurs types. Tout d'abord, on peut mentionner les récepteurs à géométrie tripodale [95, 96] qui se lient fortement aux halogènes (Figure 1.19). Des dérivés de ces récepteurs à base de ferrocène pour des applications en électrochimie ont également été décrites [97]. Pour ce type de récepteur, les constantes d'association avec les halogènes sont relativement élevées ($10^3$-$10^4$ $M^{-1}$) mais la sélectivité est généralement faible et des complexes avec des anions nitrate ou hydrogénosulphate ont également été observés. Avec cette conception en tripode, seule une étude à montré une sélectivité nettement supérieure pour les anions fluorure par rapport aux autres halogènes [98].

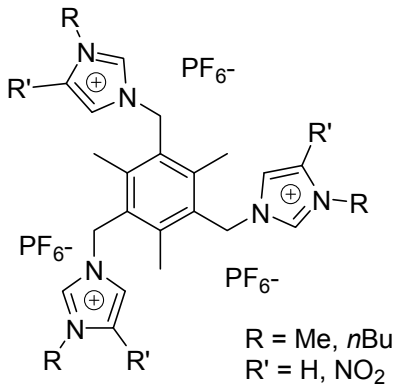


**Figure 1.19.** Récepteur anionique tripodal.

Les récepteurs basés sur des unités diimidazolium ou tétraimidazolium sont également connus [99, 100] mais les constantes d'association envers les halogènes, carboxylates et autres anions sont également relativement faibles. Un des premiers exemple de récepteur efficace et sélectif pour la complexation des anions fluorure est le calix[4]imidazolium[2]pyridine (Figure 1.20) rapporté par Kim *et al* [101]. Ce composé complexe les anions fluorure avec une constante d'association élevée de $3.10^5$ $M^{-1}$.

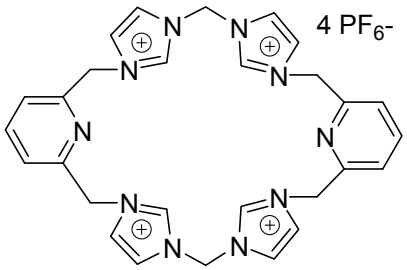


**Figure 1.20.** Récepteur Calix[4]imidazolium[2]pyridine.

D'autres anions ont également été liés sélectivement à des récepteurs basés sur des sels d'imidazolium : des récepteurs basés sur l'anthracène ont été récemment synthétisés pour complexer les ions pyrophosphate avec de fortes constantes d'association ($10^6$ $M^{-1}$) [102, 103]. Récemment, la synthèse d'un récepteur oxyanionique basé sur un calix[4]arène [104] a été rapportée (Figure 1.21). Ce système est particulièrement intéressant pour la conception d'assemblages supramoléculaires plus complexes, surtout au vu des propriétés des calixarènes.

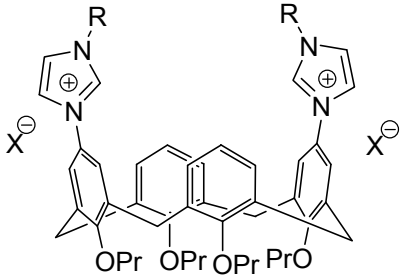


**Figure 1.21.** Récepteur *bis*(imidazolium)calix[4]arène

Dû à la présence de la charge positive du cycle imidazolium et des chaînes alkyles de différentes longueurs, il n'est pas inattendu que certains sels d'imidazolium soient capables de former des complexes d'inclusion en solution avec les macrocycles qui ont été présentés précédemment.

### 1.2.6 Complexes d'inclusion basés sur les sels d'imidazolium

Le cation imidazolium peut complexer les différents macrocycles connus en chimie supramoléculaire : une étude de complexation entre le cation imidazolium et des éther-couronnes par liaisons hydrogène a été faite [105] mais ce sont surtout les propriétés de complexation en solution aqueuse avec des cyclodextrines ou cucurbiturils qui ont été étudiées. Les interactions entre certains cations imidazolium et les macrocycles α-CD et β-CD ont été décrites [106]. Principalement, ce sont les sels *N,N'*-disubstitués de type 1-alkyl-3-méthylimidazolium (des composés ayant des propriétés de liquides ioniques) dont la complexation a été étudiée et l'effet du contre-ion sur la complexation a été largement débatue [107, 108, 109, 110, 111]. Les complexes entre ces liquides ioniques et les différentes cyclodextrines ont généralement de faibles constantes d'association et il est assez difficile de les caractériser.

Ces dernières années, ce sont surtout les complexes entre les liquides ioniques imidazolium et les macrocycles de type cucurbituril qui ont été étudiés. Il a été montré que certains liquides ioniques pouvaient augmenter significativement la solubilité du CB[6] dans l'eau [112] et l'effet de la longueur des chaînes alkyle est considérable sur les propriétés des complexes (Figure 1.22).

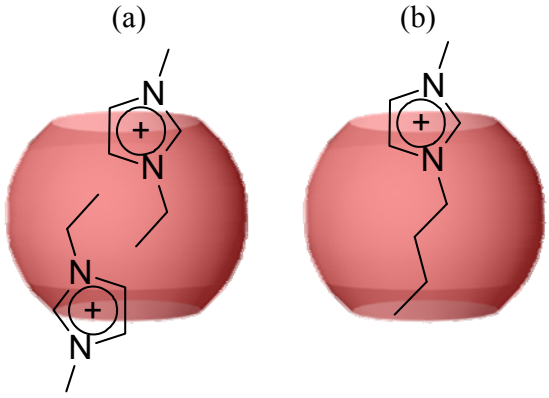


**Figure 1.22.** Complexes d'inclusion entre le CB[6] et des liquides ioniques imidazolium : (a) complexe 2:1 ; (b) complexe 1:1

En effet, un bromure de 1-éthyl-3-méthylimidazolium peut être complexé dans chacun des deux portails polaires du CB[6] alors que le bromure de 1-butyl-3-méthylimidazolium ne peut former que des complexes 1 :1 avec le CB[6]. Il y a donc principalement deux types d'interactions favorable dans ces complexes: (1) des interactions hydrophobes entre les chaînes alkyles et la cavité du CB[6]. (2) Des interactions de type ion-dipôle entre le cation imidazolium et le portail polaire des atomes d'oxygène du CB[6]. L'augmentation de la concentration de saturation en cucurbituril peut également être observe avec des cucurbiturils plus volumineux comme le CB[7] et le CB[8] : Par exemple, en utilisant du tétrafluoroborate de 1-butyl-3-méthylimidazolium, la concentration de saturation en macrocycle augmente d'un ordre de grandeur [113].

Une autre application des complexes d'inclusion avec le cucurbituril est l'inhibition des propriétés basiques du proton H(2) du cation imidazolium [114] (Figure 1.23). Cette inhibition est due aux liaisons hydrogène entre les protons H(2) des cations imidazolium et les atomes d'oxygène de la ceinture polaire du cucurbituril.

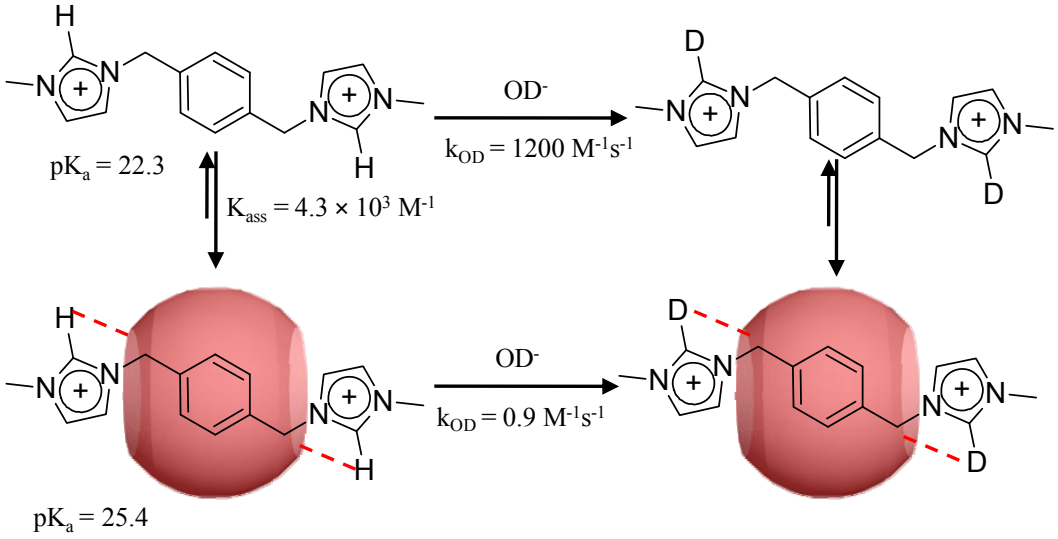


**Figure 1.23.** Complexe d'inclusion entre le CB[7] et le N,N'-diméthyl(1,4-xylylène)diimidazolium (Liaisons hydrogène entre H(2) et le CB).

Cette étude rapporte par la même occasion le premier sel de diimidazolium pouvant fortement complexer un macrocycle connu en chimie supramoléculaire, et a servi de point de départ important pour certains des travaux qui sont présentés dans cette thèse.

# 1.3 Description du projet de recherche

## 1.3.1 Objectif

L'objectif général des travaux de recherche présentés dans cette thèse a été d'étudier les propriétés supramoléculaires de sels de diimidazolium disubstitués en solution (aqueuse ou organique) ainsi qu'en phase solide ou crystal liquide. L'influence de l'espaceur entre les deux noyaux imidazolium ainsi que l'influence des substituants latéraux et des contre-ions a été étudiée (Figure 1.24). La recherche a été, dans la mesure du possible, orientée de façon à essayer de quantifier au meilleur de nos capacités les interactions supramoléculaires présentes dans les systèmes étudiés.

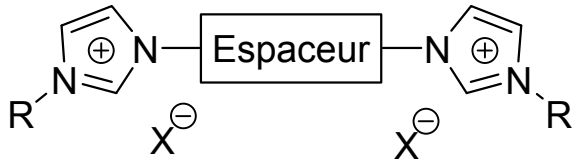


**Figure 1.24.** Schéma général des sels de diimidazolium étudiés.

L'idée initiale à l'origine du projet de recherche était la formation de pseudorotaxane à base de DB24C8 et de methylènediimidazolium disubstitué. Les deux cycles imidazolium peuvent interagir par empilement-π avec les deux cycles benzéniques riches en électrons de l'éther-couronne et les protons de l'imidazolium ainsi que ceux de l'espaceur méthylène pourraient former des liaisons hydrogène avec les oxygènes du DB24C8. À partir de ce concept, le projet sera ensuite élargi à différents macrocycles, différents conte ions, différents espaceurs et différentes chaînes latérales. Les études ont

dans un premier temps été menées en solution, pour ensuite s'étendre à la phase cristalline puis la formation de cristaux liquides.

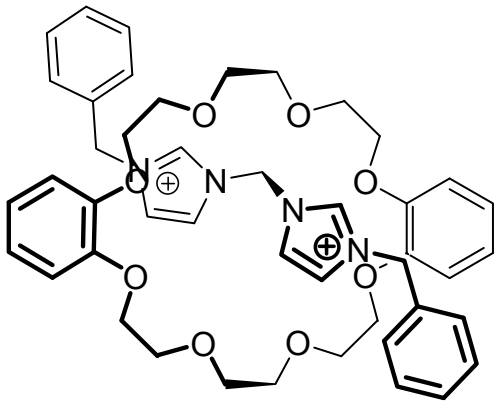

**Figure 1.25.** Pseudorotaxane à base de diimidazolium à l'origine du projet de recherche.

Les sels de diimidazolium ont été étudiés dans un premier temps par rapport à leurs propriétés de complexation par différents macrocycles connus en chimie supramoléculaire. Ces études ont été réalisées en solution aqueuse ou organique et comprennent plusieurs étapes à réaliser pour la caractérisation complète des espèces supramoléculaires formées. Dans un premier temps, il a fallu synthétiser les sels de diimidazolium et caractériser leur structure chimique. Des titrages et courbes de Job ont alors été réalisés par RMN $^{1}$H ou spectroscopie UV pour vérifier la formation des complexes. Nous avons ensuite caractérisé le mode de complexation pour comprendre la conformation adoptée par chacune des molécules lors de l'assemblage. Ceci a pu être réalisé par RMN $^{1}$H pour certains systèmes mais a nécessité une étude par RMN 2D NOESY ou ROESY. Dans les cas où un seul complexe était formé, le titrage a également permis de calculer la constante d'association du complexe. Dans d'autres cas rencontrés, plusieurs complexes ont été présents en solution et il a alors fallu estimer les paramètres de complexation par des méthodes informatiques.

Une étude de certains sels de diimidazolium a été faite en phase cristalline. Au vu de la directionnalité des trois atomes d'hydrogène présents sur chaque imidazolium, il a été possible de considérer les sels de diimidazolium comme des tectons moléculaires qui peuvent s'auto-assembler pour former un réseau cristallin. Dans ce cas, une étude par diffraction des rayons-X a été réalisée pour déterminer tous les paramètres des mailles cristallines.

Dans le cas d'un espaceur assez rigide et des chaînes latérales hydrophobes et linéaires, il a été également possible de former des cristaux liquides. Pour caractériser les mésophases, l'utilisation de la calorimétrie différentielle [115] à balayage fut importante. Elle nous a permis de déterminer avec précision les températures de transition de phase et de mesurer leur enthalpie. La stabilité des molécules utilisées a été vérifiée par analyse thermogravimétrique et une caractérisation complète des mésophases obtenues fut entreprise par microscopie optique polarisée [116] et par diffraction des rayons-X de poudre [117].

## 1.3.2 Systèmes étudiés

### 1.3.2.1 Motif méthylènediimidazolium et complexes binaires en solutions aqueuse et organique

Une première série de quatre sels de diimidazolium fut synthétisée et l'évaluation des propriétés de complexation de ces nouveaux composés avec les différents macrocycles connus dans la littérature fut entreprise. L'espaceur est ici un groupement méthylène, les contre-ions sont des bromures (étude en solution aqueuse) ou hexafluorophosphates (étude en solution organique polaire) et les substituants sont des benzyles ou phényles. Les propriétés de complexation ont été testées avec quatre différents macrocycles : le tétrapropoxycalix[4]arène (C[4]P) et le DB24C8 avec les sels d'hexafluorophosphate en solution organique ainsi que le CB[7] et la $\beta$-CD avec les bromures en solution aqueuse.

Cette première étude a donc consisté en la caractérisation de huit complexes supramoléculaires et est présentée dans le chapitre 2 de cette thèse.

#### 1.3.2.2 Motif méthylènediimidazolium et complexes ternaires en solutions aqueuse. Contrôle de l'assemblage supramoléculaire à l'interface air-eau

Cette partie de la thèse se concentre sur les complexes formés entre les bromures de diimidazolium étudiés précédemment et le quatre différents macrocycles solubles en solution aqueuse (trois types de cyclodextrines, $\alpha$-CD, $\beta$-CD et $\beta$-DIME ainsi que CB[7]). L'étude a été cette fois plus poussée et la formation de complexes ternaires a également été étudiée entre un sel de diimidazolium, une cyclodextrine et le CB[7]. En plus de l'étude de ces complexes en solution aqueuse, une étude des assemblages supramoléculaires formés à l'interface air/eau a également été réalisée. Ces résultats obtenus à la suite de nos résultats préliminaires sont présentés dans le chapitre 3.

#### 1.3.2.3 Motif phénylènediimidazolium : complexes multiples en solution aqueuse et estimation de leurs constantes d'association

Après avoir étudié la famille des composés méthylènediimidazolium disubstitués, il a pu être établi qu'existaient en solution aqueuse deux sites de complexation. Le site de complexation principal avec les cyclodextrines et le CB[7] était en fait le substituant externe avec les extrémités polaires des macrocycles qui complexaient un cation imidazolium. En rajoutant un deuxième macrocycle nous avons pu mettre en évidence un deuxième site de complexation au centre de la molécule. Pour inverser la priorité de ces sites, nous avons introduit un espaceur aromatique et des chaînes latérales alkyles (Figure 1.26)

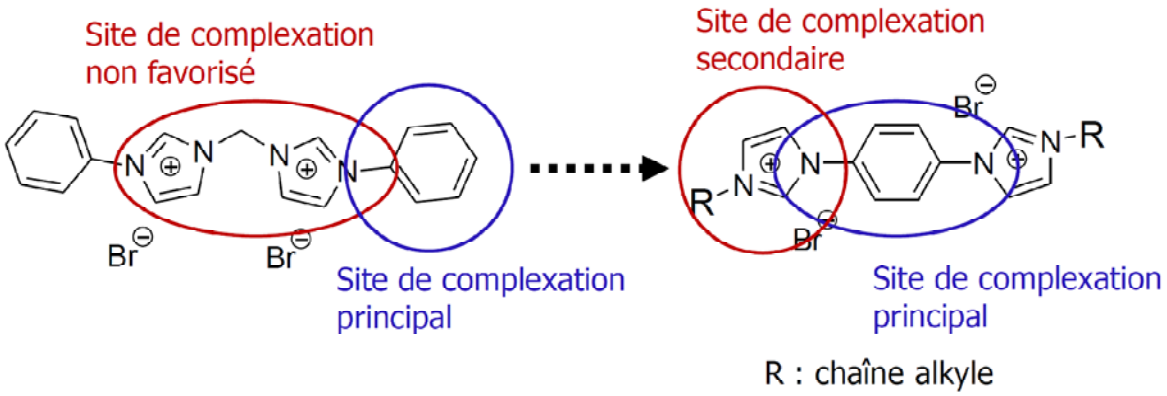


**Figure 1.26.** Sites de complexation (gauche) d'un méthylènediimidazolium et (droite) d'un phénylènediimidazolium.

La variation de la longueur des chaînes alkyles et l'étude des propriétés de complexation avec le **CB[7]** ont révélé la coexistence de plusieurs complexes en solution pour certains composés et c'est l'étude de ces complexes, ainsi que l'évaluation de leurs constantes d'association, qui est présentée dans le chapitre 4 de la thèse.

### 1.3.2.4 Cations diimidazolium diaromatiques : mise en évidence d'interactions supramoléculaires à l'état cristallin

Les études en solution des deux familles de composés diimidazolium présentées dans les premiers chapitres ont ensuite été complétées dans un premier temps par l'étude des interactions supramoléculaires en phase cristalline. Dans le chapitre 5, ce sont quatre structures cristallines de sels de diimidazolium qui sont présentées avec une étude systématique de l'organisation supramoléculaire dans les cristaux.

### 1.3.2.5 Formation de cristaux-liquides à base de sels de phénylènediimidazolium

En augmentant encore la longueur des chaînes alkyles des sels de phénylènediimidazolium étudiés au chapitre 5 et en modifiant la nature des contre-ions, des composés présentant des mésophases smectiques ont pu être obtenus. C'est à partir d'une

structure cristalline qu'il a été possible d'envisager la formation de cristaux liquides et c'est la caractérisation des mésophases obtenues pour quatre sels de diimidazolium qui est présentée dans le chapitre 6 de la thèse.

## 1.4 Références


1 J.-M. Lehn, *Supramolecular Chemistry: Concepts and Perspectives*, **1995**, VCH, Wieinheim.

2 P. Beer, P. Gale, D. Smith, *Supramolecular Chemistry*, **1998**, Oxford Chemistry Primers, England.

3 J. W. Steed, J. L. Atwood, *Supramolecular Chemistry*, **2000**, John Wiley & Sons.

4 C. J. Pedersen, *Angew. Chem.* **1988**, *100*, 1053-1059.

5 J.-M. Lehn, *Angew. Chem.* **1988**, *100*, 91-116.

6 D. J. Cram, *Angew. Chem.* **1988**, *100*, 1041-1052.

7 H. M. Powell, *ibid*. **1948**, 61-73.

8 H. Kunz, *Angew. Chem. Int. Ed.* **2002**, *41*, 4439-4451.

9 K. A. Connors, *Binding Constants*, **1987**, John Wiley & Sons: Chichester.

10 P. W. N. M. van Leeuwen, *Supramolecular catalysis*, **2008**, Wiley-VCH, Wieinheim.

11 J.-M. Lehn, *Pharm. Acta Helv.* **1995**, *69*, 205-11.

12 M. C. F. Fyfe, J. F. Stoddart *Acc. Chem. Res.* **1997**, *30*, 393-401.

13 M. Albrecht, *Chem. Soc. Rev.* **1998**, *27*, 281-288.

14 J.-M. Lehn, *Chem. Eur. J.* **2000**, *6*, 2097-2102.

15 J.-M. Lehn, *PNAS* **2002**, *99*, 4763-4768.

16 F. M. Menger, *PNAS* **2002**, *99*, 4818-4822.

17 L. Styyer, *Biochemistry*, **1995**, W. H. Freeman and Co, New York.

18 G. A. Jeffrey, *An introduction to hydrogen bonding,* **1997**, Oxford University Press, Oxford.

19 C. A. Hunter, J. K. M. Sanders, *J. Am. Chem. Soc.* **1990**, *112*, 5525-5534.

20 A. Bondi *J. Phys. Chem.***1964**, *68*, 441-451.

21 D. B. Smithrud, E. M. Sanford, I. Chao, S. B. Ferguson, D. R. Carcanague, J. D. Evanseck, K. N. Houk, F. Diederich, *Pure & Appl. Chem.* **1990**, *62*, 2227-2236.

22 M. C. Jimenez, C. Dietrich-Buchecker, J.-P. Sauvage, *Angew. Chem. Int. Ed.* **2000**, *39*, 3284-3287.

23 J. P. Collin, C. Dietrich-Buchecker, P. Gavina, M. C. Jimenez-Molero, J.-P. Sauvage, *Acc. Chem. Res.* **2001**, *34*, 477-487.

24 P. R. Ashton, R. Ballardini, V. Balzani, I. Baxter, A. Credi, M. C. T. Fyfe, M. T. Gandolfi, M. Gómez-López, M. V. Martínez-Díaz, A. Piersanti, N. Spencer, J. F. Stoddart, M. Venturi, A. J. P. White, D. J. Williams, *J. Am. Chem. Soc.* **1998**, *120*, 11932-11942.

25 P. R. Ashton, R. Ballardini, V. Balzani, I. Baxter, A. Credi, K. R. Dress, E. Ishow, C. J. Kleverlaan, O. Kocian, J. A. Preece, N. Spencer, J. F. Stoddart, M. Venturi, M. Wenger, *Chem. Eur. J.* **2000**, *6*, 3558.

26 E. Ishow, A. Credi, V. Balzani, F. Spadola, L. Mandolini, *Chem. Eur. J.* **1999,** *5*, 984-989.

27 J. D. Badjic, V. Balzani, A. Credi, S. Silvi, J. F. Stoddart, *Science,* **2004**, *303*, 1845-1849.

28 Y. Liu, A. H. Flood, P. A. Bonvallet, S. A. Vignon, B. H. Northrop, H.-R. Tseng, J. O. Jeppesen, T. J. Huang, B. Brough, M. Baller, S. Magonov, S. D. Solares, W. A. Goddard, C.-M. Ho, J. F. Stoddart, *J. Am. Chem. Soc*. **2005**, *127*, 9745-9759.

29 G. W. Gokel, *Crown Ethers*, *Royal Society of Chemistry*, **1990**.

30 C. J. Pedersen, *J. Am. Chem. Soc.* **1967**, *89*, 2495-2496.

31 T. B. Stolwijk, L. C. Vos, E. J. R. Sudhölter, D. N. Reinhoudt, *Recl. Trav. Chim. Pays Bas,* **1989**, *108*, 103-108.

32 C. M. Starks, C. L. Liotta, M. Halpern, *Phase-transfer catalysis, Fundamentals, applications and industrial perspectives*, **1994**, Chapman & Hall Inc.

33 C. D. Gutsche, *Calixarenes*, *Royal Society of Chemistry*, **1989**.

34 C. D. Gutsche, *Calixarenes 2, Royal Society of Chemistry*, **1997**.

35 L. J. Bauer, C. D. Gutsche, *J. Am. Chem. Soc.* **1985**, *107*, 6063-6069.

36 S. Kanamathareddy, C. D. Gutsche, *J. Org. Chem.* **1995**, *60*, 6070-6075.

37 E. Bilensoy, *Cyclodextrins in Pharmaceutics, Cosmetics, and Biomedicine: Current and Future Industrial Applications*, **2010**, John Wiley & Sons.

38 J. Szejtli, *Chem. Rev.* **1998**, 98, 1743-1754.

39 W. J. Shieh, A. R. Hedges, *J. Macromol. Science, Pure Appl. Chem.* **1996**, *33*, 673-683.

40 Figure tirée de J. Lagona, P. Mukhopadhyay, S. Chakrabarti, L. Isaacs, *Angew. Chem. Int. Ed.* **2005**, *44*, 4844-4870.

41 J. M. Lehn, *Science*, **2002**, *295*, 2400-2403.

42 D. J. Cram, *Angew. Chem. Int. Ed.* **1986**, *25*, 1039-1057.

43 F. M. Raymo, J. F. Stoddart, *Pure & Appl. Chem.* **1997**, *69*, 1987-1997.

44 G. Schill, H. Justus, *Liebigs Annalen der Chemie*, **1969**, *721*, 53-74.

45 S. J. Langford, L. Perez-Garcia, J. F. Stoddart, *Supramolecular* Chemistry, **1995**, *6*, 11-27.

46 A. Rescifina, C. Zagni, D. Iannazzo, P. Merino, *Curr. Org. Chem.* **2009**, *13*, 448-481.

47 P. R. Ashton, P. J. Campbell, P. T. Glink, D. Philp, N. Spencer, J. F. Stoddart, E. J. T. Chrystal, S. Menzer, D. J. Williams, P. A. Tasker*, Angew. Chem. Int. Ed.* **1995**, 34, 1865-1869.

48 S. J. Loeb, J. A. Wisner, *Chem. Commun.* **1998**, 2757-2758.

49 F. M. Raymo, K. N. Houk, J. F. Stoddart, *J. Am. Chem. Soc.* **1998**, 120, 9318-9322.

50 B. W. Matthews, P. B. Siegler, R. Hederson, D. M. Blow, *Nature* **1967**, *214*, 652-656.

51 M. K. Campbell, S. O. Farrell, *Biochemistry, Sixth Edition*, **2009**, Thomson.

52 R. Breslow, *Pure & Appl. Chem.* **1990**, *62*, 1859-1866.

53 J. Dupont, C. S. Consorti, P. A. Z. Suarez, R. F. de Souza, *Organic Syntheses* **2002**, 79-79.

54 E. P. Serjeant, B. Dempsey, *Ionization Constants of Organic Acids in Aqueous Solution*, **1979**, Pergamon, Oxford.

55 G. Bertrand, *Carbene chemistry: from fleeting intermediates to powerful reagents*, **2002**, Marcel Dekker.

56 B. Kirchner, *Topics in Current Chemistry vol 290, Ionic Liquids*, **2009**, Springer-Verlkag, Berlin.

57 C. Chiappe, D. Pieraccini, *J. Phys. Org. Chem.* **2005**, *18*, 275-297.

58 J. D. Holbrey, W. M. Reichert, R. P. Swatloski, G. A. Broker, W. R. Pitner, K. R. Seddon, R. D. Rogers, *Green Chem.* **2002**, *4*, 407-413.

59 C. C. Cassol, G. Ebeling, B. Ferrera, J. Dupont*, Adv. Synth. Catal.* **2006**, *348*, 243-248.

60 N. Noujeim, L. Leclercq, A. R. Schmitzer, *Curr. Org. Chem.* **2010**, *14*, 1500-1516.

61 J. Dupont, *J. Braz. Chem. Soc.* **2004**, *15*, 341-350.

62 L. Leclercq, A. R. Schmitzer, *Supramol. Chem.* **2009**, *21*, 245-263.

63 H. Weingartner, *Angew. Chem. Int. Ed.* **2008**, 654-670.

64 J. Dupont, P. A. Suarez, *Phys. Chem. Chem. Phys.* **2006**, *8*, 2441-2452.

65 H. Zhang, H. Liang, J. Wang, K. Li, *Z. Phys. Chem.* **2007**, *221*, 1061-1074.

66 J. Bowers, C. P. Butts, P. J. Martin, M. C. Vergara-Gutierrez, R. K. Heenan, *Langmuir* **2004**, *20*, 2191-2198.

67 S. Dorbritz, W. Ruth, U. Kragl, *Adv. Synth. Catal.* **2005**, *347*, 1273-1279.

68 I. B. Malham, P. Letellier, M. Turmine, *J. Phys. Chem. B* **2006**, *110*, 14212-14222.

69 H. Katayanagi, K. Nishikawa, H. Shimozaki, K. Miki, P. Westh, Y. Koga, *J. Phys. Chem. B* **2004**, *108*, 19451-19457.

70 C. S. Consorti, P. A. Z. Suarez, R. F. S. de Souza, R. A. Burrow, D. H. Farrar, A. J. Lough, W. Loh, L. H. M. da Silva, J. Dupont, *J. Phys. Chem. B* **2005**, *109*, 4341-4349.

71 G. R. Desiraju, *Crystal Engineering: the design of organic solids*, **1989**, Elsevier: Amsterdam.

72 R. Tilley, *Crystals and Crystal Structure*, **2006**, John Wiley, Chichester.

73 C. J. Dymek Jr, D. A. Grossie, A. V. Fratini, W. W. Adams, *J. Molec. Struct.* **1989**, *213*, 25-34.

74 A. Elaiwi, P. B. Hitchcock, K. R. Seddon, N. Srinivasan, Y. M. Tan, T. Welton, J. A. Zora, *J. Chem. Soc. Dalton Trans.* **1995**, *5*, 3467-3472.

75 J. Fuller, R. T. Carlin, H. C. Delong, D. Haworth, *J. Chem. Soc. Chem. Commun.* **1994**, 299-300.

76 F. M. Reinitzer, *Chemistry* **1988**, 9, 421-441.

77 O. Lehmann, *J. Phys. Chem.* **1989,** 4, 462-468.

78 W. L. McMillan, *Phys. Rev. A* **1973**, 8, 1921-1929.

79 R. B. Meyer, W. L. McMillan, *Phys. Rev. A* **1974**, 9, 899-906.

80 S. Singh, *Liquid Crystals Fundamentals*, **2002**, World Scientific.

81 C. K. Lee, H. W. Huang, I. J. B. Lin, *Chem. Commun.*, **2000**, 1911-1912.

82 M. Tosoni, S. Laschat, A. Baro, *Helv. Chim. Acta* **2004**, *87*, 2742-2749.

83 Y. R. Zhao, X. Chen, X. D. Wang, *J. Phys. Chem. B* **2009**, *113*, 2024-2030.

84 M. Yoshio, T. Mukai, K. Kanie, M. Yoshizawa, H. Ohno, T. Kato, *Chem. Lett.* **2002**, 320-321.

85 S. Yazaki, Y. Kamikawa, M. Yoshio, A. Hamasaki, T. Mukai, H. Ohno, T. Kato, *Chem. Lett.* **2008**, *38*, 538-539.

86 K. Hoshino, M. Yoshio, T. Mukai, K. Kishimoto, H. Ohno, T. Kato, *J. Polym. Sci. Part A*, **2003**, *41*, 3486-3492.

87 M. Yoshio, T. Mukai, H. Ohno, T. Kato, *J. Am. Chem. Soc.* **2004**, *126*, 994-995.

88 Y. Sanami, M. Funahashi, T. Kato, *J. Am. Chem. Soc.* **2008**, *130*, 13206-13207.

89 X. Cheng, X. bai, S. Jing, H. Ebert, M. Prehm, C. Tschierske, *Chem. Eur. J.* **2010**, *16*, 4588-4601.

90 K. Binnemans, *Chem. Rev.* **2005,** *105*, 4148-4204

91 S. S. Kolesnikov, A. L. Lyubarskii, E. E. Fesenko, *Vision Res.* **1984**, *24*, 1295-1300.

92 J.-M. Lehn, *Supramolecular Chemistry*, **1995**, *chapter 5*, 55-68, Wiley-VCH, Weinheim.

93 E. Alcalde, C. Alvarez-Rua, S. Garcia-Granda, E. Garcia-Rodriguez, N. Mesquida, L. Pérez-Garcia, *Chem. Commun.* **1999**, 295-296.

94 E. Alcalde, S. Ramos, L. Pérez-Garcia, *Org. Lett.* **1999**, *1*, 1035-1038.

95 K. Sato, S. Arai, T. Yamagishi, T. *Tetrahedron Lett.* **1999**, *40*, 5219-5222.

96 H. Ihm, S. Yun, H. G. Kim, J. K. Kim, K. S. Kim, *Org. Lett.* **2002**, *4*, 2897-2900.

97 J.–L. Thomas, J. Howarth, K. Hanlon, D. McGuirk, *Tetrahedron Lett.* **2000**, *41*, 413-416.

98 S. Yun, H. Ihm, H. G. Kim, C.-W. Lee, B. Indrajit, K. S. Oh, Y. J. Gong, J. Lee, J. Yoon, H. C. Lee, K. S. Kim, *J. Org. Chem.* **2003**, *68*, 2467-2470

99 H. Kim, J. Kang, *Tetrahedron Lett.* **2005**, *46*, 5443-5445.

100 S. In, J. Kang, *J. Incl. Phenom. Macrocycl. Chem.* **2006**, *54*, 129-132.

101 K. Chellappan, N. J. Singh, I.-C. Hwang, J. W. Lee, K. S. Kim, *Angew. Chem. Int. Ed.* **2005**, *44*, 2899-2903.

102 Z. Xu, S. Kim, K.-H. Lee, J. Yoon, *Tetrahedron Lett.* **2007**, *48*, 3797-3800.

103 N. J. Singh, E. J. Jun, K. Chellappan, D. Thangadurai, R. P. Chandran, I.-C. Hwang, J. Yoon, K. S. Kim, *Org. Lett.* **2007**, *9*, 485-488.

104 I. Dinares, C. Garcia de Miguel, N. Mesquida, E. Alcalde, *J. Org. Chem.* **2009**, *74*, 482-485.

105 J.-M. Lehn, P. Vierling, R. C. Hayward, *J. Chem. Soc., Chem. Commun.* **1979**, 296–298.

106 Y. A. Gao, Z. H. Li, J.-M. Du, B. X. Han, G. Z. Li, W. G. Hou, D. Shen, L. Q. Zheng, G. Y. Zhang, *Chem. Eur. J.* **2005**, *11,* 5875-5880.

107 Y. Gao, X. Zhao, B. Dong, L. Zheng, S. Zhang, *J. Phys. Chem. B* **2006**, *110*, 8576-8581.

108 N. Li, J. Liu, X. Zhao, Y. Gao, L. Zheng, J. Zhang, L. Yu, *Colloids Surf. A* **2007**, *292,* 196-201.

109 Y. François, A. Varenne, J. Siriex-Plenet, P. Gareil, *J. Sep. Sci.* **2007**, *30*, 751-760.

110 Y. He, X. Shen, *J. Photochem. Photobiol. A: Chem.* **2008**, 253-259.

111 Y. He, X. Shen, H. Gao, Y. He, *J. Photochem. Photobiol. A: Chem.* **2008**, *193,* 178-186.

112 L. Liu, N. Zhao, O. A. Scherman, *Chem. Commun.* **2008**, 1070-1072.

113 P. Montes-Navajas, A. Corma, H. Garcia, *J. Mol. Catal. A* **2008**, *279*, 165-169.

114 R. Wang, L. Yuan, D. H. Macartney, *Chem. Comm.* **2006**, 2908-2910.

115 J. A. Dean, *The Analytical Chemistry Handbook*, **1995**, McGraw Hill Inc. New York.

116 I. Dierking, *Textures of Liquid Crystals*, **2003**, Wiley-VCH, Weinhiem.

117 P. Collings, M. Hird, *Introduction to Liquid Crystals*, **1997**, Taylor and Francis, New York.

# Chapitre 2 : Motif méthylènediimidazolium et complexes binaires en solutions aqueuse et organique

# 2.0 Préface

Avant d'entreprendre ces travaux, les connaissances sur les proprieties supramoléculaires des sels de diimidazolium étaient limitées. Quelques publications rapportaient notamment les propriétés de récepteurs anioniques des sels de méthylènediimidazolium, mais la grande majorité de l'utilisation de ce type de composés était jusque là consacrée à la synthèse de carbènes *N*-hétérocycliques pour la formation de catalyseurs de réactions de couplage croisé. Une étude des propriétés de complexation de ces sels de diimidazolium avec les macrocycles les plus communs en chimie supramoléculaire était donc appropriée. Ces travaux publiés en 2008 nous ont permis de développer et de comprendre le mode de complexation de ce nouveau motif.

Ma contribution à cet article présenté au chapitre 2 a été la synthèse de tous les composés décrits ainsi que toutes les études de RMN $^{1}H$ pour les complexes supramoléculaires. J'ai également rédigé la grande majorité de l'article. La contribution de Dr Loïc Leclercq a été la réalisation et l'interprétation des spectres RMN NOESY.

Les informations expérimentales supplémentaires de cette partie se trouvent aux pages 183-199 de la thèse.

# Article 1. *N,N'*-disubstituted methylenediimidazolium salts: a versatile guest for various macrocycles

Nadim Noujeim, Loïc Leclercq and Andreea R. Schmitzer*

Département de chimie, Université de Montréal, CP 6128, Succursale Centre-Ville, Montréal, Québec, H3C 3J7, Canada

*Journal of Organic Chemistry,* **2008**, *73*, 3784-3790

## 2.1 Abstract

*N*,*N'*-Disubstituted methylenediimidazolium salts allow the formation of flexible inclusion complexes with *β*-cyclodextrin, cucurbit[7]uril, tetrapropoxycalix[4]arene, and dibenzo-24-crown-8 ether. Due to the salt nature of the imidazolium guest, the counterion largely determines its solubility in a given solvent. Moreover, by the judicious choice of the imidazolium substituents, inclusion complexes of guest salts were obtained with a variety of macrocyclic hosts, and the binding parameters of the inclusion were determined for each complex.

## 2.2 Introduction

One of the vital current tasks in supramolecular chemistry is to develop simple yet comprehensive and reliable methods to effectively hold together separate parts of complex architectures, exclusively through cooperative noncovalent interactions. For this purpose, it is beneficial to have a set of simple guest molecules which function as a molecular glue to bind a macrocycle as one complex architecture. It becomes more difficult to find an appropriate guest molecule capable of binding different host molecules with contrasting physicochemical properties and guest selectivities. Interactions such as hydrogen bonding, $\pi$-stacking, cation-$\pi$, charge transfer interactions, and electrostatic interactions play an important role in various templates, recognition, and complexation phenomena in supramolecular chemistry and in biological processes. [1] As an effective structural unit at the active sites of various proteins and nucleic acids, imidazole plays a key role in their biological function, in its nonprotonated or protonated form. The imidazolium cation has similar properties to the pyridinium cation such as holding a positive charge and possessing ionic liquid properties. It has also been exploited in the design of imidazolium- based hosts, but the methylenediimidazolium motif is absent from the literature. [2]

A literature survey helped us to identify *N*,*N'*-disubstituted methylenediimidazolium salts as valuable recognition motifs for the assembly of novel architectures with tunable physicochemical properties, in analogy with the imidazolium cation. To move closer to an understanding of molecular recognition in these systems, we have synthesized and studied the binding properties of host-guest complexes of new *N*,*N'*-disubstituted diimidazolium guests and a large diversity of macrocyclic hosts, including cyclodextrins, calixarenes, cucurbituril, and crown ethers. We have identified patterns in the binding constants of these diimidazolium salts, and we have established the interactions that are developed in each system.

Cyclodextrins (**CDs**) are water-soluble hosts that contain a hydrophobic cavity and can accommodate a variety of small organic molecules (Figure 2.1). [3] $\alpha$-Cyclodextrin is composed of six glucose residues, while $\beta$-cyclodextrin has seven and $\gamma$-cyclodextrin has eight. This means that each type of cyclodextrin provides a cavity with slightly different geometric properties and a preference for particular-sized molecules. Cyclodextrins have been reported in the literature to form inclusion complexes with imidazole, but there are no examples of complexation of imidazolium cations in the presence of these hosts.

Another synthetic host able to form host-guest complexes in water is cucurbituril (**CB**). [4] **CBs** are cyclic oligomers consisting of glycoluril repeat units. **CBs** recognize positively charged molecules such as dipyridinium, ammonium, imidazolium, dialkylimidazolium, and bis(imidazolium) cations. [5] Calixarenes have a typical cone structure that allows them to sequester a variety of hydrophobic molecules and ions, making them useful to form host-guest complexes. [6] As in the case of **CDs**, there are no examples of imidazolium cations complexed by this type of hosts. Crown ethers have the ability to strongly solvate cationic compounds. [7] It is already known that the imidazolium cation can form inclusion complexes with large crown-ether-type hosts via H-bonding. [8] New motifs for the complexation of linear cations through crown ethers are being reported regularly; recently, other types of linear cations, like *N*-benzylanilinium [9] and *bis*(benzimidazolium)ethane [10] cations, were shown to bind to dibenzo-24-crown-8 ether

with approximately the same range of association constants ($10^3$ $M^{-1}$ in acetonitrile at 25 °C) as 1,2-*bis*(pyridinium)ethane and dibenzylammonium cations. [11]

In this paper, we describe a flexible toolkit for host-guest chemistry based on the inclusion complexes of *N*,*N'*-disubstituted diimidazolium salts with various macrocycles (*β*-cyclodextrin, cucurbit[7]uril, tetrapropyloxycalix[4]arene, and dibenzo-24-crown-8 ether) (Figure 2.2). In fact, by the judicious choice of the counterion and the substituent, the solubility of the guest and the association parameters can be changed. For each complex, the stoichiometry, the association constant, and the complex geometries are discussed on the basis of 1D and 2D NMR data, mass spectrometry (MS), and molecular modeling studies.

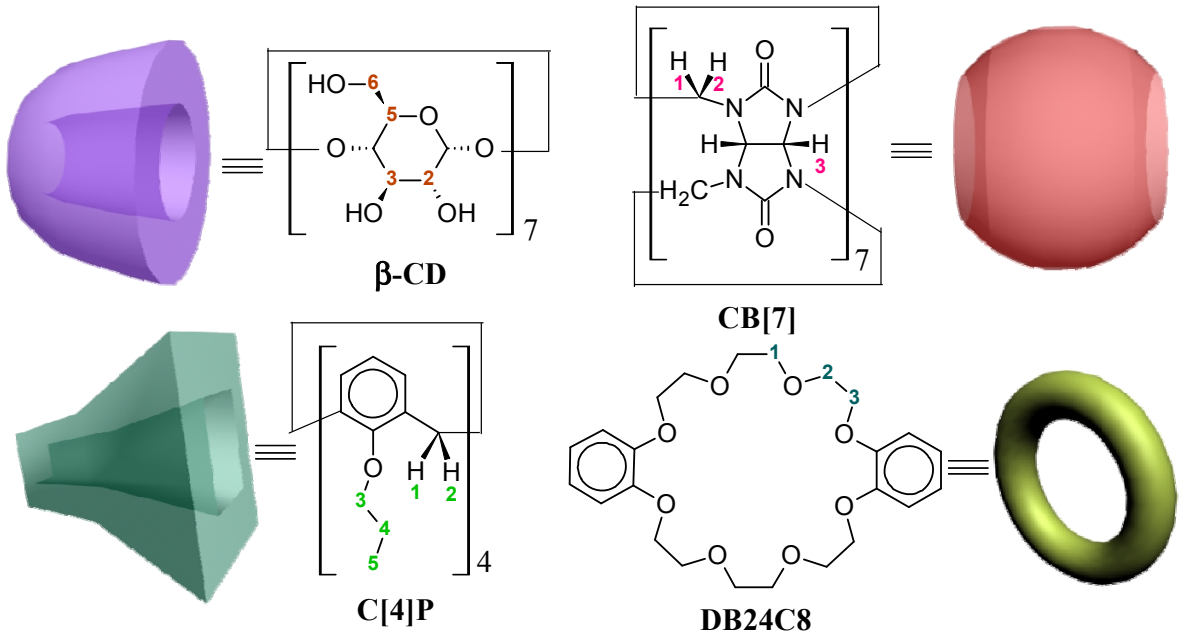


**Figure 2.1.** Structure and schematic representation of different macrocycles used in this work.

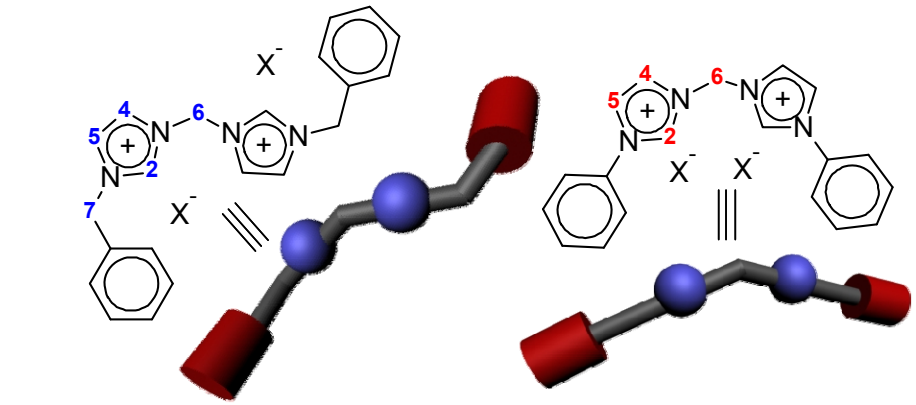


$X^-$ = Br$^-$: **[1][Br]$_2$** PF$_6^-$: **[1][PF$_6$]$_2$** Br$^-$: **[2][Br]$_2$** PF$_6^-$: **[2][PF$_6$]$_2$**

**Figure 2.2.** Diimidazolium salts and their schematic representation (blue: polar groups and red: apolar group).

## 2.3 Results and Discussion

Cucurbit[7]uril (**CB[7]**) and *β*-cyclodextrin (***β*-CD)** hosts are only soluble in water. Herein, we used dibromide diimidazolium salts for the recognition of **CB[7]** and ***β*-CD** in $D_2O$. Tetrapropyloxycalix[4]arene (**C[4]P**) and dibenzo-24-crown-8 ether (**DB24C8**) are soluble in various organic solvents. Complexation studies were performed in pure $CD_3CN$ for hexafluorophosphate cations with **DB24C8** and in a mixture of $CDCl_3/CD_3CN$ (80/20 V/V) for **C[4]P**. The methylenediimidazolium cations can provide enough noncovalent interactions to bind all the macrocycles described above, and strong association was observed in the majority of the cases. The complexation of different substituted methylenediimidazolium salts with the different hosts is described in the following sections.

The *N,N'*-disubstituted diimidazolium salts were obtained by a double $S_N2$ reaction involving *N*-substituted imidazoles and dibromomethane [12], followed by ion exchange with a hexafluorophosphate counterion (Scheme 2.1).

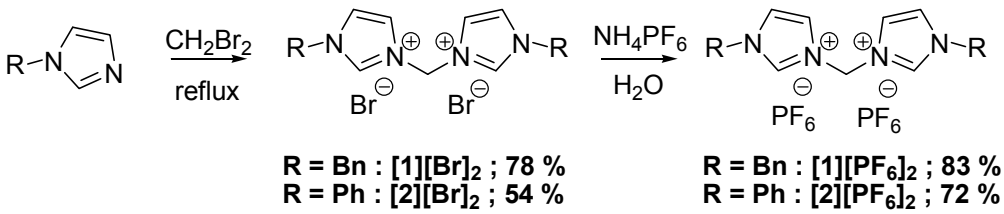


**R = Bn : [1][Br]$_2$ ; 78 %**
**R = Ph : [2][Br]$_2$ ; 54 %**

**R = Bn : [1][PF$_6$]$_2$ ; 83 %**
**R = Ph : [2][PF$_6$]$_2$ ; 72 %**

**Scheme 2.1.** Synthesis of the *N,N'*-disubstituted methylenediimidazolium compounds.

## 2.3.1 Methylenediimidazolium cation/cyclodextrin complexes

The H2 proton for both **[1][Br]$_2$** and **[2][Br]$_2$** was not observed in $D_2O$ because of deuterium exchange. In the presence of the **β-CD,** the chemical shifts of all the other protons of the diimidazolium cations were modified (Figure 2.3a, 2.3b, 2.4a and 2.4b). This is evidence for the formation of a 'host-guest' complex.[13] This feature, which is related to the geometry of the complex, is generally caused by a combination of contributions from H-bonds (expressed as a downfield) and aromatic shielding (expressed as an upfield). In the case of **[1][Br]$_2$•β-CD** and **[2][Br]$_2$•β-CD** complexes, the $H_4/H_5$ protons on the imidazolium moiety as well as $H_6$, are shifted downfield, which, in this case, is indicative of H-bonds and a more hydrophobic environment, consistent with the proximity of the **β-CD's** cavity. For these complexes, the aromatic protons of phenyl or benzyl groups are also shifted downfield. The chemical shifts of the imidazolium protons and the split of the aromatic protons of **[1][Br]$_2$** and **[2][Br]$_2$** demonstrate the formation of inclusion complexes [13]. In addition to 1D NMR experiments, mass spectrometry was used to demonstrate the formation of the inclusion complexes. Electrospray ionization (ESI) is used to "fish" loosely bonded supramolecular complexes in solution and transfer them to a mass spectrometer to investigate their assemblies. The positive ions are formed in solution and then transferred by ESI directly to the gas phase. ESI is characterized by the gentleness by which the gaseous ions are formed, and loosely bonded supramolecules can be observed, such as hydrogen-bonded amino-acid assemblies [14]. The ESI mass spectra, in the positive

ion mode, of equimolar solutions of ***β*-CD**/**[1][Br]$_2$** or **[2][Br]$_2$** give m/z peaks at 1545.1 that corresponds to (**[1][Br]•*β*-CD**)$^+$ and at 1517.0 that corresponds to (**[2][Br]•*β*-CD**)$^+$.

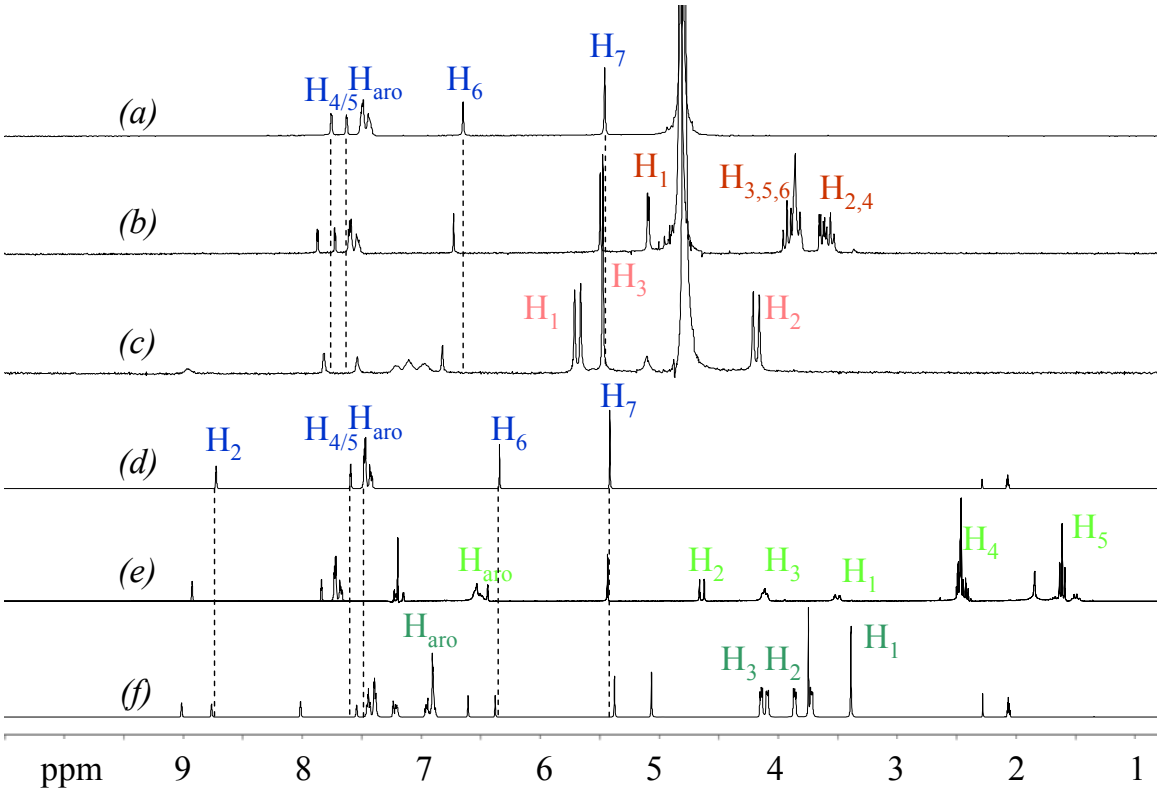


**Figure 2.3.** $^1$H NMR spectra at 25°C of: *(a)* 4 mM **[1][Br]$_2$** ($D_2O$); *(b)* 4 mM **[1][Br]$_2$** and 4 mM ***β*-CD** ($D_2O$); *(c)* 4 mM **[1][Br]$_2$** and 4 mM **CB[7]** ($D_2O$); *(d)* 25 mM **[1][PF$_6$]$_2$** ($CD_3CN$); *(e)* 25 mM **[1][PF$_6$]$_2$** and 25 mM **C[4]P** ($CDCl_3$/$CD_3CN$ (80/20 V/V)); *(f)* 25 mM **[1][PF$_6$]$_2$** and 25 mM **DB24C8** ($CD_3CN$).

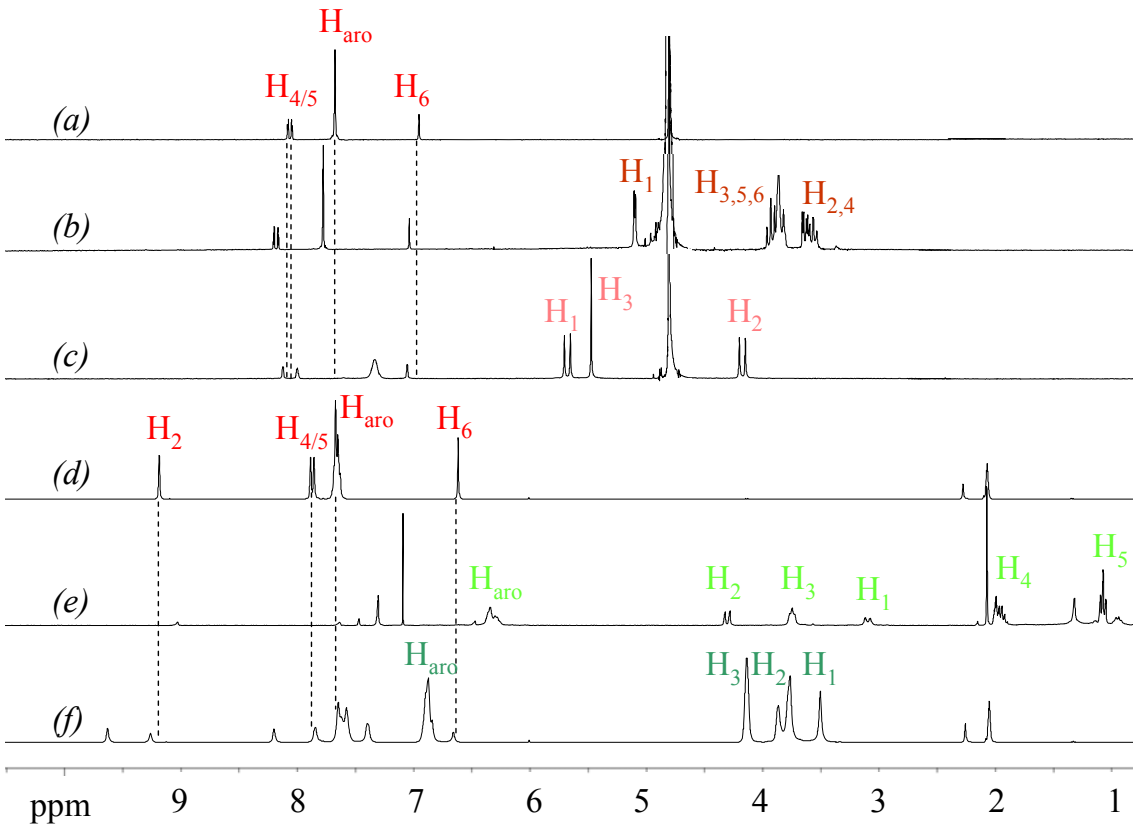


**Figure 2.4.** $^{1}$H NMR spectra at 25°C of: *(a)* 4 mM **[2][Br]$_2$** ($D_2O$); *(b)* 4 mM **[2][Br]$_2$** and 4 mM ***β*-CD** ($D_2O$); *(c)* 4 mM **[2][Br]$_2$** and 4 mM **CB[7]** ($D_2O$); *(d)* 25 mM **[2][PF$_6$]$_2$** ($CD_3CN$); *(e)* 25 mM **[2][PF$_6$]$_2$** and 25 mM **C[4]P** ($CDCl_3$/$CD_3CN$ (80/20 V/V)); *(f)* 25 mM **[2][PF$_6$]$_2$** and 25 mM **DB24C8** ($CD_3CN$).

To gain insight into the molecular interactions and the geometry of the host-guest complex, we performed a 2D NMR study in addition to the 1D NMR data presented above. NOESY experiments are well suited for the purpose; even though the COSY peaks are intense at the concentrations used, it is possible to assign the NOE signals between the diimidazolium salts and the macrocycles. The spatial distance must be less than 5Å to observe a cross peak between two protons. The NOESY spectrum of an equimolar mixture of ***β*-CD** with **[1][Br]$_2$** or with **[2][Br]$_2$** in $D_2O$ gave intense cross peaks between the

aromatic protons of phenyl or benzyl groups and the internal $H_3$ and $H_5$ protons of the **CD** (Figure 2.5a and 2.6a). These cross peaks are evidence for the formation of inclusion complexes between the **β-CD** and **[1][Br]$_2$** or **[2][Br]** in aqueous solution. Moreover, the absence of cross peaks between the hydrogens of the **β-CD** and the hydrogens located on the imidazolium residue ($H_{4/5}$) clearly shows that the interaction between the **β-CD** and the imidazolium cation occurs with the aromatic substituent of the diimidazolium cation. As both imidazolium salts contain aromatic groups at the extremities, the binding interactions seem to be dominated by the hydrophobic forces.

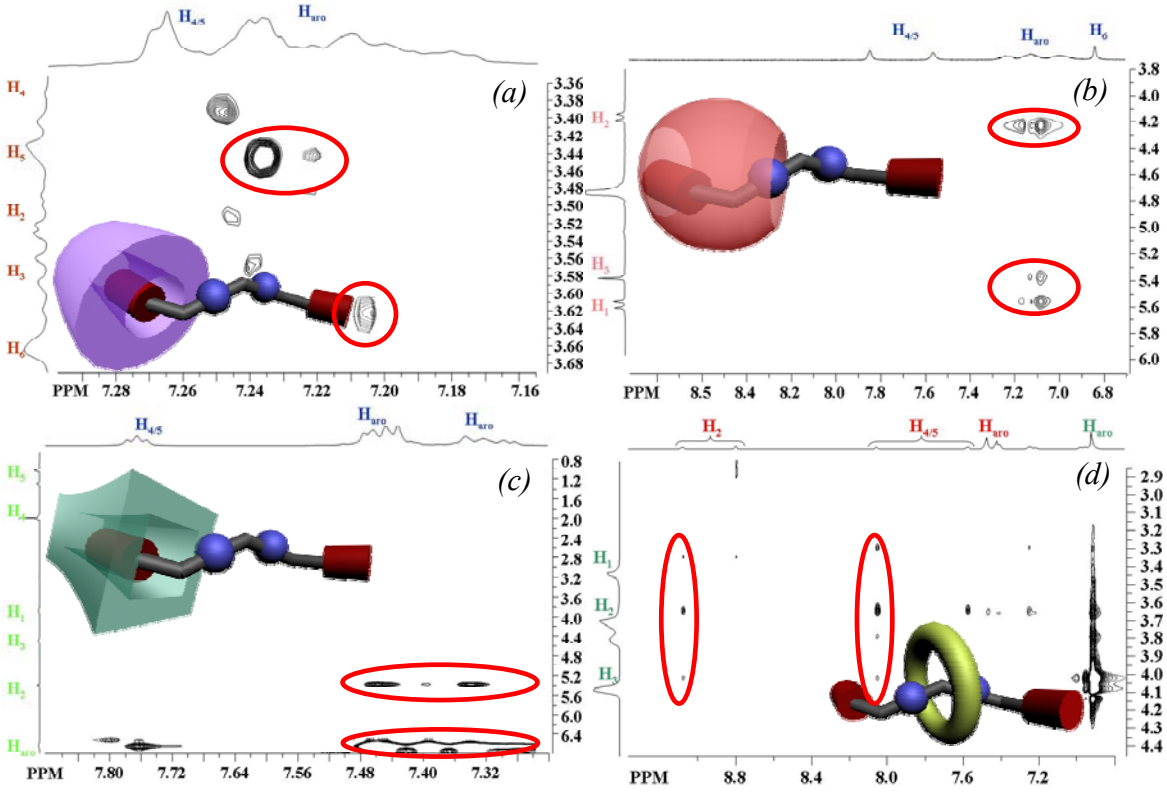


**Figure 2.5.** Partial NOESY NMR spectra at 25°C of: *(a)* 5 mM **[1][Br]$_2$** and 5 mM **β-CD** ($D_2O$); *(b)* 4 mM **[1][Br]$_2$** and 4 mM **CB[7]** ($D_2O$); *(c)* 10 mM **[1][PF$_6$]$_2$** and 10 mM **C[4]P** ($CDCl_3$/$CD_3CN$ (80/20 V/V)); *(d)* 10 mM **[1][PF$_6$]$_2$** and 10 mM **DB24C8** ($CD_3CN$).

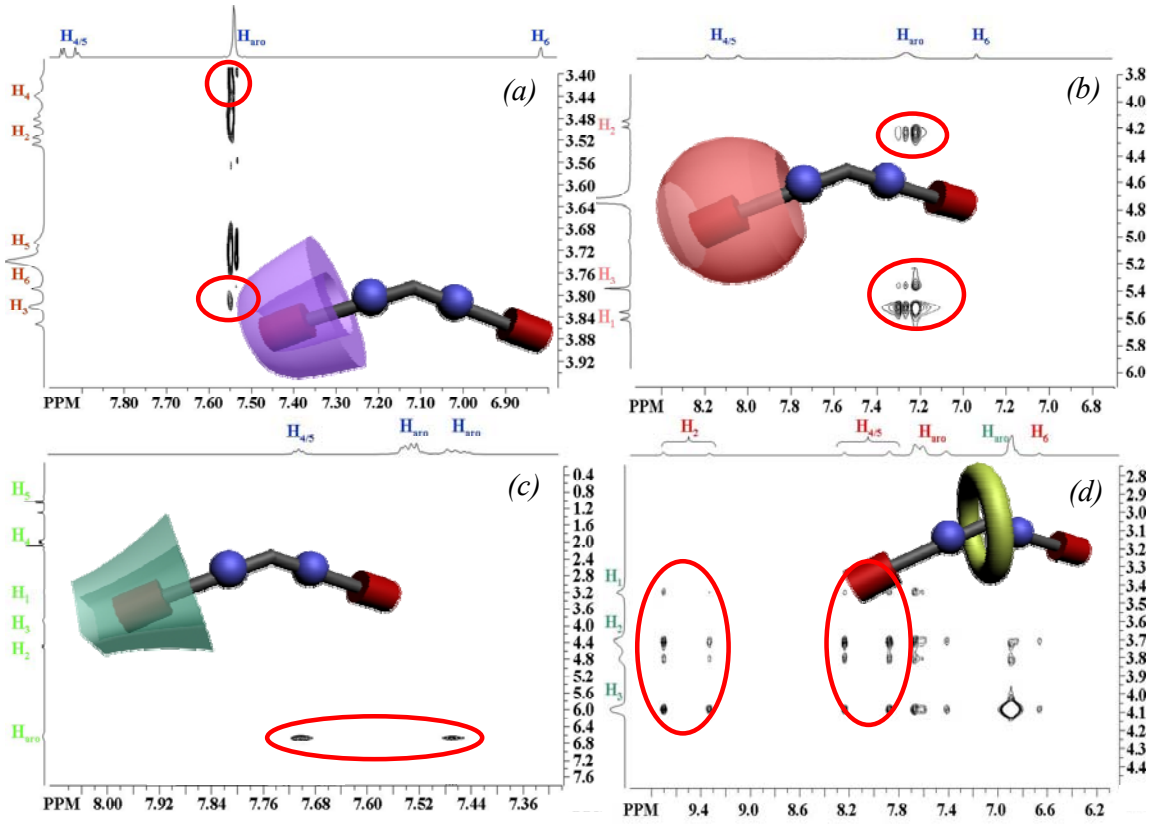


**Figure 2.6.** Partial NOESY NMR spectra at 25°C of: *(a)* 5 mM **[2][Br]$_2$** and 5 mM ***β*-CD** ($D_2O$); *(b)* 4 mM **[2][Br]$_2$** and 4 mM **CB[7]** ($D_2O$); *(c)* 10 mM **[2][PF$_6$]$_2$** and 10 mM **C[4]P** ($CDCl_3/CD_3CN$ (80/20 V/V)); *(d)* 10 mM **[2][PF$_6$]$_2$** and 10 mM **DB24C8** ($CD_3CN$).

The stoichiometry of the inclusion complexes was determined by the NMR continuous variation method [15]. A series of solutions was prepared in which the sum of ***β*-CD** and **[1][Br]$_2$** or **[2][Br]$_2$** concentrations was kept constant (10 mM in the present case), but in which the concentrations of ***β*-CD** and the imidazolium salts were systematically varied. From the variation of chemical shifts of the $^1$H NMR spectra of various ***β*-CD** /imidazolium salt mixtures, two Job's plots were drawn, one for each host-guest complex. For each imidazolim salt (**[1][Br]$_2$** and **[2][Br]**) the maximum observed at 50% of total concentration and the highly symmetric shape of the curve revealed a 1:1

stoichiometry. The **β-CD** forms inclusion complexes with one of the aromatic rings and supplementary stabilizing interactions with the imidazolium cations occur. However, it seems that these **β-CD** are too bulky to allow the formation of 2:1 complexes. For the **β-CD•[1][Br]$_2$** complex, binding constants of 6500 ± 20 $M^{-1}$ and 3000 ± 10 $M^{-1}$ for the **β-CD•[2][Br]$_2$** complex were further calculated at 25°C by the $^1$H NMR titration technique (constant concentration of imidazolium salt while varying the concentration of the **β-CD**). The difference between the two association constants must be due to the diimidazolium cation geometry. To confirm this assertion, we performed a computational study using the semi empirical PM3 energy minimization calculation using Hyperchem 7.5 program. Previous success in treating inclusion phenomena with semi-empirical methods [16] suggested that treating these systems empirically would be a judicious approximation. For computational expediency solvent effects were neglected in this work. This approximation appears not to have a significant deleterious impact on the results, a finding also reported previously by Ricketts *et al.* [17]. All structures were optimized at the molecular mechanics level to clean the physically distant contacts. To ensure thorough conformational searching, the macrocycle in the initial inclusion complex was successively rotated around and translated along the diimidazolium component manually. The rotation was performed with 36º step size and 360º range. The translation of the macrocycle for each of these 10 rotations was carried out with a step size of 1 Å and a range of 0-20 Å. The most stable complexes are formed when the cyclodextrin is positioned on the aromatic group of both imidazolium salts and the complex is more stable in the case of **β-CD•[1][Br]$_2$**.

## 2.3.2 Methylenediimidazolium cation/cucurbit[7]uril complexes

**CB[7]** is slightly more voluminous than **β-CD** and thus can bind a wider range of guests than lower order homologues (CB[5] or CB[6]). The ability of **[1][Br]$_2$** and **[2][Br]$_2$** salts to form inclusion complexes in water with **CB[7]** was studied. In aqueous solution, the aromatic protons of **[1][Br]$_2$** and **[2][Br]$_2$** are upfield shifted, consistent with the formation of an inclusion complex into the electron rich inner cavity of the **CB[7]** (Figure 2.3a, 2.3c, 2.4a and 2.4c). The effect of the complexation on the imidazolium ring proton is weaker,

which suggests that the complexation occurs primarily with the aromatic group of **[1][Br]$_2$** and **[2][Br]$_2$**. In fact, in **CB[7]**, there are different two binding regions [4]: (i) the hydrophobic cavity; and (ii) the outer disk formed by the oxygen atoms that can stabilize the positive charge. Here, the aromatic phenyl or benzyl residues are positioned in the hydrophobic cavity and the cations are situated in the cation binding region. In parallel to $^1$H NMR experiments, the inclusion complexes were also observed by MS (positive ionization mode) at m/z 1491.4 (**[1]•CB[7]**)$^+$ and 1463.3 (**[2]•CB[7]**)$^+$. We also observed that one of the positive charges is screened by the presence of **CB[7]**.

The NOESY spectra of **CB[7]** with **[1][Br]$_2$** or **[2][Br]$_2$** in $D_2O$ also show cross peaks between the aromatic protons and the $H_1$, $H_2$ and $H_3$ protons of the **CB[7]** (Figure 2.5b and 2.6b). The absence of cross-peaks between the hydrogens of the **CB[7]** and the $H_{4/5}$ hydrogens of the imidazolium residue shows once again that the interaction between the macrocycle and the imidazolium ring occurs with the aromatic substituent of the diimidazolium cation. The position of the **CB[7]** in these complexes is more surprising because this macrocycle is known to complex imidazolium or pyridinium residues [4, 5], However, in our case the aromatic group is included in the cavity. We believe that the methylene group between the two imidazolium rings destabilizes the formation of the complex directly on the diimidazolium moiety.

For both diimidazolium salts **[1][Br]$_2$** and **[2][Br]$_2$**, association constants were calculated and Job Plots were constructed. The complex **[1][Br]$_2$•CB[7]** gives a 1:1 stoichiometry whereas the **[2][Br]$_2$•CB[7]** complex gives a 1:2 stoechiometry. In the case of the latter two macrocycles can be complexed on each aromatic side, probably due to a more flexible geometry of the phenyl groups attached to the imidazolium rings. The association constants were determined to be 4200 ± 25 $M^{-1}$ for **[1][Br]$_2$•CB[7]** and 2100 ± 50 $M^{-1}$ for **[2][Br]$_2$)$_2$•CB[7]** at 25°C. As in the case of the **CDs** complexes, the PM3 calculations show that the most stable conformer is obtained when the **CB[7]** is positioned on the aromatic groups.

### 2.3.3 Methylenediimidazolium cation/tetrapropoxycalix[4]arene complexes

The hexafluorophosphate diimidazoliums **[1][PF$_6$]$_2$** and **[2][PF$_6$]$_2$** are not soluble in water, but highly soluble in polar organic solvents such as acetonitrile, methanol or nitromethane. The **C[4]P** possesses a aromatic cavity, ideal for π–π interactions and cation-π interactions with the diimidazolium groups. In the case of the **C[4]P** complexes, all the signals in the $^1$H NMR spectrum are shifted downfield for **[1][PF$_6$]$_2$** and shifted upfield for **[2][PF$_6$]$_2$** (Figure 2.3d, 2.3e, 2.4d and 2.4e). In the second case, it is clearly due to aromatic stacking between the aromatic rings of the **C[4]P** and aromatic rings of **[2][PF$_6$]$_2$**. However, the geometry of the complex is unclear because of the aromatic and imidazolium proton shifts. For **[1][PF$_6$]$_2$** the downfield shift is probably due to the formation of H-bonds between the oxygen atoms of **C[4]P** and the imidazolium ring protons of **[1][PF$_6$]$_2$**. The formation of complexes was also confirmed by the ESI/MS with characteristic m/z values of 1067.9 (**[1][PF6]•C[4]P**)$^+$ and 1038.9 (**[2][PF6]•C[4]P**)$^+$.

Globally, the same cross peaks were observed for the **C[4]P** with **[1][PF$_6$]$_2$** and **[2][PF$_6$]$_2$** in a mixture of $CDCl_3$/$CD_3CN$ (80/20 V/V) (Figure 2.5c and 2.6c). The interactions occur principally between the aromatic protons of the phenyl or benzyl residues of the diimidazolium cations and the aromatic protons of **C[4]P**. Interestingly, intense cross peaks are also observed between $H_4$ and $H_5$ of the imidazolium residue and the aromatic protons of the **C[4]P** and other less intense cross peaks are observed between $H_2$ and $H_3$ of **C[4]P** with $H_7$ of **[1][PF$_6$]$_2$,** and also between $H_1$ of **C[4]P** with $H_6$ of **[1][PF$_6$]$_2$**. This observation can be interpreted as a spatial proximity of the aromatic cavity with the imidazolium residue but the aromatic groups are positioned probably in the cavity of **C[4]P**.

For both diimidazolium salts, the stoechiometries of the complexes are 1:1. **C[4]P** forms inclusion complexes with the aromatic rings and there are stabilizing interactions with the imidazolium cations but it seems that this macrocycle are too bulky to allow the formation of 1:2 complexes. The value of association constants was estimated at 7500 ± 60

$M^{-1}$ for **[1][PF$_6$]$_2$** and 17000 ± 100 $M^{-1}$ **[2][PF$_6$]$_2$** at 25°C. Interaction of the **[1][PF$_6$]$_2$** or **[2][PF$_6$]$_2$** with **C[4]P** allowed the formation of the most stable complexes, as shown by the interaction energy obtained by PM3. This is reasonable because the interaction of the phenyl rings within a distance of 3.6 Å is very favorable. Molecular modeling did not allow interpretation of the particular stoichiometry obtained for **[2][PF$_6$]$_2$** with **C[4]P**, but it is reasonable to think that there is little repulsion between the two **C[4]P** molecules around the diimidazolium cation.

## 2.3.4 Methylenediimidazolium cation/dibenzo-24-crown-8 complexes

The complexes formed with **DB24C8** have lower association constants but they can be observed very easily by $^1$H NMR. The non-covalent interactions involved are the ion-dipole interactions with the crown ether oxygen atoms, acidic CH protons for C*H*•••O hydrogen bonding and electron poor imidazolium rings for π-interactions with the aryl groups of **DB24C8**. The rate of complexation is slower relatively on the NMR scale and the complexed components can be quantified by simple integration of the signals in the $^1$H NMR spectrum. The **[1][PF$_6$]$_2$•DB24C8** complex shows very sharp and well defined peaks. The chemical shifts of the complexed peaks are consistent with the formation of a complex in solution. The resonances due to the acidic NC*H*N proton on the imidazolium and NC$H_2$N protons on the linker are shifted downfield relative to the free imidazolium, consistent with C*H*••O hydrogen bonding. The NC*H*C*H*N protons on the imidazolium rings are shifted on opposite sides of the spectrum relative to the free **[1][PF$_6$]$_2$**, suggesting that one of the protons is engaged in C*H*••O hydrogen bonding while the other is pointing away from the crown ether. In the case of **[2][PF$_6$]$_2$** the $^1$H NMR spectrum is different from the **[1][PF$_6$]$_2$•DB24C8** complex: all the complexed and uncomplexed peaks are broad, suggesting more rapid rate of association/dissociation or multiple possible geometries for this complex.

The formation of complexes was confirmed by ESI/MS with characteristic m/z 923.36 (**[1][PF6]•DB24C8**)$^+$ and 937.37 (**[2][PF6]•DB24C8**)$^+$. For **[1][PF6]$_2$•DB24C8** (Figure 2.5d), a correlation was observed between the signals assigned to the complexed

form of **[1][PF$_6$]$_2$** and the protons of the crown ether. In the spectrum of the **[2][PF$_6$]$_2$•DB24C8** complex (Figure 2.6d), we were surprised to see that a correlation could be observed not only between the signals assigned to the complexed form of **[2][PF$_6$]$_2$** and the crown ether, but also between the signals assigned to the uncomplexed **[2][PF$_6$]$_2$** and **DB24C8**. A possible explanation for these correlation signals is a slower rate of association-dissociation for **[2][PF$_6$]$_2$•DB24C8** or the presence of different geometries for these complexes. In the case of the **DB24C8**, Job's plot experiments showed the expected 1:1 stoechiometry for both diimidazolium salts. The values of the association constants were estimated at 56 ± 10 for **[1][PF$_6$]$_2$** and 120 ± 20 $M^{-1}$ **[2][PF$_6$]$_2$** at 25°C. The computational study confirms the location of **DB24C8** symmetrically between the two imidazolium groups. The macrocycle adopts a chair-like conformation, exactly as observed in the solid state structures of other complexes obtained by X-ray diffraction.

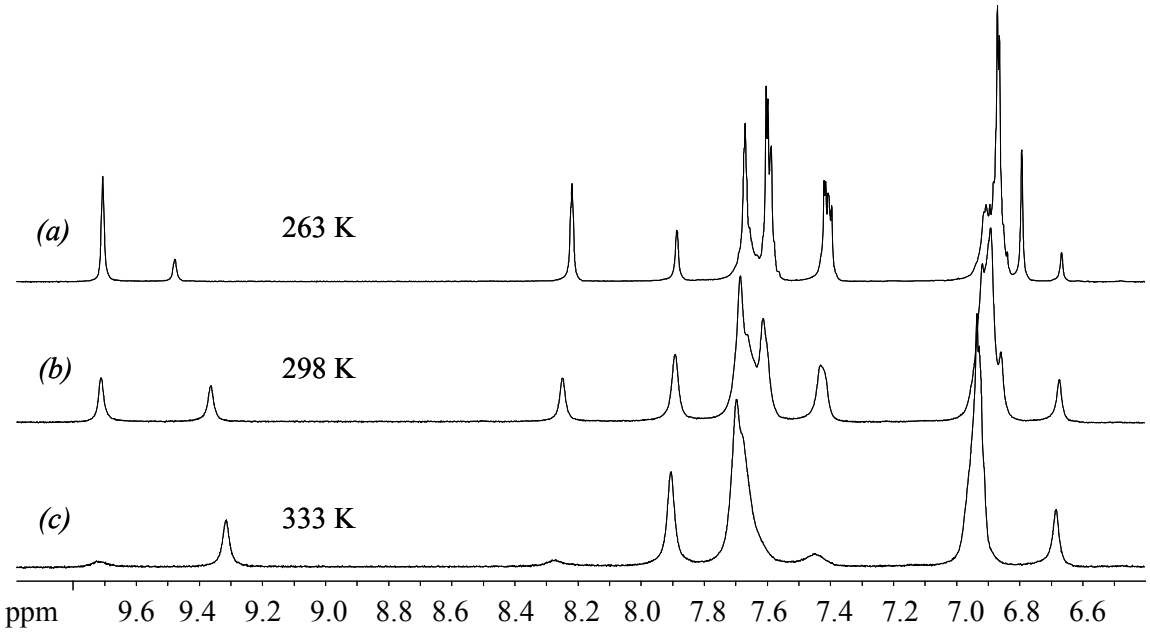


**Figure 2.7.** $^1$H NMR temperature study of **DB24C8** and **[2][PF$_6$]$_2$** (25 mM) in $CD_3CN$.

A supplementary $^1$H NMR study with temperature variation was conducted for the formation of **[2][PF$_6$]$_2$•DB24C8** complex (Figure 2.7). At 333 K, there is almost no complexed **[2][PF$_6$]$_2$,** whereas the complexed peaks are sharper and predominant at 263 K. The association constant is highly dependant on the temperature and this suggests that the enthalpy plays an important role in the formation of this complex. This experiment also allowed ruling out the formation of two different 1:1 complexes in solution at the same time.

## 2.3.5. Comparison between the Different Complexes.

**Table 2.1.** Values of the association constants for various macrocycles-diimidazolium salts

| Entry | Macrocycle | **[X]** | **[1][X]$_2$** $K_{ass}/M^{-1}$ (Host:Guest) | **[2][X]$_2$** $K_{ass}/M^{-1}$ (Host:Guest) |
|---|---|---|---|---|
| 1[d] | **β-CD** | [Br] | 6500 ± 20 [a] (1:1)[b] | 3000 ± 10 [a] (1:1)[b] |
| 2[d] | **CB[7]** | [Br] | 4200 ± 25 [a] (1:1)[b] | 2100 ± 50 [a] (2:1)[b] |
| 3[e] | **C[4]P** | [PF$_6$] | 7500 ± 60 [a] (1:1)[b] | 17000 ± 100 [a] (1:1)[b] |
| 4[f] | **DB24C8** | [PF$_6$] | 56 ± 10 [c] (1:1)[b] | 120 ± 20 [c] (1:1)[b] |

[a] Determined by $^1$H NMR titration; [b] Determined by continuous variation method (Job Plots); [c] Determined by single point method; [d] $D_2O$, 25°C (fast exchange on the NMR time scale); [e] $CDCl_3/CD_3CN$ (80/20) (fast exchange on the NMR time scale), 25°C; [f] $CD_3CN$, 25°C (slow exchange on the NMR time scale).

The association constants for **β-CD**, **CB[7]** and **C[4]P** are large (Table 2.1). A decreased association constant was observed for **[2][Br]$_2$•CB[7]** and **[2][Br]$_2$•β-CD** compared to the **[1][Br]$_2$** complexes, but a significant increase is observed for **[2][PF$_6$]$_2$•C[4]P** compared to **[1][PF$_6$]$_2$•C[4]P**. The geometry of the **[2][PF$_6$]$_2$** diimidazolium salts allows π-π interactions and enhances the possibility of additional

cation-π interactions with an imidazolium ring placed closer to the cavity of the calixarene. In the case of **DB24C8** complexes, there is a difference in the binding mode of these two cations. Even if the association constants of **[1][$PF_6$]$_2$•DB24C8** and **[2][$PF_6$]$_2$•DB24C8** are not as high as the **DB24C8** complexes reported in the literature [18], the solubility of the substituted diimidazolium *bis*(hexafluorophosphate) is higher than the previously reported recognition units (Table 2.2) in polar organic solvents. In an equimolar solution of diimidazolium salt and **DB24C8**, their initial concentration and the association constant have the same effect on the ratio of [bound imidazolium]/[unbound imidazolium] [19]. The association constant of a *bis*(pyridinium)ethane with **DB24C8** [20] is approximately $10^3$ $M^{-1}$, almost 10 times higher than **[2][$PF_6$]$_2$•DB24C8**, but its solubility is almost 20 times lower. Thus, the ratio of [bound imidazolium]/[unbound imidazolium] at a saturation concentration is almost equivalent (for calculations see Supporting Information).

**Table 2.2.** Solubilities ($mol \cdot L^{-1}$) of **[1][$PF_6$]$_2$** and **[2][$PF_6$]$_2$** at 25 °C, compared to *bis*(pyridinium)ethane bis(hexafluorophosphate) salt

| component | acetonitrile | nitromethane |
|---|---|---|
| **[1][$PF_6$]$_2$** | 1.08 | 1.21 |
| **[2][$PF_6$]$_2$** | 1.14 | 1.30 |
| *bis*(pyridinium)ethane**[$PF_6$]$_2$** | $6.5\ 10^{-2}$ | $7.7\ 10^{-2}$ |

The only undesirable effect of this high solubility is the difficulty to obtain crystals suitable for X-ray diffraction of any of the described complexes. We are currently working on using different counterions such as perchlorates or triflates to obtain less-soluble compounds suitable for the formation of crystals.

## 2.4 Conclusion

*N,N'*-disubstituted methylenediimidazolium salts with two different counter ions have been used as guests in order to obtain novel inclusion complexes with various macrocycles, such as β-cyclodextrin, cucurbit[7]uril, tetrapropoxycalix[4]arene and dibenzo-24-crown-8 ether. For most 1:1 complexes were obtained, except for **CB[7]** with the **[2][Br]$_2$** salts (in which case a 2:1 complex is observed). The highest association constant is obtained in the case of **C[4]P** and **[2][PF$_6$]$_2$**. This study underlines the versatility of *N,N'*-disubstituted methylenediimidazolium salts to form different inclusion complexes in different solvents. Work is currently underway in our laboratory to obtain a supramolecular bulky carbine derivative of these inclusion complexes for organometallic catalysis, as well as new ionic liquid media for organic reactions.

## 2.5 Experimental section

### 2.5.1 General Procedure for the Synthesis of [1][X]$_2$ and [2][X]$_2$

A mixture of *N*-substituted imidazole (11 mmol, 2.2 equiv) and dibromomethane (5 mL) in a round-bottom flask was heated at 80 °C for 18 h. The white precipitate formed was filtered off and dried under high vacuum to yield **[1][Br]$_2$** or **[2][Br]$_2$**. These compounds were dissolved in a minimum amount of hot water, and ammonium hexafluorophosphate (10 mmol, 2 equiv) in water (2 mL) was added to the solution. The white precipitate formed was filtered off and washed successively with diethyl ether, ethyl acetate, and hexane and dried under high vacuum to yield **[1][PF$_6$]$_2$** or **[2][PF$_6$]$_2$**.

### 2.5.2 Characterization

**1,1'-Dibenzyl-3,3'-methylenediimidazolium *bis*(bromide) [1][Br]$_2$** (78% yield) **$^1$H NMR** ($D_2O$, 400 MHz): δ (ppm) 7.79 (d, 2H, *J* = 2.2 Hz), 7.61 (d, 2H, *J* = 2.2 Hz), 7.46-7.47 (m, 10H), 6.67 (s, 2H), 5.44 (s, 4H). **$^{13}$C NMR** ($D_20$, 75 MHz): δ (ppm) 137.7,

133.4, 130.5, 130.3, 129.9, 124.6, 123.1, 59.8, 54.4. **HR-MS** *m/z* found: 329.17622 $(M - H)^+$, calc: 329.17661. M.p.: 278-280 ºC.

**1,1'-Diphenyl-3,3'-methylenediimidazolium *bis*(bromide) [2][Br]$_2$** (54% yield) **$^1$H NMR** ($D_2O$, 400 MHz): δ (ppm) 8.02 (m, 4H), 7.64-7.70 (m, 10H), 6.96 (s, 2H). **$^{13}$C NMR** ($D_2O$, 75 MHz): δ (ppm) 135.0, 131.6, 131.2, 124.2, 123.5, 123.3, 60.3. **HR-MS** *m/z* found: 301.14386 $(M - H)^+$, calc: 301.14529. M.p.: 270-272 ºC.

**1,1'-Dibenzyl-3,3'-methylenediimidazolium *bis*(hexafluorophosphate) [1][PF$_6$]$_2$** (83% yield from **[1][Br]$_2$**) **$^1$H NMR** ($CD_3CN$, 400 MHz): δ (ppm) 8.78 (s, 2H), 7.62 (t, 2H, $J$ = 2.0 Hz), 7.48-7.52 (m, 8H), 7.28-7.47 (m, 4H), 6.34 (s, 2H), 5.39 (s, 4H). **$^{13}$C NMR** ($CD_3CN$, 75 MHz): δ (ppm) 137.7, 133.6, 130.4, 130.2, 129.9, 124.4, 123.5, 59.7, 54.3. **HR-MS** *m/z* found: 475.1481 $(M - PF_6)^+$, calc: 475.1498. M.p.: 195-197 ºC.

**1,1'-Diphenyl-3,3'-methylenediimidazolium *bis*(hexafluorophosphate) [2][PF$_6$]$_2$** (72% yield **[2][Br]$_2$**) **$^1$H NMR** ($CD_3CN$, 400 MHz): δ (ppm) 9.26 (s, 2H), 7.92 (s, 2H), 7.89 (s, 2H), 7.64-7.75 (m, 10H), 6.62 (s, 2H). **$^{13}$C NMR** ($CD_3CN$, 75 MHz): δ (ppm) 136.9, 135.2, 131.8, 131.3, 124.0, 123.6, 60.2. **HR-MS** *m/z* found: 447.1168 $(M - PF_6)^+$, calc: 447.1169. M.p.: 238-240 ºC.

## 2.6 Acknowledgment

We are grateful to the Natural Sciences and Engineering Research Council of Canada, the Fonds Quebécois de la Recherche sur la Nature et les Téchnologies, the Canada Foundation for Innovation, and Université de Montréal for financial support. We thank Sylvie Bilodeau for the NMR studies and Dr. Alexandra Furtos and Karine Venne for mass spectrometry analysis. We also thank colleagues for careful reading and discussion of this manuscript.

## 2.7 Supporting information available

General experimental details, $^{1}$H NMR, $^{13}$C NMR, and ESI-MS of **[1][Br]$_2$**, **[2][Br]$_2$**, **[1][PF6]$_2$** and **[2][PF6]$_2$**, $^{1}$H NMR of complexes, NOESY NMR of complexes, association constants, and determination for complexes with **DB24C8**. This material is available free of charge via the Internet at http://pubs.acs.org.

## 2.8 References


1 (a) *Comprehensive Supramolecular Chemistry, Vol. 11* (Eds.: Atwood, J. L.; Davies, J. E. D.; MacNicol, D. D.; Vögtle, F.) Pergamon, Oxford, **1996**. (b) H.-J. Schneider, A. Yatsimirsky, *Principles and Methods in Supramolecular Chemistry*, Wiley, Chichester, **2000**.

2 (2) (a) Tomapatanaget, B.; Tuntulani, T.; Wisner, J. A.; Beer, P. D. *Tetrahedron Lett.* **2004**, *45*, 663-666. (b) Wisner, J. A.; Beer, P. D.; Berry, N. G.; Tomapatanaget, B. *Proc. Natl. Acad. Sci. U.S.A.* **2002**, *99*, 4983-4986. (c) Sambrook, M. R; Beer, P. D.; Wisner, J. A.; Paul, R. L.; Cowley, A. R.; Szemes, F.; Drew, M.G. B. *J. Am. Chem. Soc.* **2005**, *127* 2292-2302.

3 *Chem. Rev.* **1998**, *98*, 1741-2076 (a special edition on cyclodextrins).

4 Lagona, J.; Mukhopadhyay, Chakrabarti, Isaacs, L. *Angew. Chem. Int Ed.* **2005**, *44*, 4844-4870.

5 (a) Lee, J. W.; Samal, S.; Selvapalam, N.; Kim, H.-J.; Kim, K. *Acc. Chem. Res.* **2003**, *36*, 621-630. (b) Moon, K.; Kaifer, A. E. *Org. Lett.* **2004**, *6*, 185-188. (c) Sindelar, V.; Moon, K.; Kaifer, A. E. *Org. Lett.* **2004**, *6*, 2665-2668. (d) Ong, W.; Kaifer, A. E. *J. Org. Chem.* **2004**, *69*, 1383-1385. (e) Sindelar, V.; Cejas, M. A.; Raymo, F. M.; Kaifer, A. E. *New J. Chem.* **2005**, *29*, 280-282. (f) Ko, Y. H.; Kim, K.; Kang, J.-K.; Chun, H.; Lee, J. W.; Sakamoto, S.; Yamaguchi, K.; Fettinger, J. C.; Kim, K. *J. Am.*

*Chem. Soc.* **2004**, *126*, 1932-1933. (g) Kim, J.; Jung, I.-S.; Kim, S.-Y.; Lee, E.; Kang, J.-K.; Sakamoto, S.; Yamaguchi, K.; Kim, K. *J. Am. Chem. Soc.* **2000**, *122*, 540-541. (h) Mohanty, J.; Bhasikuttan, A. C.; Nau, W. M.; Pal, H. *J. Phys. Chem. B* **2006**, *110*, 5132-5138. (i) Ong, W.; Kaifer, A. E. *Organometallics* **2003**, *22*, 4181-4183. (j) Kim, K. *Chem. Soc. Rev.* **2002**, *31*, 96-107. (k) Rekharsky, M. V.; Yamamura, H.; Inoue, C.; Kawai, M.; Osaka, I.; Arakawa, R.; Shiba, K.; Sato, A.; Ko, Y. H.; Selvapalam, N.; Kim, K.; Inoue, Y. *J. Am. Chem. Soc.* **2006**, *128*, 14871-14880. (k) Montes-Navajas, P. ; Corma, A. ; Garcia, H. *J. Mol. Cat. A*, **2008**, *279*, 165-169. (l) Wang, R. ; Yuan, L. ; Macartney, D.H. *Chem. Commun*. **2006**, 2908-2910.

6 (a) Gutsche, C. D. *Calixarenes Monographs in Supramolecular Chemistry* Vol. 1, The Royal Society of Chemistry, Cambridge, **1989**. (b) Gutsche, C.D. *Calixarenes Revisited Monographs in Supramolecular Chemistry* Vol. 6, The Royal Society of Chemistry: Cambridge, **1998**.

7 For a review on crown ether complexes with alkali metals see: Steed, J. W. *Coordination Chemistry Reviews* **2001**, *215*, 171-221.

8 Stolwijk, T. B.; Sudhölter, E. J. R.; Reinhoudt, D. N.; Harkema, S. *J. Am. Chem. Soc.* **1989**, *54*, 1000-1004.

9 Loeb, S. J.; Tiburcio, J.; Vella, S.J. *Org. Lett.* **2005**, *22*, 4923-4926.

10 (a) Li, L.; Clarkson, G. J. *Org. Lett.* **2007**, *9*, 497–500. (b) Castillo, D.; Astudillo, P.; Mares, J.; Gonzales, F. J.; Vela, A.; Tiburcio, *J. Org. Biomol. Chem.* **2007**, *5*, 2252-2256.

11 (a) Ashton, P. R.; Philp, D.; Spencer, N.; Stoddart, J. F. *J. Chem. Soc., Chem. Commun.* **1992**, 1124-1126. (b) Loeb, S. J.; Wisner, J. A. *Angew. Chem., Int. Ed.* **1998**, *37*, 2838-2840. (c) Huang, F.; Slebodnick, C.; Ratliff, A. E.; Gibson, H. W. *Tetrahedron Lett.* **2005**, *46*, 6019-6022. (d) Huang, F.; Rheingold, A. L.; Slebodnick, C.; Ohs, A.; Switek, K. A.; Gibson, H. W. *Tetrahedron* **2005**, *61*,

10242-10253. (e) Cheng, P.-N.; Lin, C.-F.; Liu, Y.-H.; Lai, C.-C.; Peng, S.-M.; Chiu, S.-H. *Org. Lett.* **2006**, *8*, 435-438.

12 Experimental protocol based on: Lee, H. M.; Lu, C. Y.; Chen, C. Y.; Chen, W. L.; Lin, H. C.; Chiu, P. L.; Cheng, P. Y. *Tetrahedron*, **2004**, 60, 5807–5825.

13 Schneider, H;. J.; Hacket, F.; Rüdiger, V.; Ikeda, H. *Chem. Rev.* **1998**, *98*, 1755-1786.

14 (a) Koch, K. J.; Gozzo, F. C.; Nanita, S. C.; Takats, Z.; Eberlin, M. N.; Cooks, R. G. *Angew. Chem. Int. Ed.* **2002**, *41*, 1721-1724. (b) Takats, Z.; Nanita, S. C.; Cooks, R. G. *Angew. Chem. Int. Ed.* **2003**, *42*, 3521-3523. (c) Cooks, R. G.; Zhang, D. X.; Koch, K. J.; Gozzo, F. C.; Eberlin, M. N. *Anal. Chem.* **2001**, *73*, 3646-3655.

15 (a) Gil, V. M. S.; Oliveira, N. C. *J. Chem. Educ.* **1990**, *67*, 473-478. (b) Connors, K. Binding Constants. The Measurement of Molecular Complex Stability; Wiley: New York, **1987**.

16 (a) Liu, L.; Li, X. S.; Song, K. S.; Guo, Q. X. *J. Mol. Struct. THEOCHEM* **2000**, *531*, 127-134. (b) Sohlberg, K; Tarbet, B. *J. Inclusion Phenom. Mol. Recognit. Chem.* **1995**, *23*, 203-212.

17 Ricketts, H. G., Stoddart, J. F., Hann, M. M. Computational Approaches in Supramolecular Chemistry, Wipff, G. Ed.; vol. series C: Mathematical and Physical Science – V426, Kluwer Academic Publishers: Dordrecht, **1994**, 377.

18 (a) Balzani, V.; Credi, A.; Mattersteig, G.; Matthews, O. A.; Rayno, F. M.; Stoddart, J. F.; Venturi, M.; White, A. J. P.; Williams, D. J. *J. Org. Chem.* **2000**, *65*, 1924-1936. (b) Elizarov, A. M.; Chiu, S.-H.; Stoddart, J. F. *J. Org. Chem.* **2002**, *67*, 9175-9181. (c) Loeb, S. J.; Tiburcio, J.; Vella, S. J. *Chem. Commun.* **2006**, 1598-1600.

19 The ratio [bound imidazolium]/[unbound imidazolium] can be directly derived from the association constant for the formation of a 1:1 complex in the case of a slow complexation in the NMR time scale. See supporting information for details.

20 (a) Ashton, P. R.; Philp, D.; Spencer, N.; Stoddart, J. F. *J. Chem. Soc., Chem. Commun.* **1992**, 1124-1126. (b) Loeb, S. J.; Wisner, J. A. *Angew. Chem., Int. Ed.* **1998**, *37*, 2838-2840. (c) Cheng, P.-N.; Lin, C.-F.; Liu, Y.-H.; Lai, C.-C.; Peng, S.-M.; Chiu, S.-H. *Org. Lett.* **2006**, *8*, 435-438.

# Chapitre 3 : Motif méthylènediimidazolium et complexes ternaires en solutions aqueuse. Contrôle de l'assemblage supramoléculaire à l'interface air-eau

# 3.0 Préface

Après l'analyse des résultats présentés au chapitre 2, nous avons réalisé que l'étude des complexes en solution aqueuse avec la $\beta$-CD et le CB[7] pouvait être étoffée. En effet, plusieurs types de cyclodextrines peuvent former des complexes différents avec les sels de méthylènediimidazolium et nous avons même pu mettre en évidence la formation de complexes ternaires entre un sel de diimidazolium, une cyclodextrine et le cucurbituril. A travers l'étude de ces complexes ternaires, il a été possible de montrer un effet de coopérativité entre les cyclodextrines et le CB[7] lors de la complexation. De plus, il nous a été possible d'étudier les assemblages supramoléculaires à l'interface air/eau, ce qui, a notre connaissance n'avait jamais été réalisé avec des sels d'imidazolium.

Pour cet article, j'ai réalisé la synthèse des composés ainsi que les études RMN $^{1}$H et une partie de la rédaction, notamment les parties de synthèse et d'analyse des spectres RMN $^{1}$H.

Les informations expérimentales supplémentaires de cette partie se trouvent aux pages 200-217 de la thèse.

# Article 2. Study of the supramolecular cooperativity in the multirecognition mechanism of cyclodextrins/cucurbituril/disubstituted diimidazolium bromides

Loïc Leclercq, Nadim Noujeim, Samantha H. Sanon and Andreea R. Schmitzer*

Département de chimie, Université de Montréal, CP 6128, Succursale Centre-Ville, Montréal, Québec, H3C 3J7, Canada

*Journal of Physical Chemistry B,* **2008**, ***112***, 14176-14184

## 3.1 Abstract

*N*,*N'*-Disubstituted methylenediimidazolium bromide salts substituted with two aromatic groups present two different binding sites. In the binary complexes with cyclodextrins (**CDs**) or cucurbit[7]uril (**CB[7]**), the macrocycle is always positioned on the external aromatic residues. In the ternary complexes, **CB[7]** is positioned around the diimidazolium cation, where the external aromatic residue is included in the **CD**'s cavity. The unfavored position of the **CB[7]** on the cationic site in the ternary complex is the result of its cooperative supramolecular interaction with the cyclodextrin. The obtained ternary complexes possess different interfacial properties, compared to those of the binary complexes. We demonstrate these hypotheses by NMR spectroscopy, ESI-HRMS spectrometry, molecular modeling simulation, and surface tension measurements.

## 3.2 Introduction

The study of multiple interactions between two or more complex molecules is of fundamental interest by giving new insights into molecular recognition and self-assembly processes. The ability of macrocycles such as cryptands, carcerands, crown ethers, cyclodextrins, cyclophanes, calixarenes, and cucurbiturils to form stable complexes with a wide range of guest molecules makes them interesting as building blocks in the design of supramolecular assemblies [1, 2, 3, 4, 5 and 6]. The architectural complexity of supramolecular entities is controlled by hydrogen bonding, donor-acceptor interactions, and metal coordination interactions, which hold the components together [7, 8]. Thus, the control of noncovalent connections involved in bringing molecules together in aggregates with well-defined supramolecular entity is one of the most important issues in supramolecular assemblies. Cyclodextrins (**CDs**) are known as remarkable natural cyclic hosts with hydrophobic cavity forming inclusion complexes with a large variety of guest molecules, thus leading to interesting supramolecular assemblies [9]. By comparing with crown ethers, cryptands, calix[*n*]arenes, and cyclophanes, which are hosts focused on

molecular recognition of low molecular weight compounds, the **CDs** are able to recognize larger guests like clusters and polymers [10, 11 and 12]. Naturally occurring **CDs** are six, seven, or eight-membered-1,4-linked cyclic oligomers of D-glucopyranose (**$\alpha$-, $\beta$-, and $\gamma$-CD**) and are generally described as shallow truncated cones with the primary hydroxy rim of the cavity having a reduced diameter compared to the secondary hydroxy rim. The formation of pseudopolyrotaxanes based on **$\alpha$-CD**, which result from the threading [13] of several **$\alpha$-CD** rings onto a linear polymeric guest, has attracted recent attention [14, 15 and 16].

Cucurbit[*n*]urils (**CB[*n*]**) have often elicited comparisons with **CDs** [17]. The cavity sizes of **CB[6]**, **CB[7]** and **CB[8]** are similar to those of **$\alpha$-**, **$\beta$-**, and **$\gamma$-CD**, respectively. However, these size similarities should not be confused with similarities in composition and binding properties. **CBs** are prepared synthetically by the acid-catalyzed condensation of symmetric glycoluril repeating units with formaldehyde; they are achiral compounds that exhibit an equatorial symmetry plane, which does not exist in the **CDs**. A consequence of this symmetry is that both cavity openings in **CBs** are identical. In contrast to this, the two cavity openings of the opening lined by primary hydroxyl groups and the larger opening lined by twice as many secondary hydroxyl groups (Figure 3.1).

Not surprisingly, the main intermolecular interactions between molecular guests and these two classes of hosts are different. A considerable body of evidence suggests that hydrophobic interactions are primarily responsible for the stabilization of the inclusion complexes formed between **CDs** and most organic and organometallic guests [18]. The hydroxyl groups lining the **CD** cavity openings do not appear to engage in strong interactions with most included guests. In stark contrast to this, the interactions between **CBs** and included guests result from a combination of two types of intermolecular forces: (i) ion-dipole interactions between positive charges on the guest and carbonyl oxygens lining both **CB** cavity openings and (ii) hydrophobic interactions between the guest and the inner surface of the **CB** host cavity [19].

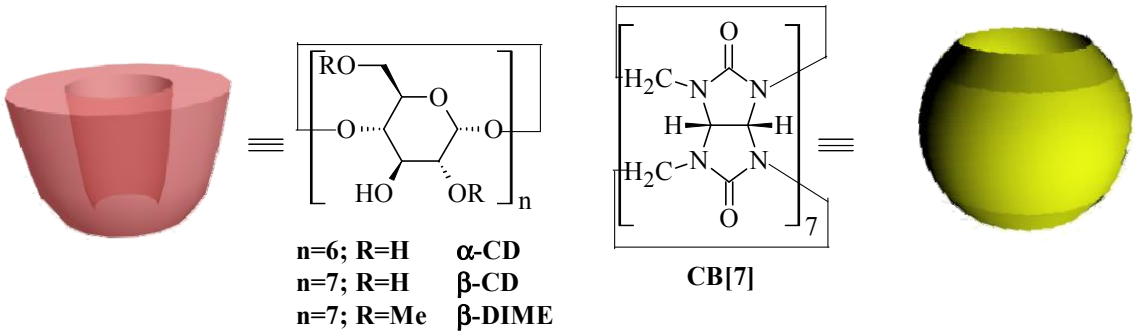


**Figure 3.1.** Structure and schematic representation of different macrocycles used in this work.

Recently, ternary complexes between **CBs**/**CD**/guest molecules have been reported [20]. However, a selective binding of **CB[7]** at an unfavorable binding position by cooperative interaction with the **CD** has not been reported before.

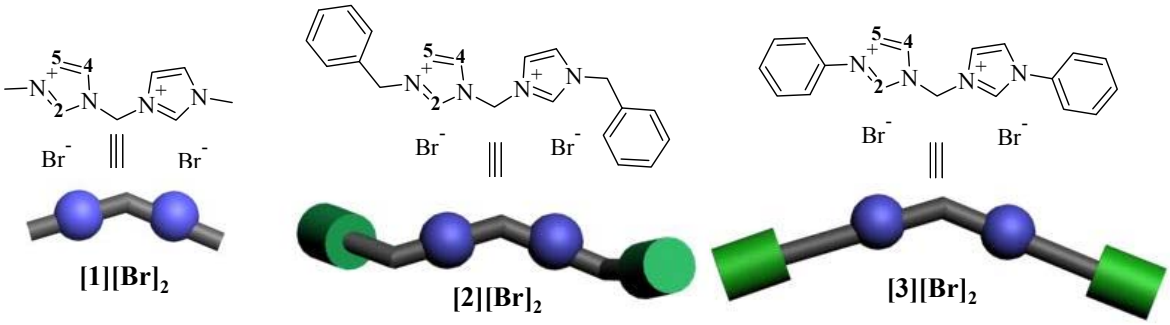


**Figure 3.2.** Structure and schematic representation of the *N,N*'-disubstituted diimidazolium bromide salts used in the work.

Although the inclusion complexation between **CDs** and some common surfactant salts has been investigated, to our knowledge there have been few reports on the combination of **CDs** and imidazolium salts [21]. In the work presented here, we focus on the multirecognition mechanism in water of **CB** and **CDs** onto three *N,N*'-disubstituted

diimidazolium salts, two bearing aromatic substituents and one bearing methyl substituents (Figure 3.2), and the interfacial properties of the different inclusion complexes. Such systems are attracting increasing interest as potential molecular switches for nanotechnological application.

## 3.3 Experimental section

### 3.3.1 Materials

$D_2O$ (99.95% isotopic purity) and all other chemicals were purchased from Aldrich and used without further purification.

### 3.3.2 NMR measurements

NMR experiments were recorded on Avance 300 or 400 Brücker spectrometers (300 or 400 MHz) with the samples nonspinning. All NMR experiments (guest titration by host, Job's plot, 2D ROESY) are obtained by the use of the sequence commercially available on Brücker spectrometers. Chemical shifts are given in ppm ($\delta$) and measured relative to the HOD signal. All NMR measurements were carried out in pure deuterated water (pH ) 6.5) because it is known that electrolyte ions also form complexes with **CDs** and **CBs** [22].

### 3.3.3 Synthesis

**1,1'-Dimethyl-3,3'-methylenediimidazolium *bis*(bromide) [1][Br]$_2$**. $^1$H NMR ($D_2O$, 400 MHz): $\delta$ (ppm) 7.64 (s, 2H), 7.47 (s, 2H), 6.57 (s, 2H), 3.84 (s, 6H). $^{13}$C NMR ($D_2O$, 75 MHz): $\delta$ (ppm) 138.3, 125.7, 122.7, 59.7, 37.2. HR-MS m/z found, 177.11277 (M - H), calc, 177.11400. mp 289 °C (decomposition is observed for T > 305 °C). (Yield 75%).

**1,1'-Dibenzyl-3,3'-methylenediimidazolium *bis*(bromide) [2][Br]$_2$**. $^1$H NMR ($D_2O$, 400 MHz): $\delta$ (ppm) 7.79 (d, 2H, J ) 2.2 Hz), 7.61 (d, 2H, J ) 2.2 Hz), 7.46-7.47 (m,

10H), 6.67 (s, 2H), 5.44 (s, 4H). $^{13}$C NMR ($D_2O$, 75 MHz): $\delta$ (ppm) 137.7, 133.4, 130.5, 130.3, 129.9, 124.6, 123.1, 59.8, 54.4. HR-MS m/z found, 329.17622 (M - H); calc, 329.17661. mp 278-280 °C. (Yield 78%).

**1,1'-Diphenyl-3,3'-methylenediimidazolium *bis*(bromide) [3][Br]$_2$**. $^1$H NMR ($D_2O$, 400 MHz): $\delta$ (ppm) 8.02 (m, 4H), 7.64-7.70 (m, 10H), 6.96 (s, 2H). $^{13}$C NMR ($D_2O$, 75 MHz): $\delta$ (ppm) 135.0, 131.6, 131.2, 124.2, 123.5, 123.3, 60.3. HRMS m/z found, 301.14386 (M - H); calc, 301.14529. mp 270-272 °C. (Yield 54%).

### 3.3.4 ESI/HRMS

ESI mass spectra were recorded with a mass spectrometer TSQ Quantum Ultra (Thermo Scientific) with accurate mass options instrument (Université de Montréal Mass Spectrometry Facility).

### 3.3.5 Molecular dynamic study

Calculations were performed on a Windows XP workstation with HyperChem 7.5 software. The initial configurations of **CDs** and diimidazolium cations have been obtained from PM3 semiempirical calculations. To investigate the conformational flexibility, we generated a unit cell containing one **$\beta$-CD** molecule in a water box with periodic boundary conditions. An initial MD run was performed for a period of 10 ps at 300 K. This solvent equilibration phase should be sufficiently extensive to allow the solvent to readjust completely to the potential field of the solute. The cutoff for nonbonded interactions was taken to be 12 Å throughout all the simulations. At the beginning, we carried out high temperature annealed MD simulations starting at 1000 K (2 ps) annealing to 0 K (10 ps). The temperature of 1000 K is necessary to enable the molecule to overcome energy barriers between different conformations and to prevent the system from getting stuck in a particular region of the conformational space. Simulations at lower temperatures yielded very similar conformations. The simulations in aqueous solution were relaxed using the steepest descent method until a gradient different of 0.01 kcal/mol was reached. After

energy minimization of the system at 0 K, the MD simulation was initialized using a time step of 1 fs for a time period of 100 ps. The temperature was kept constant at 300 K yielding a canonical ensemble (NVT).

### 3.3.6 Surface tension measurements

The processor tensiometer DCAT 11 (Dataphysics) and the Wilhelmy plate method have been used for the surface tension measurements. A concentrated solution was installed in a syringe and the addition of small volumes to ultrapure water (bidistilled water, $\sigma$ = 72.0 $mN \cdot m^{-1}$ at 25 °C) was used to increase the solution concentration. After each addition, the solution was gently stirred for 30 s. Equilibrium surface tension was measured for each concentration. All surface tension values were mean quantities of at least three measurements. The standard deviation of the mean never deviated ± 1.5% of the mean. The precision of the force transducer of the surface tension apparatus was 0.1 $mN \cdot m^{-1}$ and before each experiment, the platinum plate was cleaned in red/orange color flame. The temperature stabilization was estimated as better than ± 0.05 °C with a thermoregulated bath Lauda RC6 (25 °C).

## 3.4 Results and Discussion

### 3.4.1 Complexation study in aqueous solution

We have recently reported the synthesis and the formation of binary complexes of **[2][Br]$_2$** and **[3][Br]$_2$** salts with **CB[7]** and **$\beta$-CD** [23]. We have observed that both macrocyles recognize the aromatic unit to form inclusion complexes. However, the central diimidazolium motif can also be a binding site for **CB[7]**. To demonstrate this hypothesis, we carried out NMR studies of **[1][Br]$_2$** with **CB[7]** in $D_2O$. The NMR spectra at 298 K show a slow exchange with the **CB[7]**. The slow exchange results in a partial overlap between the peaks of the uncomplexed and the complexed diimidazolium cations. ITC

titration experiments were carried out but the limited solubility of **CB[7]** did not allow us to precisely determine the association constant. For this reason, the equilibrium constant can only be estimated to be less than 1200 $mol.L^{-1}$. We propose that the association constant of **CB[7]** with **[1][Br]$_2$** is weak due to the special geometry of the molecule (the methylene between the two imidazolim rings does not allow the perfect accommodation of the two charges at the **CB** cavity openings). Moreover, the molecule size does not allow the formation of hydrogen bonds between the oxygen of **CB[7]** and the acidic proton of the imidazolium rings; the guest may be quasi-totally included in the **CB[7]** cavity. For the association of **[1][Br]$_2$** with **$\beta$-CD**, the exchange is fast on the NMR time scale and the association constant can be estimated at 460 $mol.L^{-1}$ using $^1$H NMR titration method at 298 K. For the **$\beta$-CD**, the weak association could be explained by the very weak hydrophobicity of the diimidazolium cation.

For guests **[2][Br]$_2$** and **[3][Br]$_2$**, the methyl residues adjacent to the diimidazolium are replaced by aromatic groups benzyl and phenyl, respectively. For the **CB[7]** and the **$\beta$-CD**, the nature, the stoichiometry, and the geometry of the binary inclusion complex have already been discussed in our previous work on the basis of $^1$H NMR titration, mass spectrometry analysis, continuous variation method (Job's Plot), and 2D NOESY [23]. Complementary $^1$H NMR titration, mass spectrometry, Job's Plot method, and 2D ROESY were performed with new cyclodextins (**$\beta$-DIME** and **$\alpha$-CD**) for **[2][Br]$_2$** and **[3][Br]$_2$**. All data obtained are compatible with the formation of an inclusion complex such as in the case of **$\beta$-CD** [22]. For the **$\beta$-DIME**, the 2D NMR profile is presented in Figure 3.3. Intense cross peaks are observed between the phenyl residues (green outline in Figure 3.3) and the internal protons of the **$\beta$-DIME** (red outline).

For the imidazolium protons only very weak cross peaks are observed. This observation demonstrates the formation of a "host-guest" complex between the **$\beta$-DIME** and **[3][Br]$_2$** by complexation of the aromatic residue inside the **CD**'s cavity [23, 24]. However, the geometry of complexation is unclear because the protons of the aromatic residue give cross peaks with the OMe of the wide and narrow rims of the **CD**. Similar

ROESY spectra are observed for the other diimidazolium salts. In fact, the complexation occurs primarily on the aromatic group of **[2][Br]$_2$** and **[3][Br]$_2$** for all hosts tested in this study.

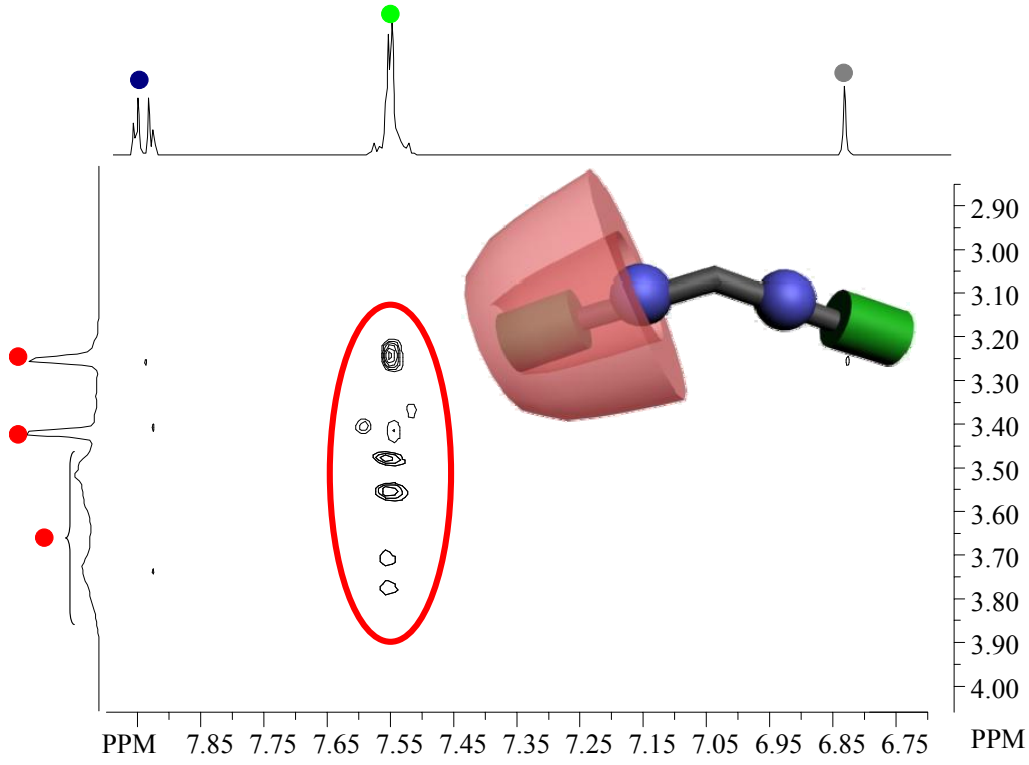


**Figure 3.3.** Partial 2D ROESY NMR spectra for an equimolar mixture of **[3][Br]$_2$** and ***β*-DIME** in $D_2O$ at 298 K (4 mM).

The association constants between the different hosts and the diimidazoium bromides, as well as the stoichiometry (obtained respectively by $^1$H NMR titration or by the integration method in the case of the slow exchange and by Job's plot methods; see Supporting Information) are presented in Table 3.1. As it was stated above, native **CD**s rarely form complexes with dicationic species. Moreover, the values of the association constants obtained for **CB[7]** with all the three diimidazolium salts demonstrate that the association with the aromatic residue is also more favored than the association with the dicationic site. The association constants of **CB[7]** and ***β*-CD** with **[2][Br]$_2$** and **[3][Br]$_2$** are

more important than the values obtained with **[1][Br]$_2$**. This observation allows us to see the aromatic disubstituted diimidazolium salts as guests presenting two different binding sites: (i) the external aromatic residues (the most favored site for all hosts) and (ii) the central diimidazolium dication (the most unfavored site). This last site is obviously disadvantaged; (i) kinetically it is accessed more slowly than the other site (as the equilibrium is slow on the NMR time scale) and (ii) thermodynamically it is more unfavored than the aromatic residue (comparing the association constant values). Employing these guests with two different binding sites, it becomes challenging to hold **CD** and **CB[7]** in one supramolecular architecture, using one favored and one unfavored binding site.

**Table 3.1.** Association constants for various macrocycles with diimidazolium salts

(all equilibria are fast exchange on the NMR timescale excepted for [b] and the stoichiometry is 1:1 type except for [e]; for the method to measure equilibrium constant, see reference 23)[a]

| | **[1][Br]$_2$** $K_{ass}$ ($M^{-1}$) | **[2][Br]$_2$** $K_{ass}$ ($M^{-1}$) | **[3][Br]$_2$** $K_{ass}$ ($M^{-1}$) (excepted[e] in $M^{-2}$) |
|---|---|---|---|
| **CB[7]** | < 1200[b] | 4200 ± 25[d] | 2100 ± 50[d,e] |
| **β-DIME** | nd[c] | 7200 ± 50 | 3200 ± 50 |
| **β-CD** | 460 ± 10 | 6500 ± 20[d] | 3000 ± 10[d] |
| **α-CD** | nd[c] | 5100 ± 30 | 2800 ± 15 |

[a]$D_2O$, 298 K. [b]Slow exchange on the NMR timescale. [c]Not determined. [d]Results published in reference 23. [e]Apparent constant ($K_1$ x $K_2$) in $M^{-2}$ for 2:1 host/guest complexes.

The complexation of **CB[7]** and **CDs** on the same diimidazolium guest has been studied by mixing in stoichiometric proportion the two hosts and the guest (**[2][Br]$_2$** or **[3][Br]$_2$**). High resolution mass spectrometry analyses were performed for the obtained

complexes. In all cases, the high resolution mass measurements using electrospray ionization showed the formation of 1:1:1 ternary complexes at 4 mM concentration of each component (Table 3.2).

**Table 3.2.** Values of the *m*/z for various macrocycles/diimidazolium salts complexes (ESI/HRMS)[a].

| Observed charged species | *m*/z found | *m*/z calculated |
|---|---|---|
| (**[2]** + **CB[7]** + **β-DIME**)$^{2+}$ | 1387.96564 | 1387 96826 |
| (**[2]** + **CB[7]** + **β-CD**)$^{2+}$ | 1313.45012 | 1313.44832 |
| (**[2]** + **CB[7]** + **α-CD**)$^{2+}$ | 1232.42267 | 1232.42191 |
| (**[3]** + **CB[7]** + **β-DIME**)$^{2+}$ | 1383.52644 | 1383.52657 |
| (**[3]** + **CB[7]** + **β-CD**)$^{2+}$ | 1299.42793 | 1299.43267 |
| (**[3]** + **CB[7]** + **α-CD**)$^{2+}$ | 1218.40828 | 1218.41187 |

[a]ESI mass spectra were recorded with a mass spectrometer TSQ Quantum Ultra (Thermo Scientific) with accurate mass options instrument.

At first glance, it is easy to imagine the formation of ternary complexes in which one external aromatic residue is complexed by the **CD**, and the other is complexed by **CB[7]**. However, in the $^1$H NMR spectra (Figures 3.4 and 3.5) of the ternary mixture, chemical shifts of the aromatic protons of the diimidazolium cation can be observed, compared to the binary mixture. The H(2) proton for both **[2][Br]$_2$** and **[3][Br]$_2$** was not observed in $D_2O$ because of H/D exchange. However for **[2][Br]$_2$** in the binary or ternary mixture, a reappearance of H(2) is observed around 9 ppm due to the complexation [25]. Encapsulation of H(2) by the macrocycle results in the inhibition of the H(2)/D exchange in the complex. It is not the case of the binary and ternary complexes of **[3][Br]$_2$** where H(2)

was not observed. This observation suggests that the binary and ternary complexes may present different geometries, depending on the imidazolium geometry.

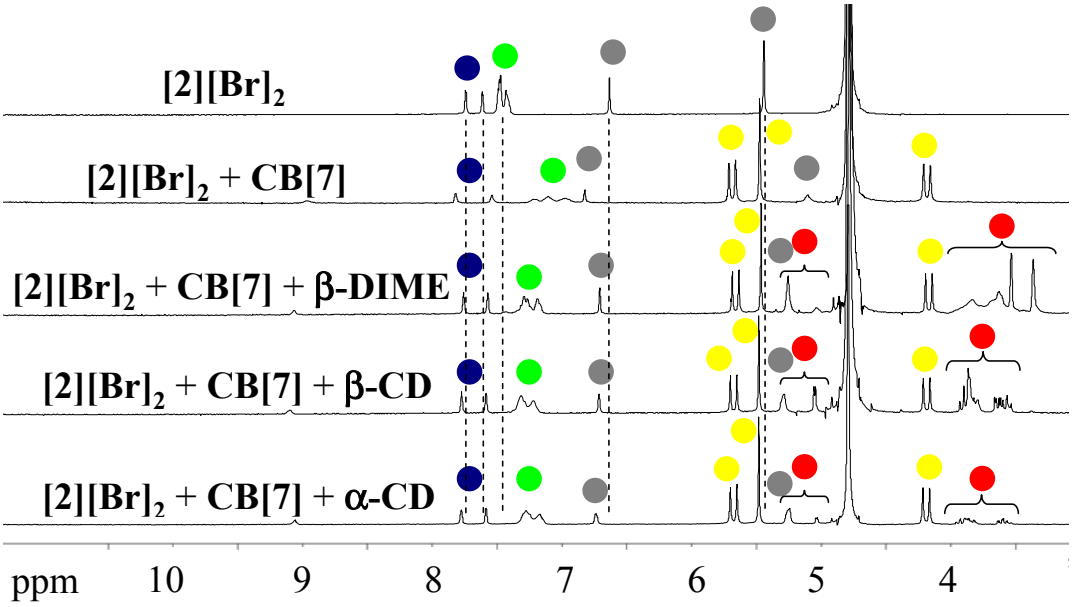


**Figure 3.4.** $^{1}$H NMR spectra at 298 K in $D_2O$ of an equimolar solution (4mM) of **[2][Br]$_2$** with various hosts (**CD**s and/or **CB[7]**).

The aromatic protons of **[2][Br]$_2$** or **[3][Br]$_2$** shift upfield in the binary mixtures with **CB[7]**, which is consistent with the formation of an inclusion complex between the aromatic residue and the electron rich inner cavity of the **CB[7]**. When the **CD** is added, the protons of the aromatic residue shift downfield compared to the binary mixture of **CB[7]**. The downfield shift observed in the ternary complexes is indicative of the positioning of the aromatic residues in a hydrophobic environment, consistent with the positioning inside the **CD**'s cavity. The NMR spectra shown in Figures 3.4 and 3.5 cannot be explained by the presence of equilibria between binary complexes. If we compare the chemical shifts of free CB[7]'s protons and those of the binary mixtures of **CB[7]** and **[3][Br]$_2$** the signal shows a 0.05 ppm upfield in the binary mixture; addition of the ***β*-DIME** to this binary mixture leads to supplementary 0.05 ppm upfield, due to the change on the binding sites of

**CB[7]**. In the case of binary mixtures of ***β*-DIME** and **[3][Br]$_2$**, the ***β*-DIME**'s signals shift 0.1 ppm upfielded and the same chemical shift is observed for the ternary mixture, as the complexation occurs on the same binding site (see Supporting Information).

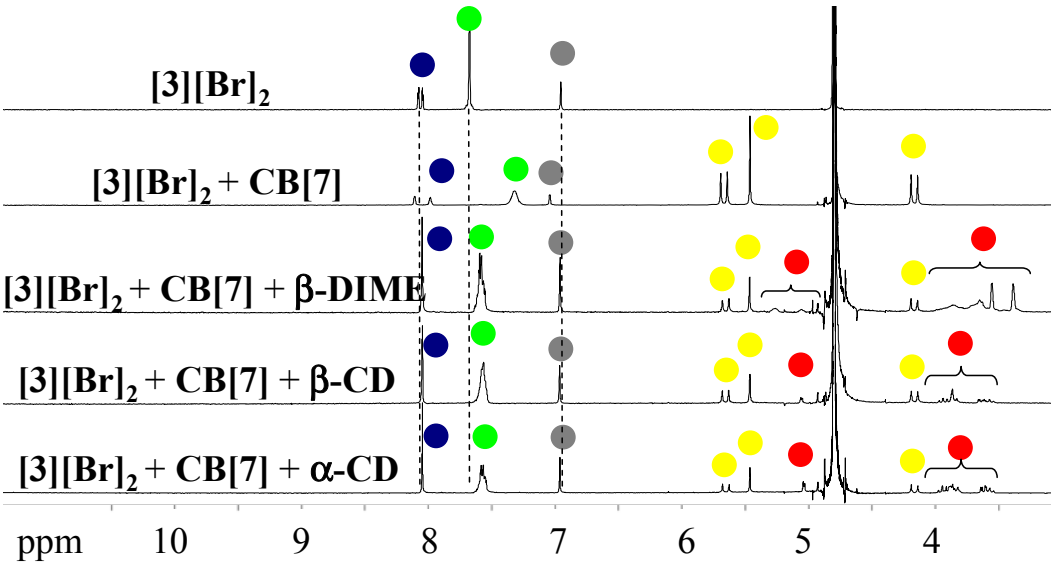


**Figure 3.5.** $^1$H NMR spectra at 298 K in $D_2O$ of an equimolar solution (4mM) of **[3][Br]$_2$** with various hosts (**CD**s and/or **CB[7]**).

To gain further insight into the geometry of the inclusion complexes, we performed 2D ROESY studies for all ternary complexes. In Figure 3.6, we present an example of ROESY spectrum, the partial profile obtained for an equimolar mixture of (a) **[3][Br]$_2$** and **CB[7]**, and (b) **[3][Br]$_2$**, **CB[7]**, and ***β*-DIME**. The spatial distance must be less than 5 Å to observe cross peaks between two nuclei. In the case of the binary complex, cross peaks are observed only between H(aro) of **[3][Br]$_2$** (green outline) and the **CB[7]** protons (yellow outline). In the case of the ternary complex, intense cross peaks can be observed between the H(aro) of **[3][Br]$_2$** (green outline) and the internal protons of the ***β*-DIME** (red outline). On the other hand, cross peaks can be observed between the protons of the **CB[7]** (yellow outline) and the H(4) and H(5) of **[3][Br]$_2$** (blue outline). These cross peaks provide evidence of the inclusion of the ***β*-DIME** and the **CB[7]** on the two different binding sites.

However, the geometry of complexation is unclear because the H(aro) give cross peaks with the OMe of the wide and narrow rims of the ***β*-DIME**.

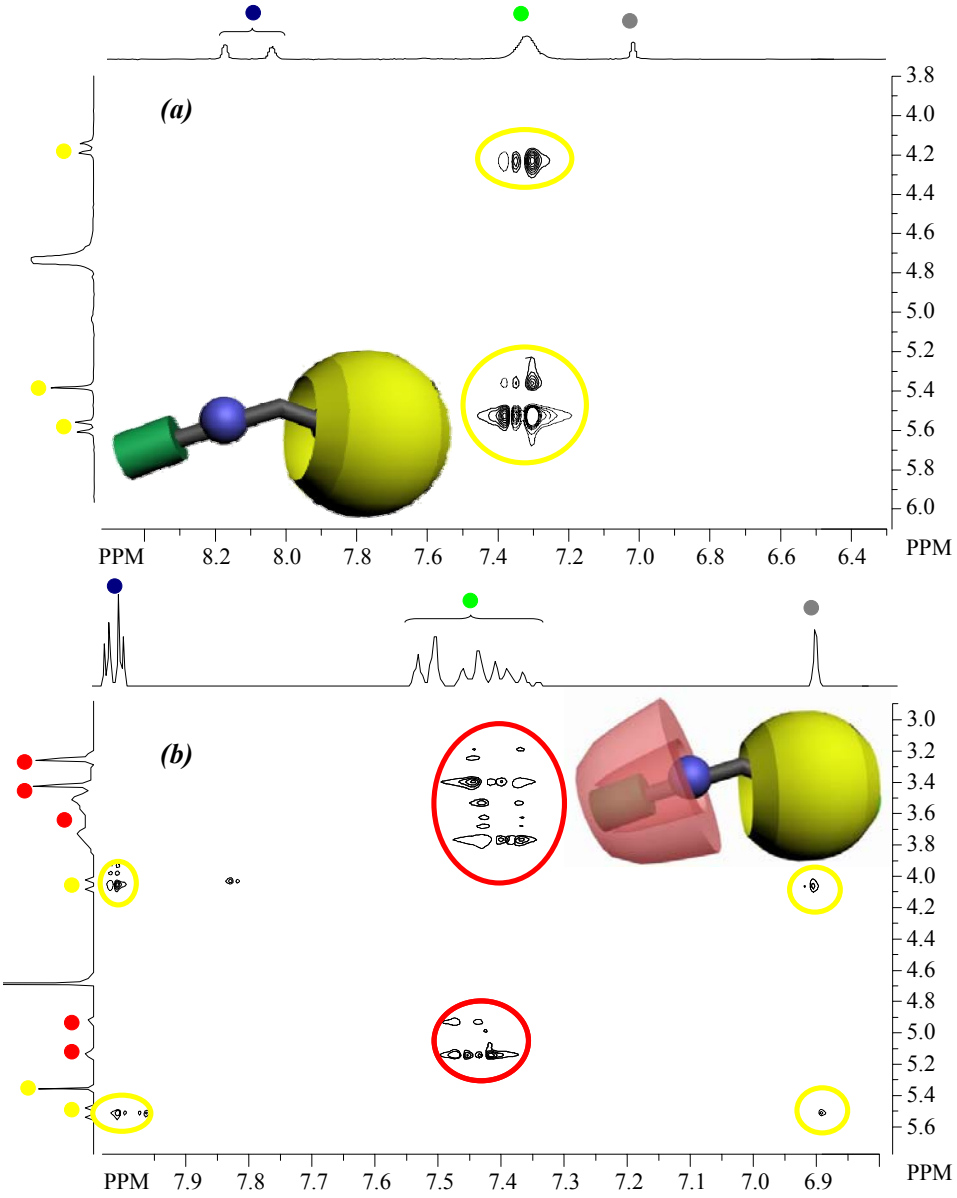


**Figure 3.6.** Partial ROESY NMR spectra for: (a) an equimolar mixture of **[3][Br]$_2$** and **CB[7]** in $D_2O$ at 298 K (4 mM); an equimolar mixture of **[3][Br]$_2$**, **CB[7]** and ***β*-DIME** in $D_2O$ at 298 K (4 mM).

It is important to note that an interaction between H(aro) of **[3][Br]$_2$** and the external proton of **CB[7]** can be observed in the binary mixture. This interaction can be seen as a proximity inetraction, where a free **CB[7]** can be close enough to **[3][Br]$_2$** to observe the correlation. This interaction is not seen in the ternary complex, where only the peaks corresponding to the cavity edges of **CB[7]** present an interaction with H(4) and H(5) of **[3][Br]$_2$**. This observation can suggest a higher stability of the ternary complex, where the binding cooperativity of the two macrocycles provide a slower decomplexation process.

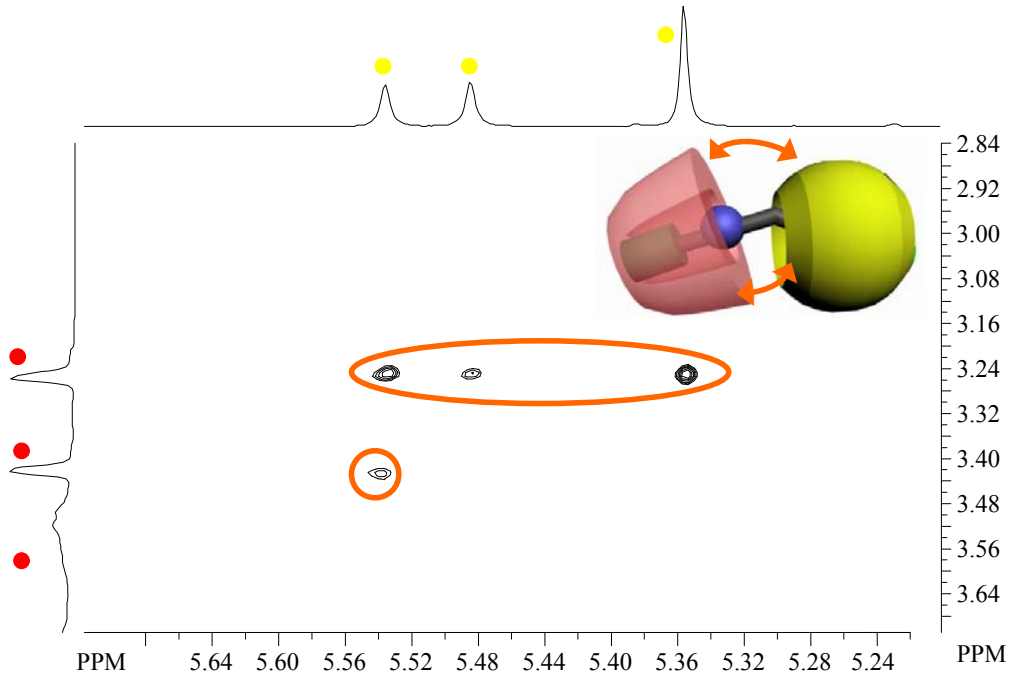


**Figure 3.7.** Partial 2D ROESY NMR spectra for an equimolar mixture of **[3][Br]$_2$**, **CB[7]** and ***β*-DIME** in $D_2O$ at 298 K (4 mM).

Moreover, for the ***β*-DIME** (red circles) clear cross-peaks can be observed between the **CD**'s methyl protons and **CB[7]** protons (yellow circles) in the ROESY spectra of the ternary complex (Figure 3.7). In the absence of diimidazolium salt, no interaction between the ***β*-DIME** and the **CB[7]** can be observed in an equimolar mixture in $D_2O$ (see

Supporting Information, Figure S15). These cross-peaks provide evidence for the two macrocycles being closely located in the ternary complex and suggest multiple point interactions (most likely multiple hydrogen bonds) leading to position **CB[7]** on the diimidazolium cation, the initially unfavored binding site. Thus, the stability of the ternary complex is determined not only by the inclusion of the aromatic residues by the macrocycles, but most importantly, by the **CD**-**CB** interactions. Plausible structures of the ternary complexes were obtained by molecular dynamics (MD) simulations. The MD simulations of binary and ternary host-guest complexes in aqueous solution were carried out in a cubic simulation box with periodic boundary conditions in all directions. For each host/guest complex, several 100 ps runs were performed with different initial relative orientations. In most cases the guest enters the host within the first 20 ps of the simulation run and remains in a stable position. The initial geometries of **CD**s were built and then fully optimized by PM3 method without any symmetrical restrictions. All guest molecules were also fully optimized by PM3.

As shown in Figure 3.8, the complexation process was simulated by making **[2][Br]$_2$** and **[3][Br]$_2$** penetrate into the cavity of the **CD** from the wider rim on one extremity and into the **CB[7]** cavity at the other extremity. The conformations with the lowest-energy of each complex during the MD simulations give visual information on the possible binding geometries of the inclusion complexes (Figure 3.8). A difference between the ternary complexes of **[2][Br]$_2$** and **[3][Br]$_2$** can be discussed relative to the CB[7] position. In the case of **[2][Br]$_2$**, **CB[7]** is positioned symmetrically around the dicationic binding site. This is due to the relative position of the **CD** on the external benzyl group: only the aromatic ring is included the cavity. In the case of **[3][Br]$_2$**, due to the linear geometry of the phenyl group, a deeper inclusion of the aromatic ring in the **CD**'s cavity can be observed and a asymmetrical positioning of **CB[7]** around the diimidazolium site is obtained. These subtle differences on the **CB** positions could explain different behavior of the H(4) and H(5) (blue outlines in Figures 3.4 and 3.5) in the 1D NMR spectra, where a more symmetrical environment on the diimidazolium motive could explain the quasi-fusion of the two protons (see Figure 3.5). These proposed structures can also explain the different

behavior of H(2) protons in the ternary complexes: in the case of **[2][Br]$_2$**, **CB[7]** is positioned symmetrically around the diimidazolium, providing a hydrophobic environment and preventing the H/D exchange; in the case of **[3][Br]$_2$**, **CB[7]** cannot fully protect the penetration of solvent molecules between the two macrocycles, as they are more distant in this case.

A)

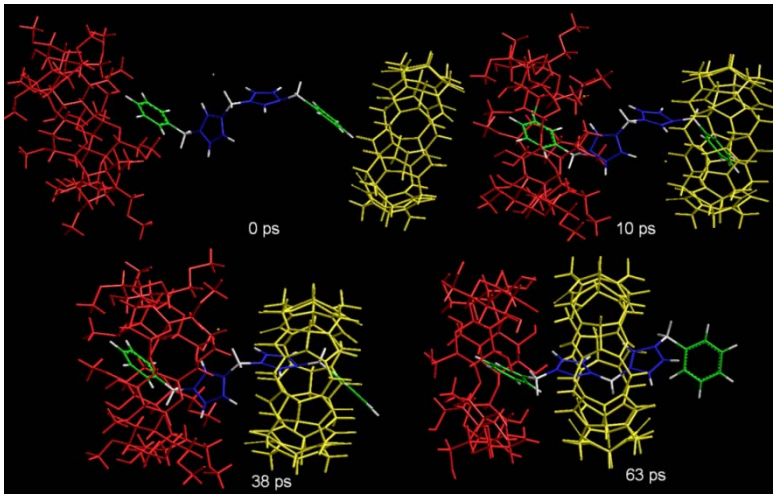


B)

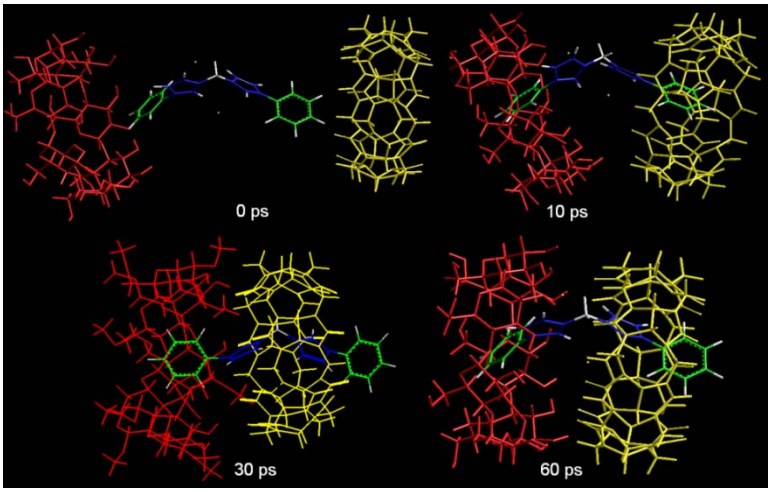


**Figure 3.8.** Snapshots of the MD simulation of (A) **[2][Br]$_2$**, **CB[7]** and ***β*-DIME** in water; (B) **[3][Br]$_2$**, **CB[7]**, and ***β*-DIME** in water. Water molecules have been removed for clarity.

### 3.4.2 Influence of β-CD and/or CB[7] on $[2][Br]_2$ and $[3][Br]_2$ Surface-Active Properties

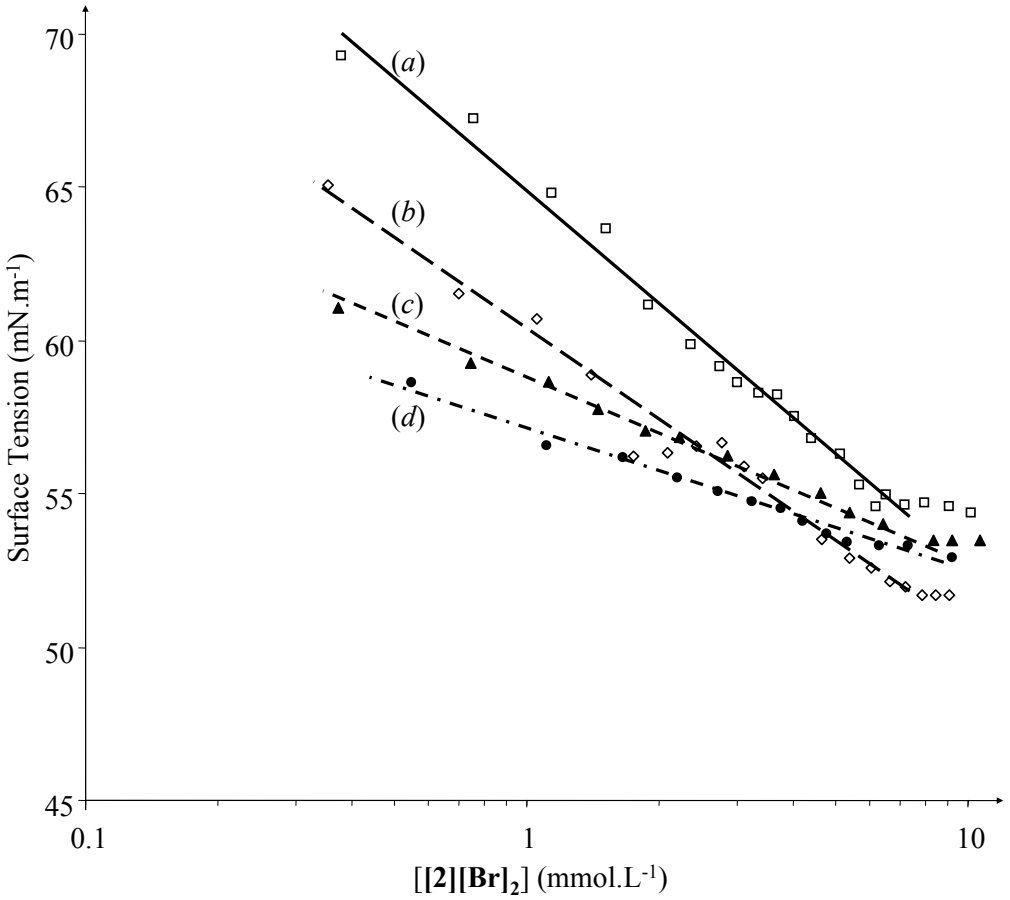


**Figure 3.9.** Surface tension (σ) variations of aqueous solutions of **$[2][Br]_2$** at 298 K without (a) and in the presence of **CB[7]** (b); in the presence of **β-CD** (c); in the presence of **β-CD** and **CB[7]** (d). Surface tensions correspond to at-equilibrium values recorded within time ranges from 1 to 20 min depending on the surfactant concentrations in the subphase. The solid, dotted and dashed lines indicate Gibbs absorption isotherm fitted by eq (1). Concentrations of **β-CD** and/or **CB[7]** in the subphase are 0.5 mM.

It was shown that imidazolium salts with a long alkyl chain group exhibited surface active property in their aqueous solutions, and these imidazolium surfactants have been

investigated by surface tension measurements [26]. Herein, the surface tensions in aqueous solutions should be distinctly affected by the different binary or ternary complexes formed at equilibrium. Variations of air-water interfacial tension ($\sigma$) for **[2][Br]$_2$** or **[3][Br]$_2$** aqueous solutions as a function of the natural logarithm of total **[2][Br]$_2$** or **[3][Br]$_2$** concentration in the aqueous subphase are shown in Figure 3.9 or 3.10, either without or in the presence of **$\beta$-CD** and/or **CB[7]**.

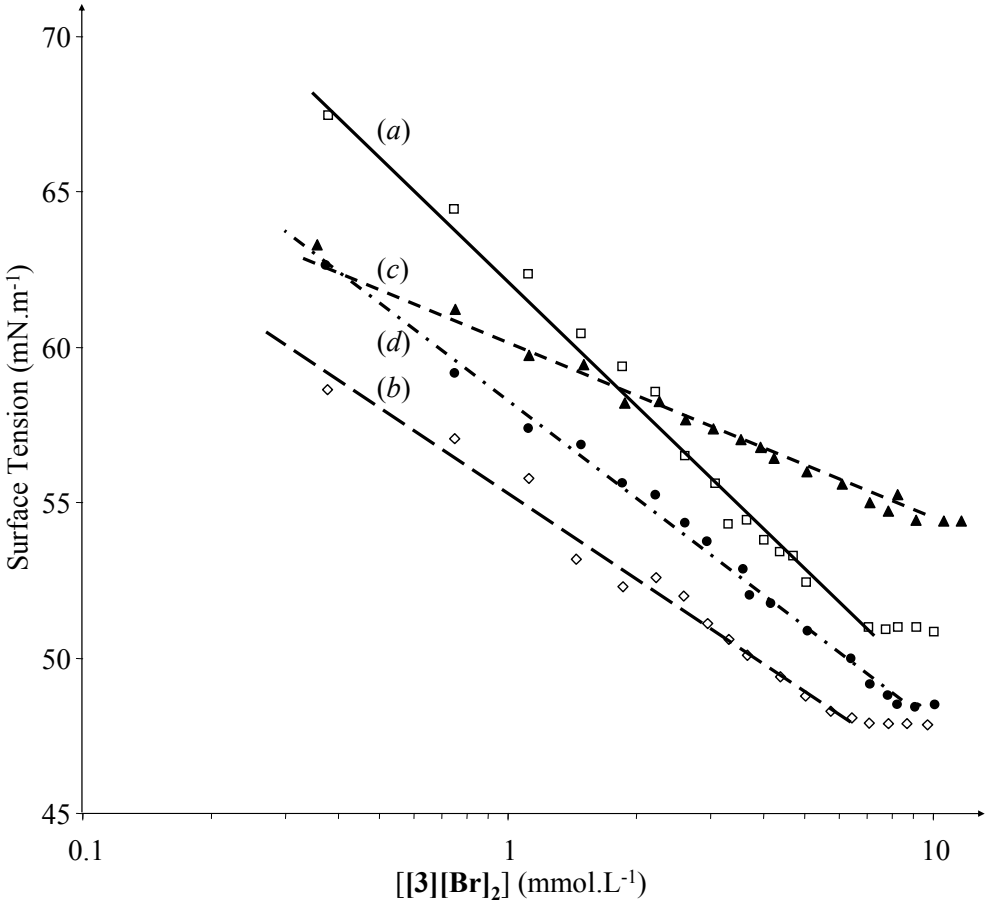


**Figure 3.10.** Surface tension ($\sigma$) variations of aqueous solutions of **[3][Br]$_2$** at 298 K without (a) and in the presence of **CB[7]** (b); **$\beta$-CD** (c); **$\beta$-CD** and **CB[7]** (d). Surface tensions correspond to at-equilibrium values recorded within time ranges from 1 to 20 min depending on the surfactant concentrations in the subphase. The solid, dotted and dashed lines indicate Gibbs absorption isotherm fitted by eq (1). Concentrations of **$\beta$-CD** and/or **CB[7]** in the subphase are 0.5 mM.

In the absence of **β-CD** and/or **CB[7]** (Figures 3.9a and 3.10a), the profile of $\sigma$ versus ln[diimidazolium salt] curve is typical of a soluble amphiphilic surfactant. In fact, at very low diimidazolium salt concentration, from 0.4 to 6 mM, the surface tension is falling almost linearly with increasing ln *c*, indicating that diimidazolium salts are being adsorbed at the air-water interface and significantly lowering the interfacial free energy. This behavior is limited to a maximum diimidazolium salt concentration from which the surface tension reaches a limiting value that does not change appreciably even though the diimidazolium concentration in the aqueous phase is further increased. This critical diimidazolium concentration in the solution coincides with the saturation of both the interface and the subphase by diimidazolium molecules. It is obvious that these **[2][Br]$_2$** and **[3][Br]$_2$** diimidazolium salts do not assemble into micelles due to their architectural design. No critical micelle concentration (cmc) of any of the diimidazolium bromides in water are observed. The experiments reported in Figures 3.9 and 3.10 were performed in such conditions, as the surface tension of each solution was measured as a function of time, until an equilibrium value was reached. The equilibrium setting time for the diimidazolium solutions studied was found in the 1 to 10 min range. We noted that for aqueous solution with **β-CD** and/or **CB[7]** the time to reach the equilibrium increased to 20 min. The difficulty of monolayer stabilization at air-water interface is characteristic of formation of inclusion complexes with water soluble macrocycles. The occupied molecular area (*A*) at the air-water interface can be calculated according to Gibbs adsorption isotherm equation (1) [27].

$$\Gamma = -\frac{1}{nRT}\left(\frac{\partial\gamma}{\partial lnc}\right)[mol.m^{-2}] \qquad (1)$$

Γ is equal to the number of moles of diimidazolium salt adsorbed at the air-water interface per unit area, *R* is the gas constant, *T* is the absolute temperature (here 298 K), and *c* the diimidazolium salt concentration in the subphase with $n = 1$. The diimidazolium salt molecular area is deduced from Γ according to (2)

$$A = \frac{10^{20}}{N\Gamma}[\text{Å}^2] \qquad (2)$$

where $N$ is Avogadro's number. Linear regression analysis (correlation coefficient > 0.97) of the $\sigma$ versus ln $c$ straight lines led to numerical equations, and from equations 1 and 2 the occupied molecular area at the air-water interface was determined and presented in Table 3.3.

**Table 3.3.** Surface excess (Γ; $\mu$mol.m$^{-2}$) and molecular occupied area (A; Å$^2$) for **[2][Br]$_2$** and **[3][Br]$_2$** with or without additives (**CB[7]** and **β-CD**) at 298 K[a]

| | **Additives** | | | | | | | |
|---|---|---|---|---|---|---|---|---|
| | None | | **CB[7]** | | **β-CD** | | **CB[7] + β-CD** | |
| | Γ | A | Γ | A | Γ | A | Γ | A |
| **[2][Br]$_2$** | 2.133 ± 0.004 | 78 ± 2 | 1.718 ± 0.005 | 97 ± 2 | 1.052 ± 0.006 | 158 ± 2 | 0.799 ± 0.009 | 208 ± 2 |
| **[3][Br]$_2$** | 2.374 ± 0.004 | 70 ± 2 | 1.598 ± 0.006 | 104 ± 2 | 1.125 ± 0.007 | 148 ± 2 | 2.201 ± 0.005 | 75 ± 2 |

[a]Obtained from Gibbs eq. and the Wilhelmy plate method at the air-water interface [27].

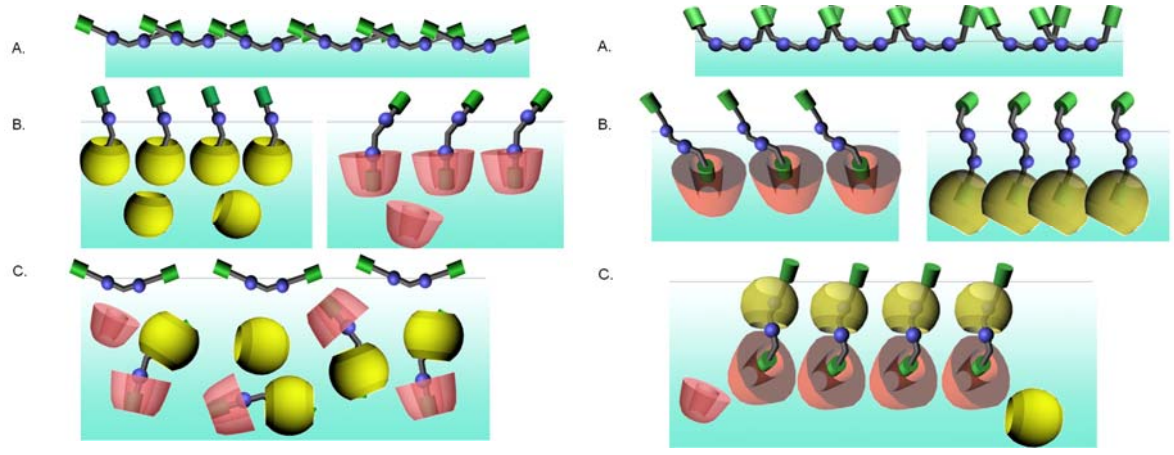


**Figure 3.11.** Schematic representation of **[3][Br]$_2$** (left) and **[2][Br]$_2$** (right) at air-water interface. (A) without macrocycle; (B) in the presence of **CB[7]** or **β-CD**; (C) in the presence of a mixture of **β-CD/CB[7]**.

In the absence of the macrocycle, the occupied molecular area is found equal to 70-78 $Å^2$, which is consistent with a monolayer arrangement of the diimidazolium molecules having closely packed in bent form the diimidazolium unit in water and the uncharged aromatic rings extended into the air phase quasi-perpendicular to the interface (Figure 3.11). Addition of both **β-CD** or **CB[7]** induces a shift of the $\sigma$ versus ln $c$ curves. The presence of the macrocyclic host modifies the number of molecules adsorbed at the air/water interface. The presence of **β-CD** or **CB[7]** induces an increase of the occupied molecular area at air/water interface. Taking into account that **β-CD** and **CB[7]** are not surface-active [28], they cannot replace the diimidazolium cations at the air-water interface. Therefore, **β-CD** and **CB[7]** contribute to the depletion and/or the modification of the diimidazolium salts at the interface. This is an indication of the formation of binary complexes of the diimidazolium bromides with **β-CD** and **CB[7]**. This fully agrees with the NMR studies, illustrating that the binary complexes are formed by the inclusion of the aromatic unit of the diimidazolium salts in the macrocyclic cavity. More interestingly, a different behavior is observed for **[2][Br]$_2$** and **[3][Br]$_2$** in the presence of **β-CD** and **CB[7]** mixture. The occupied molecular areas for the ternary complexes formation at the air/water interface are completely different, compared to those of the binary complexes. This means that macrocycles effectively act on the diimidazolium salts and a rearrangement occurs at the interface. In the case of **[2][Br]$_2$**, the higher occupied molecular area is due to a perpendicular geometry of the diimidazolium molecules, imposed by the presence of both macrocycles. In the case of the most linear diimidazolium salt, **[3][Br]$_2$/β-CD/CB[7]**, the ternary complex is completely surface inactive. The surface is only composed by **[3][Br]$_2$** molecules, exactly as in the absence of macrocycles. Processes on the surface modification in the presence of **β-CD** and **CB[7]** are summarized in Figure 3.11. These surface tension measurements are in good agreement with the proposed geometry of the ternary complexes obtained by molecular modeling. In the case of the more linear **[3][Br]$_2$**, the ternary complex hides almost the entire molecule in the deeper inclusion complex. In the ternary

complex **[2][Br]$_2$/$\beta$-CD/CB[7]**, the geometry of the imidazolium molecule does not allow its total inclusion and one aromatic unit is still exposed to the aqueous environment.

## 3.5 Conclusions

In conclusion, aromatic disubstituted diimidazolium salts have been used as guest for the assembly of ternary complexes with **CB[7]** and different **CDs**. The synergistic formation of ternary **CB[7]/CDs**/diimidazolium dibromide complex occurs through a higher order complexation for all the **CDs** used in this study. The supramolecular positive cooperativity allows the positioning of **CB[7]** on the initially unfavored dicationic binding site of the diimidazolium cation. Interfacial properties of the binary and the ternary complexes are different, depending on the diimidazolium salt. The geometry of the diimidazolium salt controls position of **CB[7]** in the complex and its surfactant properties. Work is under development in our laboratory in order to use this cooperativity in the construction of more complex architectures by controlling the exact positioning of **CB** and **CDs** for various interface applications. The air/water interface provides a good platform to construct supramolecular assemblies in this case, as the orientation and packing of the diimidazolium salts and their complexes can be arranged in a controlled manner.

## 3.6 Acknowledgment.

We are grateful to the Natural Sciences and Engineering Research Council of Canada, the Fonds Québécois de la Recherche sur la Nature et les Technologies, the Canada Foundation for Innovation, and Université de Montréal for financial support. We thank Dr. Alexandra Furtos and Karine Venne for mass spectrometry analysis. We also thank colleagues for careful reading and discussion of this manuscript.

## 3.7 Supporting information available

Synthesis, example of ESI/HRMS, 2D NMR ROESY, and MD simulation trajectory. This material is available free of charge via the Internet at http://pubs.acs.org.

## 3.8 References and notes

1 (a) Oshovsky, G. V.; Reinhoudt, D. N.; Verboom, W. *Angew. Chem. Int. Ed.* **2007**, *46*, 2366. (b) Lehn, J. M. In *Supramolecular Chemistry, Concepts and Perspectives*; Ute, A. Ed.; VCH, Weinheim, Germany, 1995.

2 Szejtli, J.; Osa, T. In *Comprehensive Supramolecular Chemistry, (Cyclodextrins)*; Atwood, J. L., Davies, J. E. D., Macnicol, D. D., Vo¨gtle, F., Eds.; Elsevier: Oxford, 1996; Vol. 3.

3 Lindoy, L. F.; Atkinson I. M. In *Self-Assembly in Supramolecular Systems*; Stoddart, J. F., Ed.; The Royal Society of Chemistry: Cambridge, England, 2000.

4 Cram, D. J. *Nature* **1992**, *356*, 29–36.

5 Escuder, B.; Rowan, A. E.; Feiters, M. C.; Nolte, R. J. M. *Tetrahedron* **2004**, *60*, 291–300.

6 Mulder, A.; Huskens, J.; Reinhoudt, D. N. *Org. Biomol. Chem.* **2004**, *2*, 3409–3424.

7 Mammen, M.; Choi, S.-K.; Whitesides, G. M. *Angew. Chem., Int. Ed. Engl,.* **1998**, *37*, 2755–2794.

8 Whitesides, G. M.; Mathias, J. P.; Seto, C. T. *Science* **1991**, *254*, 1312–1319.

9 (a) Harada, A. In *Large Ring Molecules*; Semlyen, J. A., Ed.; J. Wiley & Sons Ltd.: Chichester, England, 1996; pp 407-432. (b) Rekharsky, M. V.; Inoue, Y. *Chem. Rev.* **1998**, *98*, 1875–1918.

10 (a) Liu, L.; Guo, Q.-X. *J. Incl. Phenom. Macrocyclic Chem.* 2002, 42, 1–14. (b) Shinkai, S. Tetrahedron 1993, 49, 8933–8968. (c) Buschmann, H.-J.; Schollmeyer, E.; Mutihac, L. *Biol. J. Arm.* 2001, 50, 58–63.

11 Stoddart, J. F. *Angew. Chem., Int. Ed. Engl.* **1992**, *31*, 846–847.

12 (a) Harada, A. *Coord. Chem. Rev.* **1996**, *148*, 115–133. (b) Castronuovo, G.; Elia, V.; Fessas, D.; Giordano, A.; Velleca, F. *Carbohydr. Res.* **1995**, *272*, 31–39. (c) Rontoyianni, A.; Mavridis, I. M. *Supramol. Chem.* **1999**, *10*, 213–218. (d) Eliadou, K.; Yannakopoulou, K.; Rontoyianni, A.; Mavridis, I. M. *J. Org. Chem.* **1999**, *64*, 6217–6226.

13 When the guest species is longer than the central axis of the CD host, the latter may be viewed as "threaded" onto the former, and to be in accord with the current usage we have adopted the term "threading" in place of "inclusion".

14 (a) Harada, A.; Kamachi, M. *Macromolecules* **1990**, *23*, 2821– 2823. (b) Wenz, G.; Keller, B. *Angew. Chem., Int. Ed. Engl.* **1992**, *31*, 197–199.

15 Nepogodiev, S. A.; Stoddart, J. F. *Chem. Rev.* **1998**, *98*, 1959– 1976.

16 Herrmann, W.; Keller, B.; Wenz, G. *Macromolecules* **1997**, *30*, 4966–4972.

17 (a) Wenz, G. *Angew. Chem., Int. Ed. Engl.* **1994**, *33*, 803–822. (b) Connors, K. A. *Chem. Re*V. **1997**, *97*, 1325–1358. (c) Rekharsky, M. V.; Inoue, Y. *Chem. Re*V. **1998**, *98*, 1875–1918. (d) Szejtli, J. *Chem. Rev.* **1998**, *98*, 1743–1754.

18 (a) Inoue, Y.; Hakushi, T.; Liu, Y.; Tong, L.-H.; Shen, B.-J.; Jin, D.-S. *J. Am. Chem. Soc.* **1993**, *115*, 475–481. (b) Inoue, Y.; Liu, Y.; Tong, L.-H.; Shen, B.-J.; Jin, D.-S. *J. Am. Chem. Soc.* **1993**, *115*, 10637–10644.

19 For reviews, see: (a) Mock, W. L. In *Comprehensive Supramolecular Chemistry*; Vögtle, F., Ed.; Pergamon: Oxford, 1996; Vol. 2, p 447.

(b) Cintas, P. *J. Inclusion Phenom.* **1994**, *17*, 205–220. (c) J, W.; Samal, S.; Selvapalam, N.; Kim, H.-J.; Kim, K. *Acc. Chem. Res.* **2003**, *36*, 621–630. (d) Kim, K.; Kim, H.-J. In *Encyclopedia of Supramolecular Chemistry*; Atwood, S., Ed.; Marcel Dekker

Inc.: New York, 2004; p 390. (e) Kim, K.; Selvapalam, N.; Oh, D.-H. *J. Inclusion Phenom.* **2004**, *50*, 31–36.

20 (a) Liu, Y.; Ke, C.-F.; Zhang, H.-Y.; Wu, W.-J.; Shi, J. *J. Org. Chem.* **2007**, *72*, 280–283. (b) Ooya, T.; Inoue, D.; Choi, H. S.; Kobayashi, Y.; Loethen, S.; Thompson, D. H.; Ho Ko, Y.; Kim, K.; Yui, N. *Org. Lett.* **2006**, 3159–3162. (c) Chakrabarti, S.; Mukhopadhyay, P.; Lin, S.; Isaacs, L. *Org. Lett.* **2007**, 2349–2352. (d) Zou, D.; Andersson, S.; Zhang, R.; Sun, S.; Åkermark, B.; Sun, L. *Chem. Commun.* **2007**, 4734–4737. (e) Liu, Y.; Li, X.-Y.; Zhang, H.-Y.; Li, C.-J.; Ding, F. *J. Org. Chem.* **2007**, *72*, 3640–3645.

21 (a) Li, N.; Liu, J.; Zhao, X.; Gao, Y.; Zheng, L.; Zhang, J.; Yu, L. *Colloids Surf., A* **2007**, *292*, 196–201. (b) Gao, Y.-A.; Li, Z.-H.; Du, J.-M.; Han, B.-X.; Li, G.-Z.; Hou, W.-G.; Shen, D.; Zheng, L.-Q.; Zhang, G.-Y. *Chem. Eur. J.* **2005**, *11*, 5875–5880. (c) Gao, Y.-A.; Zhao, X.; Dong, B.; Zheng, L.-Q.; Li, N.; Zhang, S. *J. Phys. Chem. B* **2006**, *110*, 8576–8581.

22 Rohrbach, R. P.; Rodriguez, L. J.; Eyring, E. M.; Wojcik, J. F. *J. Phys. Chem.* **1977**, *81*, 944–948.

23 Noujeim, N.; Leclercq, L.; Schmitzer, A. R. *J. Org. Chem.* **2008**, *73*, 3784–3790.

24 Schneider, H. J.; Hacket, F.; Rüdiger, V.; Ikeda, H. *Chem. Rev.* **1998**, *98*, 1755–1786.

25 Wang, R.; Yuan, L.; Macartney, D. H. *Chem. Commun.* **2006**, 2908– 2910.

26 (a) Anderson, J. L.; Ding, R.; Ellern, A.; Armstrong, D. W. *J. Am. Chem. Soc.* **2005**, 593–604. (b) Law, G.; Watson, P. R. *Langmuir* **2001**, *17*, 6138–6141.

27 Myers, D. *Interfaces and colloids, principles and applications*; VCH Publishers, Inc.: New York, 1991.

28 (a) Szejtli, J. *J. Mater. Chem* **1997**, *7*, 575–587. (b) Yoshihiro, S.; Haruhisa, U.; Masahiko, A.; Takatoshi, S.; Sherril, D. C. *Colloids Surf.* **1998**, *135*, 103–108. (c) Saenger, W.; Mueller-Farhrnow, A. *Angew. Chem., Int. Ed. Engl.* **1998**, *27*, 393–

394. (d) Leclercq, L.; Bricout, H.; Tilloy, S.; Monflier, E. *J. Colloid Interface Sci.* **2007**, *307*, 481–487.

# Chapitre 4 : Motif phénylènediimidazolium : complexes multiples en solution aqueuse et estimation de leurs constantes d'association

# 4.0 Préface

Une nouvelle famille de sels de diimidazolium a été étudiée dans ce chapitre. Les travaux rapportés ici traitent de l'étude des sels de phénylènediimidazolium et des complexes multiples formés avec le **CB[7]**. En plus de l'étude classique par RMN $^{1}$H et spectrométrie de masse à haute résolution, c'est ici une méthode d'évaluation numérique des constantes d'association dans des systèmes à complexes multiples qui a été développée. Cette étude est dans la continuité des deux articles précédents même si la classe des composés est légèrement différente.

Pour cet article publié en 2009 et qui est présenté en tant que chapitre 4 de cette thèse, j'ai réalisé toute la rédaction de l'article ainsi que toutes les études de caractérisation des complexes (RMN $^{1}$H, interprétation des spectres de masse et évaluation des constantes d'association). La synthèse des composés a été réalisée par Benjamin Jouvelet selon un protocole que j'avais mis au point au préalable.

Les informations expérimentales supplémentaires de cette partie se trouvent aux pages 218-240 de la thèse.

# Article 3. Formation of inclusion complexes between 1,1'-dialkyl-3,3'-(1,4-phenylene)bisimidazolium dibromide salts and cucurbit[7]uril

Nadim Noujeim, Benjamin Jouvelet and Andreea R. Schmitzer*

Département de chimie, Université de Montréal, CP 6128, Succursale Centre-Ville, Montréal, Québec, H3C 3J7, Canada

*Journal of Physical Chemistry B,* 2009, **113**, 16159-16168

## 4.1 Abstract

*N*,*N*'-Dialkyl-(1,4-phenylene)bisimidazolium salts form inclusion complexes with cucurbit[7]uril (**CB[7]**) with high association constants. The stoichiometry of the complexes depends on the alkyl chains and on the relative concentration of the imidazolium salt and **CB[7]**. The binding interactions of **CB[7]** with these bisimidazolium salts were studied experimentally by $^{1}$H NMR, high resolution mass spectroscopy, and UV spectroscopy, and theoretically by semiempirical molecular modeling. Nonlinear regression analysis was used to calculate or estimate the binding parameters for the supramolecular inclusion complexes present in solution. The detailed study of the binding association of these imidazolium salts may allow us to understand the exact role of each recognition site in these salts and to assemble higher supramolecular complexes.

## 4.2 Introduction

An important task in supramolecular chemistry has always been the development of simple and innovative systems to hold together separate molecules using noncovalent interactions. A wide variety of macrocycles like cryptands, crown ethers, carcerands, cyclodextrins, calixarenes, cyclophanes and cucurbiturils are known to form complexes with a wide range of guest molecules. These macrocycles are already used as building blocks for complex supramolecular assemblies [1, 2, 3, 4, 5 and 6]. In these assemblies, hydrogen bonding, π-stacking, cation-π interactions, charge transfer interactions and electrostatic interactions play the most important role in the recognition processes [7, 8 and 9].

Imidazole is already known as an effective structural unit at the active site of various proteins and nucleic acids as it plays a key role in their biological function [10]. The imidazolium cation is also known to possess ionic liquid properties [11, 12 and 13]. We previously developed a new family of guests based on methylene bisimidazolium

cations that could be included within a large variety of host macrocycles in water or in organic solvents [14]. Furthermore, these methylene bisimidazolium guests were studied in a multirecognition system involving two different hosts (one cyclodextrin and one cucurbit[7]uril) [15]. We demonstrated that methylene bisimidazolium guests possess two different binding sites, but only in the ternary complexes with a cyclodextrin and cucurbit[7]uril (**CB[7]**) the secondary binding site can be reached. In the ternary complexes, the **CB[7]** is positioned on the unfavored binding site (on the methylene spacer between the two imidazolium moieties), while the cyclodextrin is exclusively located on one of the external aromatic groups (Figure 4.1). As an extension of our previous work, we have inverted the order of the recognition sites, by placing a phenylene unit between the two alkyl-substituted imidazolium units.

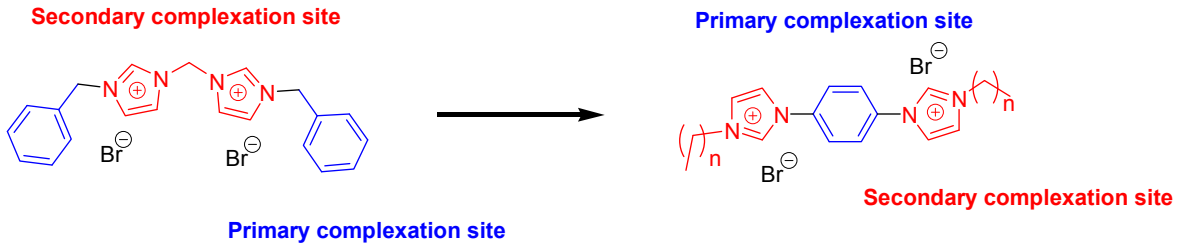


**Figure 4.1.** Methylene bisimidazolium guests previously studied (left); Phenylene bisimidazolium guests used in this study (right)

We focus in this paper on the supramolecular interactions between dialkyl-substituted phenylene bisimidazolium salts and **CB[7]** (Figure 4.2). The different complexes obtained in aqueous solution were studied by NMR spectroscopy, UV spectroscopy, and high resolution mass spectroscopy. The stability of the different inclusion complexes was evaluated by molecular dynamics followed by a semiempirical calculation. The intimate knowledge of the complexation equilibria of these imidazolium salts with **CB[7]** provides useful information for the understanding of each recognition unit

in these systems and how they can be used for the formation of higher supramolecular complexes.

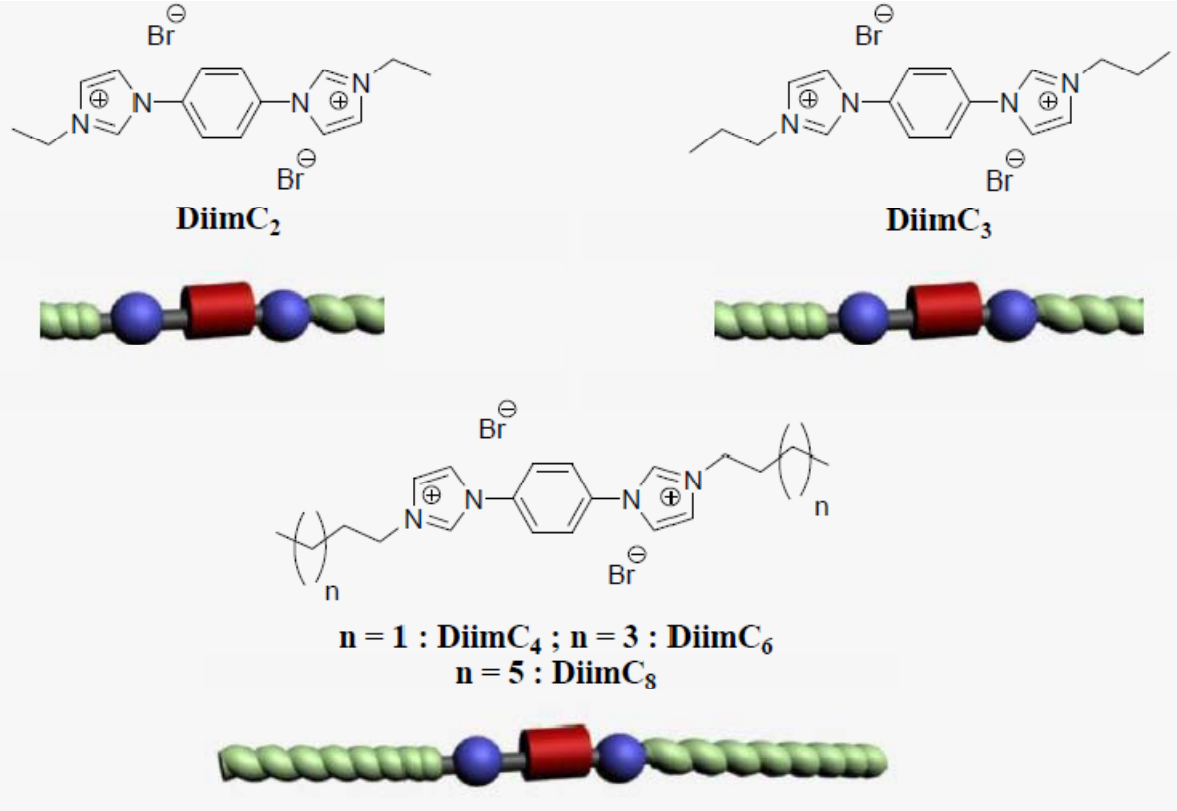


**Figure 4.2.** Bisimidazolium cations used in this work and their schematic representation

The binding parameters were calculated for the complex **DiimC$_2$·CB[7]** and estimated for the complexes formed between **DiimC$_3$** and **CB[7]**, by comparing theoretical and experimental values using a non-linear algorithm. For the complexes **DiimC$_4$**, **DiimC$_6$**, **DiimC$_8$** with **CB[7]**, too many binding parameters are involved and the precise determination of the binding constants is too complex. However, the interpretation of the UV-visible titration curves, correlated with the HR-MS data, allowed us to understand the binding equilibria in solution.

## 4.3 Experimental section

### 4.3.1 Materials

$D_2O$ (99.95% isotopic purity), $CD_3OD$ (99.95% isotopic purity), and all other chemicals were purchased from Aldrich and used without further purification.

### 4.3.2 NMR experiments

$^1H$ NMR experiments for characterization of the compounds were recorded on an Advance 400 Brücker spectrometer operating at 400 MHz. All $^{13}C$ NMR experiments were recorded on an Advance 300 Brücker spectrometer operating at 75 MHz. $^1H$ NMR complexation experiments were recorded on an Advance 700 Brücker spectrometer operating at 700 MHz. Chemical shifts are given in ppm (δ) and measured relative to the solvents residual peaks. All complexation experiments were carried out in pure deuterated water (pH = 6.5) because it is known that electrolyte ions also form complexes with **CBs** [16].

### 4.3.3 ESI/HR-MS

ESI mass spectra were recorded with a TSQ Quantum Ultra (Thermo Scientific) Mass Spectrometer with accurate mass options instrument (Université de Montréal Mass Spectrometry Facility).

### 4.3.4 UV Spectroscopy

UV absorption measurements were done on a Varian Cary-100 spectrometer using 1 cm quartz cells.

## 4.3.5 Synthesis

**1-[4-(1*H*-Imidazol-1-yl)phenyl]-1*H*-imidazole** was synthesized following a previously reported procedure [16]. The $^{1}H$ and $^{13}C$ NMR spectra of this compound were found to be in accordance with the literature.

**General procedure for the synthesis of 1,1'-dialkyl-3,3'-(1,4-phenylene)bisimidazolium *bis*(bromide) salts:** To a solution of 1-[4-(1*H*-Imidazol-1-yl)phenyl]-1*H*-imidazole (1 mmol, 210 mg, 1 eq) in acetonitrile (10 mL) was added the appropriate alkyl bromide (10 mmol, 10 eq). The solution was heated to reflux and stirred for 24 h and then filtered. The bisimidazolium salts were dried under high vacuum for 24h.

**1,1'-diethyl-3,3'-(1,4-phenylene)bisimidazolium *bis*(bromide) ($DiimC_2$):** $^{1}H$ NMR ($D_2O$, 400 MHz): $\delta$ (ppm) 9.28 (s, 2H), 7,85 (s, 2H), 7.79 (s, 4H), 7.64 (s, 2H), 4.26 (q, $J$ = 7.5 Hz, 4H), 1.48 (t, $J$ = 7.5 Hz, 6H). $^{13}C$ NMR ($D_2O$, 75 MHz): $\delta$ (ppm) 136.8, 124.8, 123.9, 122.3, 46.2, 14.8. HR-MS m/$z$ found: 134.0840 ($[M - 2Br]^{2+}$), calc: 134.0844, m.p. 284-288 °C (decomposition) (yield 85 %)

**1,1'-dipropyl-3,3'-(1,4-phenylene)bisimidazolium *bis*(bromide) ($DiimC_3$):** $^{1}H$ NMR ($CD_3OD$, 400 MHz): $\delta$ (ppm) 8.21 (d, $J$ = 2.0 Hz, 2H), 8.07 (s, 4H), 7.93 (d, $J$ = 2.0 Hz, 2H), 4.33 (t, $J$ = 7.3 Hz, 4H), 2.03 (sext, $J$ = 7.3 Hz, 4H), 1.05 (t, $J$ = 7.3 Hz, 6H). $^{13}C$ NMR ($CD_3OD$, 75 MHz): $\delta$ (ppm) 136.8, 124.8, 124.3, 122.3, 52.4, 23.8, 10.4. HR-MS m/$z$ found: 148.0995 ($[M - 2Br]^{2+}$), calc: 148.1006, m.p. > 300 °C (yield 73 %)

**1,1'-dibutyl-3,3'-(1,4-phenylene)bisimidazolium *bis*(bromide) ($DiimC_4$):** $^{1}H$ NMR ($CD_3OD$, 400 MHz): $\delta$ (ppm) 9.77 (s, 2H), 8.24 (s, 2H), 8.10 (s, 4H), 7.97 (s, 2H), 4.39 (t, $J$ = 7.3 Hz, 4H), 2.02 (quint, $J$ = 7.3 Hz, 4H), 1.49 (Sext, $J$ = 7.3 Hz, 4H), 1.06 (t, $J$ = 7.30 Hz, 6H). $^{13}C$ NMR ($CD_3OD$, 75 MHz): $\delta$ (ppm) 136.8, 124.8, 124.3, 122.3, 50.7, 32.4, 20.0, 13.2. HR-MS m/$z$ found: 162.1153 ($[M - 2Br]^{2+}$), calc: 162.1157, m.p. > 300 °C (yield 75 %)

**1,1'-dihexyl-3,3'-(1,4-phenylene)bisimidazolium *bis*(bromide):** $^{1}H$ NMR ($CD_3OD$, 400 MHz): $\delta$ (ppm) 9.77 (s, 2H), 8.24 (t, $J$ = 1.8 Hz, 2H), 8.09 (s, 4H), 7.97 (t, $J$

= 1.8 Hz, 2H), 4.38 (t, *J* = 7.4 Hz, 4H), 2.03 (quint, *J* = 6.9 Hz, 4H), 1.52-1.38 (m, 12H), 0.96 (t, *J* = 6.9 Hz, 6H). $^{13}$C NMR ($CD_3OD$, 75 MHz): $\delta$ (ppm) 136.8, 124.8, 124.3, 122.4, 51.0, 31.7, 30.4, 26.4, 22.9, 13.7. HR-MS m/*z* found: 190.1466 ($[M - 2Br]^{2+}$), calc: 190.1464, m.p. > 300 °C (yield 91 %)

**1,1'-dioctyl-3,3'-(1,4-phenylene)bisimidazolium *bis*(bromide):** $^1$H NMR ($D_2O$, 400 MHz): $\delta$ (ppm) 7,82 (s, 2H), 7.75 (s, 4H), 7.60 (s, 2H), 4.19 (t, *J* = 7.1 Hz, 4H), 1.81 (quint, *J* = 6.7 Hz, 4H), 1.26-1.08 (m, 20H), 0.70 (t, *J* = 6.6 Hz, 6H). $^{13}$C NMR ($CD_3OD$, 75 MHz): $\delta$ (ppm) 136.8, 124.8, 124.3, 122.3, 51.0, 32.4, 29.7, 29.6, 26.8, 23.2, 14.0. HR-MS m/*z* found: 218.1786 ($[M - 2Br]^{2+}$), calc: 218.1788, m.p. > 300 °C (yield 93 %)

## 4.3.6 Molecular modeling

Calculations were performed on a Windows® XP workstation with HyperChem 7.5 software [17]. The initial configurations of the bisimidazolium cations and **CB[7]** were obtained from PM3 semi-empirical calculations [18]. An initial molecular dynamics (MD) [19] run was performed, for a period of 10 ps at 300 K. This solvent equilibration phase should be sufficiently extensive to allow the solvent to readjust completely to the potential field of the solute. The cut-off for non-bonded interactions was taken to be 12 Å throughout all the simulations. We carried out high temperature annealed MD simulations starting at 1000 K (2 ps), annealing to 0 K (10 ps). The temperature of 1000 K is necessary to enable the molecule to overcome energy barriers between different conformations and to prevent the system from getting stuck in a particular region of the conformational space. Simulations at lower temperatures (500 K or 750 K) yielded in very similar conformations. The simulations in aqueous solution were relaxed using the steepest descent method until a gradient difference of 0.01 kcal/mol was reached. After energy minimization of the system at 0 K, the MD simulation was initialized using a time step of 1 fs for a time of 100 ps. The temperature was kept constant at 300 K yielding a canonical ensemble (NVT). The heat of formation for all the host: guest complexes were obtained from PM3 semi-empirical calculation.

## 4.4 Results and discussion

The synthesis of the 1,4-phenylenediimidazole **2** was carried out as described in the literature [20]. The bisimidazolium dibromide salts were obtained by a double $S_N2$ reaction involving a linear alkyl bromide and **2**. The *N,N'*-disubstituted (1,4-phenylene)bisimidazolium bromides **DiimC$_n$** were isolated in good yields, as shown in Scheme 4.1.

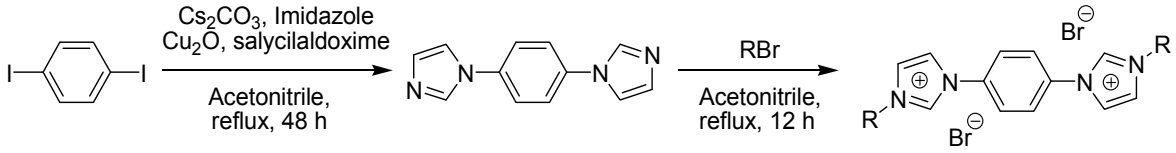


**1** **2**

**DiimC$_2$ : R = Et, 85 %**
**DiimC$_3$ : R = *n*Pr, 73 %**
**DiimC$_4$ : R = *n*But, 75 %**
**DiimC$_6$ : R = *n*Hex, 91 %**
**DiimC$_8$ : R = *n*Oct, 93 %**

**Scheme 4.1.** Synthesis of the *N,N*'-disubstituted (1,4-phenylene) *bis*imidazolium bromide salts

Titration curves for the formation of complexes between the bisimidazolium salts **DiimC$_n$** and **CB[7]** were obtained by UV-visible spectroscopy and the complexes were characterized by HR-MS and $^1$H NMR. While **DiimC$_2$** showed only the formation of a 1:1 complex with **CB[7]**, evidence of multiple complexes in solution was obtained for **DiimC$_{3-8}$** with **CB[7]**. A comparison between the experimental titration curves and a theoretical model allowed us to estimate the association constants for some of the complexes, as described below.

### 4.4.1 $^1$H NMR study of the complexation in $D_2O$

We previously studied the complexation between methylene bridged bisimidazolium salts bearing aromatic substituents and **CB[7]** [13, 14]. For the majority of the previously used guests, the complexation was fast on the NMR timescale and the binding constants were calculated for a 1:1 or a 1:2 complexation exclusively. In the case of the bisimidazolium guests studied here, two problems occurred. First, the complexation is slow on the NMR timescale. While this is usually an advantage in host-guest chemistry, as the association constants can be obtained with one experiment by integrating the peaks corresponding to the complexed and uncomplexed components, the association constant for **DiimC$_2$** is too high for an accurate measurement. Secondly, for all the other guests **DiimC$_{3-8}$**, new complexation peaks were observed after 1 equivalent of **CB[7]** was added. This observation may be attributed to the presence of multiple complexes in solution at the same time.

Nonetheless, $^1$H NMR enabled us to understand the geometry of the complexes and the positioning of the macrocyclic **CB[7]** host on the different moieties of the guest. **CB[7]** has readily interpretable $^1$H NMR signals when considering the complexed and uncomplexed protons of the guests [21]. Guest protons located within the hydrophobic cavity of the **CB[7]** are shielded (upfield shift ; $\Delta\delta < 0$), while the guest protons located at the more polar outer C=O cavity are deshielded (downfield shift ; $\Delta\delta > 0$).

Complexation of **DiimC$_2$** with **CB[7]** was the simplest equilibrium to undestand for this new family of bisimidazolium guests: in absence of **CB[7]**, the $^1$H NMR signals of the aromatic and imidazolium protons presented the expected chemical shifts [22], with $H_4$ and $H_5$ between 7.5-7.9 ppm, $H_{Ar}$ as a singlet and the imidazolium $H_2$ proton not observed because of the deuterium exchange. When 0.25 equivalent of **CB[7]** was added, peaks corresponding to the complexed and uncomplexed components were observed simultaneously for all signals (even if the $H_4$ and $H_5$ protons could not be differentiated in this complex) which demonstrated a slow complexation on the NMR timescale. Furthermore, the broadening of the signals was also indicative of slow complexation. At 1

equivalent of **CB[7]**, the peaks corresponding to the uncomplexed guest completely disappeared. An upfield shift of all the aromatic and imidazolium protons was observed, meaning that these protons are located in the hydrophobic cavity of **CB[7]**. The alkyl protons were shifted downfield, indicating that they are located in the more polar outer cavity of the **CB[7]**. No change was observed when more **CB[7]** was added, even at a high excess (more than 2 equivalents), where the same equilibrium was achieved, as no changes were observed in the $^{1}$H NMR spectra (not shown). Considering the position of the macrocycle around the guest, only a 1:1 complex can be formed between **DiimC$_2$** and **CB[7]**.

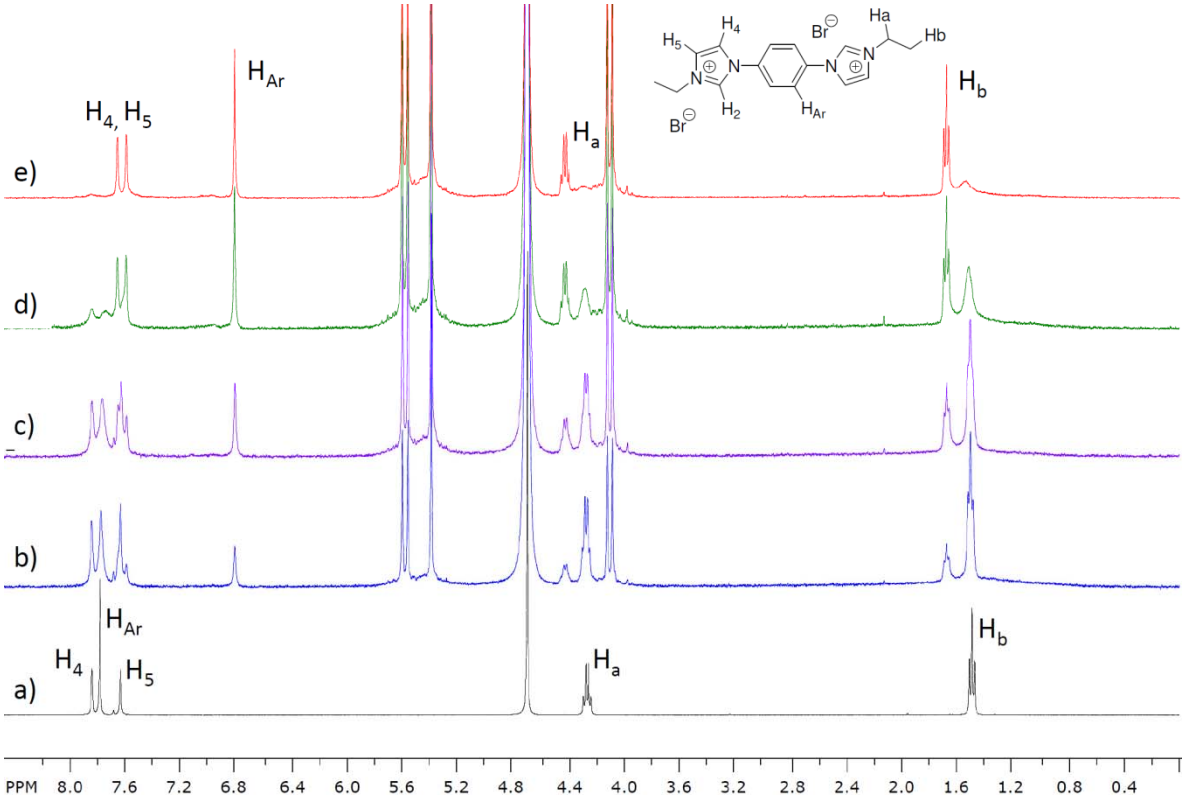


**Figure 4.3.** Partial $^{1}$H NMR spectra at 298 K in $D_2O$ of a solution of **DiimC$_2$** ($10^{-3}$ M) with increasing equivalents of host **CB[7]**: a) no **CB[7]** added ; b) 0.25 eq of **CB[7]** c) 0.5 eq of **CB[7]** ; d) 0.75 eq of **CB[7]** ; e) 1 eq of **CB[7]**

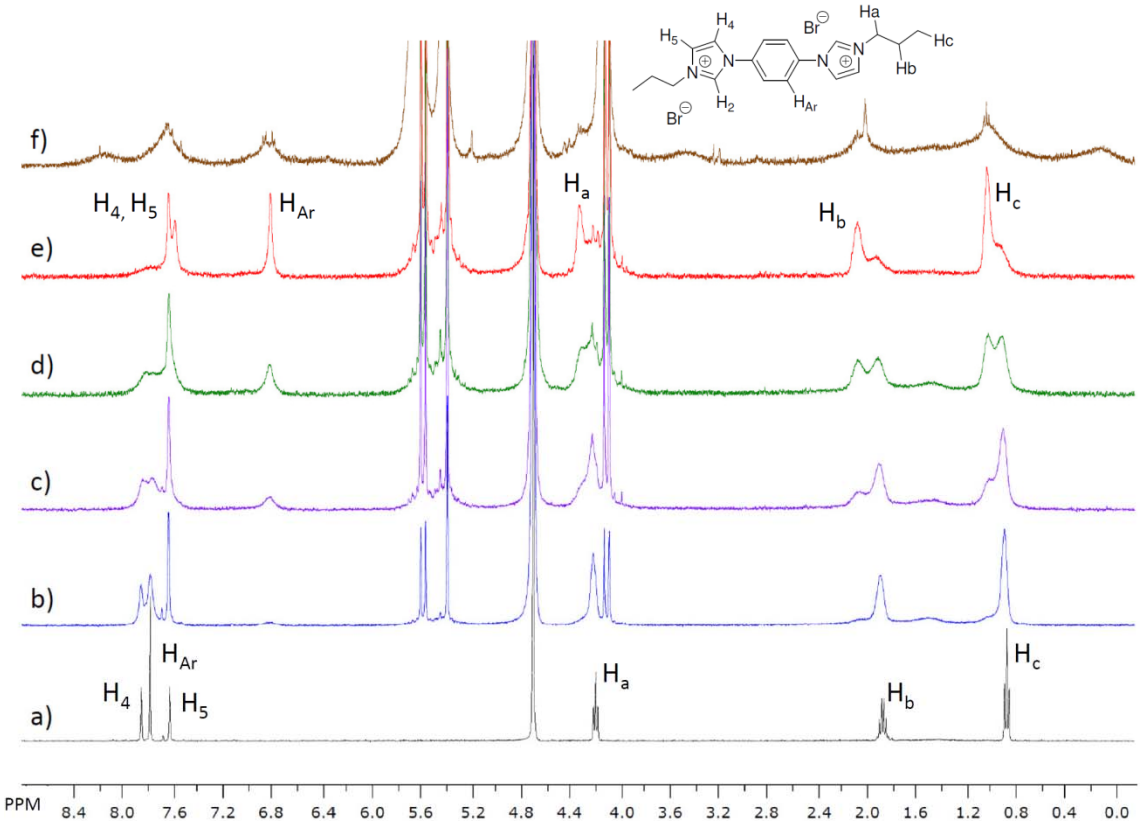


**Figure 4.4.** Partial $^{1}$H NMR spectra at 298 K in $D_2O$ of a solution of **DiimC$_3$** ($10^{-3}$ M) with increasing equivalents of host **CB[7]**: a) no **CB[7]** added ; b) 0.25 eq of **CB[7]** ; c) 0.5 eq of **CB[7]** ; d) 0.75 eq of **CB[7]** ; e) 1 eq of **CB[7]** ; f) 2 eq of **CB[7]**

The binding equilibrium of **DiimC$_3$** with of **CB[7]** was different and more difficult to interpret according to $^{1}$H NMR spectra. A greater broadening of the signals was observed when 0.25 equivalent of **CB[7]** was added. While the same shifts were obtained when 1 equivalent of **CB[7]** was added, as in the **DiimC$_2$·CB[7]** complex, the peaks remained broad and the system continued to change as more **CB[7]** was added, as seen in Figure 4.4. At 2 equivalents of **CB[7]** added, even if the limit of solubility is almost reached, another set of peaks can be observed, even if very broad. The alkyl protons, that were shifted as with the **DiimC$_2$·CB[7]** complex until 1 eq of **CB[7]** added are now shifted upfield at 2 eq of macrocycle, notably with a signal around 0.2 ppm for the $H_c$ protons and

around 3.5 ppm for the $H_a$ protons. In this same spectrum, a new broad signal can be seen at 8.3 ppm, which indicates that either $H_{Ar}$, $H_4$ or $H_5$ signals have shifted downfield. These shifts point to the formation of another complex, either another 1:1 complex or a 2:1 complex where the alkyl protons are located inside the cavity of the **CB[7]** while the imidazolium and aromatic protons are located in the outer C=O cavity. This type of complex was not observed for **DiimC$_2$** and the addition of only 1 carbon to the sidechains allowed for this different behavior.

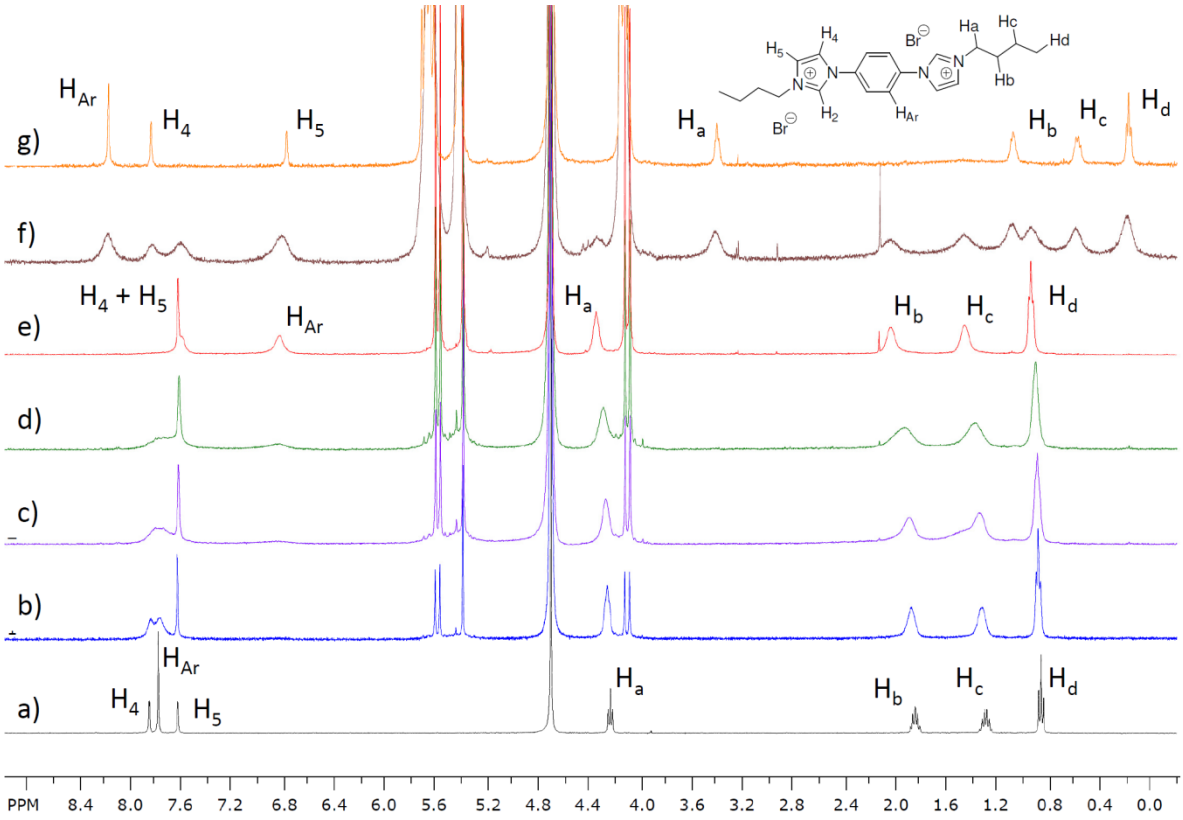


**Figure 4.5.** Partial $^1$H NMR spectra at 298 K in $D_2O$ of a solution of **DiimC$_4$** with increasing equivalents of host **CB[7]**: a) no **CB[7]** added ; b) 0.25 eq of **CB[7]** ; c) 0. 5 eq of **CB[7]** ; d) 0.75 eq of **CB[7]** ; e) 1 eq of **CB[7]** ; f) 2 eq of **CB[7]** ; g) 4 eq of **CB[7]**

At lower stoichiometries than 1 equivalent of **CB[7]** added to a **DiimC$_4$** aqueous solution, the $^1$H NMR spectra were different than the previously studied complexes: The observed complexation is fast on the NMR timescale as multiple sets of peaks were not observed, even in the aliphatic region. At 1 equivalent of **CB[7]** added however, the spectrum is similar to the **DiimC$_2$·CB[7]** complex, with the **CB[7]** positioned on the aromatic unit of the bisimidazolium salt. Even if the peaks for the **DiimC$_4$·CB[7]** are broader and the separation between the $H_4$ and $H_5$ protons can't be seen, the chemical shifts of all the signals are similar to the already studied 1:1 complexation between **DiimC$_2$** and **CB[7]**. A completely different behavior is observed with increased amounts of **CB[7]** added: at 2 equivalents, a new set of peaks can be seen. A slow complexation on the NMR timescale is observed where the aliphatic protons are all shifted upfield. This indicates that it's the alkyl chains that are positioned inside the hydrophobic cavity of the **CB[7]**. This geometry is further confirmed by having only the $H_5$ proton of the imidazolium moieties shifting upfield, with all the signals of the aromatic protons of the phenyl ring and the $H_4$ protons shifted downfield relative to the 1:1 complex. The initial 1:1 complex was no longer observed and a higher order complex was formed, presumably a 1:2 **DiimC$_4$·CB[7]$_2$** complex. No further spectral differences were recorded as more **CB[7]** was added after 4 equivalents.

## 4.4.2 High Resolution Mass Spectrometry

To confirm the stoichiometry of the complexes present in solution, a mass spectrometry study was conducted. For each compound **DiimC$_{2\text{-}8}$**, solutions of guest and **CB[7]** at a 4:1, 1:1 and 1:2 stoichiometry were prepared. The HR-MS results are shown in the Table 4.1. The results obtained for **DiimC$_2$** and **DiimC$_3$** were not surprising. In the case of **DiimC$_2$**, even at very low or very high ratios of **CB[7]**, only the 1: 1 complex was observed complex. It was the same case for **DiimC$_3$** at **CB[7]** ratios inferior or equal to 1, where only the 1:1 complex was detected. However, at high ratios of **CB[7]**, the 1:2 complex was observed. Starting with **DiimC$_4$** and for all bisimidazolium guests, a new 2:1 complex was detected at low ratios of **CB[7]**. For **CB[7]** ratios superior to 1, a mixture of

all possible complexes was observed by MS. It is important to note that even at a large excess of bisimidazolium in $D_2O$, it was not possible to observe these 2:1 complexes by $^1H$ NMR because the complex-induced chemical shift for the **CB[7]** protons is too small to be accurately measured.

**Table 4.1.** Values of the *m*/z for the complexes obtained by HR-MS

| **Guest** | Im/CB[7] | *m*/z found | *m*/z *calc.* | Stable complex(es) in the gas phase |
|---|---|---|---|---|
| **DiimC$_2$** | 4:1 | 715.2560 | 715.2562 | **1:1** $(C_{58}H_{62}N_{28}O_{14})^{2+}$ |
| | 1:1 | 715.2565 | 715.2562 | **1:1** |
| | 1:2 | 715.2564 | 715.2562 | **1:1** |
| **DiimC$_3$** | 4:1 | 729.2727 | 729.2712 | **1:1** $(C_{60}H_{66}N_{32}O_{14})^{2+}$ |
| | 1:1 | 729.2727 | 729.2712 | **1:1** |
| | 1:2 | 1310.4429 and 729.2721 | 1310.4430 and 729.2712 | **1:2** $(C_{102}H_{108}N_{60}O_{28})^{2+}$ and **1:1** |
| **DiimC$_4$** | 4:1 | 984.3209 | 984.3209 | **2:1** $(C_{82}H_{98}Br_2N_{36}O_{14})^{2+}$ |
| | 1:1 | 743.2876 | 743.2869 | **1:1** $(C_{62}H_{70}N_{32}O_{14})^{2+}$ |
| | 1:2 | 1324.9585 and 743.2873 | 1324.9610 and 743.2869 | **1:2** $(C_{104}H_{112}N_{60}O_{28})^{2+}$ and **1:1** |
| **DiimC$_6$** | 4:1 | 1040.3831 | 1040.3835 | **2:1** $(C_{90}H_{114}Br_2N_{36}O_{14})^{2+}$ |
| | 1:1 | 771.3198 and 1352.4892 | 771.3182 and 1352.4899 | **1:1** $(C_{66}H_{78}N_{32}O_{14})^{2+}$ and **1:2** $(C_{108}H_{120}N_{60}O_{28})^{2+}$ |
| | 1:2 | 1352.4892 and 771.3195 | 1352.4899 and 771.3182 | **1:2** and **1:1** |
| **DiimC$_8$** | 4:1 | 799.3492 and 1016.5197 | 799.3495 and 1016.5199 | **1:1** $(C_{70}H_{86}N_{32}O_{14})^{2+}$ and **2:1** $(C_{98}H_{128}N_{36}O_{14})^{2+}$ |
| | 1:1 | 799.3503 and 1380.5250 | 799.3501 and 1380.5248 | **1:1** and **1:2** $(C_{112}H_{128}N_{60}O_{28})^{2+}$ |
| | 1:2 | 799.3510 and 1380.5191 | 799.6501 and 1380.5248 | **1:1** and **1:2** |

### 4.4.3 $DiimC_2$ and $DiimC_3$: UV Spectroscopy and Titration Curves.

The $^1$H NMR titration method is usually helpful to measure binding parameters if the binding constants are relatively low (< $10^4$ $M^{-1}$). In our case, the complexation was slow on the NMR timescale and the association constants appeared to be higher than this value. It was not possible to obtain either a mean chemical shift for all the species present in solution, or a sample at a concentration high enough to allow the perfect separation of the signals and the precise integration for an accurate measurement. UV Spectroscopy was used to study the binding equilibrium and the stoichiometry of the complexes. For the complexation of **$DiimC_2$** with **CB[7]**, the stoichiometry was determined by the continuous variation technique (Job's plot) [23], based on relative UV absorbance of guest **$DiimC_2$,** measured in the presence of **CB[7]**. Equimolar solutions of **$DiimC_2$** and **CB[7]** were prepared and mixed for each measurement, while keeping the sum of the concentrations constant. For this guest, the Job's plot, with a maximum value of relative absorbance for a ratio of 0.5, clearly indicates a 1:1 stoichiometry (Figure 4.6b). A UV-visible titration was performed, keeping the concentration of **$DiimC_2$** constant while varying the **CB[7]** concentration (Figure 4.6a). The absorption maxima remained at 243 nm throughout the titration. Non-linear regression analysis of the resulting difference curve (Figure 4.6b) showed that the association constant for the formation of the **$DiimC_2$·CB[7]** complex was $K_{11}$ = (7.6 ± 0.8)x$10^5$ $M^{-1}$. The information gathered from the HR-MS, $^1$H NMR, UV-visible spectra and the titration curve/Job's plot clearly illustrate that the only complex formed is a 1:1 complex, where the only complexation site is the phenylene moiety with the imidazolium cations. In this case, the ethyl sidechains do not appear to play any role in the complexation.

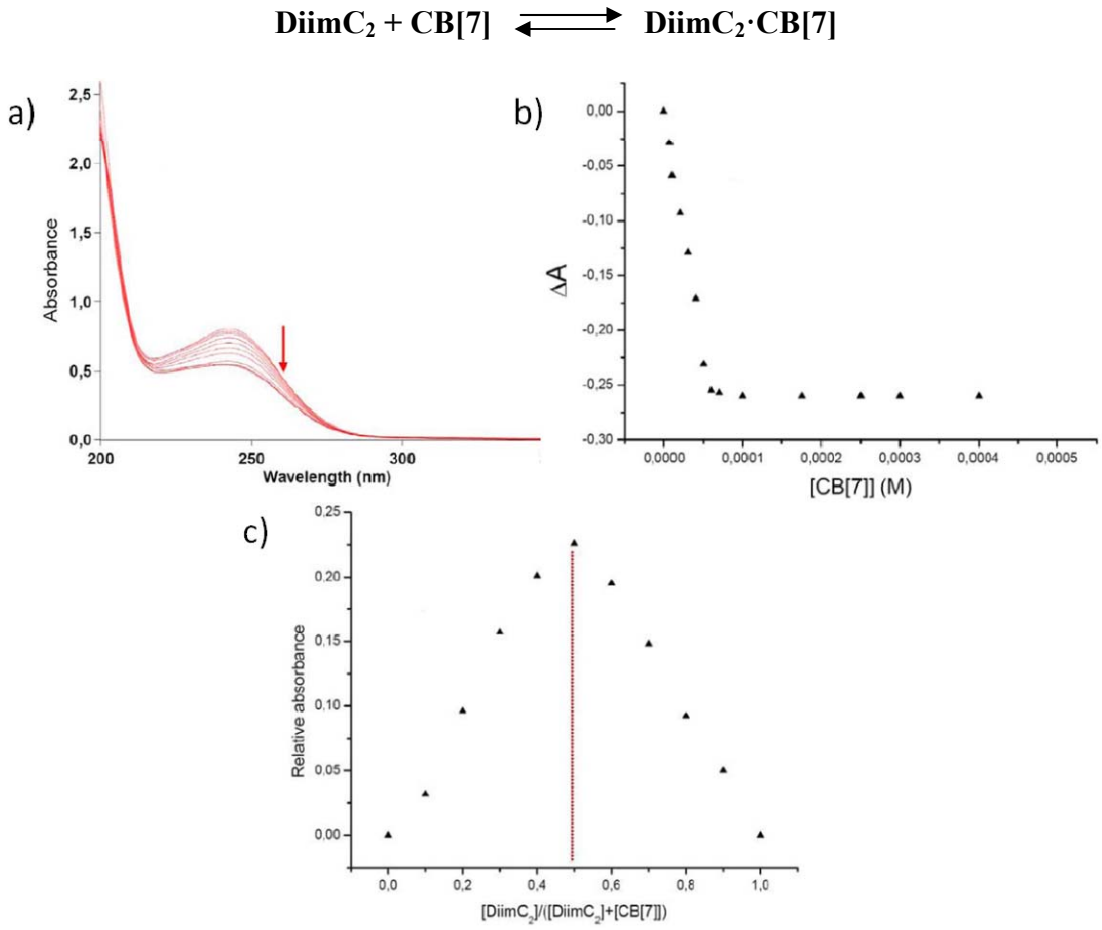


**Figure 4.6.** a) UV-Visible spectra for the titration of **DiimC$_2$** (5 x $10^{-5}$ M) by increasing amounts of **CB[7]** (0 to 8 equivalents). b) UV titration curve. c) Job's plot for the **DiimC$_2$·CB[7]** complex.

We studied the complexation between **DiimC$_3$** and **CB[7]** in order to investigate the impact of sidechain length on the binding equilibrium. As for **DiimC$_2$·CB[7]**, a Job's plot was constructed, as well as a titration curve. A very different behaviour was observed, as presented in Figure 4.7. First, although the Job's plot showed a global maximum at 0.5, it was consistent with more complex binding equilibrium since it was atypical, particularly in the zone of **CB[7]** excess. This suggests the formation of a higher order complex, as was observed by HR-MS (1:2 complex observed in the gas phase). The UV-visible spectra for

the titration of **DiimC$_3$** by **CB[7]** showed always absorption maxima at a constant 246 nm, but no saturation of the relative absorption was observed. The relative absorption ($\Delta A$) decreased below 1 equivalent of **CB[7]**, remained constant until 1.5 equivalents and increased until the end of the titration.

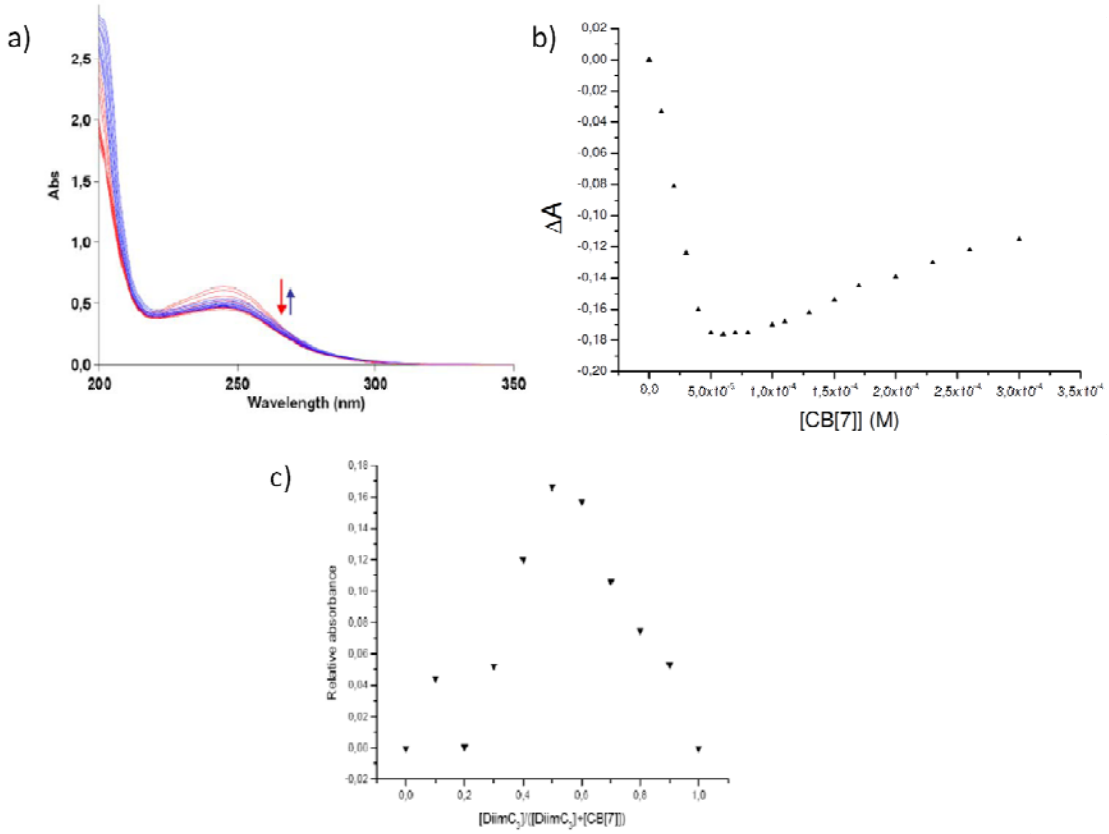


**Figure 4.7.** a) UV-Visible spectra for the titration of **DiimC$_3$** (5 x $10^{-5}$ M) by increasing amounts of **CB[7]** (0 to 7 equivalents). b) UV titration curve. b) Job's plot for the complexation between **DiimC$_3$** and **CB[7]**.

The UV, HR-MS, and $^1$H NMR data suggest a competition between the formation of 1:1 and 1:2 complexes. A 1:1 complexation is predominant until about 1 equiv of **CB[7]** is added and the 1:2 complex starts to be formed in nonnegligible quantities at this point. The variation in $\Delta A$ is also indicative of a completely different binding mode. The $\Delta A$

increase, compared to the initial decrease attributed to the position of the macrocycle mainly on the center of the guest, can be correlated to a complexation on the alkyl side chains and the imidazolium cations. From these observations, a binding mechanism can be proposed for **DiimC$_3$**, based on the different complexes present in solution at the same time.

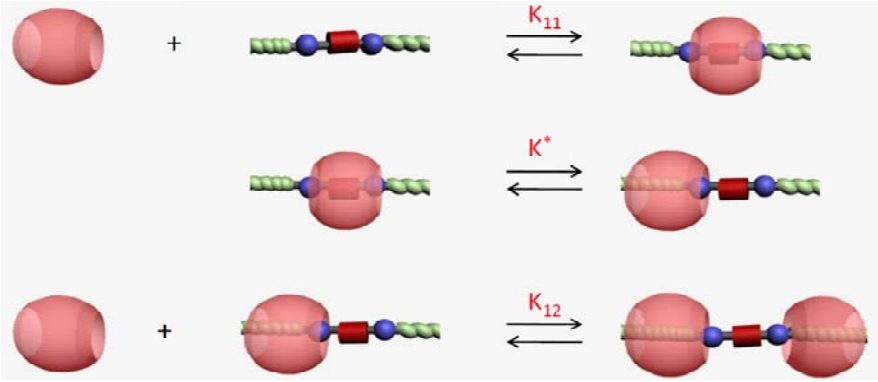


**Figure 4.8.** Plausible mechanism for the complexation between **DiimC$_3$** and **CB[7]**

At a low **CB[7]** ratio, the same complex as in the case of **DiimC$_2$** is formed. Since this complex is formed by the complexation of the phenylene moiety in the hydrophobic cavity of the **CB[7]** and the imidazolium rings in the outer C=O cavity, we can assume that the association constant $K_{11}$ will be very similar for all guests. As such, we chose to use the same $K_{11}$ constant as an initial value to help approximate the other binding parameters. At increased **CB[7]** concentrations, the **DiimC$_3$·CB[7]$_2$** complex is formed. To allow its formation, a different 1:1 complex must first be formed, where the **CB[7]** is positioned on the secondary binding site of the bisimidazolium salt. This secondary 1:1 complex can then accommodate a second **CB[7]** macrocycle to form the 1:2 complex. No evidence of this secondary 1:1 complex was obtained by $^1$H NMR. It clearly has a lower association constant ($K^* < 1$), is a necessary step to allow the formation of the 1:2 complex (combining steps 2 and 3 of the mechanism could be possible in a less accurate description of the system). Considering that saturation was not reached even at 7 equivalents of **CB[7]**, we can assume that $K_{12}$ is lower than $K_{11}$ for **DiimC$_3$**. We estimated the binding constants of

this complex binding equilibrium using a non-linear regression analysis with 3 experimental data sets. As multiple complexes are present in solution simultaneously, the binding constants presented below are estimates only and not actual measurements as in the case of **DiimC$_2$**. Nonetheless, it is still useful to estimate the order of magnitude of the binding parameters for these bisimidazolium salts. The modeled mechanism was the one presented in Figure 4.7. A non-linear algorithm was performed according to the theoretical model equations. The theoretical and experimental values were compared using a merit function [24] which was minimized in order to obtain the best estimates possible. All details can be found in the Supplementary Information. With $K_{11}$ kept constant at 7.6 x $10^5$ $M^{-1}$, we estimated the other constants to be approximately $K_{12}$ = 5 x $10^4$ $M^{-1}$ and K* = 5.7 x $10^{-2}$, with a merit function minimized at 2.65 %. The subsequent variation of the value of $K_{11}$ did not allow a better fit, which confirmed our choice of keeping it constant and equal to the **DiimC$_2$·CB[7]** association constant.

### 4.4.4 DiimC$_4$, DiimC$_6$, and DiimC$_8$: UV Spectroscopy and Titration Curves.

These three phenylene bisimidazolium salts were studied in the same way as the previous two. Although the resulting Job's plots did not provide readily interpretable information about the complexation (no apparent maximum was observed in any case and the plots were asymmetrical), the HR-MS data suggest a 2:1 majority complex present in solution at a low **CB[7]** ratio. With this information in mind, UV titration curves were plotted for these three compounds for a qualitative estimation of the equilibria. The estimation of the binding constants may require more advanced methods in order to accurately describe these complex equilibria in solution. Direct observation of the titration curves at different equivalents of **CB[7]** and by correlation with the previous HR-MS study, allowed a rough understanding of the supramolecular behavior of these bisimidazolium guests in the presence of **CB[7]**.

The same observations can be made for the three bisimidazolium salts: a) saturation is obtained at high **CB[7]** ratios; b) a similar absorbance variation is obtained in all cases. Moreover, the complexation sites being very similar, we can assume that $K_{11}$ and $K_{12}$ calculated and respectively estimated for **DiimC$_2$** and **DiimC$_3$** will have very similar values for these compounds.

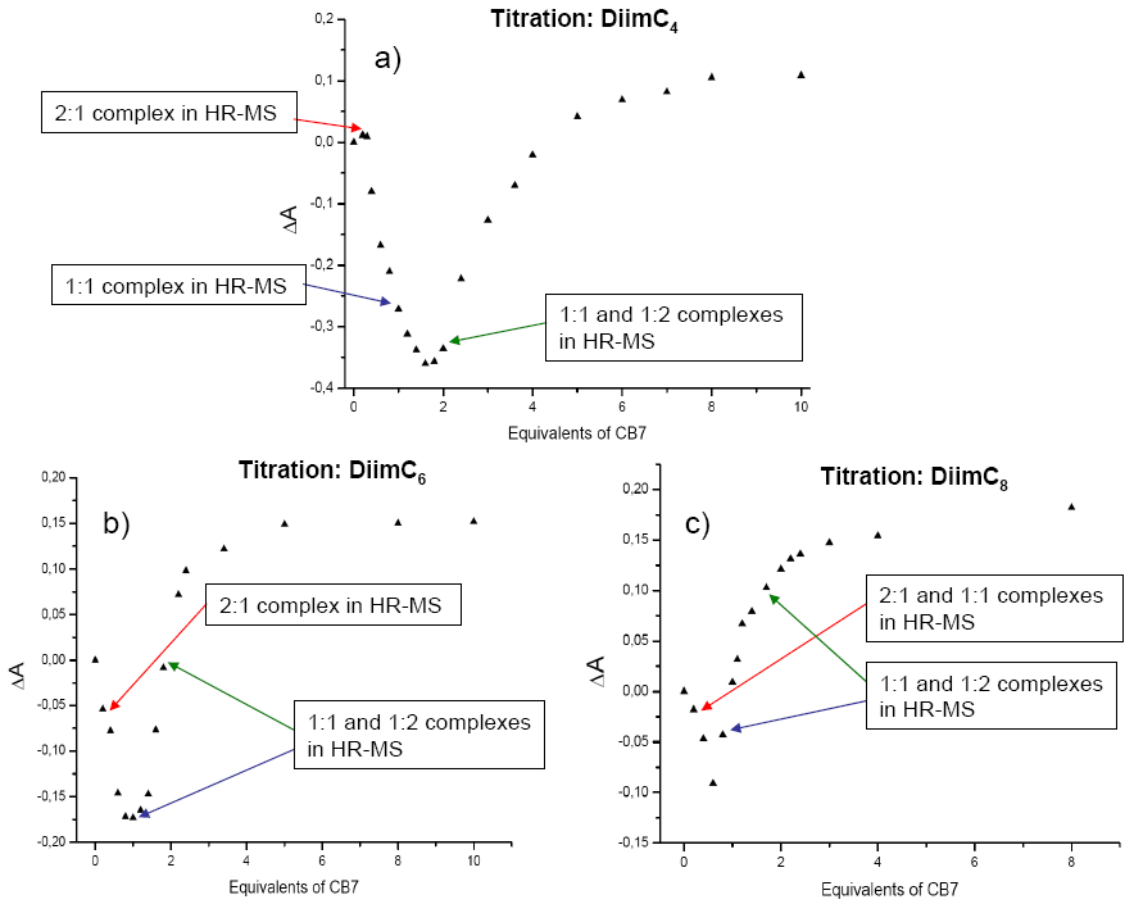


**Figure 4.9.** Titration curves for the complexation of **CB[7]** with : a) **DiimC$_4$** ; b) **DiimC$_6$**; c) **DiimC$_8$** (**[DiimC$_x$]** = 5 x $10^{-5}$ M).

For the **DiimC$_4$** guest, the relative absorption increased at the beginning of the titration (at low **CB[7]** ratio). This very distinctive behaviour in the UV-visible spectra is consistent with the formation of 2:1 (**2DiimC$_4$·CB[7]**) complexes with butyl sidechains

from two different **DiimC$_4$** molecules inserted in the same **CB[7]** macrocycle (Figure 4.10). For **DiimC$_6$** and **DiimC$_8$**, no such increase was observed, although the 2:1 complex was observed in the gas phase. The $K_{21}$ value may be lower for **DiimC$_6$** and **DiimC$_8$** compared to **DiimC$_4$**, because of the increase of the sidechain length. The decrease in the relative absorption is similar to the first two complexes studied with **DiimC$_2$** and **DiimC$_3$** guests, corresponding to the 1:1 complexes. Between 1 and 2 equivalents of **CB[7]**, the ΔA began to increase, which can be associated with the formation of 1:2 complexes. A mechanism can be written similarly to the one previously theorized.

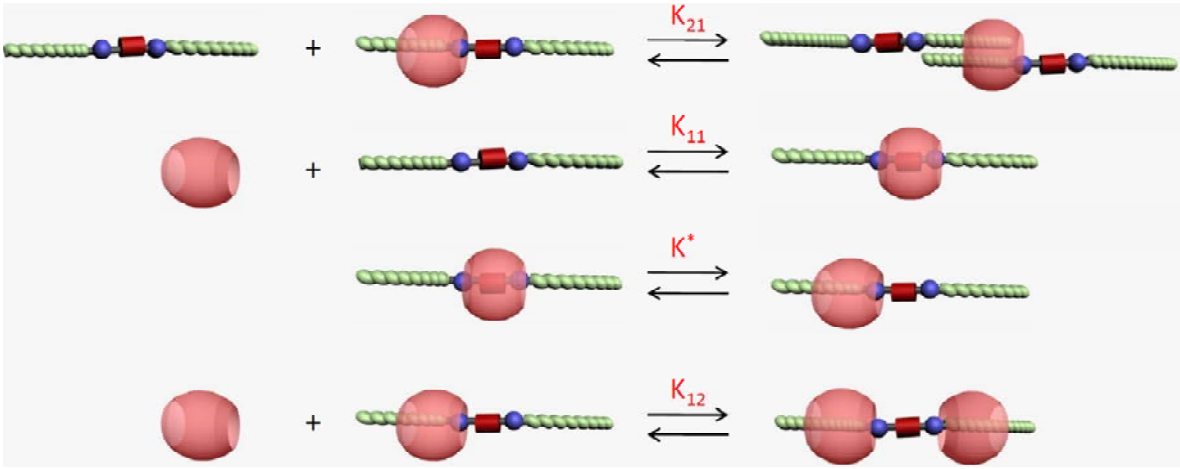


**Figure 4.10.** Proposed mechanism for the complexation of guests **DiimC$_n$** (n = 4, 6, 8) and **CB[7]**.

The mechanism presented here is consistent with the obtained titration curves, with the same equilibrium for the formation of the 1:1 complex and with the **CB[7]** being positioned on the secondary binding site. The number of binding parameters present in these equilibria is too high to be able to estimate them accurately. However, it was possible to extract the product $K_{12}$ x K* by fitting the titration curve starting at 2 equivalents of **CB[7]** added and assuming that there are no more free bisimidazolium guests or 2:1 complexes in solution. The values that were obtained are by no means actual measurements but help visualize and compare the formation of the 1:2 complexes when the only variation

is the length of the alkyl sidechains. The fitted curves can be found in the supplementary information and the summary of the results can be found in table 4.2. The value for **DiimC$_3$** was calculated from the $K_{12}$ and K* values previously estimated for the **DiimC$_3$/CB[7]** complexation.

**Table 4.2.** Estimated values of the product $K_{12}$ x K* for the **DiimC$_{3\text{-}8}$/CB[7]** systems

| | **DiimC$_3$** | **DiimC$_4$** | **DiimC$_6$** | **DiimC$_8$** |
|---|---|---|---|---|
| $K_{12}$ x K* ($M^{-1}$) | 2.8 x $10^3$ | 2.5 x $10^4$ | $10^5$ | 1.2 x $10^5$ |

For all the guests, the estimated values of $K_{12}$ x K* were lower than $K_{11}$ which is coherent with the fact that the 1:1 complex is predominant before enough **CB[7]** is added to form 1:2 complexes. It can also be noted that the value of $K_{12}$xK* increases with the length of the alkyl sidechains which confirm once again that the secondary 1:1 complexation and the 1:2 complexation are highly dependent on this parameter. The product increases by almost an order of magnitude from **DiimC$_3$** to **DiimC$_4$** and from **DiimC$_4$** to **DiimC$_6$**. Considering that K* is lower than 1 in all cases (since it was proven by $^1$H NMR that the primary 1:1 complex was the one where the **CB[7]** was complexed on the phenylene moiety), the only possibility with the values obtained is that K* increases only slightly when a carbon is added to the sidechain (up to **DiimC$_6$**) and it's mainly the increase of $K_{12}$ that accounts for the increase in the product $K_{12}$ x K*. For **DiimC$_8$** however, only a slight increase in the product is observed: this could be due to a decrease in $K_{12}$ since the alkyl chain is starting to be too bulky to fit as well as a hexyl in the cavity of a **CB[7]**. To confirm these hypotheses, a more direct estimation of the association constants is needed. We are currently working on estimating the association constants and validating the proposed mechanism using the software Dynafit® 3 [25], with a similar methodology to that used by Stoddart *et al.* to study the complexation of viologen with macrocycles [26].

### 4.4.5 Molecular Modeling.

Plausible structures of the ternary complexes were obtained by molecular dynamics (MD) simulations. The MD simulations of the host-guest complexes in aqueous solution were carried out in a cubic simulation box with periodic boundary conditions in all directions. For each host:guest complex, several 100 ps runs were performed with different initial relative orientations. In most cases the guest enters the host within the first 20 ps of the simulation run and remains in a stable position. The initial geometries of **DiimC$_n$** and **CB[7]** were built and then fully optimized by the PM3 method without any symmetrical restrictions.

For many self association processes the entropy effect is small and it is the enthalpy change (ΔH) that mainly determines whether the association can take place spontaneously. The enthalpy change is essentially due to the difference in the bond energies (including resonance and strain energies) between the different free components of the supramolecular complex and the complex itself. Since in this case the entropy effect can be considered the same for the formation of all the inclusion complexes, the calculated enthalpy variations can be used in order to discuss the stability of the different complexes (Table 4.3).

**Table 4.3.** Enthalpy variations (kcal·mol$^{-1}$) for the formation of the different inclusion complexes.[a]

| **DiimC$_n$** | **DiimC$_n$·CB[7]** | **DiimC$_n$·CB[7]*** | **2DiimC$_n$·CB[7]** | **DiimC$_n$·CB[7]$_2$** |
|---|---|---|---|---|
| **DiimC$_2$** | - 29.75 | - 0.25 | + 2.05 | + 8.96 |
| **DiimC$_3$** | - 30.14 | - 16.51 | + 2.36 | - 4.56 |
| **DiimC$_4$** | - 25.17 | - 22.12 | - 52.96 | - 26.46 |
| **DiimC$_6$** | -27 | - 32.44 | - 54.17 | - 27.94 |

[a] Calculated using Hyperchem with PM3 geometry optimization, restricted shell. The geometries of the calculated complexes on which the schematic representations in Figures 4.7 and 4.9 are based are provided in the Supporting Information

Since the entropy effect was not considered in this study, one obvious observation can be made about the stability of the inclusion complexes: the most stables complexes were obtained for **DiimC$_6$**, although the differences with **DiimC$_4$** are very small. Other interesting result is that for **DiimC$_2$** the formation of 1:2 or 2:1 complexes are not enthalpy driven, as it is the case for its superior analogs. If in the case **DiimC$_3$** only the formation of 1:2 complex can take place spontaneously, for **DiimC$_4$** and **DiimC$_6$** all the complexes can be formed, as their self-assembly is exothermic. In the case of **DiimC$_4$** and **DiimC$_6$** the enthalpy change is very similar for the formation of the 1:1 or the 1:2 complex, which could explain their different behavior even at low **CB[7]** ratio, compared to **DiimC$_2$** and **DiimC$_3$**.

## 4.5 Conclusion

In conclusion, different dialkyl-3,3'-(1,4-phenylene)bisimidazolium salts formed inclusion complexes with **CB[7]**. Depending on the length of the alkyl chains and the **CB[7]** concentration, different supramolecular associations were obtained by the threading of the imidazolium salts into the **CB[7]** cavity. In all the cases the most stable complex was obtained when **CB[7]** was positionned around the central phenylene bisimidazolium recognition site. However, by the judicious choice of the **CB[7]** concentration, in the case of longer alkyl chains, the stoichiometry of the supramolecular complexes can be controlled. The detailed study of the binding association of these imidazolium salts may allow us to understand the exact role of each recognition site in these salts and to assemble higher supramolecular complexes.

## 4.6 Acknowledgment.

We are grateful to the Natural Sciences and Engineering Research Council of Canada, the Fonds Quebécois de la Recherche sur la Nature et les Technologies, the Canada Foundation for Innovation and Université de Montréal for financial support. We thank Dr. Alexandra Furtos and Karine Venne for mass spectrometry analysis. We also thank colleagues for careful reading and discussion of this manuscript.

## 4.7 Supporting information available:

$^{1}$H and $^{13}$C NMR of **DiimC$_2$**, **DiimC$_3$**, **DiimC$_4$**, **DiimC$_6$**, and **DiimC$_8$**; association constant for the formation of **DiimC$_2$·CB[7]** complex by UV titration; estimation of the association constants for the formation of complexes between **DiimC$_3$** and **CB[7]** by UV titration; estimates of $K_{12} \times K^*$ for **DiimC$_4$**, **DiimC$_6$**, and **DiimC$_8$**; mass spectra of the observed complexes; structures of the inclusion complexes and heats of formation obtained by molecular modeling. This material is available free of charge via the Internet at http://pubs.acs.org.

## 4.8 References and notes

1 (a) Oshovsky, G. V.; Reinhoudt, D. N.; Verboom, W. *Angew. Chem. Int. Ed.* **2007**; *46*, 2366. (b) J.-M. in Supramolecular Chemistry, Concepts and Perspectives, VCH, Weinheim, 1995.

2 Szejtli, J.; Osa, T. in Comprehensive Supramolecular Chemistry Vol. 3 (Cyclodextrins), Elsevier, Oxford, 1996.

3 Lindoy, L. F.; Atkinson, I.M. in Self-Assembly in Supramolecular Systems, The Royal Society of Chemistry, Cambridge, 2000.

4 Cram, D. J. *Nature*, **1992**, *356*, 29-36.

5 Escuder, B.; Rowan, A. E.; Feiters, M. C.; Nolte, R. J. M. *Tetrahedron*, **2004**, *60*, 291-300.

6 Mulder, A.; Huskens, J.; Reinhoudt, D. N. *Org. Biomol. Chem.*, **2004**, *2*, 3409-3424.

7 Mammen, M.; Choi S.-K.; Whitesides, G. M. *Angew. Chem. Int. Ed. Engl,*. **1998**, *37*, 2755-2794.

8 Whitesides, G. M.; Mathias, J. P.; Seto, C. T. *Science*, **1991**, *254*, 1312-1319.

9 Wyman, I. W.; Macartney, D. H. *Org. Biomol. Chem.*, **2009**, *7*, 4045-4051

10 Sambrook, M. R.; Beer, P. D.; Wisner, J. A.; Paul, R. L.; Cowley, A. R.; Szemes, F.; Drew, M.G. B. *J. Am. Chem. Soc.* **2005**, *127* 2292-2302.

11 Dupont, J. *J. Braz. Chem. Soc.* **2004**, *15*, 341-350.

12 Leclercq, L.; Schmitzer, A. R. *Supramol. Chem.* **2009**, *21*, 245-263.

13 Weingartner, H. *Angew. Chem. Int. Ed.* **2008**, 654-670.

14 Noujeim, N.; Leclercq, L.; Schmitzer, A. R. *J. Org. Chem.* **2008**, *73*, 3784-3790.

15 Leclercq, L.; Noujeim, N.; Sanon, S.; Schmitzer, A. R. *J. Phys. Chem. B.* **2008**, *112*, 14179-14184.

16 Lagona, J.; Mukhopadhyay, P.; Chakrabarti, A.; Isaacs, L. *Angew. Chem. Int Ed.* **2005**, *44*, 4844-4870.

17 *HyperChem. 7.52 for Windows*; Hypercube Inc., 2007.

18 Stewart J.J.P. *J. Comp. Chem.* **1991**, *12*, 320-341.

19 Beachy, M.D.; Chasman, D; Murphy, R.B.; Halgren, T.A.; Friesner, R.A. *J. Am. Chem. Soc.* **1997**, *119***,** 5908-5920.

20 Cristau, H-J.; Cellier, P. P.; Spindler, J-F.; Taillefer, M. *Chem. Eur. J.* **2004**, *10*, 5607-5622.

21 Wyman, I. W.; Macartney, D. H.; *Org. Biomol. Chem.* **2008**, *6*, 1796-1801.

22 Kolman, V.; Marek, R.; Strelcova, Z.; Kulhanek, P.; Necas, M.; Svec, J.; Sindelar, V. *Chem. Eur. J.* 2009, 15, 6926-6931.

23 Job, P. *Ann*. *Chim*. **1928**, *9*, 113-134.

24 a) See Supporting Information section for details. b) Korendovych, I.V.; Cho, M.; Makhlynets, O.V.; Butler, P. L.; Staples, R.J.; Rybak-Akimova, E.V. *J. Org. Chem.* **2008**, *73*, 4771–4782.

25 Kuzmic, P. *Anal. Biochem.* **1996**, *237*, 260-273.

26 Gasa, T. B.; Spruell, J. M.; Dichtel, W. R.; Sorensen, T. J.; Philp, D.; Stoddart, J. F.; Kuzmic, P. *Chem. Eur. J.* **2009**, *15*, 106-116.

# Chapitre 5 : Cations diimidazolium diaromatiques : mise en évidence d'interactions supramoléculaires à l'état cristallin

# 5.0 Préface

À ce stade dans l'avancée des travaux, les propriétés supramoléculaires en solution des sels de diimidazolium sont bien connues. La majorité des interactions intermoléculaires présentes en auto-association ou dans des complexes avec des macrocycles ont pu être identifiées. Nous nous sommes donc demandés si ces composés avaient la possibilité d'agir en tant que tectons moléculaires lors de la cristallisation et de former des réseaux de sels de diimidazolium à l'état cristallin. En prenant en compte toutes les interactions présentes, et après une étude de modélisation moléculaire, nous avons essayé de prédire la structure cristalline de quatre sels de diimidazolium. Les cristaux ont ensuite été obtenus et les structures cristallines résolues.

Pour ces travaux publiés en 2009 et réalisés en collaboration avec Dr Loïc Leclercq, j'ai obtenu et résolu deux des quatre structures cristallines présentées dans cet article. J'ai également contribué à la rédaction de l'article.

Les informations expérimentales supplémentaires de cette partie se trouvent aux pages 241-245 de la thèse.

# Article 4. Development of *N,N*'-diaromatic diimidazolium cations: arene interactions for highly organized crystalline materials

Loïc Leclercq, Nadim Noujeim and Andreea R. Schmitzer*

Département de chimie, Université de Montréal, CP 6128, Succursale Centre-Ville, Montréal, Québec, H3C 3J7, Canada

*Crystal Growth and Design,* **2009**, *9*, 4784-4792

## 5.1 Abstract

We applied concepts developed in the context of molecular recognition of aromatic rings in solution to design molecular tectons capable of generating molecular networks based on aromatic stacking in the crystalline phase. In this respect, *N,N'*-diaromatic diimidazolium cations are interesting tectons because they offer electron-rich (aromatic) and electron-poor (imidazolium) rings able to develop aromatic stacking interactions. Two positive charges and six acidic protons divergently oriented on the diimidazolium dication are involved in strong electrostatic charge-charge interactions and H-bonding with anions. Incorporation of aromatic rings modifies the rigidity of these dications. Depending on the flexibility of the molecules, incorporation of water molecules in the crystal lattice is possible, and channels are created in the solid network.

## 5.2 Introduction

"The field of crystal engineering has undergone tremendous growth over the past ten years [1]. Recently, a number of crystalline organic and metal-organic materials that exhibit micro- and nano-porous behaviour have been reported with crystalline structures that are stable upon removal of guest or solvent molecules [2]. Such porous materials have potential for commercial application in areas such as molecular separations, catalysis, storage, photonic materials and synthetic zeolytes [3]. Consequently, there is a growing interest to develop strategies and methodologies to construct new types of crystalline materials with properties that can be designed and predicted. Current efforts in this area are aimed at controlling parameters such as the size and shape of channels and cavities and the nature of surface-exposed functional groups, toward functional properties including trapping or exchange of guest molecules, molecular recognition and selectivity[4]."

In parallel, recent studies have demonstrated that pure 1,3-disubstituted imidazolium salts are better described as H-bonded polymeric supramolecules, notably in

the solid state [5]. The supramolecular organization of imidazolium salts in the solid phase was proposed to be maintained to a great extent in the liquid and gas phase [5]. Imidazolium-based salts possess preorganized structures mainly through H-bonds that induce structural directionality contrary to classical salts in which the aggregates are mainly formed through ionic bonds (charge-ordering structure) [5]. The imidazolium cation possesses three ring-borne H-bond donors, where the three acidic protons oriented in a divergent fashion. Moreover, other attractive intermolecular interactions can also occur, such as electrostatic and aromatic stacking (Figure 5.1) [5]. "An overview of recent X-ray studies of 1,3-dialkylimidazolium salts [6] reveals a typical trend: in the solid state they form an extended network of cations and anions connected by H-bonds. The monomeric unit is always constituted of one imidazolium cation surrounded by at least three anions and each anion is surrounded by at least three imidazolium cations (Figure 5.1a) [7]. The strongest H-bond always involves the most acidic $H_2$ ($pK_a$ = 23.0 for the 1,3-dimethyl imidazolium cation) [8] followed by $H_4$ and $H_5$ of the imidazolium ring". These H-bonds are weak to moderate (H•••X bond lengths > 2.2 Å; C-H•••X bond angles between 100-180°) [9]. In 3D, imidazolium rings form channels by aromatic stacking (Figure 5.1b; the number of anions that surround the cation (and vice-versa) and the aromatic stacking varies according to the size of the anion and the nature of the *N*-imidazolium substituents).

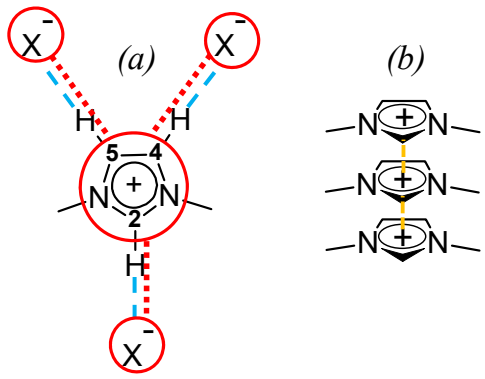


**Figure 5.1.** Intermolecular interactions for an imidazolium cation: (*a*) H-bond donors (blue dotted lines) and electrostatic interactions (red dotted lines); (*b*) aromatic stacking interaction (orange dotted lines).

It is assumed that aromatic stacking interactions of the imidazolium rings are less important than the H-bonds [10]. Imidazolium cations are electron-poor rings such that the interaction between the π-electrons is weak [11]. Aromatic stacking is caused by intermolecular overlapping of the p orbitals in π-conjugated systems and is strengthened as the number of π-electrons increases. Three stacking interactions can be obtained in these systems which contain imidazolium and phenyl rings: (i) π-stacking of similar aromatic rings; (ii) π-stacking between two different aromatics rings; (iii) T-stacking between the hydrogen of one aromatic system that points perpendicular to the center of the aromatic plane of the other aromatic system. Generally, these two last stackings are more stable because the interactions take place between an electron-rich and an electron-poor aromatic system, where we can talk of a stacking charge-transfer complex (Figure 5.2) [12].

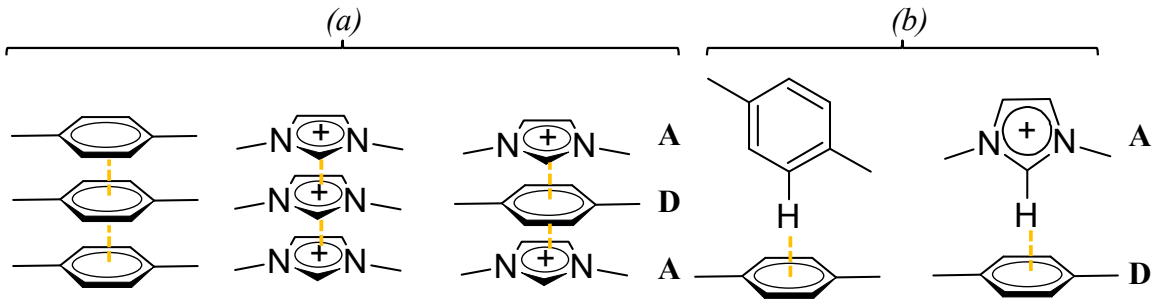


**Figure 5.2.** Aromatic stacking interactions (dotted orange lines) between imidazolium cations and aromatic rings: (*a*) π-stacking; (*b*) T-stacking (the acceptor is called A and the donor D).

While aromatic stacking is less important than H-bonds in the conventional organization of imidazolium salts, we have recently reported that dibenzylimidazolium halide salts present an increased cohesion in the solid state and self-assemble in dimers by aromatic T-stacking interactions in polar and nonpolar solutions [13a]. On the basis of that study, the aromatic stacking appears to be an important contributor to the crystalline

structure of these imidazolium cations and can be extended to their organization in solution [13a]. However, the dibenzylimidazolium bromide salt forms dimers due to the poor flexibility and the small size of the cation. Moreover, the size of the anion dictates the arrangement in the solid state [13b]. A recent study also confirms the aromatic stacking of 1-benzyl-3-(pentafluorobenzyl)imidazolium bromide salts in the solid phase [14]. As charge-transfer stacking interactions can be exploited in these aromatic imidazolium salts (in addition to electrostatic and H-bond interactions) and considering the applications of imidazolium salts in various fields [15], we investigated their potential use as supramolecular building blocks for crystal engineering. We report here four imidazolium cations, substituted by aromatic residues. Two central motifs were used: (i) methylene and (ii) xylylene-bridged *N*-substituted diimidazolium salts and two variations of each were investigated: *N,N'*-(diphenyl-methylene) diimidazolium (**[PM][Br]$_2$**), *N,N'*-(diphenylxylylene) diimidazolium dibromide (**[PX][Br]$_2$**), *N,N'*-(dibenzylmethylene) diimidazolium (**[BM][Br]$_2$**) and *N,N'*-(dibenzylxylylene)-diimidazolium dibromide (**[BX][Br]$_2$**) (Chart 5.1).

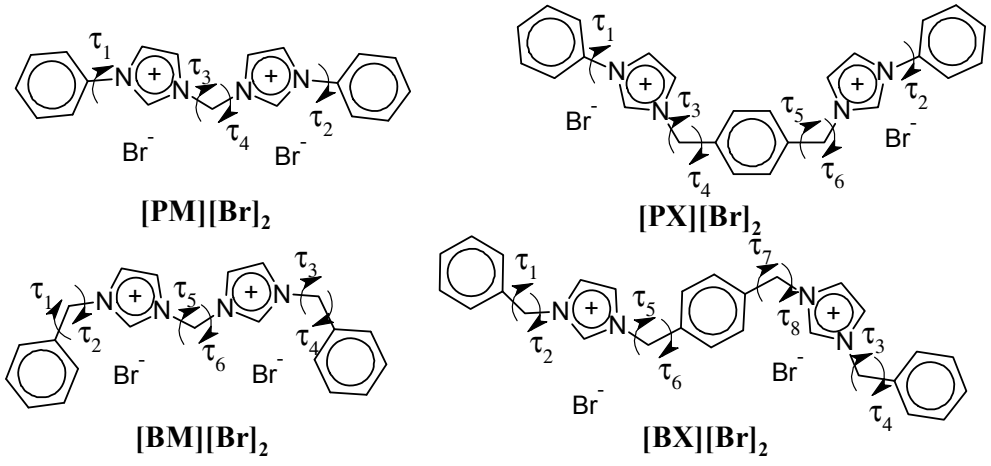


**Chart 5.1.** Structure of the diimidazolium dibromide salts used in this work and torsion angles used to illustrate their flexibilities.

## 5.3 Results and discussion

### 5.3.1 Rational and design of the cations

We have chosen to work with methylene or xylylene-bridged *N*-substituted diimidazolium cations, as they offer different flexibilities. Both diimidazolium cations are substituted by two phenyl (**[PM][Br]$_2$** and **[PX][Br]$_2$**) or benzyl residues (**[BM][Br]$_2$** and **[BX][Br]$_2$**, see Chart 1). In the structures investigated here, the alternation of electron-rich donor (benzyl or phenyl) and electron-poor acceptor (imidazolium) rings in their structures may allow the formation of strong and directional stacking. On the basis of our previous results, we exploited aromatic stacking as the most important interaction dictating the organization in the solid phase [13, 14]. However, higher flexibility within a tecton makes it difficult to predict its self assembly in the solid state. Actually, the central dications can be described as rigid imidazolium units linked by flexible methylene or xylylene spacers. External aromatic rings are attached directly, or by flexible methylene to the central dications. Theoretical calculations were performed to determine the most stable structures of these diimidazolium cations. We used the Ghemical computational chemistry package for Linux workstations to apply semiempirical methods (AM1, MOPAC7) for geometry calculations, as it was previously described that this method can predict the crystal structure of small organic salts without predominant H bonds [16, 17 and 18]. For all the calculations, the bromide anions were omitted. To study the molecular structures of the diimidazolium cations and their energies in detail, we plotted the energy of the conformers (2D and 3D) as a function of the torsion angles values (Figure 5.3).

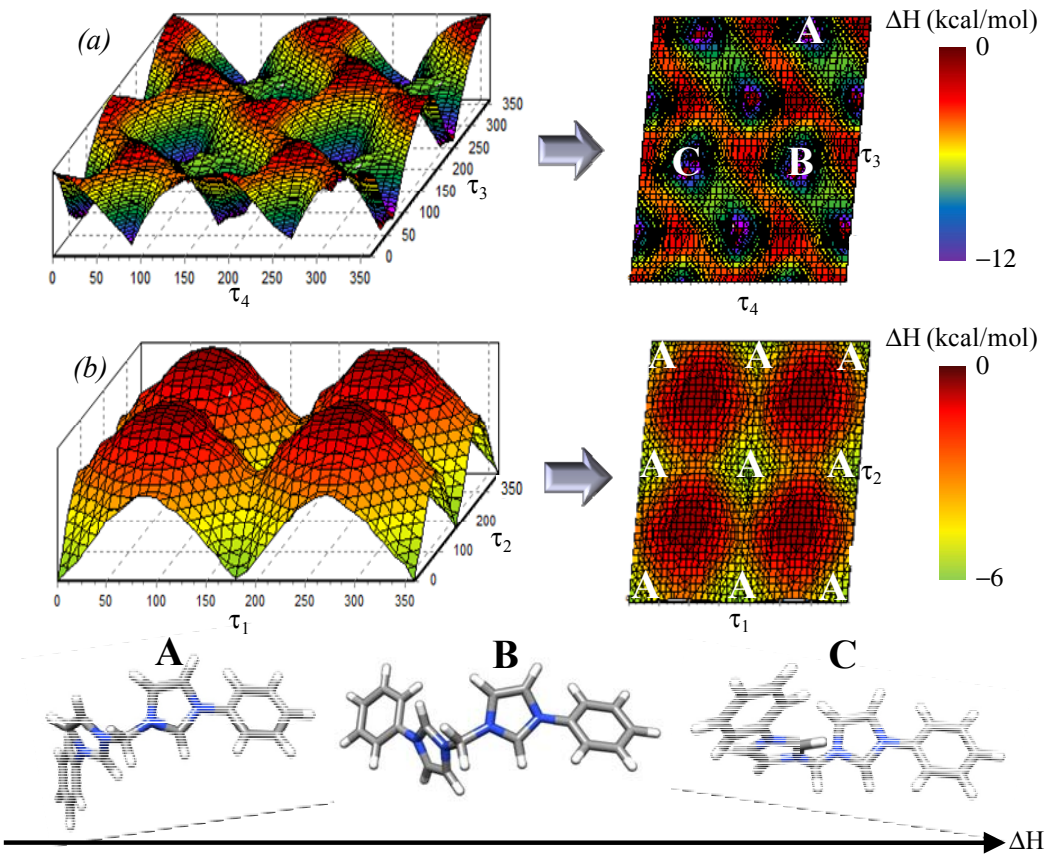


**Figure 5.3.** Study of **[PM]** dication molecular structures and most stable conformers (**A**, **B** and **C**) as function of the torsion angles defined in Chart 1 (obtained using AM1, MOPAC7): (*a*) $\tau_3$ and $\tau_4$ torsion angles as variables and $\tau_1$ and $\tau_2$ fixed, (*b*) $\tau_1$ and $\tau_2$ torsion angles as variables and $\tau_3$ and $\tau_4$ fixed (see Chart 1 for the definition of torsion angles).

After a global geometry minimization of the molecular structure, the methodology we applied was the following: (i) the influence of the torsion angles was investigated from the central to the lateral position, (ii) the minimal energy geometry of the conformer obtained was kept constant and the atoms fixed, (iii) the two previous operations were repeated until the last two torsion angles were optimized. For example, the **[PM]** dication has four different torsion angles ($\tau_1$, $\tau_2$, $\tau_3$, and $\tau_4$; see Chart 1). After a global geometry optimization, the influence of the torsion angles $\tau_3$ and $\tau_4$ were investigated. The most stable

geometry (A) was kept and then torsions $\tau_1$ and $\tau_2$ were optimized. Finally, the most stable conformation was kept (C; see Figure 5.3). The four most stable conformers of the **[PM]** dication, as well as the most stable conformers for the other dications, are presented in Figure 5.4. To simplify the further representation of the diimidazolium cations, we adopted a schematic representation, obtained by the projection of the structures in a plane (Figure 5.4).

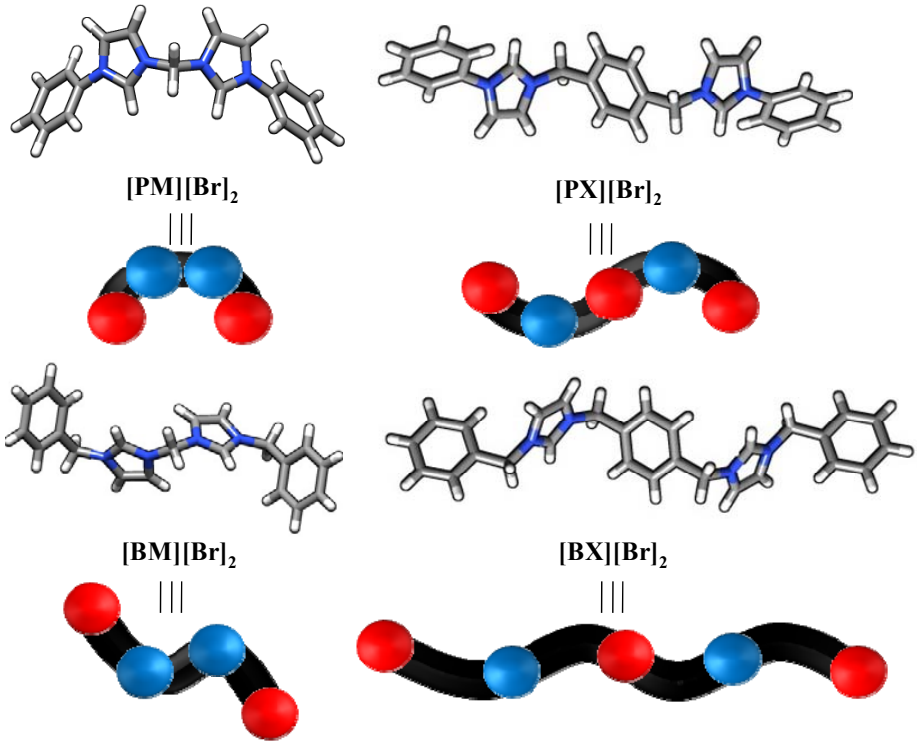


**Figure 5.4.** Schematic representation of the optimized structures of the diimidazolium cations.

In the 3D networks, the global organization will be directed by the global flexibility of the diimidazolium cations and the number of aromatic electron-rich rings. Figure 5.5 presents the predicted organization in the crystalline structures. These schematic representations are based on molecular dynamics study of the dications in vacuo, using

HyperChem (Amber force field, see Supporting Information). It is noteworthy that in all cases the aromatic stacking seems to be more important than electrostatic or H-bonds interactions. On the basis of this theoretical study, multiple π-stacking interactions can be developed between the aromatic electron-poor and electron-rich rings. In other words, the stabilization of the structure can be ensured principally by aromatic stacking and not by H-bonds. Moreover, for the four structures investigated, the weak steric hindrance of the anion may favor the stacking interactions. All obtained organizations are in agreement with the classical crystal growth rules and the previous reported imidazolium crystalline structures [9, 14 and 15]]: to simplify the representation, the bromide anions were omitted and the schematic representation of the dications was used (the localization of anions and eventually crystallization solvents are omitted for clarity).

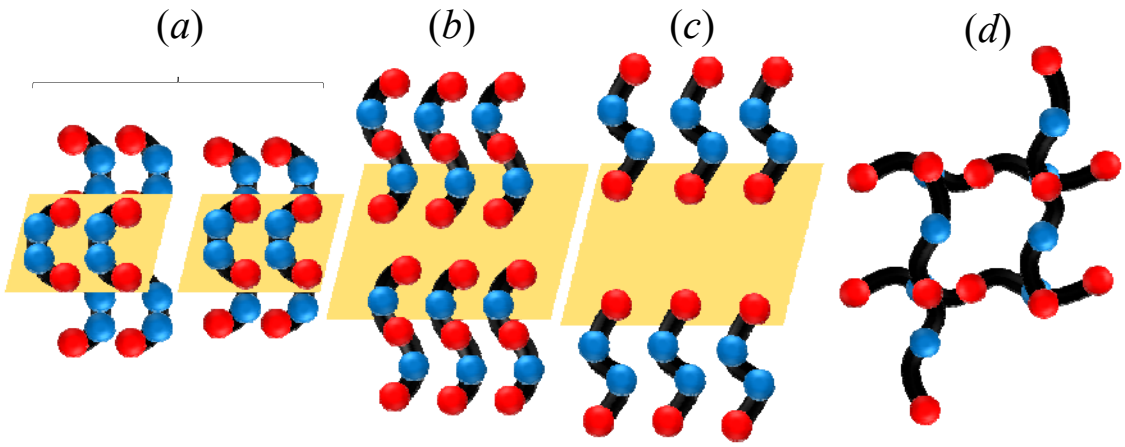


**Figure 5.5.** Schematic representations of the predicted molecular networks (projection of the structures in a plane) for the diimidazolium tectons: (*a*) **[PM][Br]$_2$**, (*b*) **[PX][Br]$_2$**, (*c*) **[BM][Br]$_2$**, and (*d*) **[BX][Br]$_2$**.

For **[PM][Br]$_2$**, two 3D organizations were obtained: one where the aromatic stacking takes place between two electron- rich rings and one where the aromatic stacking takes place between one electron-rich and one electron-poor ring. For **[PX][Br]$_2$** and **[BM][Br]$_2$**, the 3D organization is the same in terms of aromatic stacking as for **[PM][Br]$_2$**.

For **[BX][Br]$_2$** salts, the maximization of the stacking interactions results in the formation of a more porous structure. The diimidazolium moiety bearing the two imidazolium rings acts as an anion receptor. Because of the relative conformation of the imidazolium moieties, the six acidic protons can be involved in two sets of three H-bond networks, on each side of the molecule. Moreover, the diimidazolium cation offers two positive charges allowing strong electrostatic charge-charge interactions with the anions. Therefore, in the presence of anions as H-bonds acceptors, the **[BX][Br]$_2$** motif allows the repetition of the self-association process; one may expect the formation of H-bonded molecular networks based on both electrostatic charge-charge interactions and strong and directional H-bonds.

## 5.3.2 Synthesis, Crystal Informations, and Structure of the Dications.

The diimidazolium salts were obtained by a double $S_N2$ reaction involving *N*-substituted imidazoles and dibromomethane without solvent (or α,α'-dibromo-*p*-xylene in toluene, see Scheme 5.1 and ESI) [19].

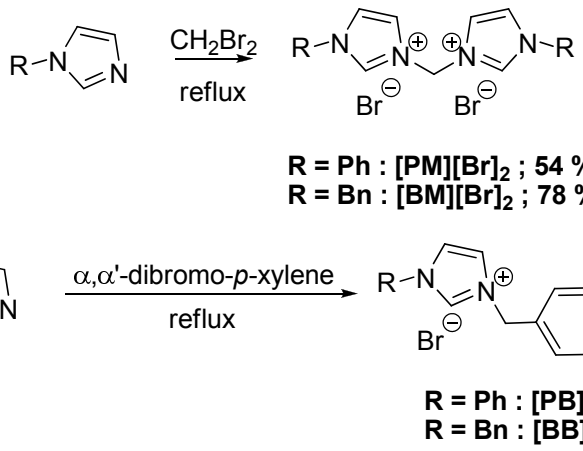


**Scheme 5.1.** Synthesis of the *N,N'*-disubstituted methylene- or xylylene-diimidazolium tectons.

To investigate the structures adopted in the solid phase, a crystallographic study of the diimidazolium cations was performed. We found that crystallization of the

diimidazolium salts can be carried out efficiently from aqueous solutions of the respective salt. For example, when a diimidazolium salt aqueous solution was warmed until homogenisation and then left at room temperature, small crystals suitable for X-ray analysis appeared after one week. It is noteworthy that all obtained crystalline materials were partially soluble in water. X-ray diffraction studies on single crystals revealed that the crystalline materials obtained are triclinic for **[PM][Br]$_2$** and monoclinic for the three others. The space groups obtained are: $P\bar{1}$ for **[PM][Br]$_2$**, $P2_1/n$ for **[PX][Br]$_2$**, $C2/c$ for **[BM][Br]$_2$** and $P2_1/c$ for **[BX][Br]$_2$** (Table 5.1). For **[PX][Br]$_2$** and **[BX][Br]$_2$**, the crystalline materials obtained are isostructural and all space groups obtained, here, have common symmetry elements, for instance: the center of inversion.

From a constitutional point of view, **[PM][Br]$_2$** crystals have an asymmetric lattice. **[PM][Br]$_2$** and **[PX][Br]$_2$** have incorporated water molecules in the lattice (one for **[PM][Br]$_2$** and four for **[PX][Br]$_2$**). In other words, the cohesion in the solid state is not ensured only by the ionic components. The presence of the phenyl groups on the imidazolium units imposes a steric hindrance for H-bonds between cations and anions: the presence of a phenyl group attached directly to the imidazolium nitrogen implies a great rigidity and a greater space between the two bromide anions. To obtain a crystal packing and to ensure its cohesion, the structure should include structuring solvent molecules (especially water, as it is an H-bond donor and acceptor). For the **[PX][Br]$_2$** salt, the presence of the xylylene spacer implies four time more water molecules in the crystal, compared to **[PM][Br]$_2$**. The **[BM][Br]$_2$** and **[BX][Br]$_2$** salts are more flexible than their phenyl analogs. As a result, the molecules can easily come together and blend into the crystal. In these cases, water molecules are necessary to ensure the cohesion of the crystal.

The dications **[PM]**, **[PX]**, **[BM]** and **[BX]** can be described as a succession of aromatic rigid units linked directly, or by flexible methylene bridges (Figure 5.6 and large ORTEP in ESI). It should be noted that for the asymmetric lattice (**[PM][Br]$_2$**), we adopted the atom numbering that uses the first digit of the atom's labeling as indication of the corresponding moiety (Figure 5.6).

**Table 5.1.** Crystal data of crystals **[PM][Br]$_2$**, **[PX][Br]$_2$**, **[BM][Br]$_2$** and **[BX][Br]$_2$**.[a]

| Compound | **[PM][Br]$_2$**[b] | **[PX][Br]$_2$**[c] | **[BM][Br]$_2$**[c] | **[BX][Br]$_2$**[c] |
|---|---|---|---|---|
| Cation and Anion Formula | $C_{19}H_{18}N_4$; $Br_2$ | $C_{26}H_{24}N_4$; $Br_2$ | $C_{21}H_{22}N_4$; $Br_2$ | $C_{28}H_{28}N_4$; $Br_2$ |
| Water | $H_2O$ | 4 $H_2O$ | - | - |
| Molecular weight | 480.21 | 624.38 | 490.25 | 580.36 |
| Crystal system | Triclinic | Monoclinic | Monoclinic | Monoclinic |
| Space group | $P\bar{1}$ | $P2_1/n$ | C2/*c* | $P2_1/c$ |
| *a*/Å | 9.8029 (3) | 12.2729 (11) | 32.8179 (8) | 10.6090 (3) |
| *b*/Å | 12.4532 (4) | 7.3230 (8) | 5.0964 (2) | 11.4607 (4) |
| *c*/Å | 16.2953 (5) | 16.1223 (14) | 12.4602 (3) | 10.5336 (4) |
| $\alpha$/deg | 89.420 (1) | 90 | 90 | 90 |
| $\beta$/deg | 89.667 (1) | 111.966 (3) | 102.4950 (10) | 97.6150 (10) |
| $\gamma$/deg | 77.057 (2) | 90 | 90 | 90 |
| *V*/Å$^3$ | 1938.64 (10) | 1343.8 (2) | 2034.65 (11) | 1269.45 (7) |
| *Z* | 4 | 2 | 4 | 2 |
| Color | colorless | colorless | colorless | colorless |
| Crystal dim./mm | 0.18×0.16×0.07 | 0.18×0.10×0.05 | 0.16×0.10×0.03 | 0.23×0.08×0.02 |
| $\mu$/mm$^{-1}$ | 5.430 | 4.147 | 5.150 | 4.227 |
| Temperature/K | 150 (2) | 150 (2) | 150 (2) | 150 (2) |
| $D_{calc.}$/Mg.m$^{-3}$ | 1.645 | 1.543 | 1.600 | 1.518 |
| *F*(000) | 960 | 636 | 984 | 588 |
| $\theta$ range for collection/deg. | 2.71 to 72.83 | 3.90 to 67.96 | 2.76 to 66.93 | 4.2 to 67.85 |
| Limiting indices | $-11 \le h \le 12$ | $-14 \le h \le 14$ | $-38 \le h \le 38$ | $-12 \le h \le 12$ |
| | $-15 \le k \le 15$ | $-7 \le k \le 7$ | $-5 \le k \le 5$ | $-13 \le k \le 13$ |
| | $-20 \le l \le 20$ | $-19 \le l \le 19$ | $-14 \le l \le 14$ | $-11 \le l \le 11$ |
| Refl. collected / unique | 26186/7426 | 10033/2240 | 14044/1711 | 19740/2139 |
| $R_{int}$ | 0.037 | 0.070 | 0.036 | 0.050 |
| Completeness to $\theta$ max./% | 0.958 | 0.917 | 0.945 | 0.951 |
| Data/restraints/parameters | 7426/6/482 | 2240/6/175 | 1711/0/123 | 2196/0/154 |
| Final *R* indices $R_1$ | 0.0343 | 0.0521 | 0.0298 | 0.0289 |
| $[I > 2\sigma(I)]$ $wR_2$ | 0.0909 | 0.1468 | 0.1230 | 0.0784 |
| *R* indices (all data) $R_1$ | 0.0362 | 0.0525 | 0.0312 | 0.0295 |
| $wR_2$ | 0.0923 | 0.1471 | 0.1283 | 0.0792 |
| Goodness-of-fit on $F^2$ | 1.034 | 1.102 | 0.834 | 1.073 |
| Largest diff. peak and hole/eA$^{-3}$ | 0.453; -1.070 | 0.681; -0.624 | 0.409; -0.440 | 0.691; -0.251 |

[a]Absorption correction: Empirical (SADABS), Refinement method: Full-matrix least-squares on $F^2$. [b]Diffractometer: Bruker Platform, equipped with a Bruker SMART 4K Charged-Coupled Device (CCD) Area Detector using the program APEX II and a Nonius FR591 rotating anode equipped with Montel 200 optics. [c]Diffractometer: Bruker microstar equipped with a Platinum 135 CCD Detector, a Helios optics and a Kappa goniometer.

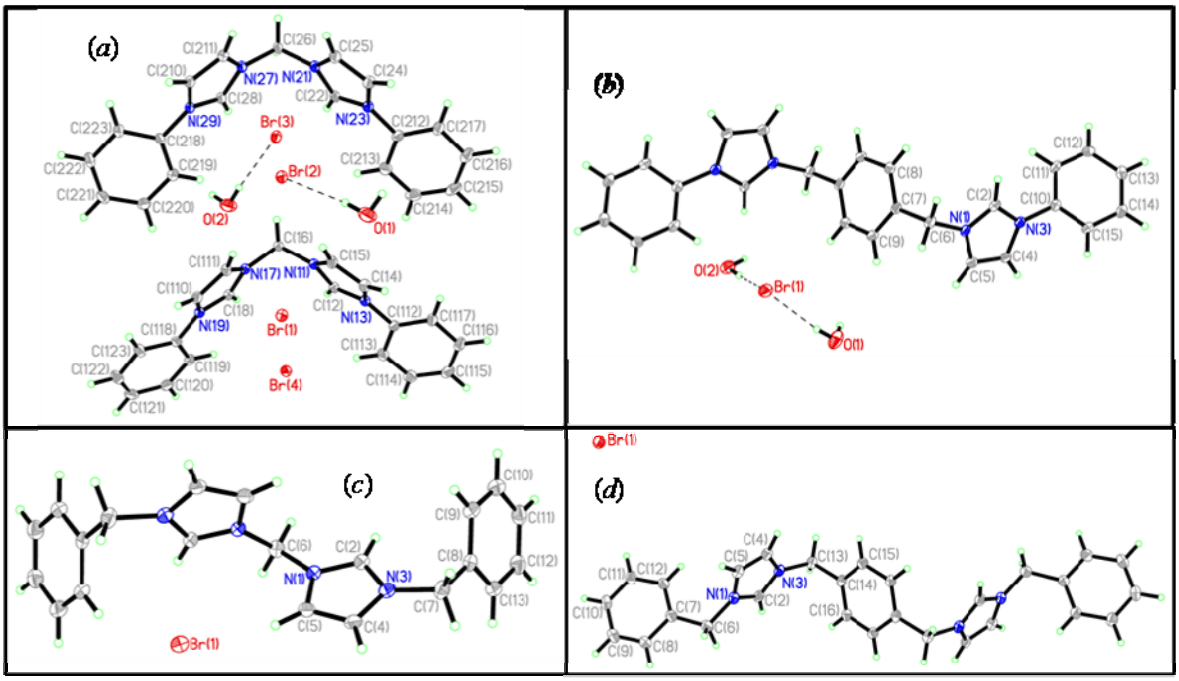


**Figure 5.6.** ORTEP view of the (*a*) **[PM][Br]$_2$**, (*b*) **[PX][Br]$_2$**, (*c*) **[BM][Br]$_2$**, and (*d*) **[BX][Br]$_2$** with the numbering scheme adopted. Ellipsoids are drawn at 50% probability level.

The **[PM]** and **[PX]** dications show a similar organization. In fact, when an aromatic ring is directly attached to the imidazolium unit, we observe the absence of the coplanarity between the imidazolium and the aromatic rings, which suggests a lack of electron delocalization. The **[BM]** and **[BX]** dications present an *anti* conformation of the aromatic rings. This observation suggests an increase of the complexity of the dication structure with the incorporation of methylene residues between the aromatic units. The simplest organization is obtained for the **[PM]** cation, which can be described as a bent molecule via the central methylene linker. The most complicated structure (the **[BX]** cation) adopts a stair conformation (Figure 5.6). This stair conformation is due to the *anti* conformation of the aromatic rings that implies the appearance of parallel planes (see the

inter-plane distances between aromatic rings in ESI, Table S1). It is noteworthy that these conformations are very close to those obtained by molecular modeling (see Figure 5.4).

## 5.3.3 Supramolecular Organization

### 5.3.3.1 Aromatic Stacking

The organization obtained in the dicationic network is governed by stacking interactions of the aromatic rings (Figure 5.7 and Supporting Information).

Crystal organization of the diimidazolium cations is in close agreement with the theoretical organization predicted by molecular modeling, except for **[BM][Br]$_2$**. For this last molecule, the conformation is responsible for the special organization observed in the solid state: the molecules are stacked on each other with a distance of 5 Å between the same rings. This long distance suggests that stacking interactions are quite weak. For **[PM][Br]$_2$**, the aromatic stacking takes place between the phenyl residues with a distance of 4 Å. It is important to note that π-ring overlap is partially due to the interaction of the p-electrons and electron charge transfer. The *cisoid*-type conformation of **[PM][Br]$_2$** is responsible for the organization observed in the solid state. In this structure, as well as in the **[BM][Br]$_2$**, the succession of two imidazolium rings separated by a methylene spacer is not favorable to the formation of charge transfer interaction. Two reasons can be highlighted: (i) the steric hindrance of this motif, and (ii) the non-juxtaposition of electron-rich and electron-poor rings. The last hypothesis is corroborated by **[PX][Br]$_2$** and **[BX][Br]$_2$** structures, where aromatic stacking occurs between electron-rich (phenyl, benzyl or xylylene) and electron-poor rings (imidazolium). The distance between two identical rings is comprised between 3.4 and 3.6 Å. A global alternation of electron-rich and electron-poor rings along the axis of the molecule is also important for the supramolecular organization. For example, the most flexible and alternating molecules (**[PX][Br]$_2$** and **[BX][Br]$_2$**) are more involved in charge transfer aromatic stacking interactions in the solid phase. In **[PX][Br]$_2$**, as well as in **[BX][Br]$_2$**, π-stacking occurs between the different aromatic rings, but for **[BX][Br]$_2$**, which is more flexible than

**[PX][Br]$_2$**, classical aromatic stacking between two benzyl rings can also observed, as well as T-stacking between a phenyl proton and another phenyl ring with a distance of 3.2 Å.

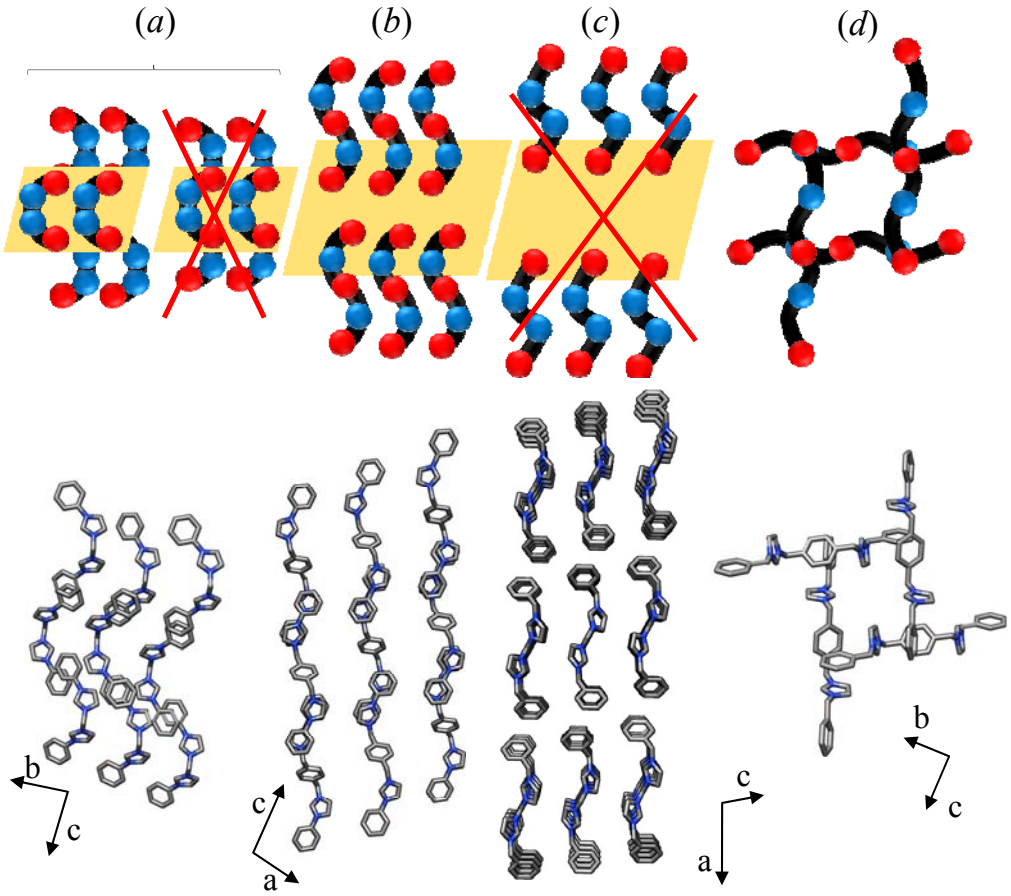


**Figure 5.7.** Crystal packing of the diimidazolium dications: predicted (above) and obtained by X-rays diffraction (below): (a) **[PM]**, (b) **[PX]**, (c) **[BM]** and (d) **[BX]**. Hydrogen atoms, bromide anions and water molecules are omitted for clarity.

### 5.3.3.2 Complementary interactions

In each structure, complementary interactions to stacking exist: H-bonds and electrostatic interactions. The H-bonds occur between the acidic proton of imidazolium

rings and bromide anions and/or the oxygen of water molecules. As in the previous reported structures, all the H•••X distances are inferior to 3.2 Å and the C-H•••X angles vary between 138 and 176° (Tables 5.2, 5.3, 5.4 and 5.5) [9].

**Table 5.2.** Distances and angles of X-H•••Br hydrogen bonds in **[PM][Br]$_2$**.[a]

| | X•••H (Å) | H•••Br (Å) | X•••Br (Å) | X–H•••Br (°) | Symmetry operators for Br[b] |
|---|---|---|---|---|---|
| H-bonds between cation 1 and Br | | | | | |
| $C_{12}$-$H_{12}$•••$Br_1$ | 0.95 | 2.7298 | 3.6007 | 152.74 | x, y, z |
| $C_{18}$-$H_{18}$•••$Br_1$ | 0.95 | 2.6295 | 3.5169 | 155.66 | x, y, z |
| $C_{15}$-$H_{15}$•••$Br_2$ | 0.95 | 2.8207 | 3.6731 | 149.82 | x, y, z |
| $C_{110}$-$H_{110}$•••$Br_2$ | 0.95 | 2.7957 | 3.7005 | 159.50 | 1-x, 1-y, 2-z |
| $C_{111}$-$H_{111}$•••$Br_2$ | 0.95 | 3.1190 | 3.9405 | 145.71 | x, y, z |
| $C_{14}$-$H_{14}$•••$Br_3$ | 0.95 | 2.8548 | 3.6862 | 146.75 | 1+x, y, z |
| H-bonds between cation 2 and Br | | | | | |
| $C_{24}$-$H_{24}$•••$Br_1$ | 0.95 | 2.8149 | 3.6488 | 147.05 | x, 1+y, z |
| $C_{22}$-$H_{22}$•••$Br_3$ | 0.95 | 2.7037 | 3.5713 | 152.14 | x, y, z |
| $C_{28}$-$H_{28}$•••$Br_3$ | 0.95 | 2.7084 | 3.5900 | 154.64 | x, y, z |
| $C_{25}$-$H_{25}$•••$Br_4$ | 0.95 | 2.7631 | 3.6192 | 150.33 | -1+x, 1+y, z |
| $C_{210}$-$H_{210}$•••$Br_4$ | 0.95 | 2.8815 | 3.7941 | 161.40 | 1-x, 1-y, 2-z |
| $C_{211}$-$H_{211}$•••$Br_4$ | 0.95 | 2.7906 | 3.6495 | 150.81 | -1+x, 1+y, z |
| H-bonds between water and Br | | | | | |
| $O_1$-$H_{1A}$•••$Br_1$ | 0.84 | 2.4940 | 3.3319 | 175.45 | x, 1+y, z |
| $O_1$-$H_{1B}$•••$Br_2$ | 0.84 | 2.6409 | 3.4692 | 169.02 | x, y, z |
| $O_2$-$H_{2A}$•••$Br_3$ | 0.84 | 2.5399 | 3.3783 | 176.03 | x, y, z |
| $O_2$-$H_{2B}$•••$Br_4$ | 0.84 | 2.6511 | 3.4866 | 173.27 | -1+x, y, z |

[a] Only H•••Br that have significant interactions are reported. [b] Symmetry operator for the other atoms are x, y, z.

**Table 5.3.** Distances and angles of X-H•••Y hydrogen bonds in **[PX][Br]$_2$**.[a]

| | X•••H (Å) | H•••Y (Å) | X•••Y (Å) | X–H•••Y(°) | Symmetry operators for Y[b] |
|---|---|---|---|---|---|
| H-bonds between cation and water | | | | | |
| $C_2$-$H_2$•••$O_2$ | 0.95 | 2.2776 | 3.2031 | 164.49 | -x, 1-y, 1-z |
| $C_4$-$H_4$•••$O_2$ | 0.95 | 2.4840 | 3.3882 | 159.02 | 1/2+x, 1/2-y, -1/2+z |
| $C_5$-$H_5$•••$O_2$ | 0.95 | 2.4095 | 3.3579 | 176.02 | 1/2-x, 1/2+y, 3/2-z |
| H-bonds pentagonal ring | | | | | |
| $O_1$-$H_{1A}$•••$Br_1$ | 0.84 | 2.4585 | 3.2927 | 172.18 | x, y, z |
| $O_1$-$H_{1B}$•••$Br_1$ | 0.84 | 2.5533 | 3.3552 | 160.05 | 1/2-x, -1/2+y, 3/2-z |
| $O_2$-$H_{2A}$•••$Br_1$ | 0.84 | 2.4357 | 3.2646 | 169.17 | x, y, z |
| $O_2$-$H_{2B}$•••$O_1$ | 0.84 | 1.9289 | 2.7313 | 159.42 | 1/2-x, -1/2+y, 3/2-z |

[a]Only H•••Y that have significant interactions are reported. [b]Symmetry operator for the other atoms are x, y, z.

These H-bonds are weak to moderate.[12] For two structures (**[PM][Br]$_2$** and **[PX][Br]$_2$**), water molecules are incorporated in the crystal to ensure its cohesion. However, the incorporation of water is different in the both structures. For **[PM][Br]$_2$**, the presence of the methylene between the imidazolium rings implies direct H-bonds between the most acidic proton of the imidazolium ring and the anions, and the insertion of water helps to connect some bromide anions. The H-bonds between the anions and water molecules are very local and any particular geometry can be highlighted (Figure 5.8a and Tables 5.2 and 5.3).

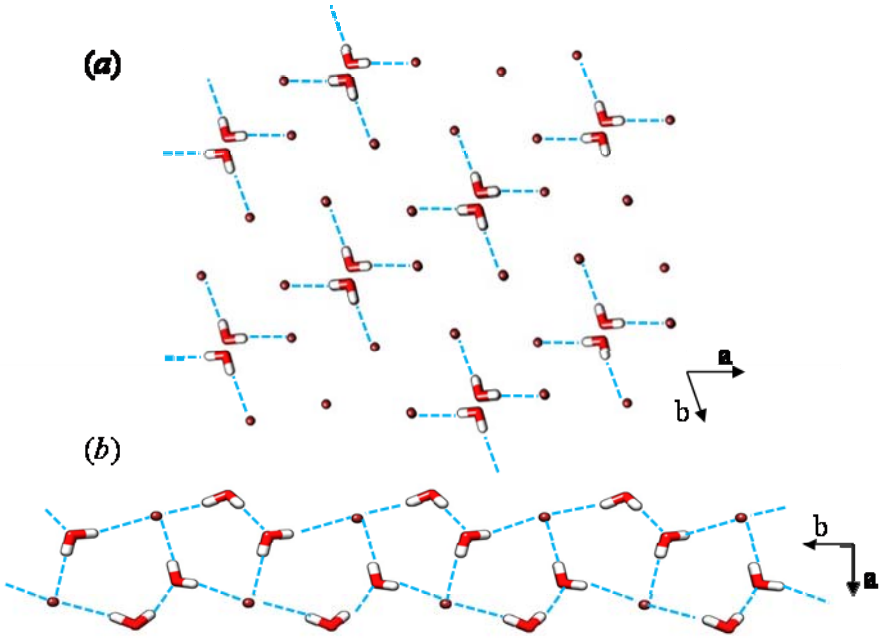


**Figure 5.8.** Structural water in: (*a*) **[PM][Br]$_2$** and (*b*) **[PX][Br]$_2$** (H-bonds: blue dotted lines).

In the case of **[PX][Br]$_2$**, the water molecules are directly connected by H-bonds to the acidic proton of the imidazolium rings and the bromide anions help to connect all the water molecules. For this last compound, H-bonds allow the formation of a pentagonal ring formed by two bromides and three water molecules. These pentagonal rings are inter-connected via water bromide H-bonds to form a filament of rings (Figure 5.8b). In the **[PM][Br]$_2$** structure, each bromide is connected by H-bonds to the imidazolium rings (principal H-bonds), which can suggest that the water H-bonds are not essential in the solid state: the water molecules are locally connected, but not inter-connected (secondary H-bonds), whereas, in the **[PX][Br]$_2$** structure, all the pentagonal ring filaments are linked via H-bonds between the acid protons of the dication and the water oxygen atom. In other words, this structure shows an extended H-bonds network and all dications, anions and water molecules are connected (Figure 5.9).

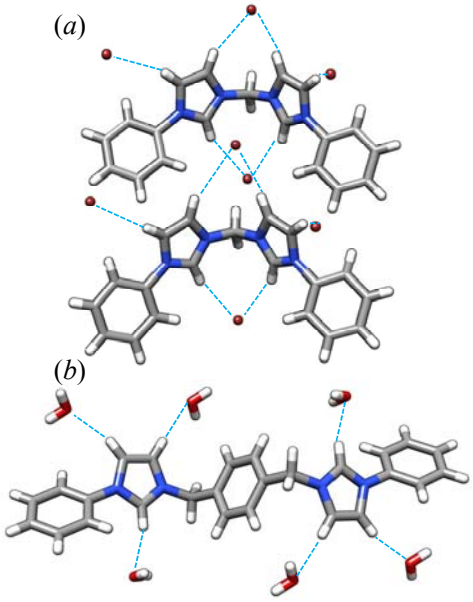


**Figure 5.9.** Local H-bonds (dotted blue lines) close to a dication: (*a*) **[PM][Br]$_2$** and (*b*) **[PX][Br]$_2$**.

In **[BM][Br]$_2$** and **[BX][Br]$_2$**, the lattice packing reveals that H-bond interactions occur between cations and bromide anions. In **[BM][Br]**$_2$, six H-bonds close to a dication are developed (two between the most acidic proton H(2) of the imidazolium and bromide anions and four between H(4) or H(5) and bromide anions, distance H•••Br < 3 Å, see Figure 5.10a and Tables 5.4 and 5.5).

In the case of **[BX][Br]$_2$**, only four H-bonds exist (two between the most acidic proton H(2) of the imidazolium and bromide anions and two between H(4) and bromide anions, see Figure 5.10b). An interesting observation can be made: when the stacking is important in the solid state, the H-bonds are weak and vice-versa. For example, in **[PM][Br]$_2$** and **[BM][Br]$_2$**, the stacking is weak and the interactions take place between similar rings, i.e. π-orbital overlap is only partial. As a result, the stacking distance is superior to 4 Å. However, in these two structures, compensation by H-bonding is obtained in the solid state.

**Table 5.4.** Distances and angles of C-H•••Br hydrogen bonds in **[BM][Br]$_2$**.[a]

| | C•••H (Å) | H•••Br (Å) | C•••Br (Å) | C–H•••Br (°) | Symmetry operators for Br[b] |
|---|---|---|---|---|---|
| $C_2$-$H_2$•••$Br_1$ | 0.95 | 2.7326 | 3.5744 | 148.09 | 1-x, 1+y, 3/2-z |
| $C_4$-$H_4$•••$Br_1$ | 0.95 | 2.7197 | 3.6380 | 162.79 | 1-x, -y, 1-z |
| $C_5$-$H_5$•••$Br_1$ | 0.95 | 2.7233 | 3.6386 | 161.97 | x, y, z |

[a] Only H•••Br that have significant interactions are reported. [b] Symmetry operator for the other atoms are x, y, z.

**Table 5.5.** Distances and angles of C-H•••Br hydrogen bonds in **[BX][Br]$_2$**.[a]

| | C•••H (Å) | H•••Br (Å) | C•••Br (Å) | C–H•••Br (°) | Symmetry operators for Br[b] |
|---|---|---|---|---|---|
| $C_2$-$H_2$•••$Br_1$ | 0.95 | 2.5951 | 3.5082 | 161.30 | x, -1+y, z |
| $C_4$-$H_4$•••$Br_1$ | 0.95 | 3.0434 | 3.8111 | 138.92 | -x, -1/2+y, 3/2-z |

[a] Only H•••Br that have significant interactions are reported. [b] Symmetry operator for the other atoms are x, y, z.

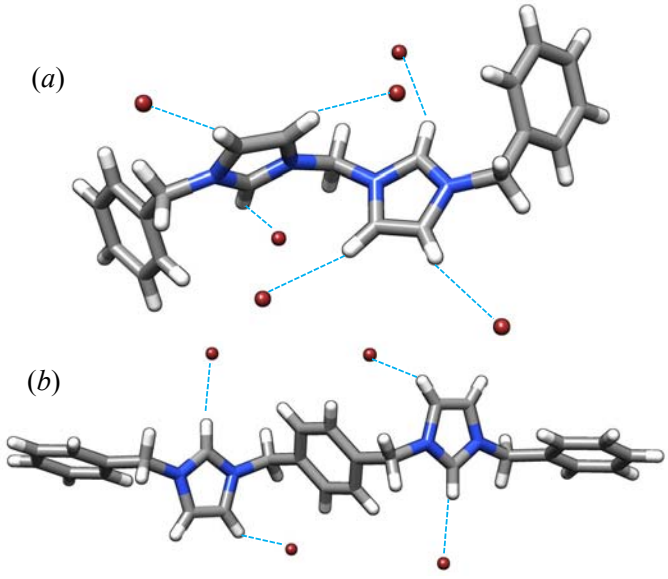


**Figure 5.10.** Local H-bonds (dotted blue lines) close to a dication: (*a*) **[BM][Br]$_2$** and (*b*) **[BX][Br]$_2$**.

## 5.4 Conclusions

In summary, the detailed structures of four new diimidazolium cations with bromide anions have been obtained. Given the precise X-ray crystal data and the molecular modeling, we are able to understand the structural organization in the solid state. The structure of the dication (as well as the structure of the anion, not studied here) is essential in dictating the self assembly of dications, anions and eventually the inclusion of water molecules in the solid state. This study has highlighted some important parameters in the self-assembly governed by stacking interactions : (i) a perfect alternation of electron rich and electron poor ring is necessary to maximize the interactions all along the molecule; (ii) the presence of a flexible spacer (methylene) between the aromatics rings is important to maximize this stacking. In the most flexible molecules, stacking becomes the principal interaction at the expense of H-bonds (**[PX][Br]$_2$** and **[BX][Br]$_2$**). For the most flexible and stacked structure, **[BX][Br]$_2$**, the dication packing can be described as a channeled structure. In line with current interest in the development of new supramolecular crystalline structures in the field of molecular tectonics, this knowledge can aid in the design of self-assembly of imidazolium cations and anions to form highly organized structures, in particular channeled structures. We demonstrated here that imidazolium cations are versatile tectons that can be further decorated with functional groups in order to obtain crystalline materials with predictable properties.

## 5.5 Acknowledgment.

We are grateful to the Natural Sciences and Engineering Research Council of Canada, the Fonds Québécois de la Recherche sur la Nature et les Technologies, the Canada Foundation for Innovation and Université de Montréal for financial support. We thank Dr. Michel Simard for X-ray acquisitions. We also thank colleagues for careful reading and discussion of this manuscript.

## 5.6 Supporting Information Available

Synthesis, characterization, large ORTEP views, supplementary figures, and crystallographic information are available free of charge via the Internet at http://pubs.acs.org

## 5.7 References

1 (a) Khan, M.; Enkelmann, V.; Brunklaus, G. *Cryst. Growth & Des.* **2009**, *9*, 2354–2362. (b) Palma, C. A.; Bonini, M.; Breiner, T.; Samori, P. *Adv. Mater.* **2009**, *21*, 1383–1386. (c) Men, Y. B.; Sun, J.; Huang, Z. T.; Zheng, Q. Y. *Angew. Chem., Int. Ed.* **2009**, *48*, 2873–2876. (d) Desiraju, G. R. *Crystal Engineering: The Design of Organic Solids*; Elsevier: New York, **1989**; Vol. 54. (e) Zaworotko, M. *J. Chem. Soc. Rev.* **1994**, 283–288. (f) Batten, S. R. J. *Angew. Chem. Int. Ed.* **1998**, *37*, 1461–1494. (g) Hagrman, P. J. J. *Angew. Chem., Int. Ed.* **1999**, *38*, 2638–2684.

2 (a) Kawamichi, T.; Kodama, T.; Kawano, M.; Fujita, M. *Angew. Chem., Int. Ed.* **2008**, *47*, 8030–8032. (b) Dalrymple, S. A.; Shimizu, G. K. H. *J. Am. Chem. Soc.* **2007**, *129*, 12114–12119. (c) Higuchi, M.; Horike, S.; Kitagawa, S. *Supramol. Chem.* **2007**, *19*, 75–78. (d) Du, M.; Zhang, Z. H.; Tang, L. F.; Wang, X. G.; Zhao, X. J.; Batten, S. R. *Chem. Eur. J.* **2007**, *13*, 2578–2586. (e) Eddaoudi, M. *J. Am. Chem. Soc.* **2000**, *122*, 1391–1397. (f) Kepert, C. J. *Chem. Commun.* **1998**, 31–32. (g) Kepert, C. J. *J. Am. Chem. Soc.* **2000**, *122*, 5158–5168. (h) Kondo, M. *Chem. Mater.* **2000**, *12*, 1288–1299. (i) Seo, J. S. *Nature* **2000**, *404*, 982–986.

3 (a) Dalgarno, S. J.; Thallapally, P. K.; Barbour, L. J.; Atwood, J. L. *Chem. Soc. Rev.* **2007**, *36*, 236–245. (b) Sarkar, M.; Biradha, K. *Cryst. Growth & Des.* **2007**, *7*, 1318–1331. (c) Palmore, G. T. R.; MacDonald, J. C. *In The Amide Linkage: Structural Significance in Chemistry, Biochemistry and Materials Science*;

Greenberg, A., Breneman, C. M., Liebman, J. F., Eds.; John Wiley and Sons: New York, **2000**; pp 291-336. (d) Vogtle, F. *Supramolecular Chemistry: An Introduction*; John Wiley and Sons: New York, **1991**.

4 (a) Zaworotko, M. J. *Cryst. Growth & Des.* **2007**, *7*, 4–9. (b) Yaghi, O. M.; Li, G.; Li, H. *Nature* **1995**, *378*, 6558. (c) Yaghi, O. M.; Li, G. *Angew. Chem., Int. Ed.* **1995**, *34*, 307-308.

5 (a) Dupont, J. *J. Braz. Chem. Soc.* **2004**, *15*, 341–350. (b) Avent, A. G.; Chaloner, P. A.; Day, M. P.; Seddon, K. R.; Welton, T. *J. Chem. Soc., Dalton Trans.* **1994**, 3405–3413.

6 (a) Gordon, C. M.; Holbrey, J. D.; Kennedy, A. R.; Seddon, K. R. *J. Mater. Chem.* **1998**, *8*, 2627–2636. (b) Dupont, J.; Suarez, P. A. Z.; de Souza, R. F.; Burrow, R. A.; Kintzinger, J. P. *Chem. Eur. J.* **2000**, *6*, 2377–2381. (c) van den Broeke, J.; Stam, M.; Lutz, M.; Kooijman, H.; Spek, A. L.; Deelman, B.-J.; van Koten, G. *Eur. J. Inorg. Chem.* **2003**, 2798–2811. (d) Holbrey, J. D.; Reichert,W. M.; Nieuwenhuyen, J. S.; Seddon, K. R.; Rogers, R. D. *Chem. Commun.* **2003**, 1636–1837. (e) Saha, S.; Hayashi, S.; Hamaguchi, H. *Chem. Lett.* **2003**, *32*, 740–741. (f) Downard, A.; Earle, M. J.; Hardacre, C.; McMath, S. E. J.; Nieuwenhuyzen, M.; Teat, S. J. *Chem. Mater.* **2004**, *16*, 43–46. (g) Holbrey, J. D.; Reichert,W. M.; Rogers, R. D. *Dalton Trans.* **2004**, *15*, 2267–2271. (h) Golovanov, D. G.; Lyssenko, K. A.; Antipin, M. Y.; Vygoskii, Y. S.; Lozinskaya, E. I.; Shaplov, A. S. *Cryst. Eng. Comm.* **2005**, *6*, 53–56. (i) Fujimoto, T.; Kawahata, M.; Nakakoshi, Y.; Yamaguchi, K.; Machinami, T.; Nischikawa, K.; Tashiro, M. *Anal. Sci.* **2007**, *23*, 107–108. (j) Nakakoshi, Y.; Shiro, M.; Fujimoto, T.; Machinami, T.; Seki, H.; Tashiro, M.; Nischikawa, K. *Chem. Lett.* **2006**, *35*, 1400–1401. (k) Getsis, A.; Mudring, A.-V. *Acta Crystallogr.* **2005**, *E61*, 2945–2946. (l) Leclercq, L.; Suisse, I.; Nowogrocki, G.; Agbossou-Niedercorn, F. *J. Mol. Struct.* **2008**, *892*, 433–437.

7 Dupont, J.; Suarez, P. A. Z. *Phys. Chem. Phys. Chem.* **2006**, *8*, 2441–2452.

8 (a) Amyes, T. L.; Diver, S. T.; Richard, J. P.; Rivas, F. M.; Toth, K. *J. Am. Chem. Soc.* **2004**, *126*, 4366–4374. (b) Alder, R. W.; Allen, P. R.;Williams, S. J. *J. Chem. Soc., Chem. Commun.* **1995**, 1267–1268.

9 Jeffrey, G. A. *An Introduction to Hydrogen Bonding;* Oxford University Press: Oxford, **1997**.

10 (a) Schalley, C. A. *Handbook of Spectroscopy*; Gauglitz, G.; Vo-Dinh. T., Eds.; Wiley-VCH: Weinheim, **2003**, pp 2-4. (b) Vilar, R. *Supramolecular Assembly via Hydrogen Bonds II*, Mingos, D. M. P.; Braga, D., Eds.; Springer: New-York, **2004**; p 114.

11 (a) Gabriel, G.; Iverson, B. *J. Am. Chem. Soc.* **2002**, *124*, 15174– 15175. (b) Klarner, F. G.; Kuchenbrandt, M. C. *Strategies and Tactics in Organic Synthesis*; Harmata, M.; Stork, G.; Eds.; Academic Press: New York, **2004**; p 119.

12 Ghosh, S.; Ramakrishnan, S. *Angew. Chem. Int. Ed.* **2004**, *43*, 3264–3268.

13 (a) Leclercq, L.; Schmitzer, A. R. *J. Phys. Chem. A* **2008**, *112*, 4996– 5001. (b) Leclercq, L.; Simard, M.; Schmitzer, A. R. *J. Mol. Struct.* **2009**, *918*, 101–107.

14 Serrano-Becerra, J. M.; Herm_andez-Ortega, S.; Morales-Morales, D.; Valdes-Martinez, J. *Cryst. Eng. Comm.* **2009**, *11*, 226–228.

15 (a) Zhao, H.; Malhotra, S. V. *Aldrich Acta* **2002**, *35*, 75–83. (b) Chauvin, Y.; Olivier-Bourbigou, H. *CHEMTECH* **1995**, *25*, 26–30. (c) Seddon, K. R. *J. Chem. Technol. Biotechnol.* **1997**, *68*, 351–356. (d) Sheldon, K. R. *Chem. Commun.* **2001**, 2399–2407. (e) Leclercq, L.; Suisse, I.; Nowogrocki, G.; Agbossou Niedercorn, F. *Green Chem.* **2007**, *9*, 1097–1103. (f) Leclercq, L.; Suisse, I.; Agbossou Niedercorn, F. *Chem. Commun.* **2008**, 311–313. (g) Song, C. E. *Chem. Commun.* **2004**, 1033–1043. (h) Park, S.; Kazlauskas, R. *J. Curr. Opin. Biotechnol.* **2003**, *14*, 432–437. (i) Kragl, U.; Eckstein, M.; Kaftzik, N. *Curr. Opin. Biotechnol.* **2002**, *13*, 565–571. (j) Poole, C. F. *J. Chromatogr. A* **2004**, 1037, 49–82. (k) Stalcup, A. M.; Cabovska, B. *J. Liq. Chromatogr. Relat. Technol.* **2004**, *27*, 1443–1459. (l) Antonietti, M.;

Kuang, D. B.; Smarsly, B.; Yong, Z. *Angew. Chem. Int. Ed.* **2004**, *43*, 4988–4992. (m) Geetha, S.; Trivedi, D. C. *Bull. Electrochem.* **2003**, *19*, 37–48.

16 For examples of semiempirical calculations that predict the conformation in crystal structures see: (a) Bock, H.; Nagel, N.; Eller, P. Z. *Kristallogr.* **2000**, *215*, 39–44. (b) Kabak, M. *J. Mol. Struct.* **2003**, *655*, 135–139. (c) Elerman, Y.; Kabak, M.; Elmali, A. Z. *Naturforsch.* **2002**, *57*, 651–656.

17 (a) Hassinen, T.; Perakyla, M. *J. Comput. Chem.* **2001**, *22*, 1229– 1242. (b) For more details about Ghemical, please visit http://www.uku.fi/~thassine/projects/ghemical/.

18 For more details about MOPAC7, please visit http://sourceforge.net/projects/mopac7/.

19 (a) Noujeim, N.; Leclercq, L.; Schmitzer, A. R. *J. Org. Chem.* **2008**, *73*, 3784–3790. (b) Leclercq, L.; Noujeim, N.; Sanon, S.; Schmitzer, A. R. *J. Phys. Chem. B* **2008**, *112*, 14176–14184.

# Chapitre 6 : Formation de cristaux-liquides à base de sels de phénylènediimidazolium

# 6.0 Préface

Les sels de diimidazolium étudiés au chapitre 4 pour leurs propriétés de complexation avec le CB[7] ont été modifiés pour former des mésophases smectiques. C'est la caractérisation complète de ces mésophases qui est présentée dans ce chapitre 6, en plus de l'étude d'une structure cristalline qui a fortement suggéré la possibilité d'obtenir des phases liquide-cristallines. L'étude détaillée des patrons de diffraction des rayons-X de poudre ainsi que des vues en microscopie optique polarisée ont permis de classer les mésophases et de proposer un mode d'organisation de ces sels de diimidazolium dans ces mésophases.

J'ai réalisé toutes les études physico-chimiques et de caractérisation des mésophases pour les quatre sels de diimidazolium présentés à l'exception d'une des quatre études de diffraction des rayons-X réalisée par Ludovic Eberlin. La synthèse des quatre molécules a été réalisée par Samantha H. Sanon et Ludovic Eberlin selon un protocole expérimental que j'ai mis au point.

Les informations expérimentales supplémentaires de cette partie se trouvent aux pages 246-253 de la thèse.

# Article 5. Dialkyl(1,4-phenylene)diimidazolium salts: a new class of ionic liquid crystals

Nadim Noujeim, Ludovic Eberlin, Samantha H. Sanon and Andreea R. Schmitzer*

Département de chimie, Université de Montréal, CP 6128, Succursale Centre-Ville, Montréal, Québec, H3C 3J7, Canada

*Soumis pour publication*

## 6.1 Abstract

A new family of dialkyl(1,4-phenylene)diimidazolium salts has been synthesized. Various salts containing triflate and *bis*(trifluoromethanesulfonyl)imide anions and different alkyl chains have been prepared. The molecular structure of didodecyl(1,4-phenylene)diimidazolium salt was determined by single crystal X-ray diffraction, in order to have a better understanding of the structure relation between the solid and liquid crystal.The mesomorphic properties of all the compounds were investigated.

## 6.2 Introduction

Studies of ionic liquids (IL) have shown many useful properties such as high thermal and chemical stability, low volatility, non-flammability and a wide electrochemical window [1]. Imidazolium-based ionic liquids are well known and have already found wide applications in electrochemical devices, ion transport systems and dye-sensitized solar cells [2]. Some imidazolium based ILs have also recently been shown to be useful in catalysis, either as solvents for bioorganic catalysis [3] or as emulsion regulators in biphasic processes [4]. Recently, imidazolium-based thermotropic and lyotropic liquid crystals (LC) were reported [5], by combining the self-organization properties of LCs with the unique solvent properties and ion-conducting properties of imidazolium ILs yielding imidazolium-based ionic liquid crystals (ILC). The properties of ILs differ significantly from those of conventional liquid crystals [6].

For further application of imidazolium-based ILCs the study of the liquid crystalline properties depending on the molecular structure is essential. The imidazolium-based LCs can currently be classified into four classes: 1) Imidazolium-based LCs with one or two alkyl chains [7] incorporating in some cases an aromatic ring, generally exhibiting smectic mesophases. 2) Taper shaped imidazolium salts with multiple alkyl chains [8], with properties directly related to their strong amphiphilic character and space filling of the

lipophilic chains. 3) Rodlike and disc like mesogens with connected imidazoliums units by long flexible spacers [9].Usually, smectic and columnar phases are stabilized with these compounds. 4) Bent molecules where the imidazolium group is part of the rigid core unit are the least investigated class of imidazolium-based ILCs [10].

We report here the synthesis and study of a new symmetrical type of imidazolium-based LC which incorporate more than one of the characteristics of the four classes mentioned above. The rigid core is composed of a diimidazolium disubstituted benzene ring and two long alkyl chains are attached to this central core, one on each imidazolium moiety, to give a symmetrical compound. The length of the alkyl chains and the nature of the counter-ion were varied in order to investigate their influence on the mesomorphic properties of these salts (Scheme 6.1).

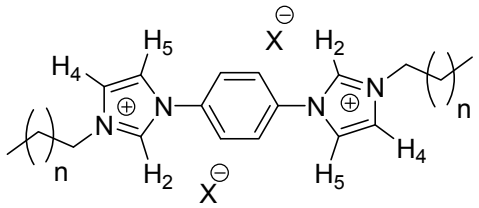


X = Br ; n = 10 (**1a**) X = Br ; n = 14 (**1b**)
X = $CF_3SO_3$ ; n = 10 (**2a**) X = $CF_3SO_3$ ; n = 14 (**2b**)
X = $N(SO_2CF_3)_2$ ; n = 10 (**3a**) X = $N(SO_2CF_3)_2$ ; n = 14 (**3b**)

**Scheme 6.1.** Dialkyl(1,4-phenylene)diimidazolium salts.

## 6.3 Results and discussion

We previously reported the synthesis and supramolecular properties of similar dialkyl(1,4-phenylene)diimidazolium bromide salts with shorter alkyl chains [11]. The increase of the length of the alkyl chains and variation of the counter-ions allowed us to obtain mesogenic compounds. Some of these compounds display LC properties in a very large temperature range. These salts were obtained in a three-step procedure (Scheme 6.2). The first step is a copper (I) catalyzed Ullman-type coupling carried out in anhydrous

acetonitrile. The second step is a double nucleophilic substitution of either 1-bromododecane or 1-bromohexadecane on the diimidazole intermediate. This step yielded dialkyl(1,4-phenylene)diimidazolium bromide salts **1a-b** which were engaged in anion metathesis to afford compounds **2a-b** and **3a-b**. All the salts were air stable and were characterized by $^{1}H$, $^{13}C$ NMR and high resolution mass spectrometry.

Single crystals of **2a** suitable for X-ray diffraction were obtained by direct crystallization from acetonitrile. Both crystal and molecular structures are shown in Figure 6.1. The crystalline material obtained is triclinic, and the obtained space group is P-1. Consequently, both imidazolium moieties and alkyl chains are symmetrical with the center of the benzene ring as a center of symmetry. The two acidic imidazolium H2 protons are thus pointing in opposite directions, as we previously predicted by molecular modeling [11].

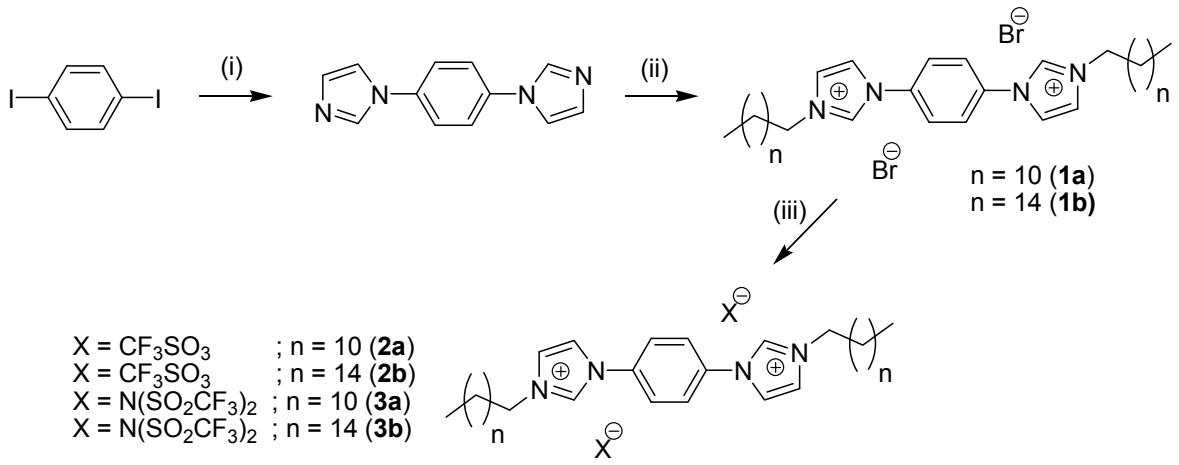


**Scheme 6.2.** Synthesis of the Dialkyl(1,4-phenylene)diimidazolium salts. (i) $Cs_2CO_3$, imidazole, $Cu_2O$, salycilaldoxime, acetonitrine, reflux, 48h, 81 % (ii) Alkyl bromide, acetonitrile, reflux, 12h; (iii) $NH_4CF_3SO_3$ or $LiN(SO_2CF_3)_2$, water/methanol, r.t. 30 mins 67-88 % (2 steps).

The crystal packing, as shown in Figure 6.1, can be described as a lamellar system in the (bc) plane. The only supramolecular interactions observed in the crystal structure are

the hydrophobic interactions between the alkyl chains and H-bonding between the acidic H2 imidazolium proton and the oxygen atom of the triflate anion. No π-stacking or T-stacking were observed in this crystal structure, which is usually very common for this kind of diimidazolium compounds, as previously described by our research group [12]. In the crystal structure of **2a**, the alkyl chains are separated from each other by 4.4 Å in the (bc) plane, and by 8.5 Å along the (a) axis, which further demonstrates the lamellar structure. The symmetry within the crystal and the angles between the imidazolium moieties and the alkyl chains give a unique S-like shape to the molecule. This class of diimidazolium salt cannot be described as rod or cylinder-shaped molecules, but can be described as containing two 16 Å long cylinders linked to a smaller 10 Å cylinder with angles of 45°. The interpenetration of the alkyl sidechains is not complete, but a four carbon gap can be observed. For example, the C4 of a sidechain is closer to the C8 of the next sidechain. With the triflate counter-ion, no direct interactions were observed between the imidazolium cores and the anions. With a bigger anion like the $NTf_2$, it could be possible to obtain intermolecular ionic bridges between the imidazolium cores and the anions.

While compounds **1a-b** decompose before their fusion point, no other transition to a mesophase was observed before their decomposition. Thermogravimetric analyses of compounds **2a-b** and **3a-b** showed that they were stable in a wide temperature range. The triflate salts **2a-b** exhibited two phase transitions below the isotropic phase, while the *bis*(trifluoromethylsulfonyl)imidate ($NTf_2$) salts **3a-b** exhibited only one transition, but at a lower temperature. For all the compounds, their mesomorphic properties and phase transition temperatures were investigated by differential scanning calorimetry (DSC), polarizing optical microscopy (POM), and X-ray powder diffractometry (XRD). To avoid hydration of the imidazolium salts, all the compounds were dried under vacuum before X-ray and DSC analyses. The phase transition temperatures and the corresponding enthalpy changes derived for compounds **2a-b** and **3a-b** in both healing and cooling cycles are shown in Table 6.1. Results are also summarized in Figure 6.2 for a visual comparison of the phase transition temperatures.

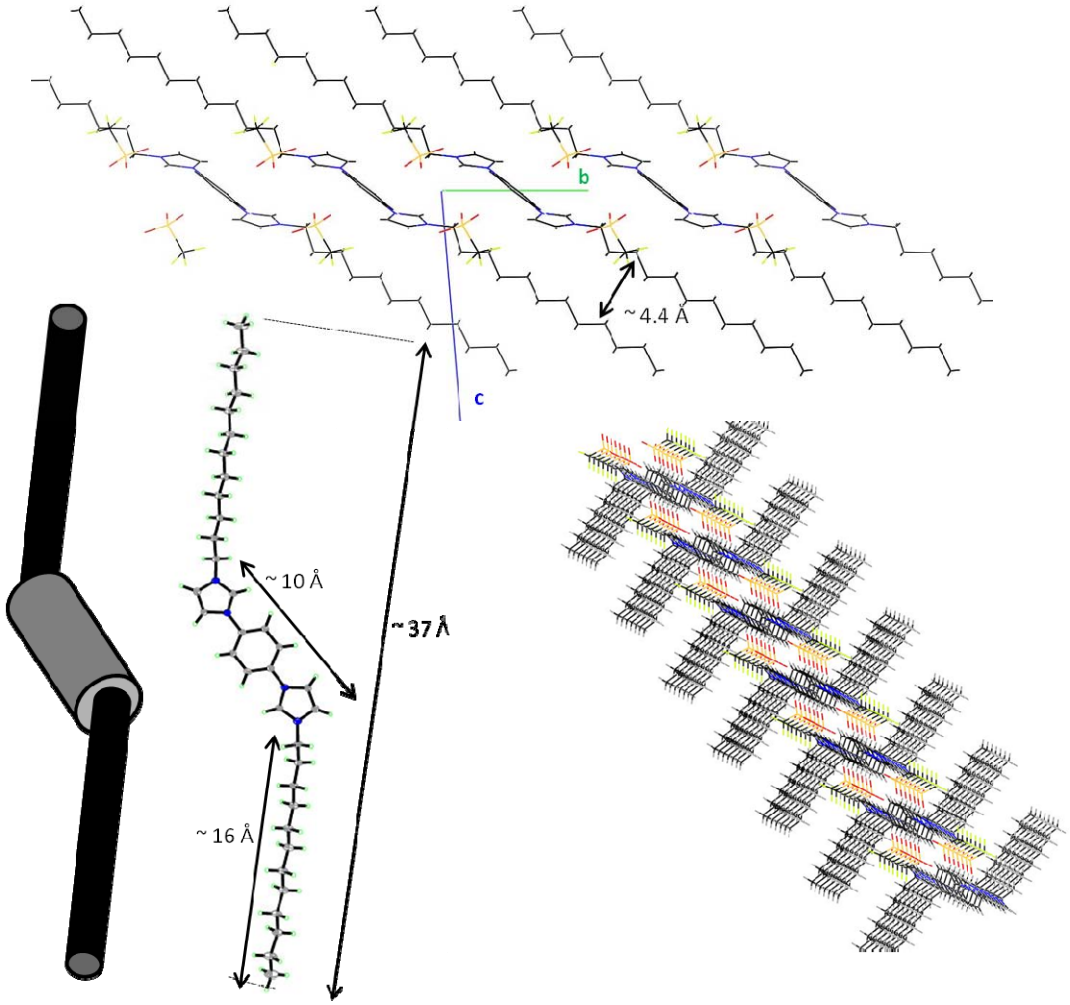


**Figure 6.1.** Top: Partial crystal packing of the compound **2a** projected on the (bc) plane. Bottom left: Schematic representation and ORTEP view of the symmetric diimidazolium salt **2a** (counterions were omitted for clarity). Bottom right: Partial crystal packing of **2a** showing the lamellar structure.

**Table 6.1.** Phase transition temperatures[a] and corresponding enthalpies $\Delta H$ determined from the 1st heating and the 1st cooling DSC thermograms.

| Compound on heating | T/°C Cr1 –> Cr2 ($\Delta H$/J.g$^{-1}$) | T/°C Cr2 –> LC ($\Delta H$/J.g$^{-1}$) | T/°C LC –> I ($\Delta H$/J.g$^{-1}$) |
|---|---|---|---|
| **2a** | 148 (26.9) | 169 (42.9) | 184 (3.4) |
| **2b** | 141[b] | 149[b] | Degradation at 250 °C |
| **3a** | ---- | 55[c] (54.0) | 136 (7.8) |
| **3b** | ---- | 75 (48.8) | 172 (6.8) |
| Compound on cooling | T/°C Cr1 <– Cr2 ($\Delta H$/J.g$^{-1}$) | T/°C Cr2 <– LC ($\Delta H$/J.g$^{-1}$) | T/°C LC <– I ($\Delta H$/J.g$^{-1}$) |
| **2a** | 110 (-27.2) | 151 (-43.6) | 183 (-3.3) |
| **2b** | 104 (-30.9) | 130 (-56.3) | Degradation at 250 °C |
| **3a** | ---- | 46[c] (-28.0) | 133 (-7.2) |
| **3b** | ---- | 56 (-46.2) | 169 (-4.9) |

[a]Abbreviations: Cr1 and Cr2 = Cristalline phases, LC = Liquid Crystal phase, I = Isotropic phase. [b]$\Delta H$ = 83.9 J.g$^{-1}$ was determined on heating for Cr1 –> Cr2 –> LC. The $\Delta H$ could not be determined for Cr1 –> Cr2 and Cr2 –> LC due to the proximity of the transition temperatures. [c]For compound **3a**, a minor phase transition was observed ($\Delta H$ = 2.5 J.g$^{-1}$) at 105°C, between two smectic phases.

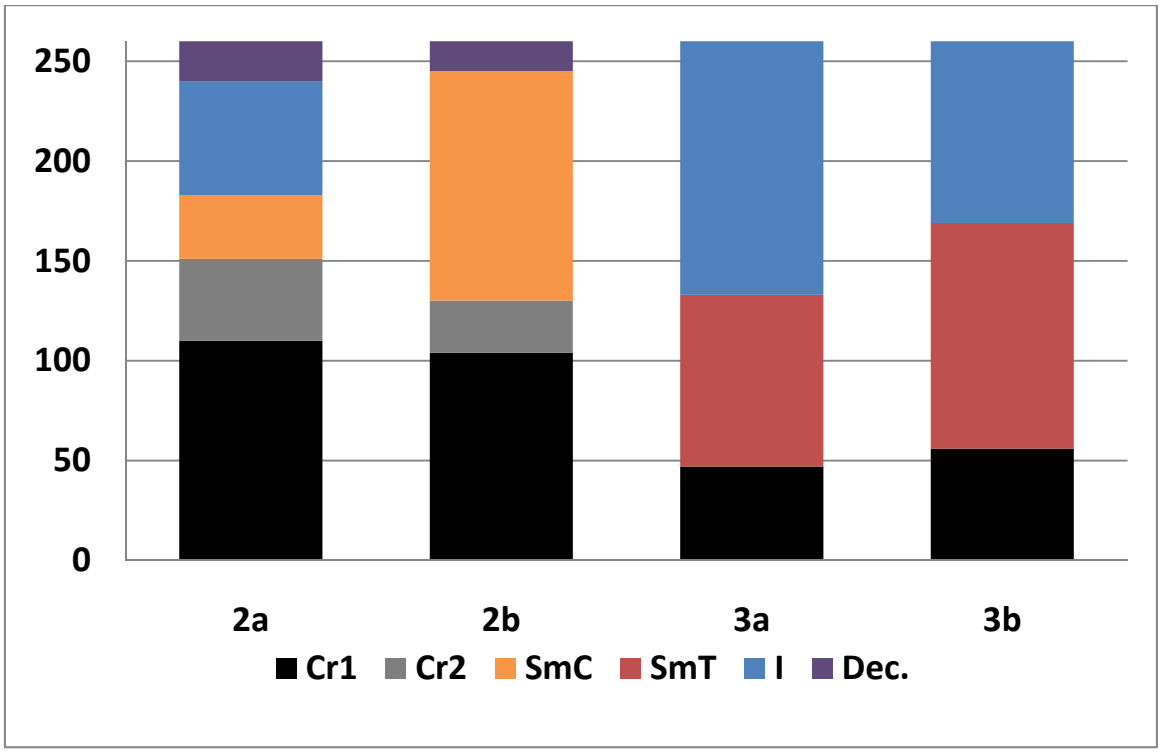


**Figure 6.2.** Phase transition temperatures of compounds **2a-b** and **3a-b** upon cooling. **Cr1** and **Cr2**: Crystalline phases; **SmC**: Smectic C mesophase; **SmT**: Smectic T mesophase; **I**: Isotropic phase; **Dec:** Decomposition.

For both triflate salts **2a** and **2b**, the smectic C structure was investigated by XRD as well as POM (Figure 6.3). Compound **2a** exhibited a fan-shaped texture often seen in SmC phases. This texture was observed on cooling from the isotropic melt between 181 and 153 °C. Compound **2b** predominantly exhibited a focal conic fan texture upon cooling from the isotropic melt, but other types of 2D organization (e.g. a different orientation of the director of the focal conic aggregates) were also present simultaneously in the sample (Figure 6.4). One sharp reflection in the small angle region related to the smectic layering, as well as a broad band in the wide angle region, related to the disordered alkyl chains and possibly to liquid-like lateral correlations of the aromatic cores within the layers is seen. The *d*-spacing values obtained were *d*= 26.8 Å for **2a** and d= 31.3 Å for **2b**. In both cases,

the *d*-spacing is shorter than the length of a single molecule (*d*/L =0.72 for **2a** and d/L = 0.67 for **2b**), resulting in tilting which confirms the characterization of this mesophase as a smectic C and an interdigitation of the alkyl chains within the mesophase.

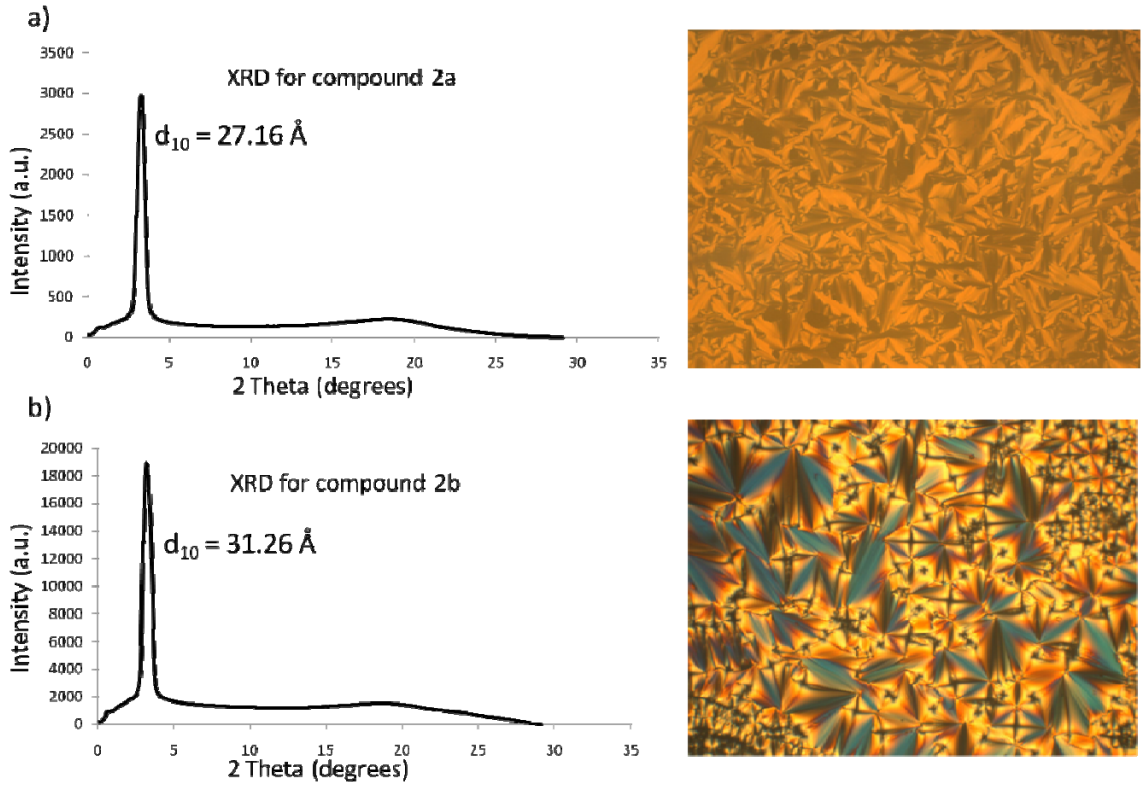


**Figure 6.3.** a) Left: XRD pattern of **2a** at 175 °C; Right: x200 POM view of **2a** at 175 °C exhibiting a fan-shaped texture of a SmC phase. b) Left: XRD pattern of **2b** at 170 °C; Right: x200 POM view of **2b** at 170 °C exhibiting a focal conic fan texture of a SmC phase.

With these *d*-spacing values and the crystal structure of compound **2a** described above, we can estimate that these triflate salts are organized in a monolayered SmC phase as shown in Figure 6.5, with partial intercalation of the alkyl chains. The *trans* conformation of the diimidazolium salt also gives the liquid crystalline structure an inherent tilt angle.

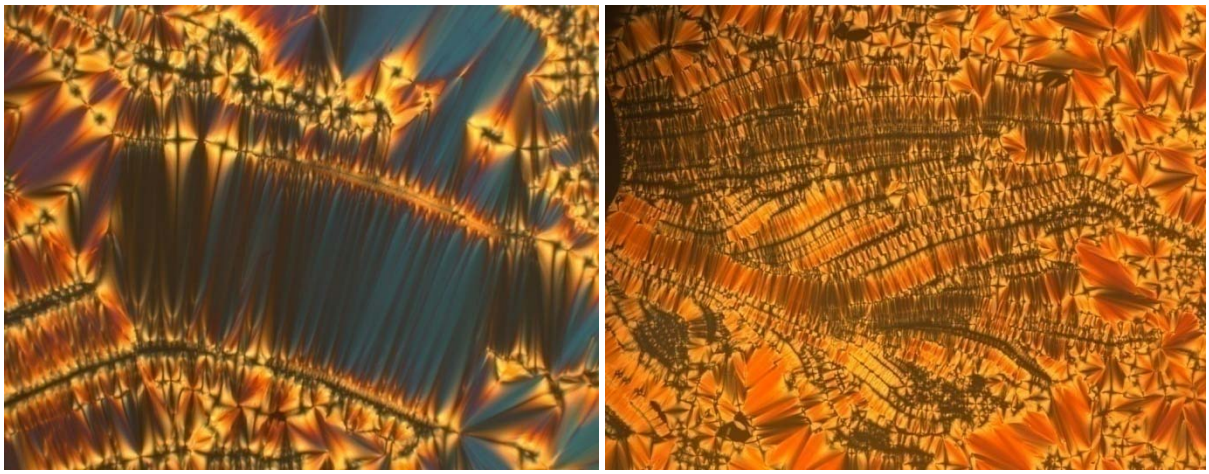

**Figure 6.4.** Different textures observed by POM for compound **2b** in the same sample at 170 °C. Left: x200 view of a closely packed SmC phase. Right: x100 view showing the 2D organization at long range.

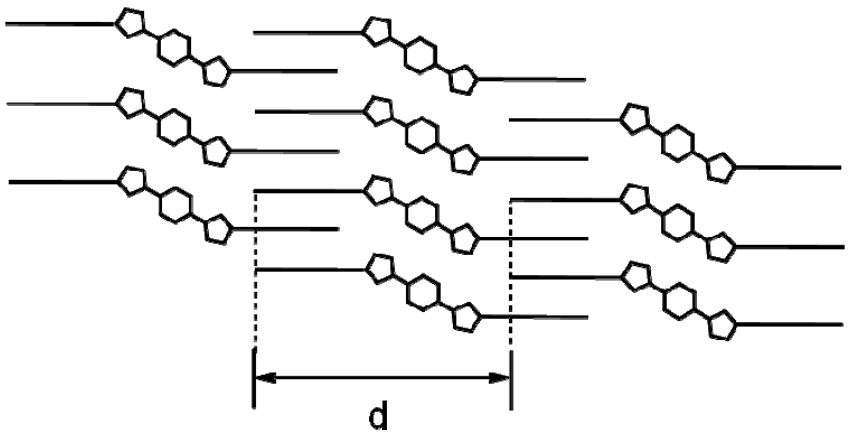


**Figure 6.5.** Schematic representation of the organization of compound **2a.**

Compounds **3a-b** had very different mesomorphic properties compared to the triflates **2a-b**. The structure of the mesophases was investigated by XRD and POM (Figure 6.6). The mesomorphic phase had a wider temperature range, with smectic transitions starting as low as 50 °C. These two $NTf_2$ salts can thus be described as ionic liquid crystals.

A first sharp reflection with high intensity is observed followed by three more equidistant reflections of low intensity in the small angle region for **3a**. For compound **3b,** the first high intensity sharp reflection is followed by two equidistant reflections of low intensity. As previously seen for compounds **2a-b**, the supramolecular forces involved in the formation of the smectic layers are predominantly hydrophobic interactions, but in this case there is at least another important interaction. This interaction can be either aromatic interactions or interactions between the acidic H2 proton of the imidazolium group and the anions. The anions can serve as bridges between the diimidazolium units and allow more cohesion in the structure, as shown in Figure 6.7. The peaks at around 2θ = 17° are related to the in-plane organization, probably at the level of the ionic groups.

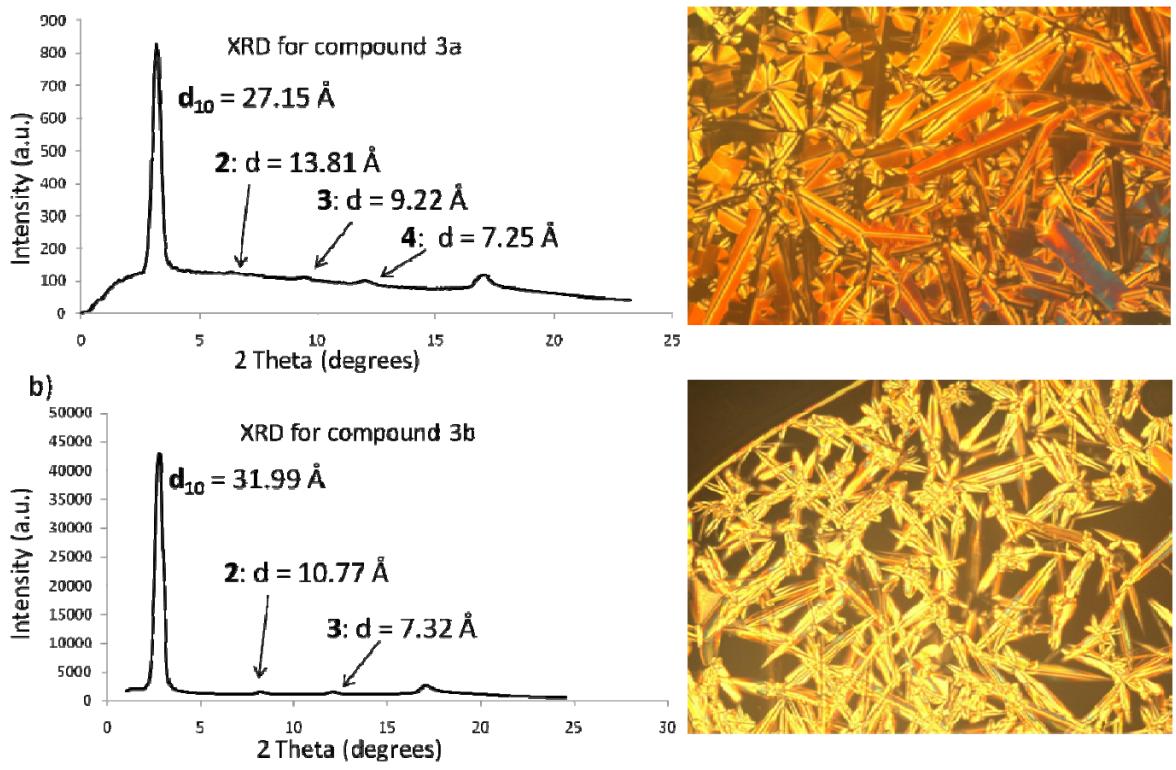


**Figure 6.6.** a) Left: XRD pattern of **3a** at 120 °C; Right: x100 POM view of **3a** at 175 °C exhibiting a lancet-like texture of a SmT phase. b) Left: XRD pattern of **3b** at 120 °C; Right: x100 POM view of **3b** at 120 °C exhibiting a lancet-like texture of a SmT phase.

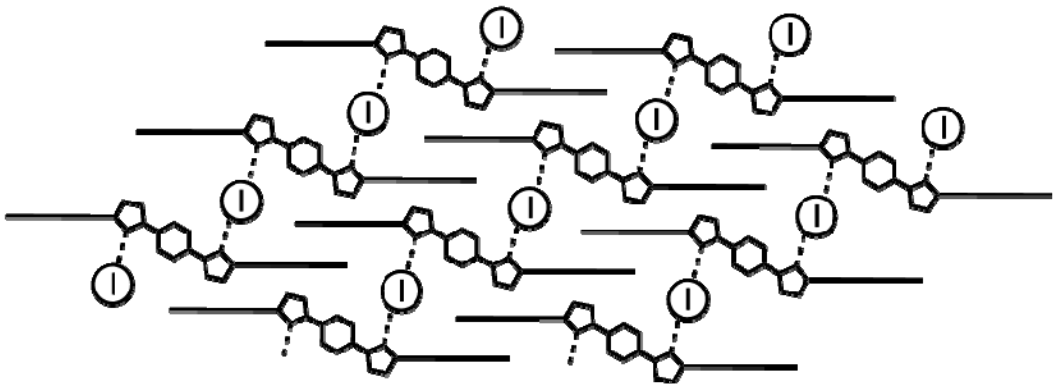

**Figure 6.7.** Schematic representation of the organization of compound **3a.**

For both compounds **3a** and **3b**, a slow growing lancet-like texture was observed upon cooling from the isotropic melt. This texture closely resembles that of growing crystals but both compounds can be described as viscous liquids after the first phase transition around 50°C, which is a very common property of imidazolium ionic liquids in this temperature range. The same lancet-like texture has been reported also for smectic T (SmT) phases [13].Furthermore, for compound **3a**, a transition between two different smectic T phases was observed by DSC at 105 °C, with a $\Delta H$ of about 2.5 $J.g^{-1}$. No change in the XRD was observed, as the *d*-spacings remain the same, as well as the shape of the diffraction pattern. Only a slight difference is observed by POM between these two phases (Figure 6.8) when cooling from the isotropic melt. As a result, we believe that we can correlate this to a minor reorganization of the smectic phase at 105 °C. This phase transition was not observed for compound **3b** which has longer side-chains.

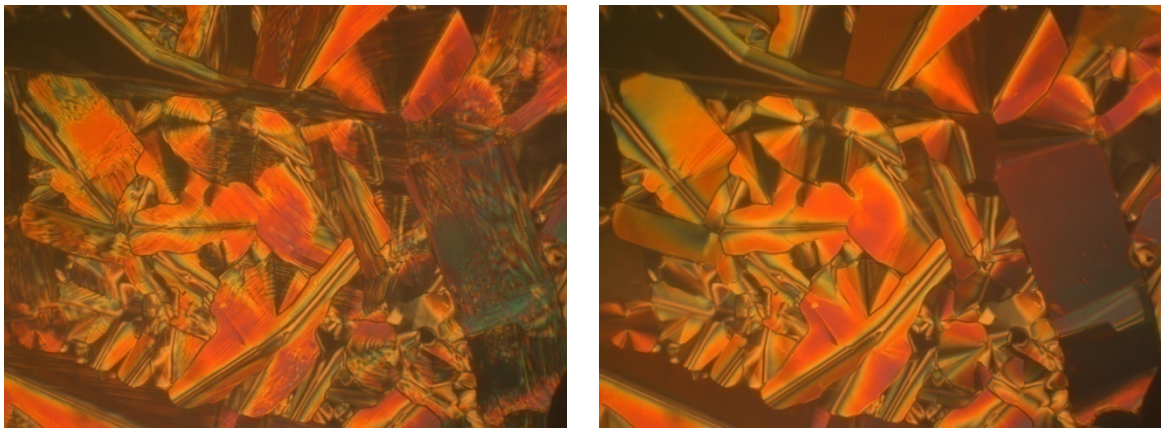

**Figure 6.8.** Left: x200 view of **3a** at 100 °C. Right: x200 view of **3a** at 110 °C

## 6.4 Syntheses

**1-[4-(1*H*-Imidazol-1-yl)phenyl]-1*H*-imidazole** was synthesized following a previously reported procedure14. The $^{1}H$ and $^{13}C$ NMR spectra of this compound were found to be in accordance with the literature.

**General procedure for the synthesis of dialkyl(1,4-phenylene)diimidazolium salts:** To a solution of **1-[4-(1*H*-Imidazol-1-yl)phenyl]-1*H*-imidazole** (1 mmol, 210 mg, 1 eq) in acetonitrile (10 mL) was added the appropriate alkyl bromide (10 mmol, 10 eq). The solution was refluxed and stirred for 24 h and then filtered. The diimidazolium bromide salts were dried under high vacuum for 24h then solubilised in 10 mL of methanol. Either Lithium *bis*(trifluoromethylsulfonyl)imidate or ammonium triflate (2.1 mmol, 2.1 eq) were added and the solution was refluxed for 2 h. After evaporation of the solvent, water was added and the subsequent salts were filtered and dried under high vacuum.

**1,1'-didodecyl-3,3'-(1,4-phenylene)diimidazolium *bis*(triflate) (2a):** $^{1}H$ NMR ($CD_3OD$, 400 MHz): $\delta$ (ppm) 8.21 (s, 2H), 8.07 (s, 4H), 7.95 (s, 2H), 4.37 (t, $J$ = 7.4 Hz, 4H), 2.08 (sext, $J$ = 6.1 Hz, 4H), 1.27-1.53 (m, 36H), 0.91 (t, $J$ = 6.06 Hz, 6H). $^{13}C$ NMR ($CD_3OD$, 100 MHz): $\delta$ (ppm) 135.6, 123.5, 123.0, 121.1, 49.8, 31.3, 29.2, 29.0, 28.9, 28.7,

28.6, 28.3, 25.6, 21.9, 12.6. HR-MS m/*z* found: 274.2412 ([M - 2TfO]$^{2+}$), calc: 274.2403, yield 88 %.

**1,1'-dihexadecyl-3,3'-(1,4-phenylene)diimidazolium *bis*(triflate) (2b):** $^{1}$H NMR ($CD_3OD$, 400 MHz): $\delta$ (ppm) 8.21 (s, 2H), 8.07 (s, 4H), 7.95 (s, 2H), 4.37 (t, *J* = 7.4 Hz, 4H), 2.03 (m, 4H), 1.25-1.51 (m, 52H) 0.92 (t, *J* = 6.6 Hz, 6H). $^{13}$C NMR ($CD_3OD$, 100 MHz): $\delta$ (ppm) 135.6, 123.5, 123.0, 121.1, 49.8, 31.3, 29.2, 29.0, 28.9, 28.7 (multiple peaks), 28.6, 28.3, 25.6, 21.9, 12.6. HR-MS m/*z* found: 330.3045 ([M - 2TfO]$^{2+}$), calc: 330.3029, yield 71 %.

**1,1'-didodecyl-3,3'-(1,4-phenylene)diimidazolium *bis*[*bis*(trifluoromethane-sulfonyl)imidate] (3a):** $^{1}$H NMR ($CD_3OD$, 400 MHz): $\delta$ (ppm) 8.18 (d, *J* = 1.4 Hz, 2H), 8.05 (s, 4H), 7.93 (d, *J* = 1.4 Hz, 2H), 4.36 (t, *J* = 7.4 Hz, 4H), 2.03 (m, 4H), 1.27-1.50 (m, 36H), 0.91 (t, *J* = 6.79 Hz, 6H). $^{13}$C NMR ($CD_3OD$, 100 MHz): $\delta$ (ppm) 135.6, 123.6, 123.1, 121.1, 49.8, 31.3, 29.2, 29.0, 28.8, 28.7, 28.6, 28.3, 25.5, 21.9, 12.6. HR-MS m/*z* found: 274.2411 ([M - 2NTf$_2$]$^{2+}$), calc: 274.2403, yield 83 %.

**1,1'-dihexadecyl-3,3'-(1,4-phenylene)diimidazolium *bis*[*bis*(trifluoromethane-sulfonyl)imidate] (3b):** $^{1}$H NMR ($CD_3OD$, 400 MHz): $\delta$ (ppm) 8.19 (d, *J* = 1.4 Hz, 2H), 8.06 (s, 4H), 7.94 (d, *J* = 1.4 Hz, 2H), 4.36 (t, *J* = 7.3 Hz, 4H), 2.03 (m, 4H), 1.25-1.51 (m, 52H) 0.92 (t, *J* = 6.6 Hz, 6H). $^{13}$C NMR ($CD_3OD$, 75 MHz): $\delta$ (ppm) 133.8, 124.8, 124.3, 122.3, 118.5, 51.0, 32.5, 30.4, 30.2 (multiple peaks), 30.1, 30.0, 29.9, 29.8, 29.5, 26.7, 23.1, 13.8. HR-MS m/*z* found: 330.3043 ([M - 2NTf$_2$]$^{2+}$), calc: 330.3029, yield 67 %

## 6.5 Conclusion

In conclusion, we have investigated the mesomorphic properties of a new family of diimidazolium salts by varying the counterions and the length of the alkyl chains. The counterion has a great impact on the mesomorphism and the temperature of the phase transitions. Only Smectic C phases could be identified with the TfO$^-$ counterion with a

much larger range of liquid crystal phase for the longer $C_{16}$ alkyl sidechains. When $NTf_2^-$ counterions were used, the first phase transition into a liquid crystalline phase occurs at around 50 °C, 120 °C lower than the triflate compounds. The ionic liquid crystalline phases obtained have been classified into Smectic T phases. The thermotropic mesomorphism of these ionic liquid crystals opens the possibility to use them as ordered solvents or organized reaction media. In these anisotropic solvents other chemo- and regioselectivities besides those in conventional solvents can be obtained for several types of reactions. Moreover, their spontaneous alignment in one direction may find applications in optical and electrical devices.

## 6.6 Acknowledgment.

This work was supported by the Natural Sciences and Engineering Research Council of Canada, the Canada Foundation for Innovation and Université de Montreal for financial support. We thank Sylvain Essiembre for the help in the use of the powder X-ray diffractometer and Pierre Ménard-Tremblay for his help on POM. We would also like to thank Professor G. Bazuin from our department for her help with identification of the liquid crystalline phases and very helpful discussion of this manuscript.

## 6.7 References

1 (a) P. Wasserscheid and T. Welton, Ionic Liquids in Synthesis, *Wiley-VCH, Weinheim,* 2003; (b) J. Dupont, R. F. de Soula and P. A. Suarez, *Chem. Rev.*, 2002, **102**, 3667.

2 H. Ohno, Electrochemical Aspect of Ionic Liquids, *Wiley-Interscience*, 2005.

3 V. Gauchot, W. Kroutil and A. R. Schmitzer, *Chem. Eur. J.*, 2010, **16**, 6748.

4 L. Leclercq, M. Lacour, S. H. Sanon and A. R. Schmitzer, *Chem. Eur. J.*, 2009, **15**, 6327.

5 (a) C. J. Bowlas, D. W. Bruce and K. R. Seddon, *Chem. Commun.*, 1996, 1625; (b) C. M. Gordon, J. D. Holbrey, A. R. Kennedy and K. R. Seddon, *J. Mater. Chem.*, 1998, **8**, 2627;(c) A. E. Bradley, C. Hardacre, J. D. Holbrey, S. Johnston, S. E. J. McMath and M. Nieuwenhuyzen, *Chem. Mater.*, 2002, **14**, 629; (d) K. M. Lee, Y. T. Lee and J. B. Lin, *J. Mater. Chem.*, 2003, **13**, 1079; (e) J. De Roche, C. M. Gordon, C. T. Imrie, M. D. Ingram, A. R. Ingram, A. R. Kenedy, F. LoCelso and A. Triolo, *Chem. Mater.*, 2003, **15**, 2003; (f) S. Kumar and S. Kumar Pal, *Tetrahedron Lett.*, 2005, **46**, 2607; (g) J. Motoyagani, T. Fukushima and T. Aida, *Chem. Commun.*, 2005, 101; (h) J. M. Suisse, S. Bellemin-Laponnaz, L. Douce, A. Maisse-François and R. Welter, *Tetrahedron Lett.*, 2005, **46**, 4303.

6 W. Dobbs, L. Douce, L. Allouche, A. Louati, F. Malbosc, R. Welter, New Ionic Liquids Based on Imidazolium Salts, *New J. Chem.*, 2006, **30**, 528.

7 (a) C. K. Lee, H. W. Huang, I. J. B. Lin, *Chem. Commun.*, 2000, 1911; (b) M. Tosoni, S. Laschat, A. Baro, *Helv. Chim. Acta* 2004, **87**, 2742; (c) Y. R. Zhao, X. Chen, X. D. Wang, *J. Phys. Chem. B* 2009, **113**, 2024; (d) M. Yoshio, T. Mukai, K. Kanie, M. Yoshizawa, H. Ohno, T. Kato, *Chem. Lett.* 2002, 320.

8 (a) S. Yazaki, Y. Kamikawa, M. Yoshio, A. Hamasaki, T. Mukai, H. Ohno, T. Kato, *Chem. Lett.* 2008, **38**, 538; (b) K. Hoshino, M. Yoshio, T. Mukai, K. Kishimoto, H. Ohno, T. Kato, *J. Polym. Sci. Part A*, 2003, **41**, 3486; (c) M. Yoshio, T. Mukai, H. Ohno, T. Kato, *J. Am. Chem. Soc.* 2004, **126**, 994.

9 (a) Y. Sanami, M. Funahashi, T. Kato, *J. Am. Chem. Soc.* 2008, **130**, 13206; (b) L. Chui, L. Zhu, *Liq. Cryst.* 2005, **32**, 143.

10 X. Cheng, X. bai, S. Jing, H. Ebert, M. Prehm, C. Tschierske, *Chem. Eur. J.* 2010, **16**, 4588.

11 N. Noujeim, B. Jouvelet, A. R. Schmitzer, *J. Phys. Chem. B* 2009, **113**, 16159.

12 (a) L. Leclercq, N. Noujeim. A. R. Schmitzer, *Crystal Growth & Design*, 2009, **9**, 4784; (b) L. Leclercq, M. Simard, A. R. Schmitzer, *J. Mol. Struct.* 2009, **918**, 101.

13 (a) E. Alami, H. Levy, R. Zana, P. Weber, A. Scoulios, *Liq. Cryst.* 1993, 201-212; (b) K. Goossens, K. Lava, P. Nockemann, K. Van Hecke, L. Van Meervelt, K. Driesen, C. Garller-Walrand, K. Binnemans, T. Cardinaels, *Chem. Eur. J.* 2009, **15**, 656

14 J. Lagona, P. Mukhopadhyay, A. Chakrabarti, L. Isaacs, *Angew. Chem. Int. Ed.* 2005, **44**, 4844-4870

# Chapitre 7 : Conclusion et perspectives

Le but du projet de recherche a été dans un premier temps l'étude des propriétés supramoléculaires des sels de diimidazolium disubstitués en solution, et donc leurs propriétés de complexation avec divers macrocycles connus en chimie supramoléculaire. Dans un second temps, l'obtention et la résolution de plusieurs structures cristallines nous a permis d'étudier les interactions supramoléculaires présentes en phase solide et d'obtenir et caractériser des mésophases basées sur des sels de diimidazolium.

C'est donc d'abord une étude des propriétés de complexation en solution aqueuse ou organique de sels de méthylènediimidazolium disubstitués avec quatre macrocycles connus en chimie supramoléculaire (les DB24C8, C[4]P, CB[7] et $\beta$-CD) qui a été réalisée. Ce sont majoritairement des complexes 1:1 qui ont été obtenus et cette étude démontre surtout qu'un substrat de type méthylènediimidazolium disubstitué est très polyvalent et peut former différents types de complexes supramoléculaires aussi bien en solution aqueuse qu'organique. Deux observations importantes sont à retenir : en solution aqueuse, les complexes formés avec le CB[7] et la $\beta$-CD ont de fortes constantes d'association et il est donc enviseageable de pouvoir former des assemblages supramoléculaires plus élaborés en utilisant ces sels de diimidazolium en solution aqueuse. Pour l'étude en solution organique polaire, le complexe de type pseudorotaxane avec le DB24C8 n'a pas une aussi forte constante d'association que les autres systèmes similaires développés par les groupes de Stoddart et Loeb, mais la solubilité de ces sels est environ dix fois supérieure que les benzylammonium ou *bis*(pyridinium) couramment utilisés. Ceci laisse penser qu'il serait possible d'utiliser un tel site de liaison pour synthétiser un rotaxane basé sur un sel de diimidazolium avec une roue DB24C8.

Par la suite, l'étude des propriétés de complexation avec des macrocycles en solution aqueuse des sels de bromure de méthylènediimidazolium disubstitués a été approfondie. Cette fois, c'est l'assemblage de complexes ternaires avec un CB[7] et une cyclodextrine qui est réalisé. Nous avons pu mettre en évidence une coopération supramoléculaire positive qui permet le positionnement du CB[7] sur un site de liaison initialement défavorisé : sur la partie dicationique du substrat. Les propriétés interfaciales des complexes binaires et ternaires ont également été étudiées et sont différentes selon le

sel de diimidazolium utilisé. Nous avons pu montrer que c'est la géométrie du sel de diimidazolium qui contrôle la position du CB[7] dans le complexe, ainsi que ses propriétés interfaciales. L'interface air/eau est une bonne plateforme pour la construction d'assemblages supramoléculaires et dans ce cas, c'est l'orientation et l'arrangement des sels de diimidazolium et des complexes qui est contrôlé.

Une modification de la structure des sels de diimidazolium fut ensuite entreprise et ce sont donc les complexes entre des sels de phénylènediimidazolium et le CB[7] qui ont été étudiés. Dépendement de la longueur des chaînes alkyles et de la concentration en CB[7], différentes associations supramoléculaires ont été obtenues. Le complexe le plus stable est toujours celui pour lequel le CB[7] est positionné sur le cycle aromatique central, mais des complexes de stoechiométrie supérieure peuvent être obtenus de manière contrôlée. Le rôle de chaque site de reconnaissance dans ces composés a donc été compris et il est maintenant enviseageable d'utiliser ces complexes supramoléculaires pour former des assemblages plus élaborés.

Les interactions en solution avec différents macrocycles ayant été étudiées, il a ensuite été intéressant de comprendre l'auto-association de ces sels de diimidazolium en phase cristalline. À travers l'étude de quatre structures cristallines, nous avons été capables de comprendre l'organisation de ces sels à l'état solide : la structure du dication est essentielle dans l'auto-assemblage, et même dans l'inclusion éventuelle de molécule d'eau pendant le processus de cristallisation. Cette étude a pu montrer que les paramètres les plus importants pour un auto-assemblage optimal étaient les interactions de type empilement-$\pi$ et les liaisons hydrogène couplées à la présence d'un espaceur flexible (espaceur méthylène dans deux des quatre structures présentées) qui permet de maximiser ces interactions. Dans les structures les plus flexibles, l'interaction principale devient l'empilement-$\pi$, au dépend des liaisons hydrogène. Des canaux à l'état cristallin ont été obtenus dans certaines structures, qui ont démontré que les sels de diimidazolium étaient des tectons flexibles et efficaces qu'il serait intéressant de décorer par d'autres groupes fonctionnels pour obtenir des structures cristallines qu'il serait moins difficile à prédire.

Finalement, c'est le dernier état de la matière attaignable avec ces sels de diimidazolium qui a été étudié, à savoir l'état cristal-liquide. En utilisant des triflates et des *bis*(trifluorométhanesulfonyl)imidates de phénylènediimidazolium, nous avons obtenu des mésophases smectiques C et T sur de longues plages de température. L'obtention de telles mésophases montre qu'il nous est possible de modifier l'architecture initiale pour obtenir les propriétés désirées. Grâce aux travaux présentés, il est maintenant possible de concevoir et de synthétiser des sels de diimidazolium pour diverses applications. Plusieurs autres projets de recherche qui ont pour base les résultats présentés dans cette thèse ont pu ainsi être entamés dans le groupe Schmitzer et diverses applications directement liées à la connaissance des propriétés supramoléculaires des sels de diimidazolium sont maintenant en cours de développement.

Pour les complexes en solution, la maîtrise des propriétés supramoléculaires des sels de diimidazolium a déjà permis le développement de différents systèmes de catalyse par transfert de phase dans notre groupe de recherche. Il est également enviseageable d'obtenir des assemblages supramoléculaires plus élaborés comme des rotaxanes et le développement d'une voie de synthèse d'un rotaxane basé sur un sel de méthylènediimidazolium est en ce moment en cours.

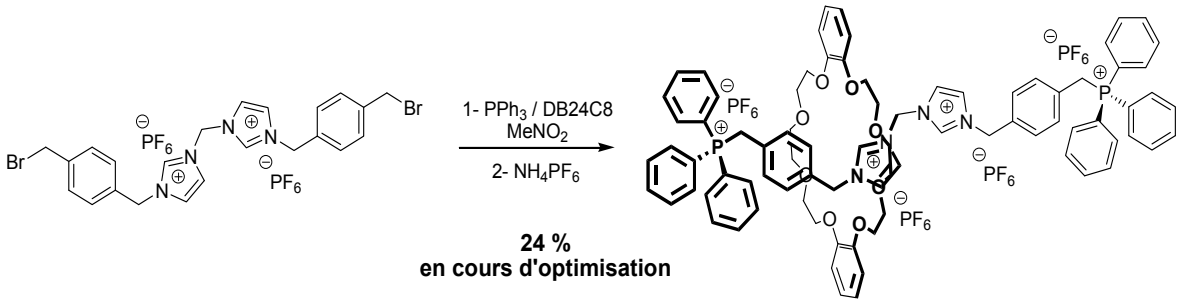


**Schéma 7.1.** Rotaxane basé sur un sel diimidazolium.

Un nouveau sel de méthylènediimidazolium ayant des propriétés de transporteur d'anion à travers une bicouche lipidique est en ce moment à l'étude. Il s'agirait à notre connaissance du premier transporteur cationique dont le transport d'anion peut être activement et efficacement inhibé par l'ajout d'un macrocycle : la formation des complexes

supramoléculaires entrerait dans ce cas en compétition avec l'inclusion dans la bicouche lipidique du transporteur de type diimidazolium.

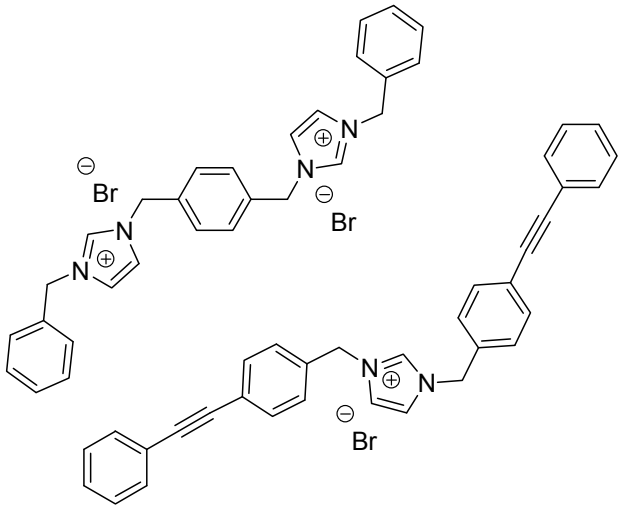


**Schéma 7.2.** Transporteur d'anions dont l'activité est inhibée par ajout de macrocycle.

En ce qui concerne les cristaux liquides, il est enviseageable d'introduire de la chiralité dans la structure de ces sels. L'utilisation de contre-ions chiraux sur l'architecture phénylènediimidazolium ou l'introduction d'un centre chiral sur le cation ont été envisagées. L'utilisation de ces cristaux liquides ioniques en tant que catalyseurs ou solvants de diverses réactions est également enviseageable.

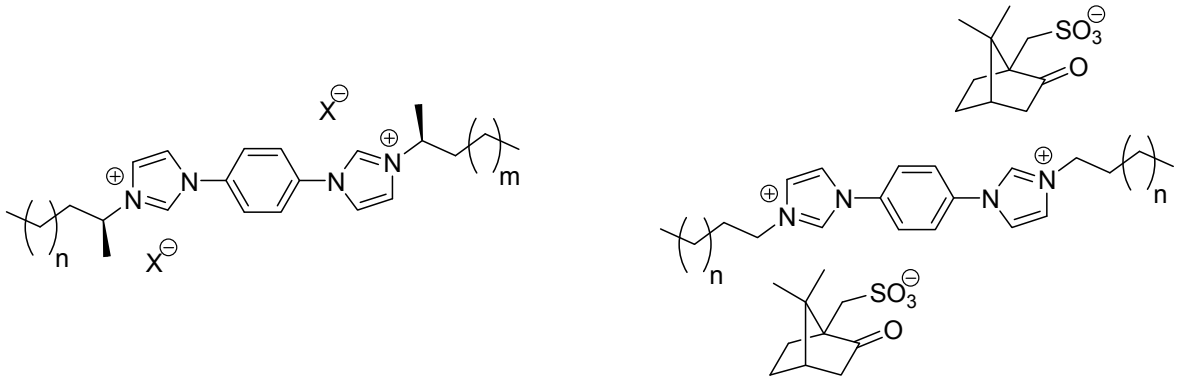


**Schéma 7.3.** Exemples de cristaux liquides chiraux potentiels à base de sels de diimidazolium.

# Partie expérimentale

Tous les réactifs utilisés pour les synthèses ont été achetés chez Aldrich et utilisés sans purification supplémentaire. Toutes les réactions ont été réalisées dans de la verrerie préalablement séchée à l'étuve. Les solvants anhydres ont été obtenus par un système de purification de solvants GlassContour (Irvine CA).

Les expériences de RMN ont été enregistrées sur des spectromètres Avance 300 (opérant à 300 MHz pour la RMN $^{1}H$ et 75 MHz pour la RMN $^{13}C$) Avance 400 (opérant à 400 MHz pour la RMN $^{1}H$ ou 100 MHz pour la RMN $^{13}C$) ou Avance 700 (opérant à 700 MHz pour la RMN $^{1}H$) de Brüker. Les déplacements chimiques sont donnés en ppm ($\delta$) et mesurés relativement aux tétraméthylsilane. Les données ont été traitées avec le logiciel Spinworks 2.5.5. L'acétonitrile deutérée ($CD_3CN$) a été acheté chez CDN et les autres solvants deutérés chez Aldrich et ont été utilisés sans purification supplémentaire.

Les spectres ESI/HRMS ont été enregistrés sur un spectromètre de masse Quantum TSQ Ultra (Thermo Scientific®) du Centre Régional de Spectrométrie de Masse de l'Université de Montréal. Pour tous les sels de diimidazolium caractérisés par cette méthode ainsi que pour les complexes d'inclusion, le mode d'ionisation positif a été utilisé.

Les mesures de tension de surface ont été réalisées sur un tensiomètre DCAT 11 (Dataphysics®) par la méthode de la lame de Wilhelmy. Toutes les valeurs de tension de surface obtenues sont le résultat d'une série d'au moins trois mesures. La température a été réglée par un bain thermorégulé Lauda RC6 à 25 °C.

Les calculs de modélisation moléculaire utilisés pour les études en solution ont été réalisés sur un poste de travail équipé du système d'exploitation Windows XP® et en utilisant le logiciel Hyperchem 7.5®. Les conformations initiales des sels de diimidazolium et des macrocycles ont été obtenues par la méthode semi-empirique PM3. Pour l'étude des sels de diimidazolium en phase cristalline, les calculs de modélisation moléculaires ont été réalisés sur un poste de travail équipé d'un système d'exploitation Linux en utilisant le logicial Ghemical 2.95 permettant d'utiliser MOPAC7. Les conformations initiales des cations diimidazolium ont été obtenues par la méthode semi-empirique AM1 en phase gazeuse. Pour l'étude détaillée des structures, les énergies relatives ont été calculées en fonction des différents angles de torsion.

Les analyses de calorimétrie différentielle à balayage ont été réalisées sur un calorimètre Q2000 de TA instruments®.

Les analyses de diffraction des rayons-X de poudre ont été réalisées sur un diffractomètre Brüker D8 Discover équipé d'un détecteur Hi-Star. La collecte des données a été effectuée en utilisant le logiciel GADDS 4.1.1.4 et EVA 8.0.0.2 a été utilisé pour l'analyse de données. La source utilisée a été une source au cuivre (énergie $K_\alpha$ de 8.04 KeV et $\lambda$ = 1.541838 Å). La plateforme utilisée a été une plateforme XYZ faite sur mesure et possédant un contrôleur de température préalablement calibré.

Toutes les données de diffraction des rayons-X de monocristaux pour résolution des structures cristallines ont été réalisées à 150 K. Les structures ont été résolues par la méthode directe ShelxS-97. Deux appareils ont été utilisés pour la collecte des données : un diffractomètre Brüker microstar équipé d'un detecteur CCD Platinum 135 avec une distance détecteur-cristal de 4.0 cm a été utilisé pour trois structures. Un diffractomètre Brüker équipé d'un détecteur CCD SMART 4K utilisant le programme APEX II et une anode rotative Nonius FR591 a été utilisé pour deux structures. Les fichiers CIF comprenant toutes les données cristallographiques peuvent être obtenus sur les sites internet des éditeurs des différents articles. Ces sites sont mentionnés à la fin de chacun des articles concernés et présentés dans cette thèse.

Les données expérimentales des travaux présentés sont disponibles en anglais directement dans les sections expérimentales des différents articles ou dans les annexes. Les annexes sont composées des données supplémentaires (« supplementary information ») qui ont été envoyées aux éditeurs lors de la soumission des différents articles pour publication.

# Annexe 1 : « Supporting information » de l'article 1: *N,N'*-disubstituted methylenediimidazolium salts: a versatile guest for various macrocycles

**General experimental details**

All the reagents were purchased from Aldrich chemicals and used without further purification. NMR spectra were recorded in the indicated solvents. Chemical shifts (δ) are reported in parts per million (ppm) relative to tetramethylsilan. NMR spectra were recorded on a Brüker Avance 400 spectrometer (operating at 400 MHz for $^{1}H$ NMR and at 100 MHz for $^{13}C$ NMR) or Brüker Avance 300 spectrometer (operating at 300 MHz for $^{1}H$ NMR and at 75 MHz for $^{13}C$ NMR) locked to the deuterated solvent. The following abbreviations are used to explain the multiplicities: s= singlet, d= doublet, t= triplet, q= quartet, p= pentet, m= multilpet. Accurate mass measurements were performed on a LC-MSD-Tof instrument from Agilent technologies in positive electrospray.

## $^{1}$H NMR, $^{13}$C NMR and ESI-MS of $[1][Br]_2$, $[2][Br]_2$, $[1][PF_6]_2$ and $[2][PF_6]_2$

### 1,1'-Dibenzyl-3,3'-methylenediimidazolium dibromide $[1][Br]_2$

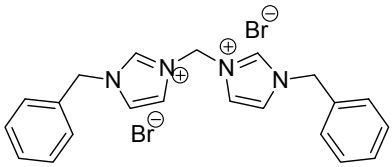


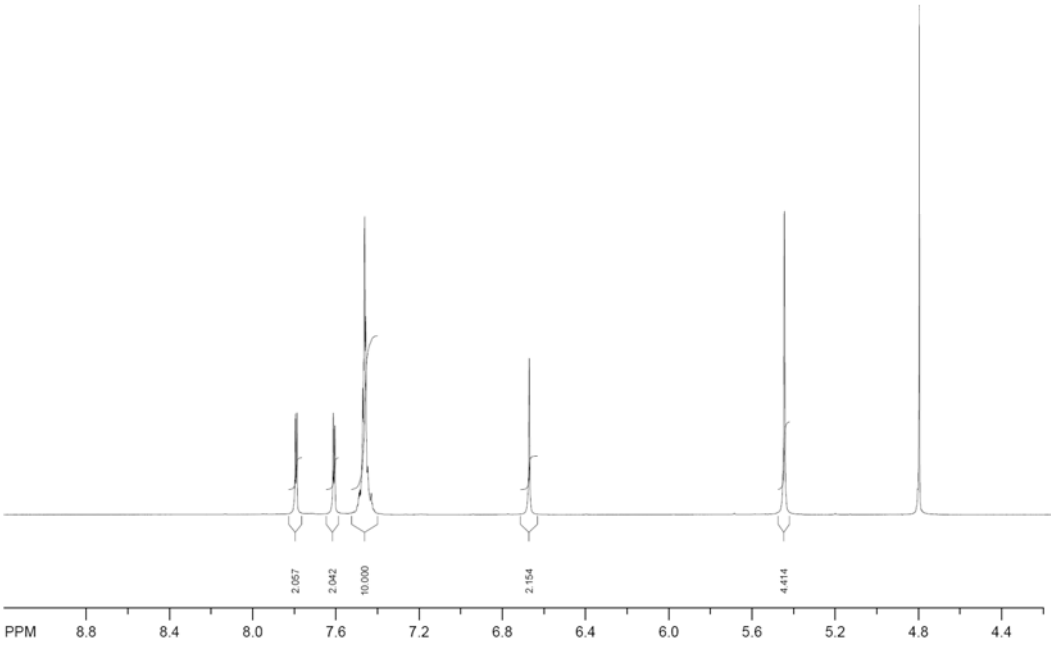


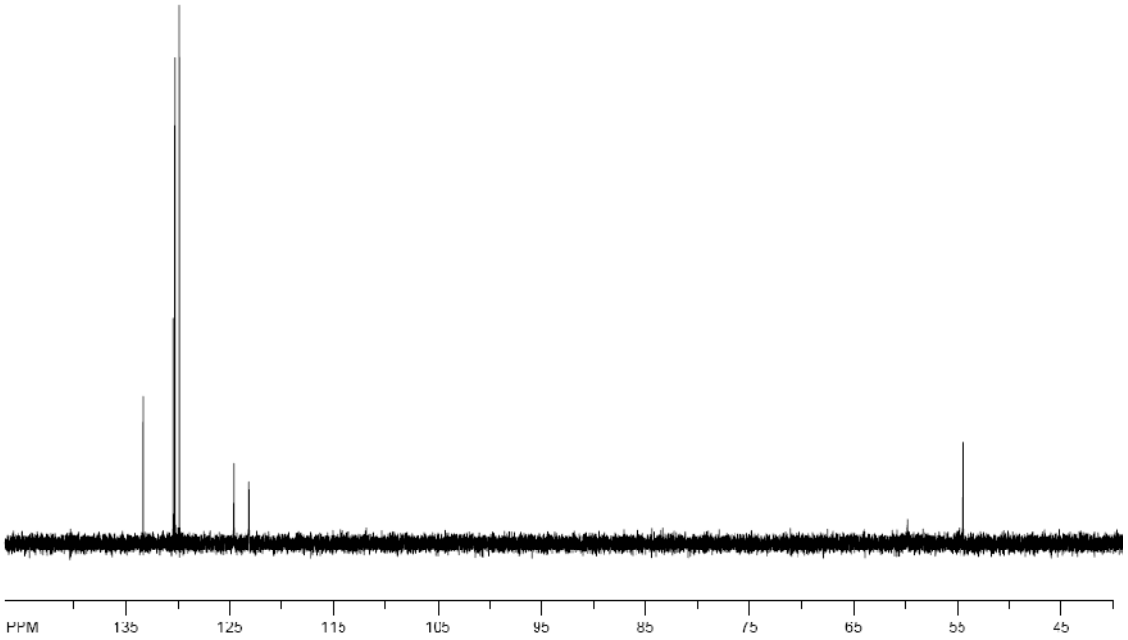

**1,1'-Diphenyl-3,3'-methylenediimidazolium dibromide [2][Br]$_2$**

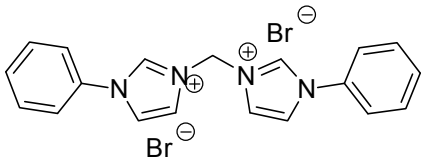


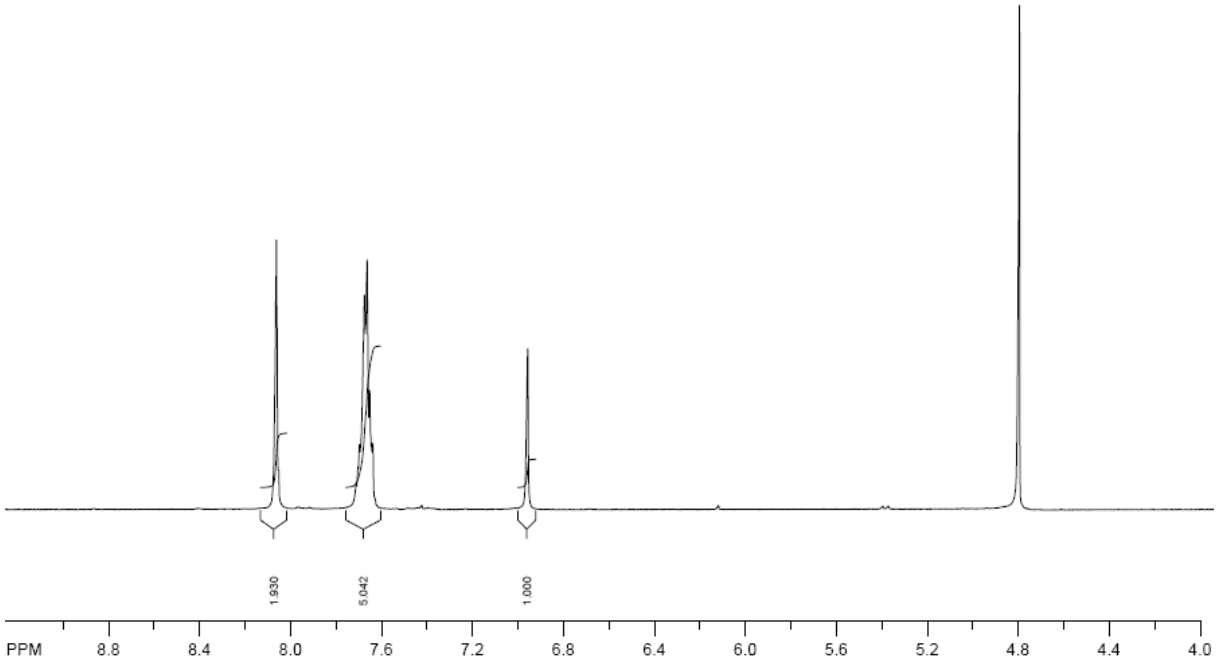


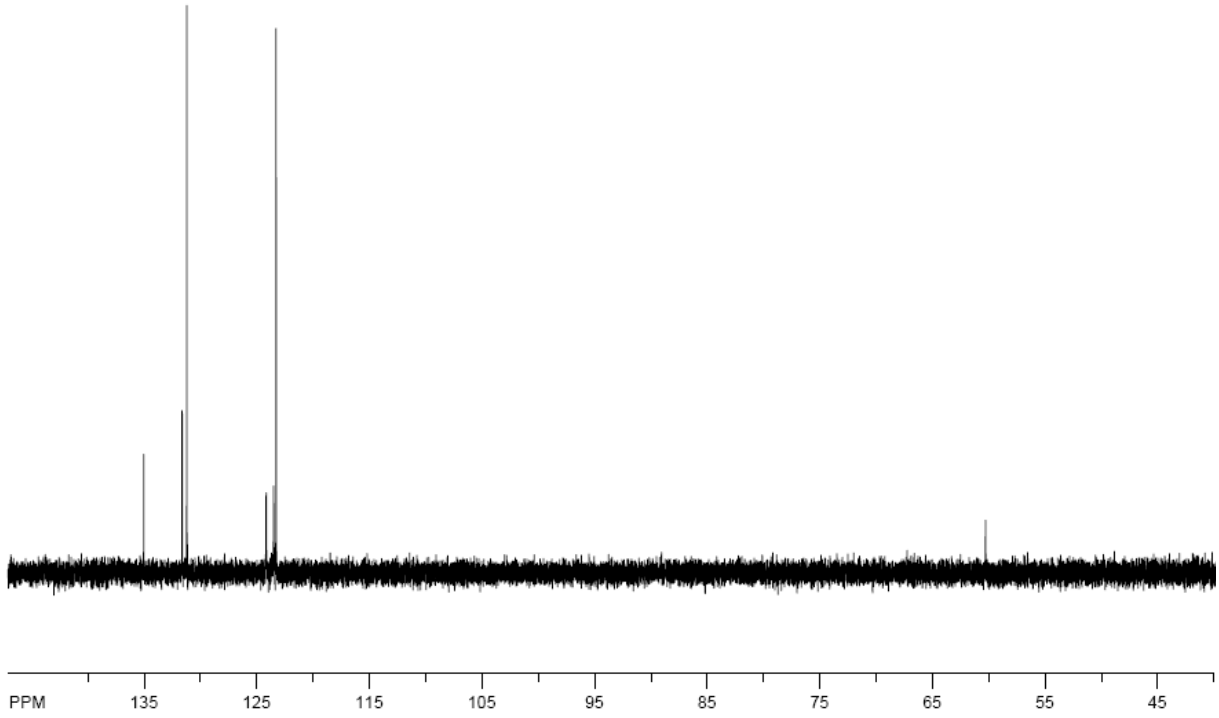

**1,1'-Dibenzyl-3,3'-methylenediimidazolium *bis*(hexafluorophosphate) [1][$PF_6$]$_2$**

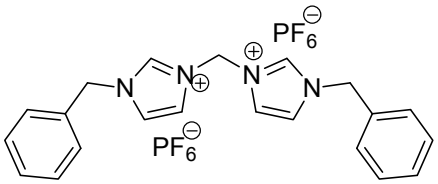


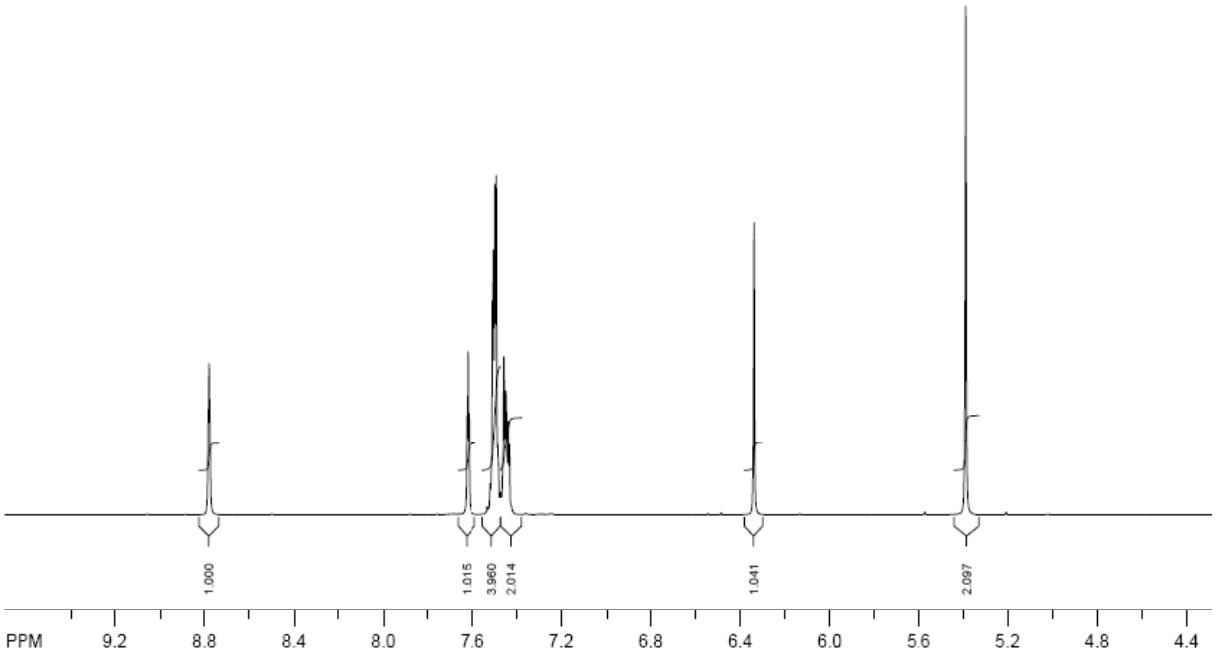


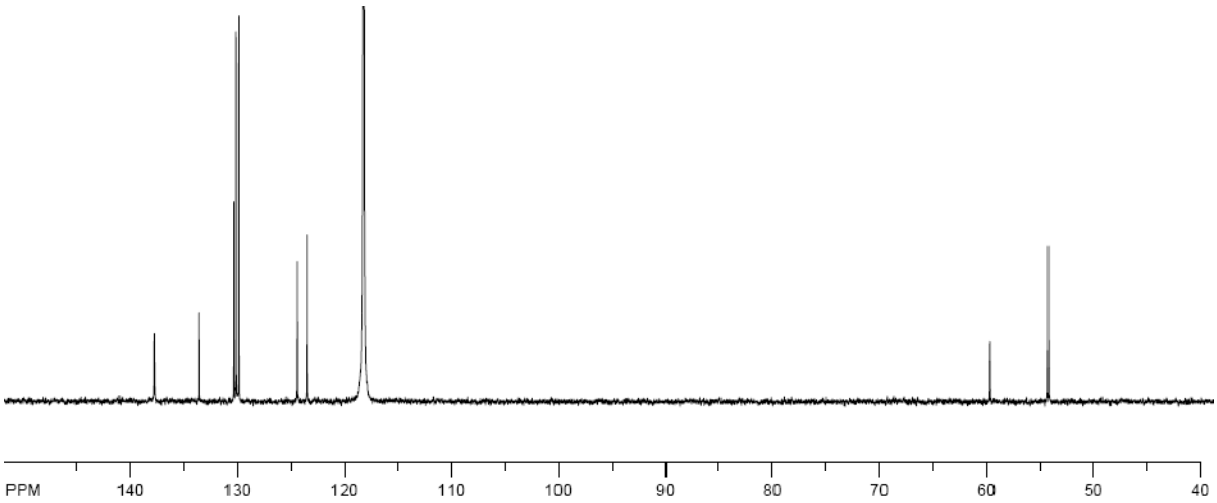

**1,1'-Diphenyl-3,3'-methylenediimidazolium *bis*(hexafluorophosphate) [2][$PF_6$]$_2$**

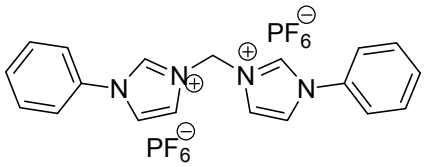


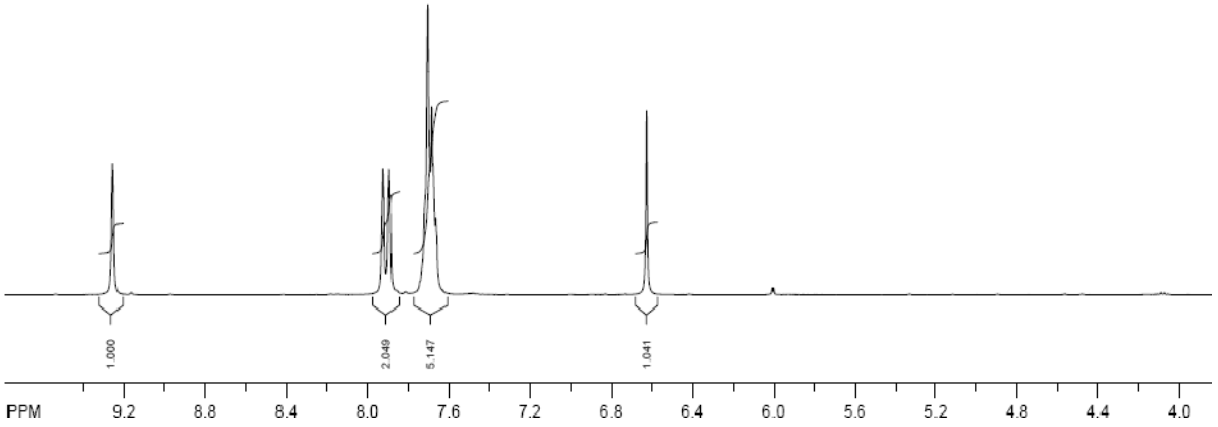


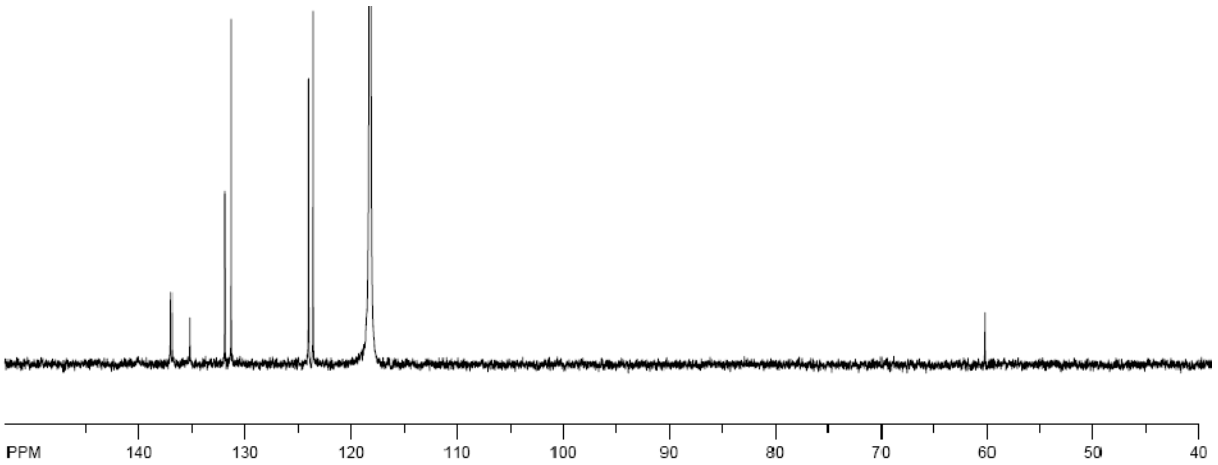

**Association constants determination for complexes with DB24C8**

The association constant $K_{ass}$ was determined (see Adrian, J.C., Jr; Wilcox, C.S. *J. Am. Chem. Soc.* **1991**, *113*, 678-680) from Equation 1 which was derived as follows for an equimolar solution of Thread (T) and Crown ether (C):

$$T + C = T.C$$

$$K_{ass} = \frac{[TC]}{[T].[C]}$$

$$K_{ass} = \frac{[T.C]}{(C_0 - [T.C])^2} = \frac{\chi_{TC}}{C_0(1-\chi_{TC})^2} \qquad \textbf{Equation 1}$$

Where $C_0$ is the initial concentration of thread and crown ether and

$$\chi_{TC} = \frac{\int complexed}{\int complexed + \int uncomplexed}$$

$K_{ass}$ can be written with the ratio $\rho = \frac{\int complexed}{\int uncomplexed}$ as follows:

$$K_{ass} = \frac{1}{C_0}\left(\rho^2 + \rho\right)$$

This gives the following equation 2 that leads to the mathematical expression of $\rho$:

$$\rho^2 + \rho - K_{ass}.C_0 = 0 \qquad \textbf{Equation 2}$$

$$\rho = \frac{1}{2}\left(\sqrt{1 + 4.K_{ass}.C_0} - 1\right) \qquad \textbf{Equation 3}$$

The equation 3 shows that in the case of an equimolar solution of thread and crown ether, the effect of the association constant and the initial concentration (solubility) is exactly the same.

**NOESY NMR of complexes**

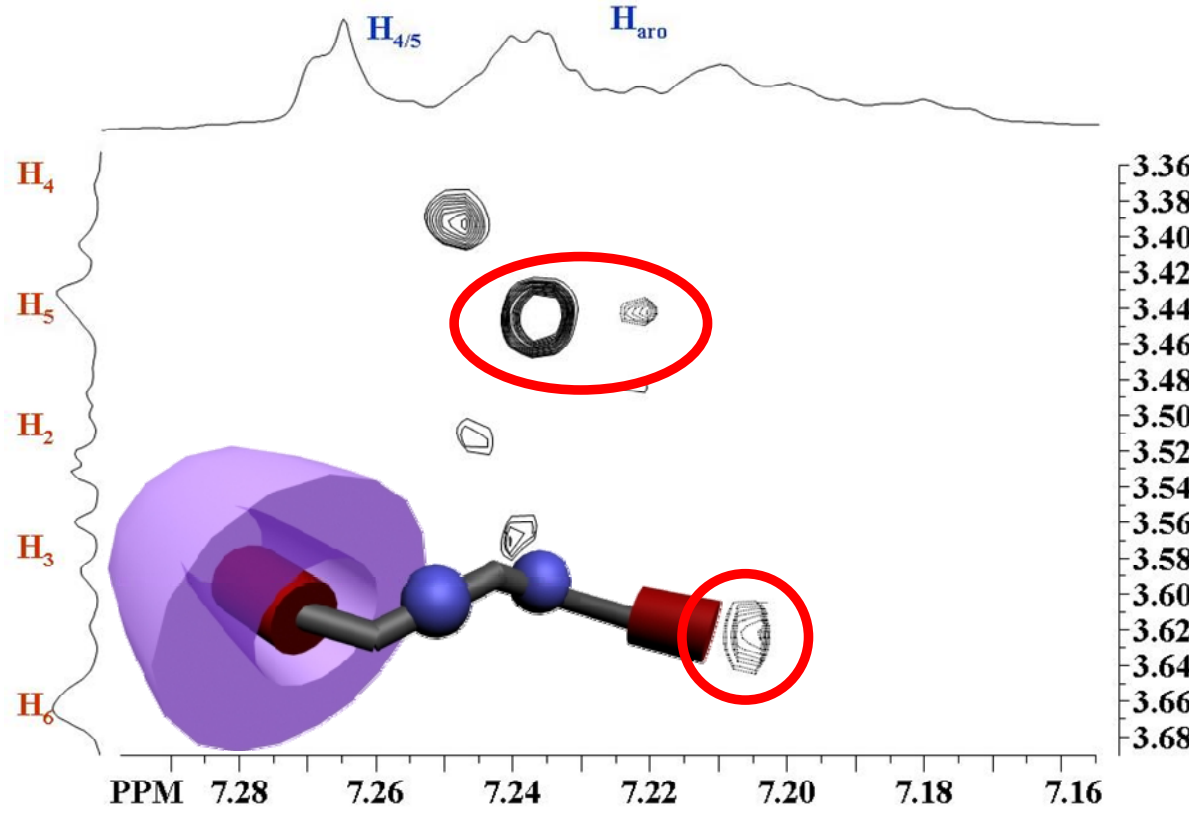


Partial NOESY NMR spectra at 25°C of 5 mM **[1][Br]$_2$** and 5 mM **β-CD** ($D_2O$).

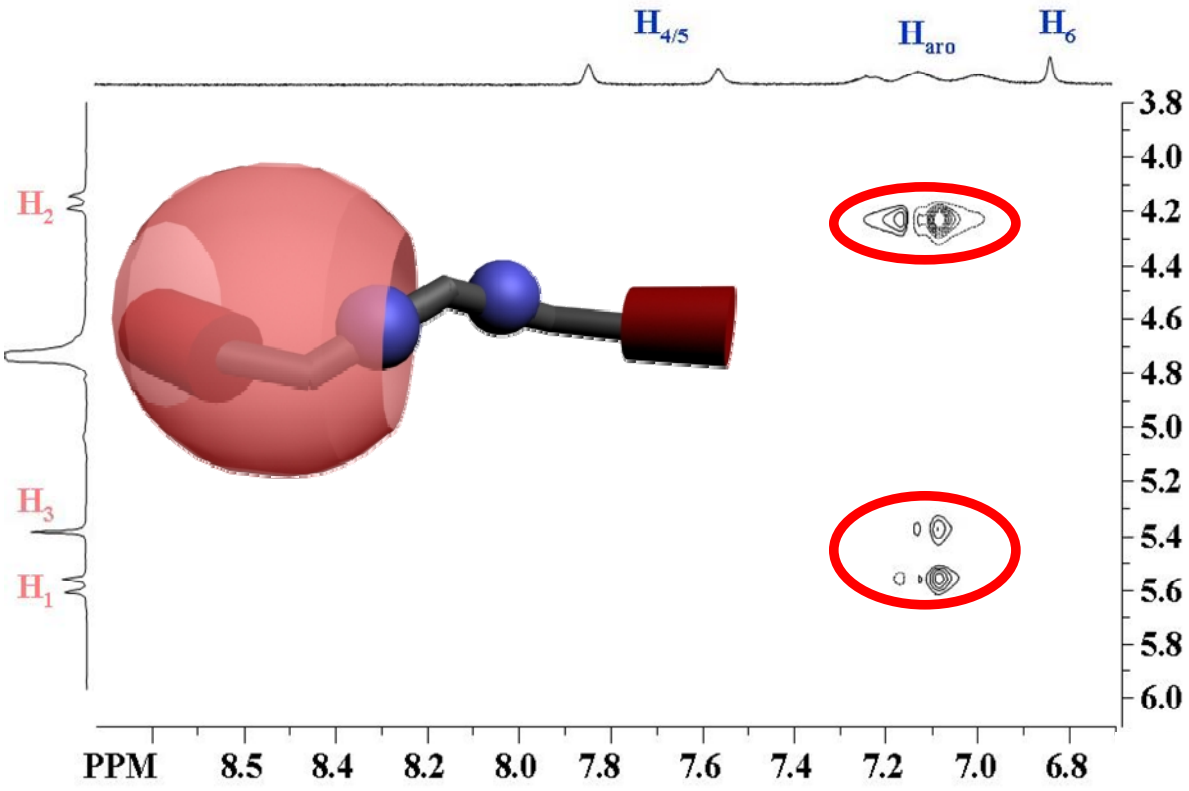


Partial NOESY NMR spectra at 25°C of 4 mM **[1][Br]$_2$** and 4 mM **CB[7]** ($D_2O$).

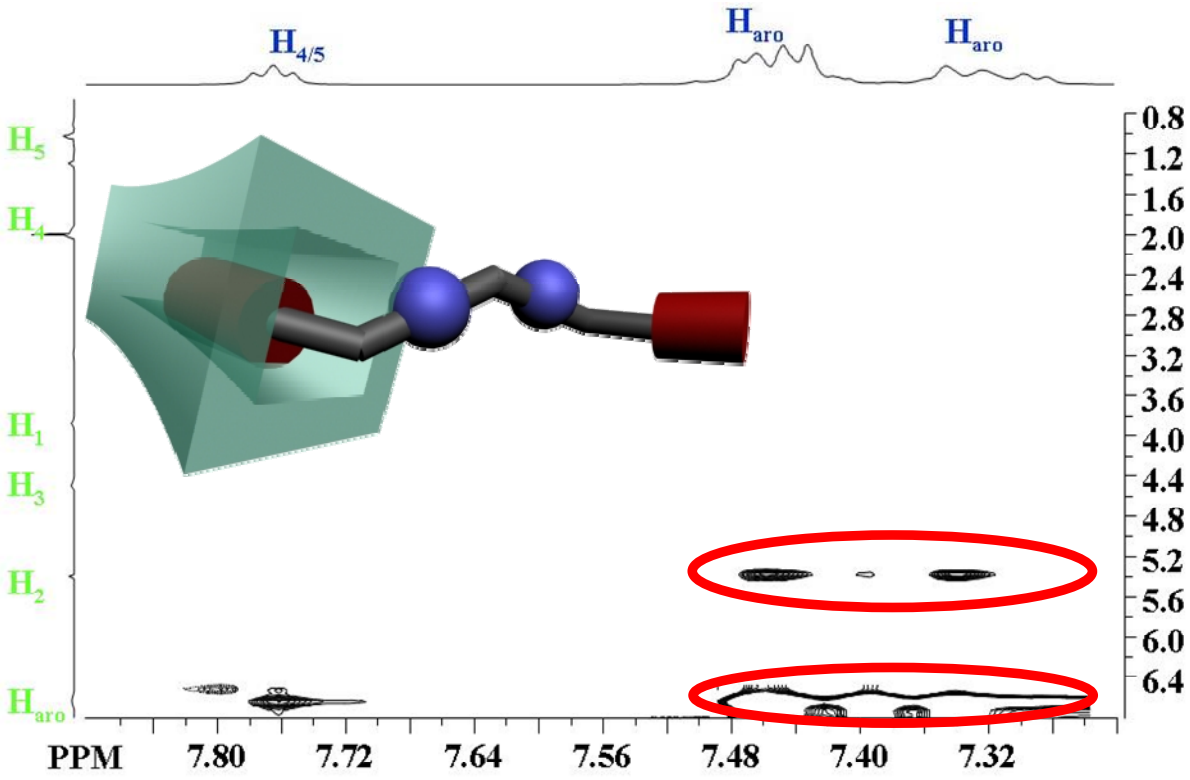


Partial NOESY NMR spectra at 25°C of 10 mM **[1][$PF_6$]$_2$** and 10 mM **C[4]P** ($CDCl_3$/$CD_3CN$ (80/20 V/V)).

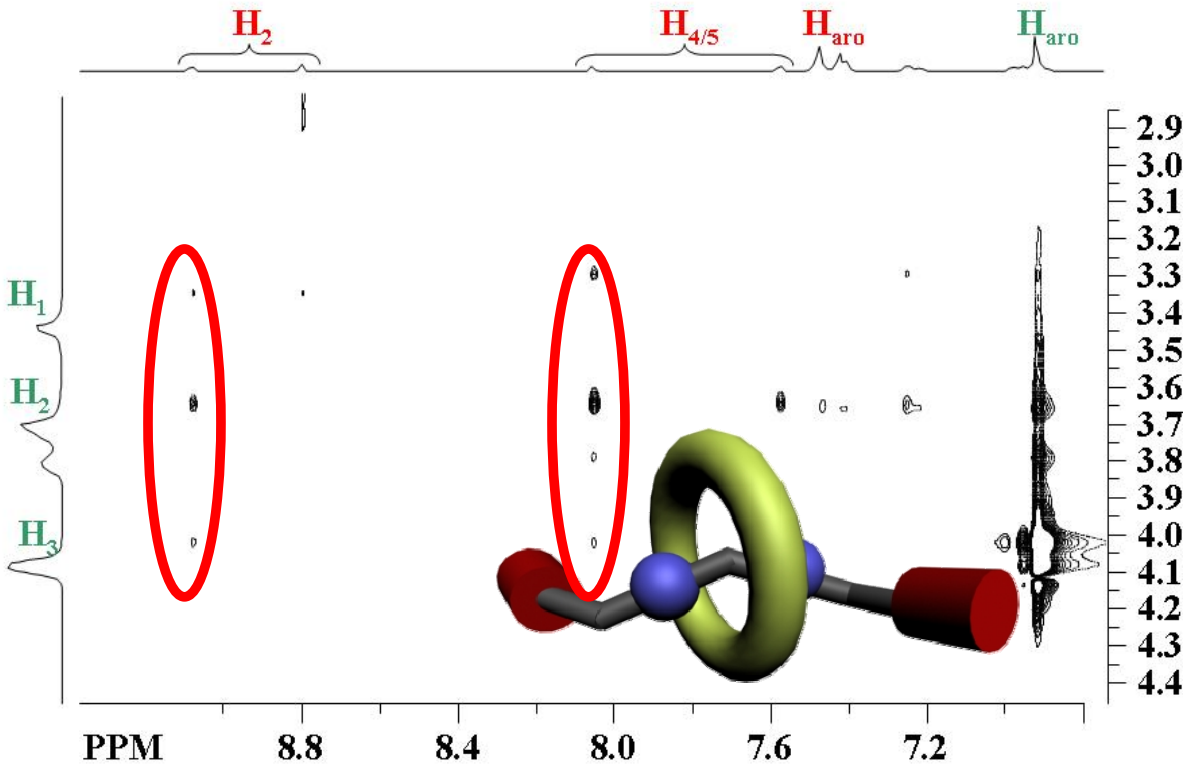


Partial NOESY NMR spectra at 25°C of 10 mM **[1][$PF_6$]$_2$** and 10 mM **DB24C8** ($CD_3CN$).

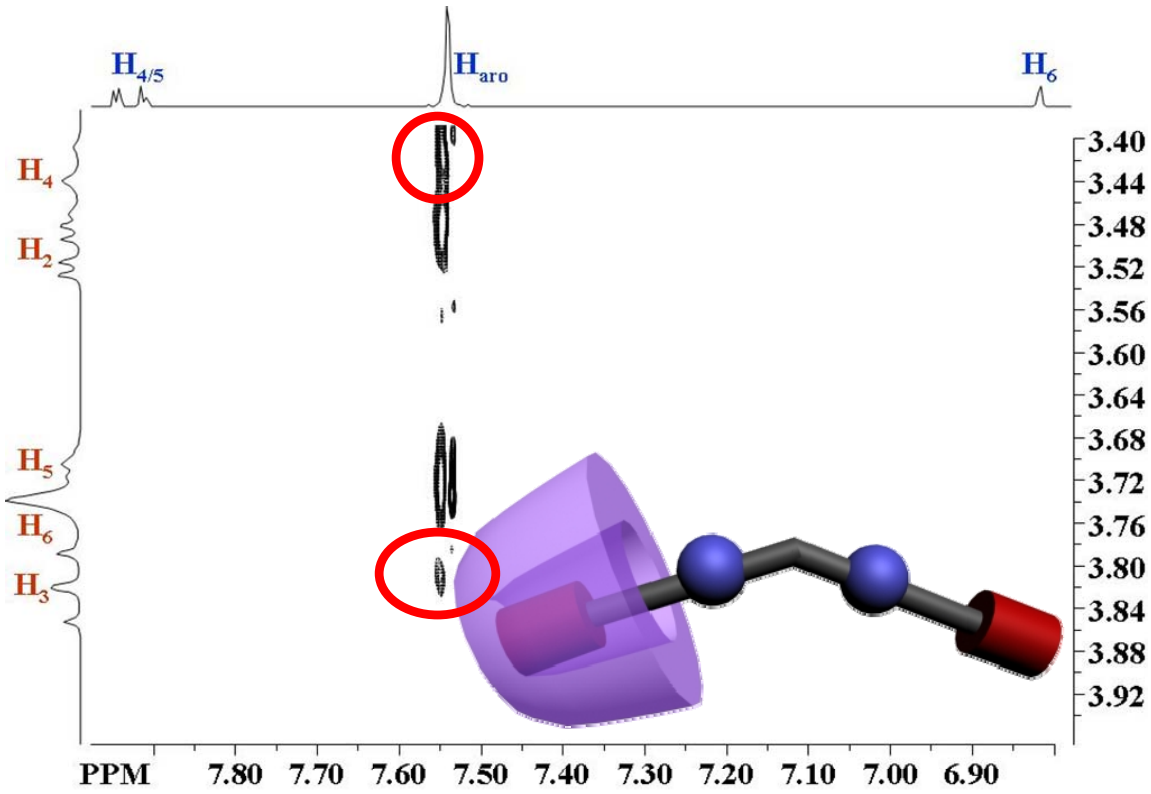


Partial NOESY NMR spectra at 25°C of 5 mM **[2][Br]$_2$** and 5 mM **β-CD** ($D_2O$).

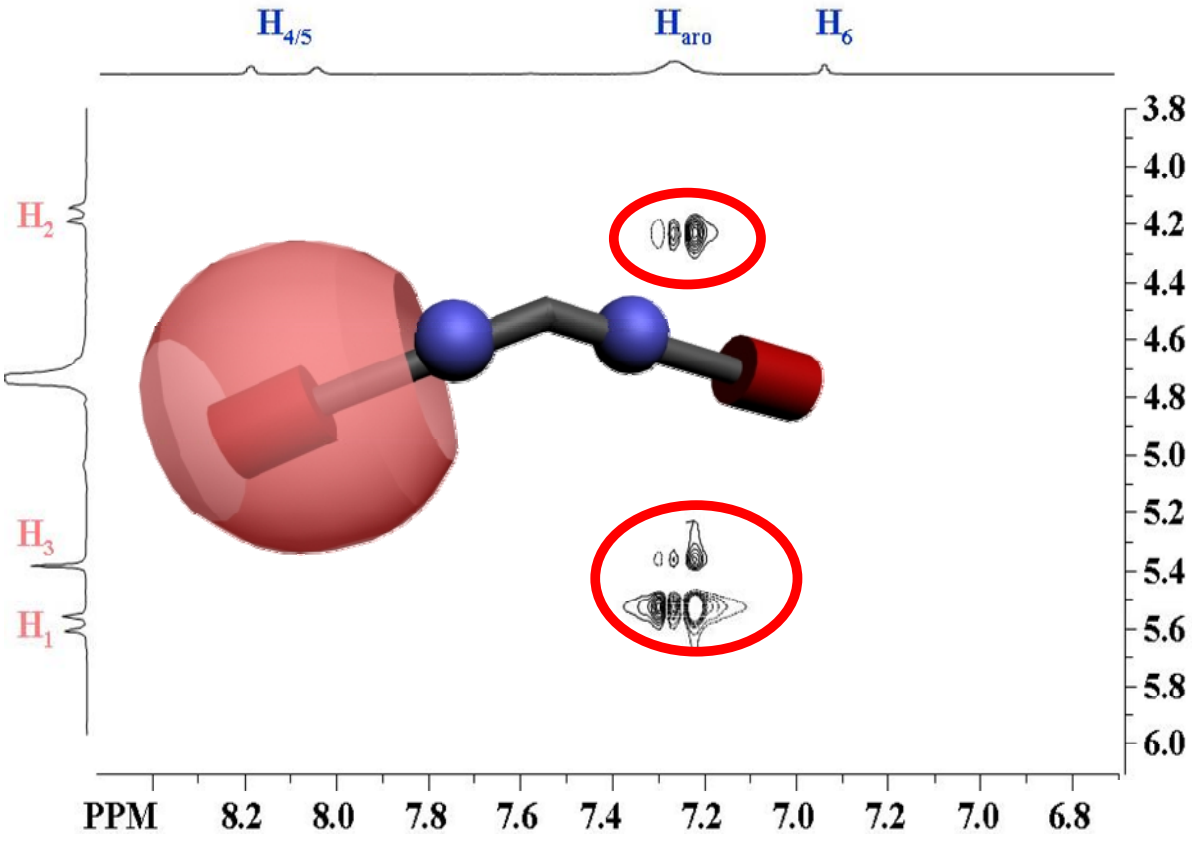


Partial NOESY NMR spectra at 25°C of 4 mM **[2][Br]$_2$** and 4 mM **CB[7]** ($D_2O$).

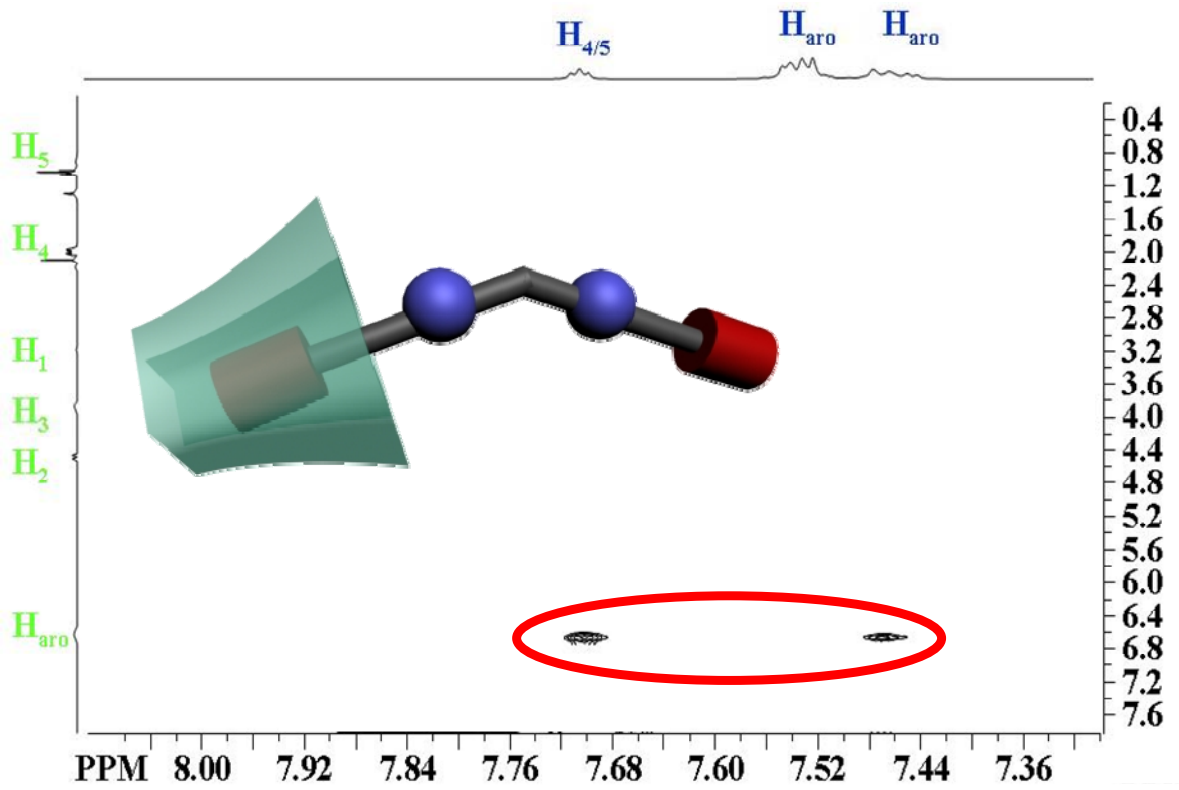


Partial NOESY NMR spectra at 25°C of 10 mM **[2][$PF_6$]$_2$** and 10 mM **C[4]P** ($CDCl_3$/$CD_3CN$ (80/20 V/V)).

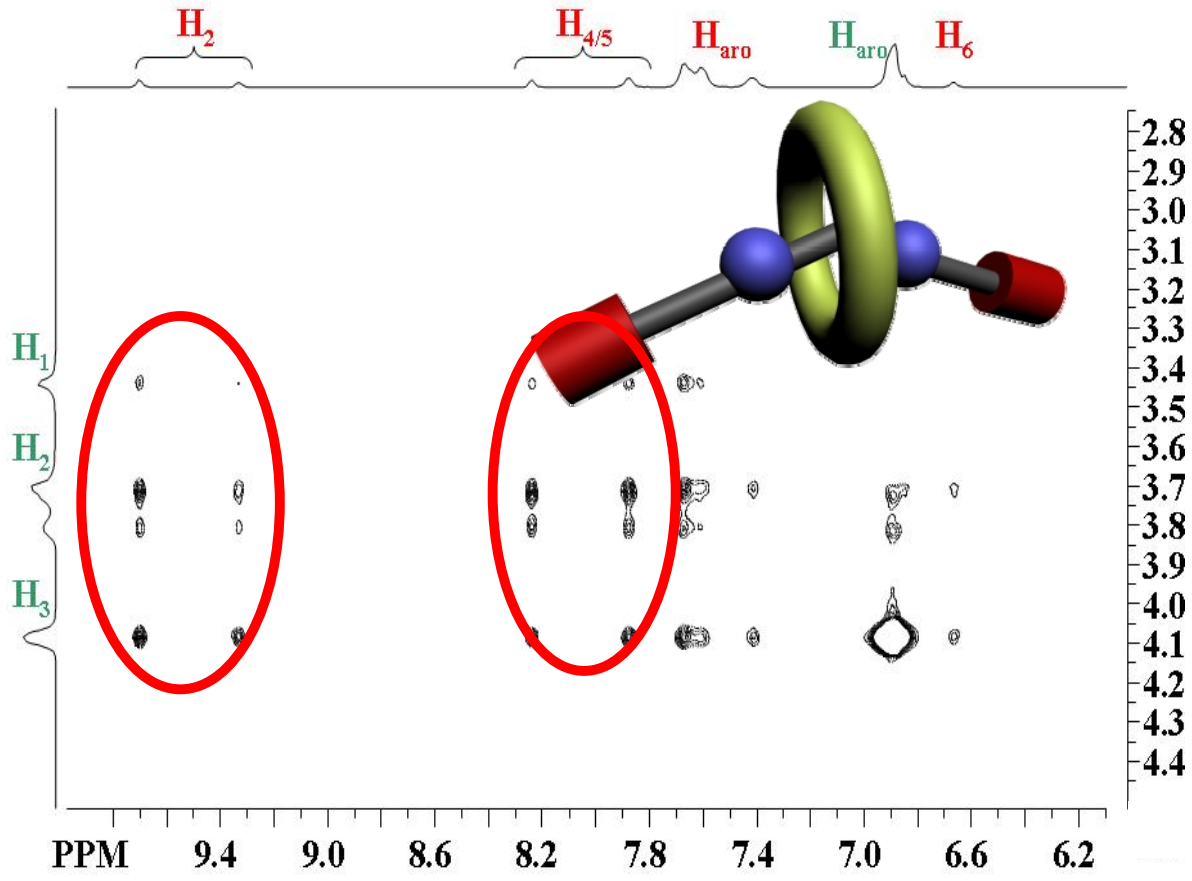


Partial NOESY NMR spectra at 25°C of 10 mM **[2][$PF_6$]$_2$** and 10 mM **DB24C8** ($CD_3CN$).

**Sample of $^1$H NMR titration and Job Plot.**

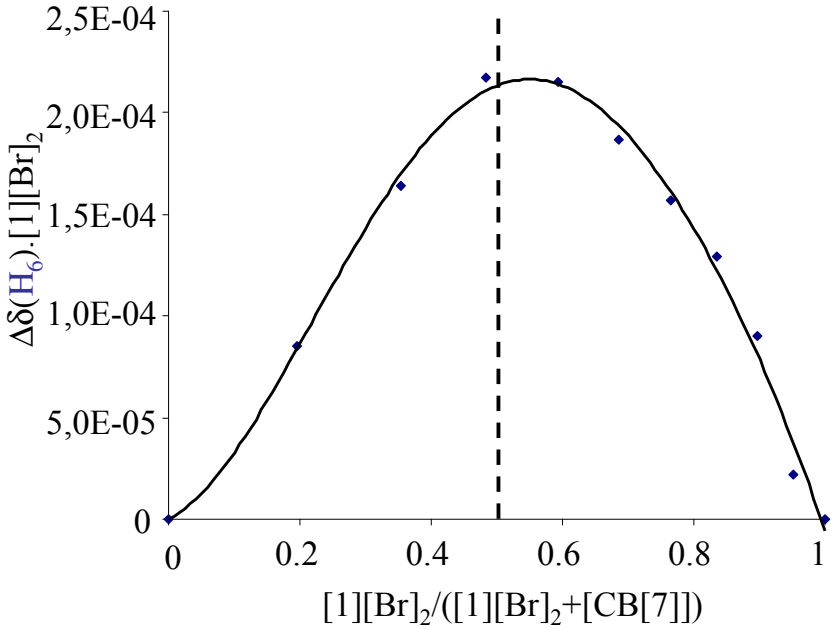


Continuous variation plot (Job's plot) derived from the $^1$H NMR data for the $H_6$ of imidazolium in $D_2O$ of **[1][Br]$_2$**.

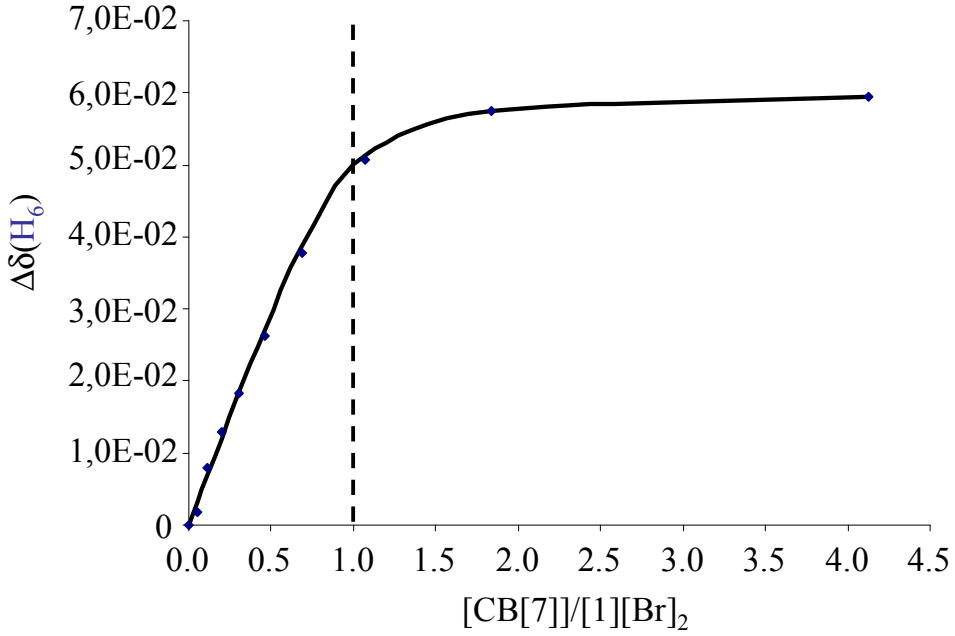


Binding isotherms for the $H_6$ of imidazolium in $D_2O$ of **[1][Br]$_2$**. The solid lines show the best fitted curve for a 1:1 association.

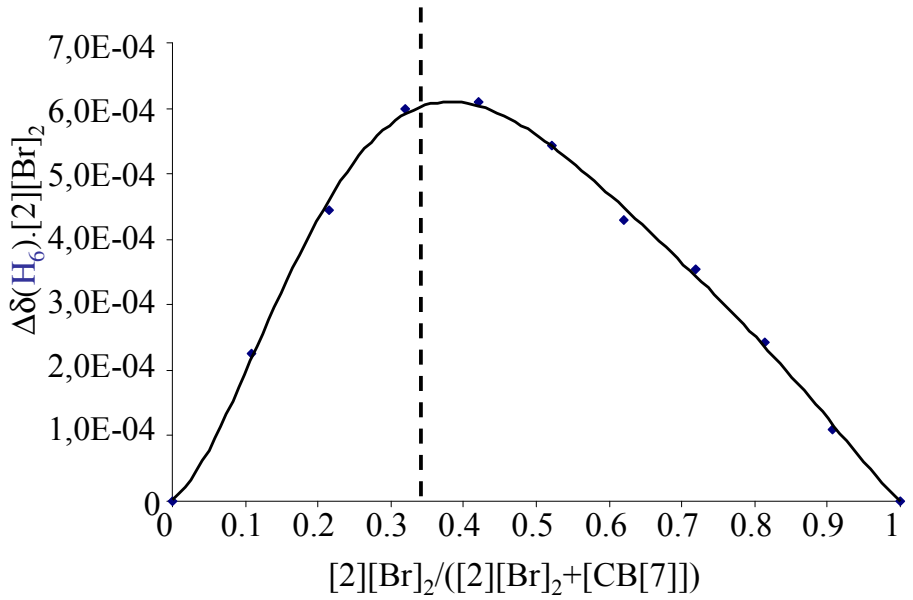


Continuous variation plot (Job's plot) derived from the $^1$H NMR data for the $H_6$ of imidazolium in $D_2O$ of **[2][Br]$_2$**.

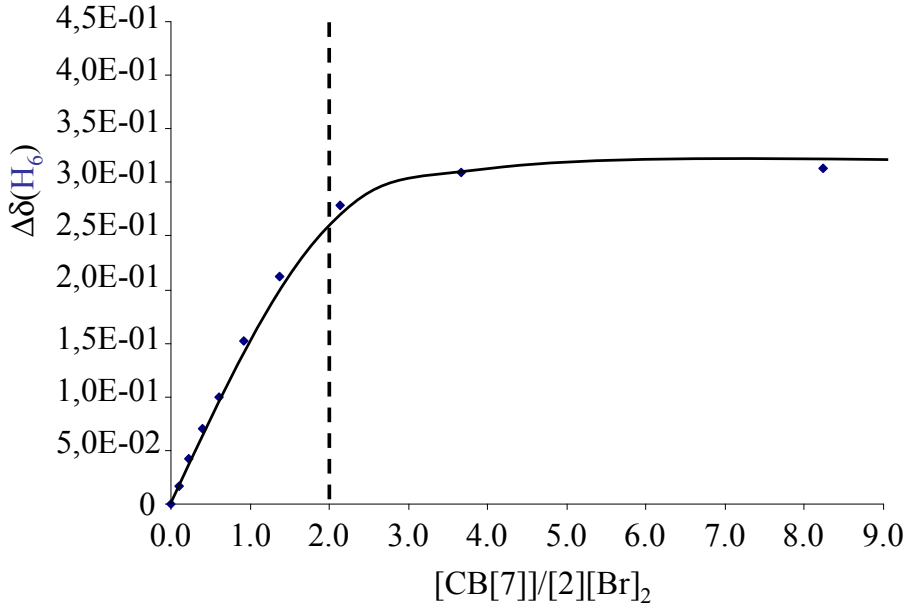


Binding isotherms for the $H_6$ of imidazolium in $D_2O$ of **[2][Br]$_2$**. The solid lines show the best fitted curve for a 2:1 association (For the method see Hao, Y.-Q.; Wu, Y.; Liu, J.; Luo, G.; Yang, G. *Journal of Inclusion Phenomena and Macrocyclic Chemistry* **2006**, *54*, 171).

# Annexe 2 : « Supporting information » de l'article 2 : Study of the supramolecular cooperativity in the multirecognition mechanism of cyclodextrins/cucurbituril/disubstituted diimidazolium bromides

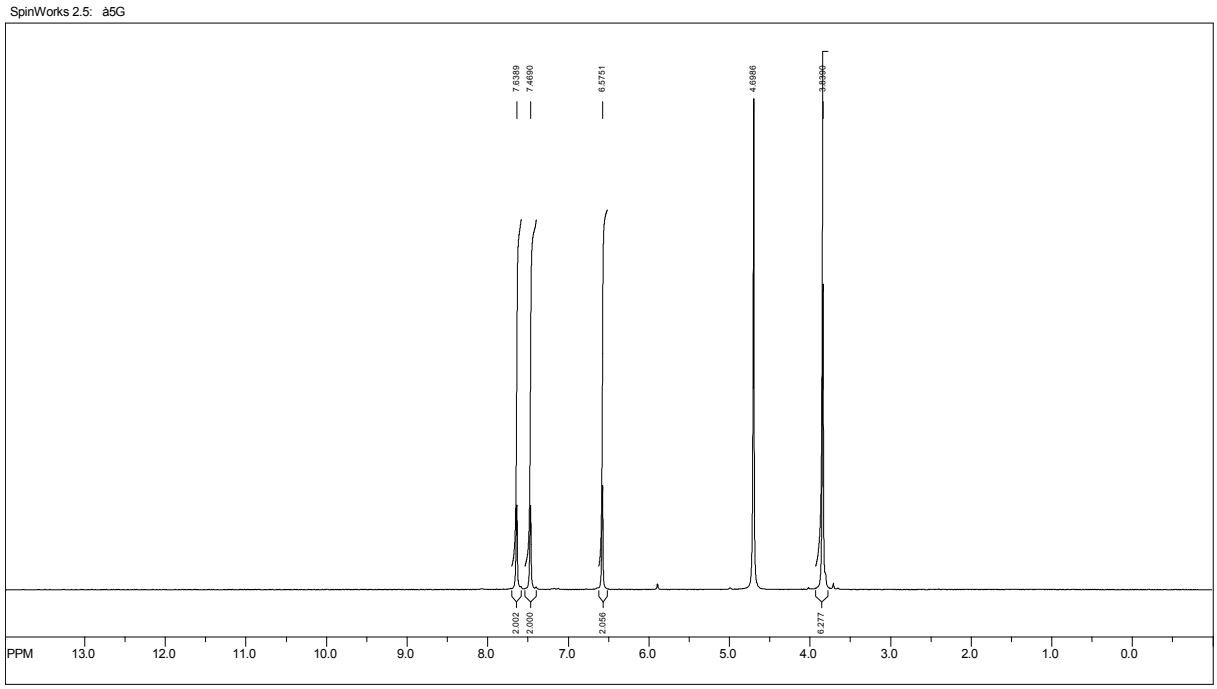


$^1$H NMR of **[1][Br]$_2$**.

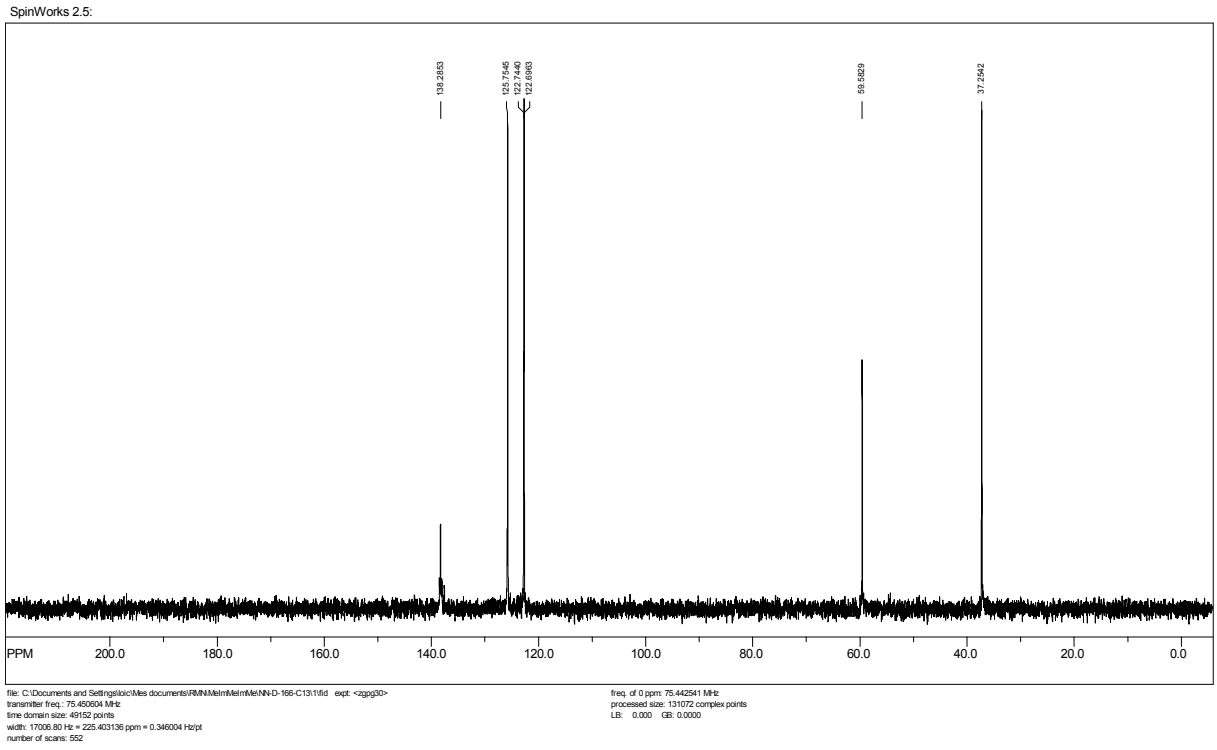


$^{13}$C NMR of **[1][Br]$_2$**.

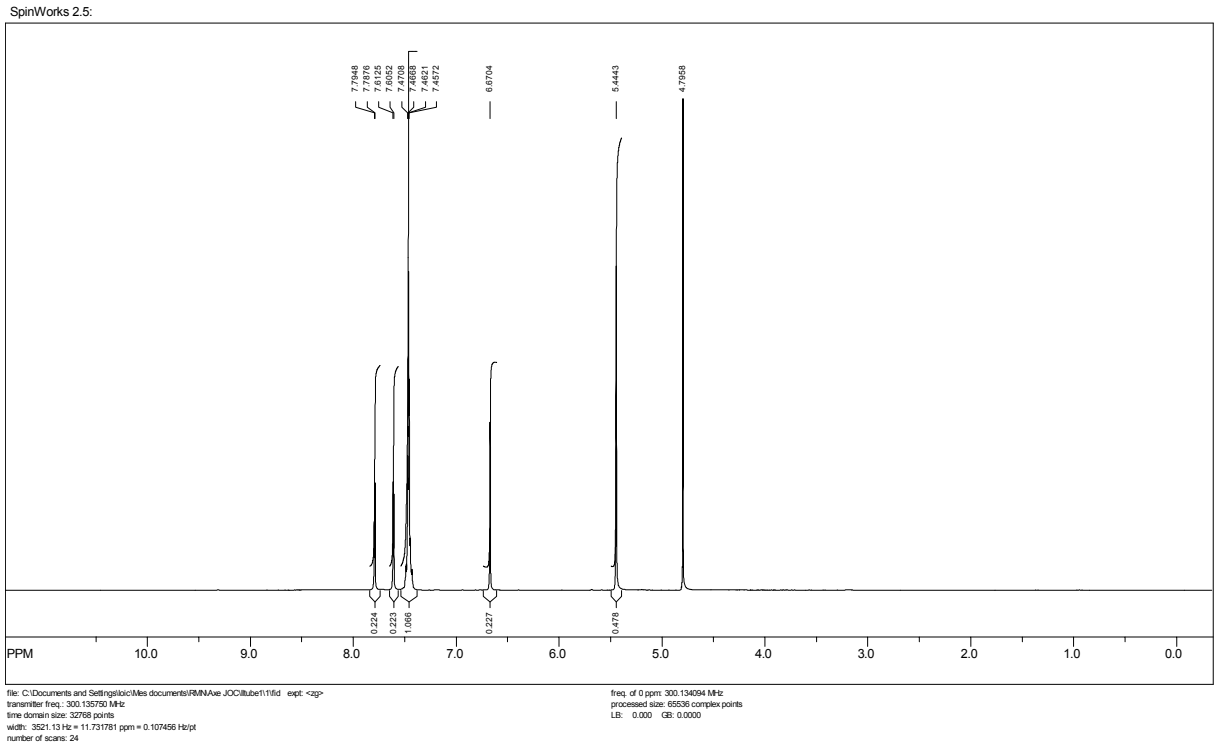


$^1$H NMR of **[2][Br]$_2$**.

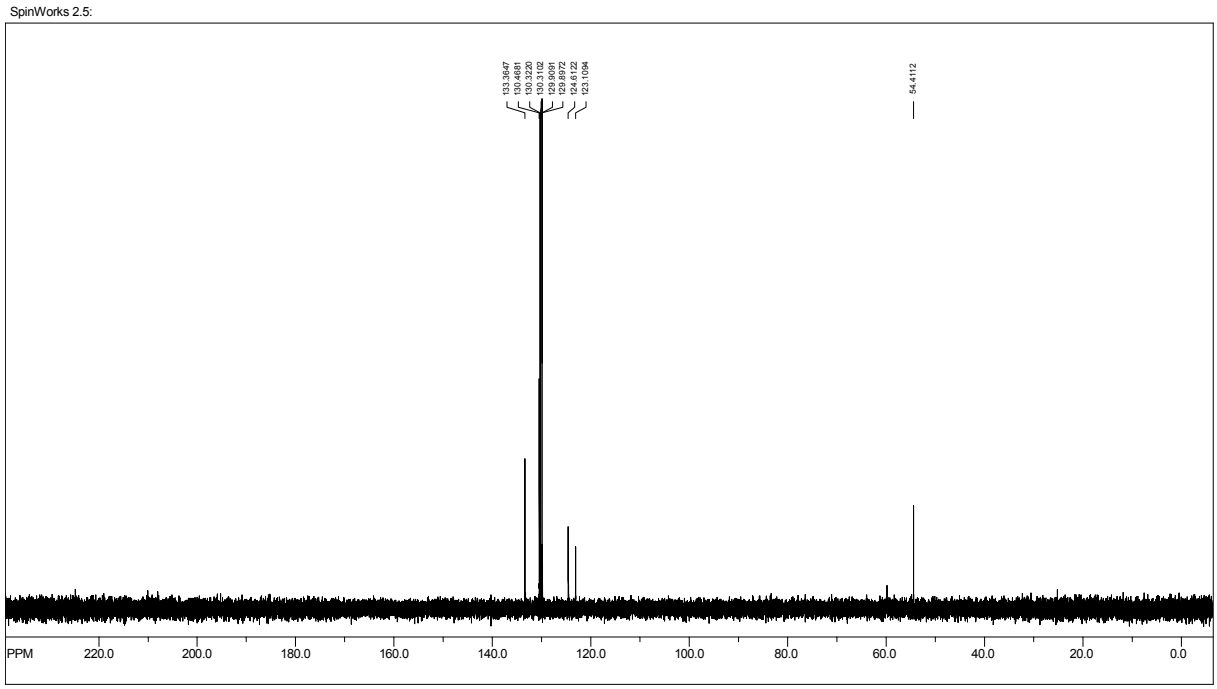


$^{13}$C NMR of **[2][Br]$_2$**.

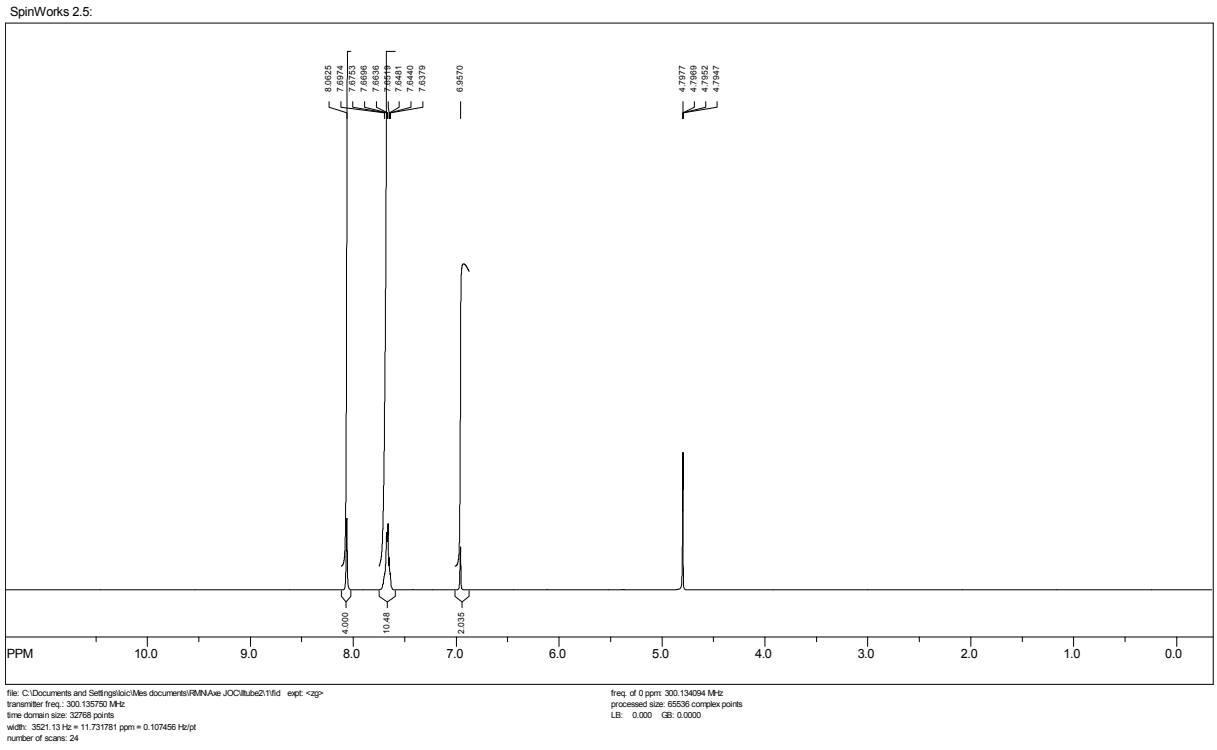


$^{1}$H NMR of **[3][Br]$_2$**.

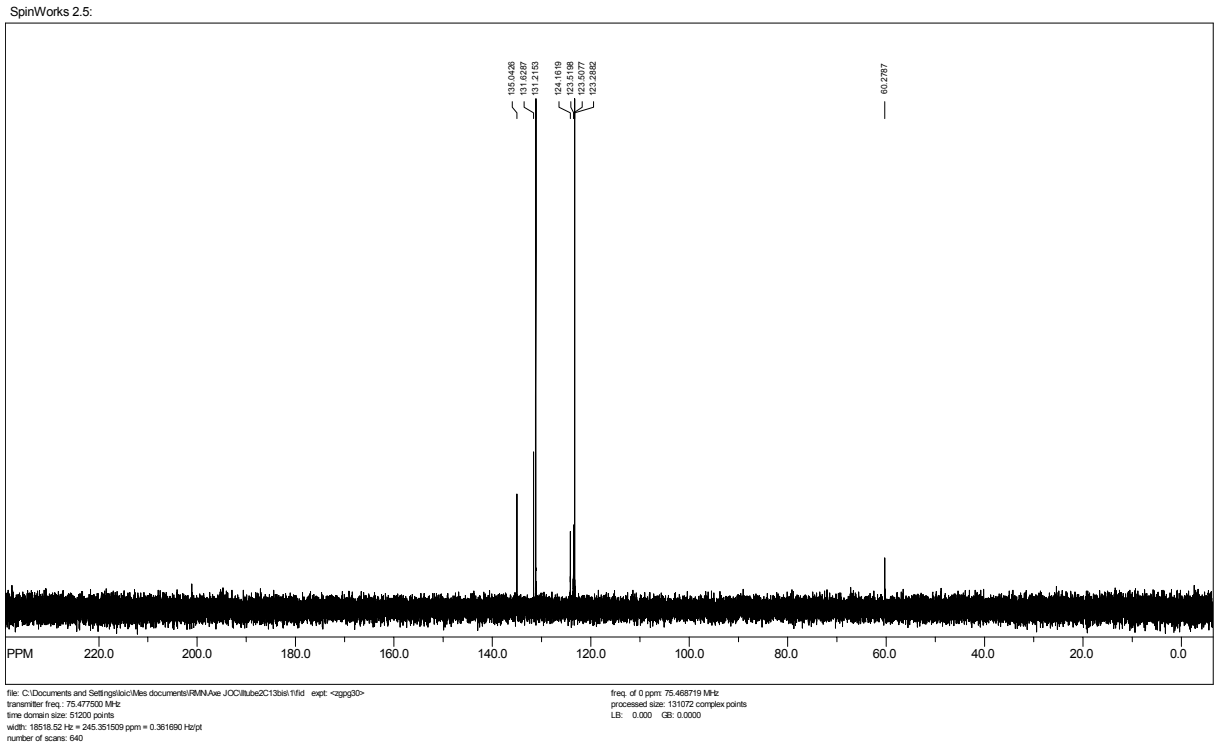


$^{13}C$ NMR of **[3][Br]$_2$**.

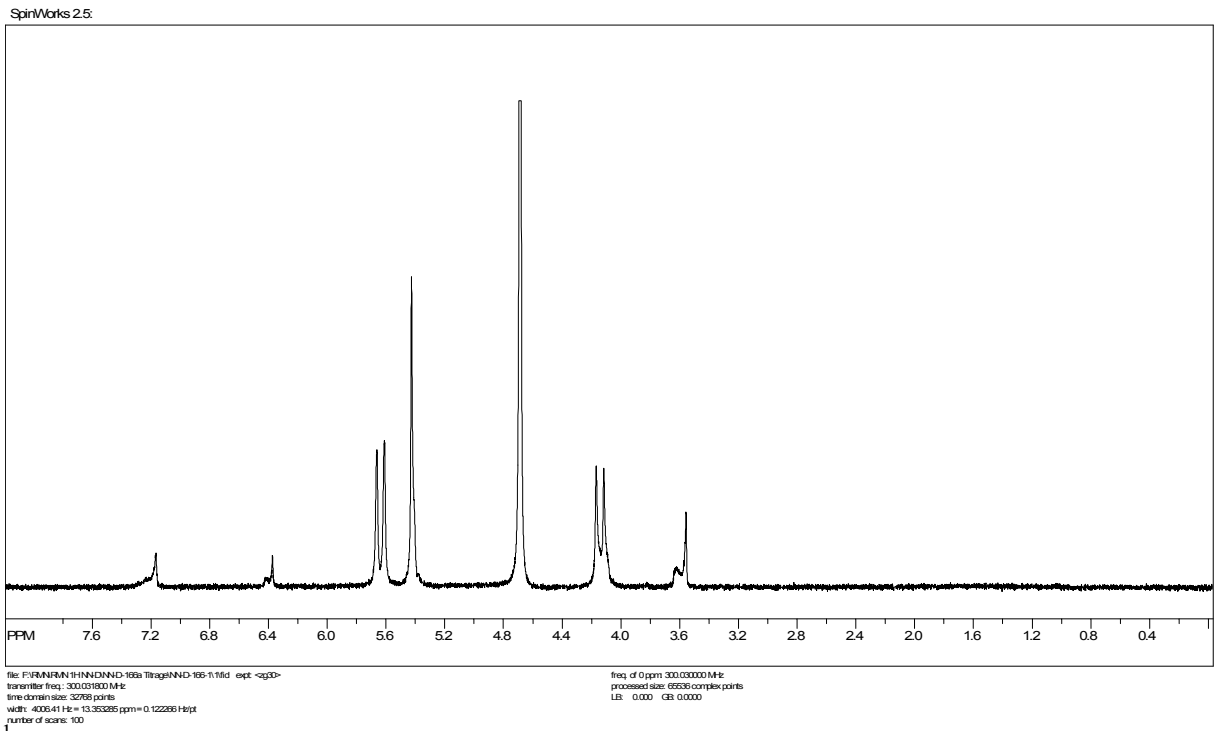


$^1$H NMR of **[1][Br]$_2$** and **CB[7]** (1 mM equimolar solution in $D_2O$).

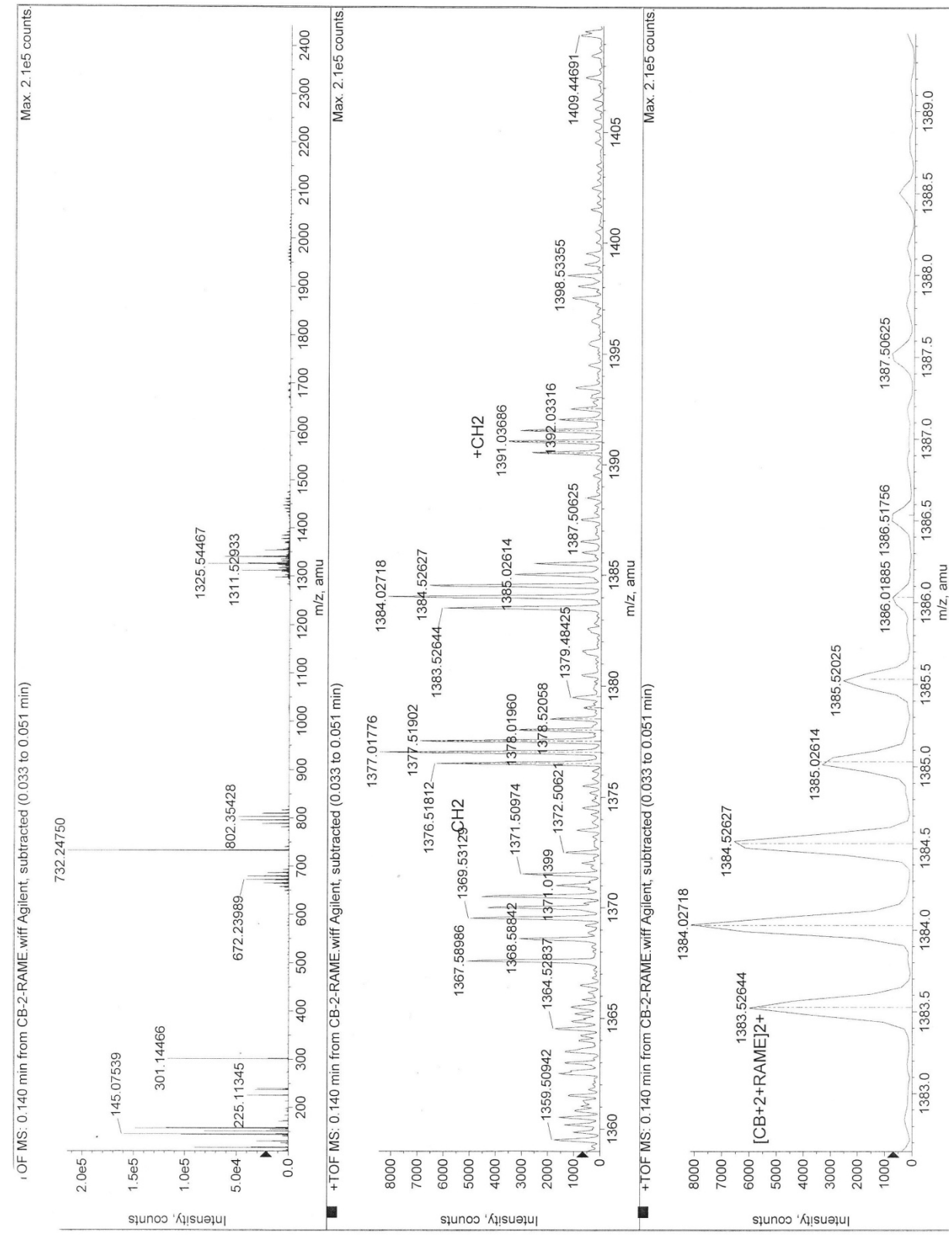


ESI/HRMS **[3][Br]$_2$**, **CB[7]** and **β-DIME**.

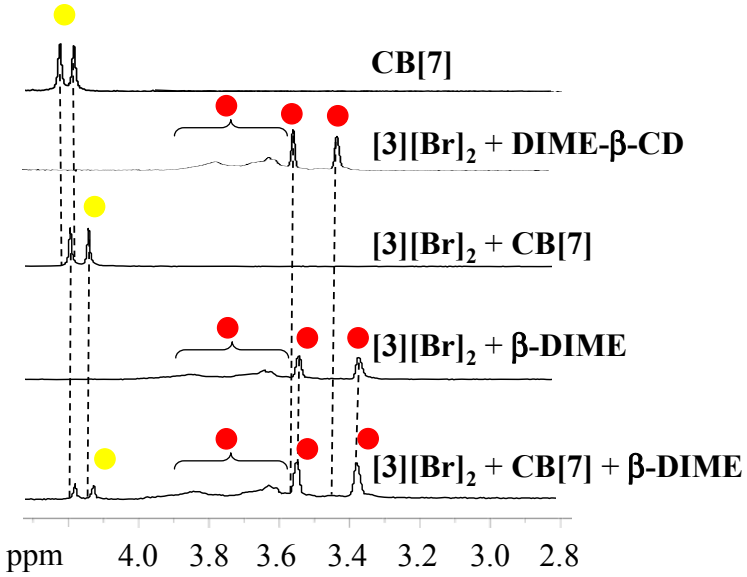


Partial $^{1}H$ NMR spectra at 298K in $D_2O$ of equimolar solution (4mM) of **[3][Br]$_2$** with various hosts (**β-DIME** and/or **CB[7]**).

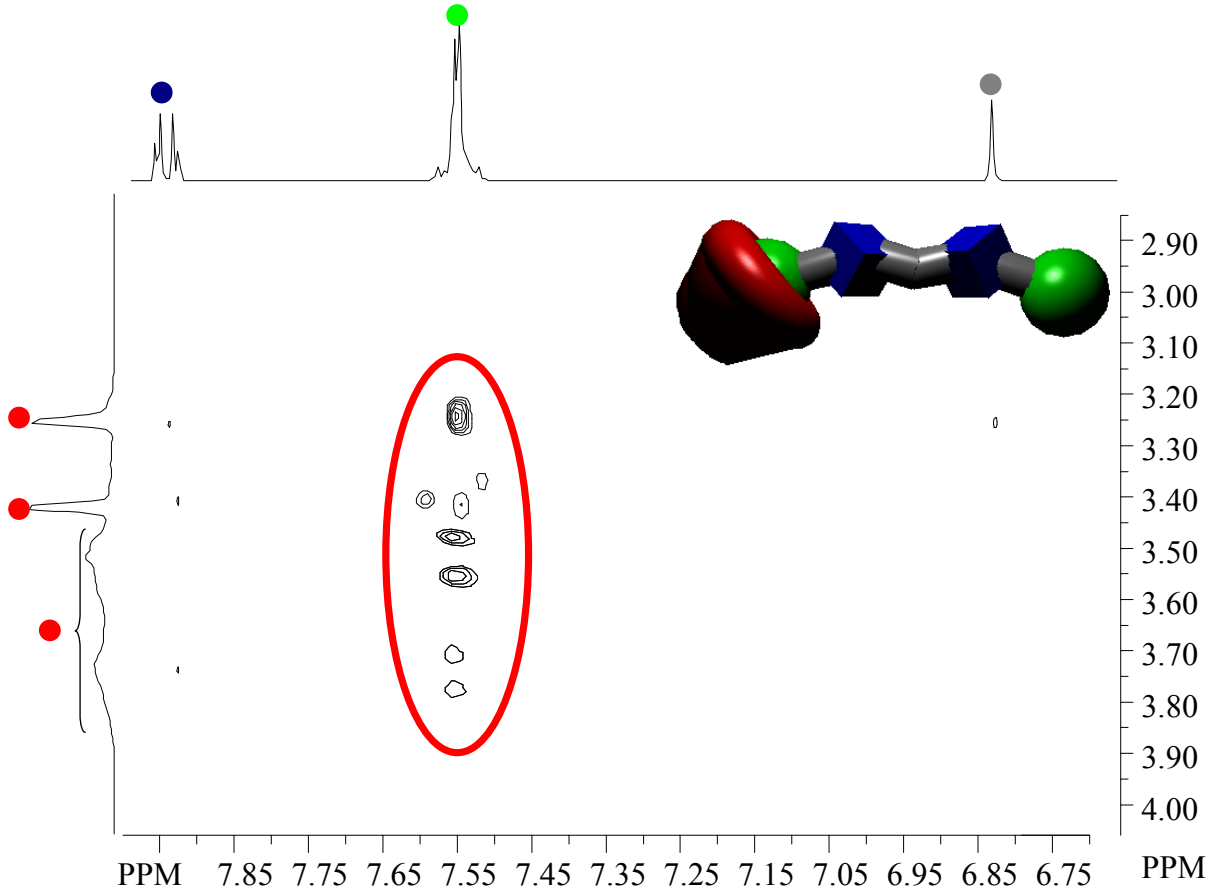


Partial 2D ROESY NMR spectra for an equimolar mixture of **[3][Br]$_2$** and **β-DIME** in $D_2O$ at 298K (4mM).

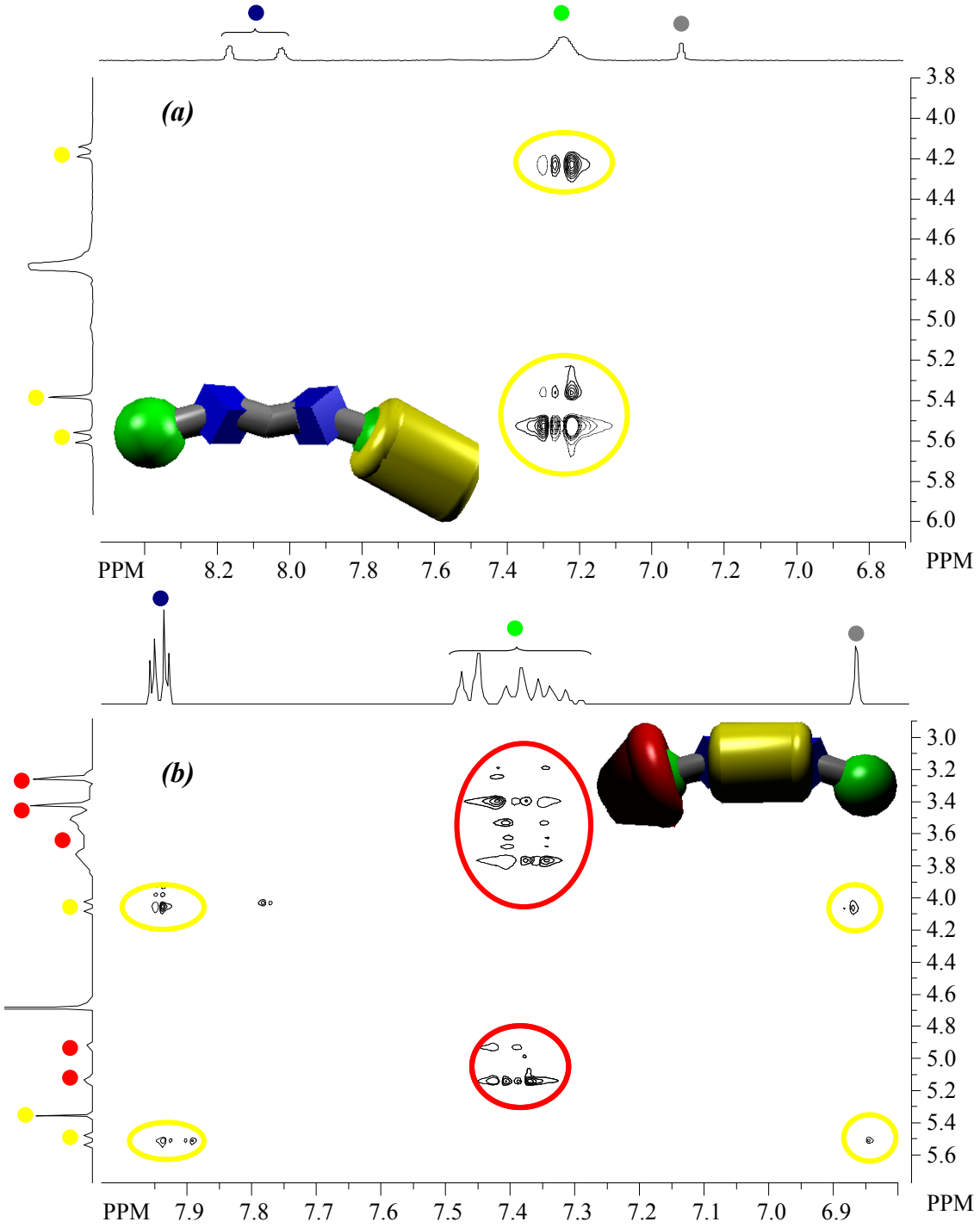


Partial 2D ROESY NMR spectra for: *(a)* an equimolar mixture of **[3][Br]$_2$** and **CB[7]** in $D_2O$ at 298K (4mM); *(b)* an equimolar mixture of **[3][Br]$_2$**, **CB[7]** and **β-DIME** in $D_2O$ at 298K (4mM).

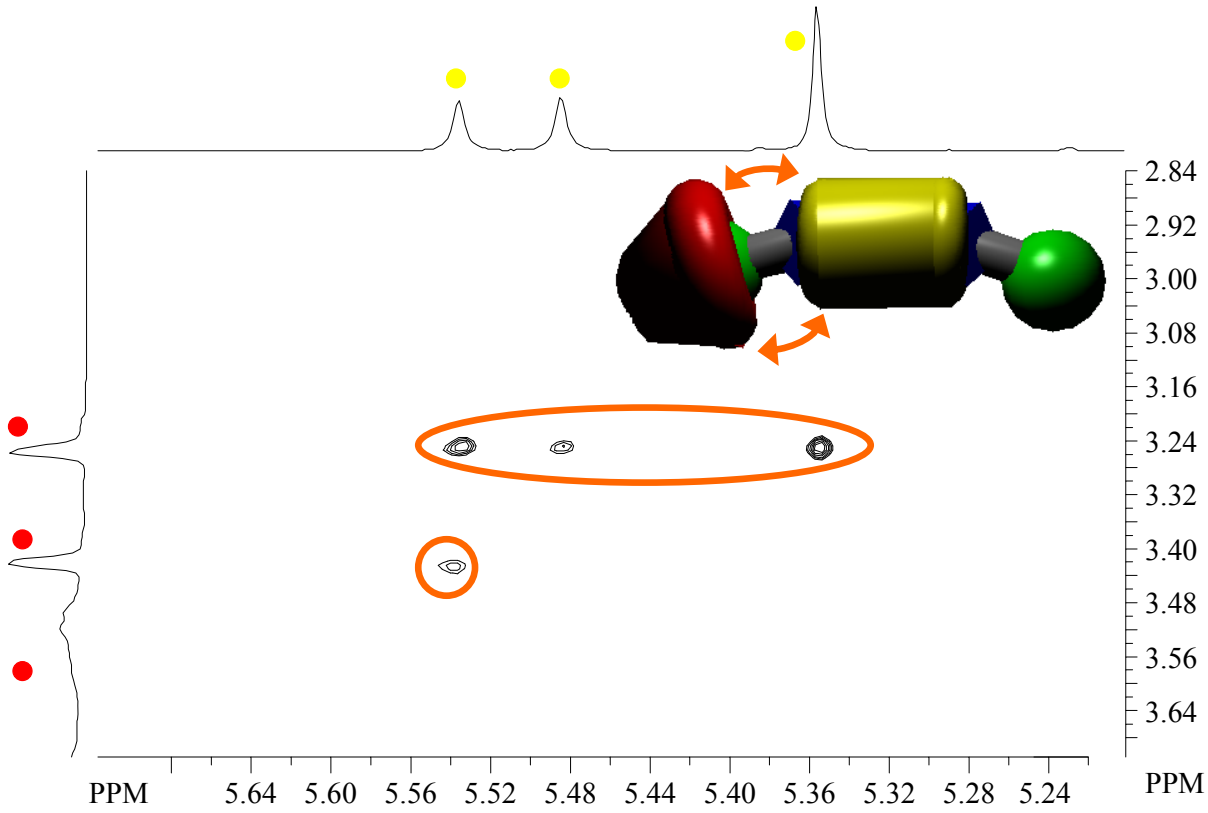


Partial 2D ROESY NMR spectra for an equimolar mixture of **[3][Br]$_2$** , **CB[7]** and **β-DIME** in $D_2O$ at 298K (4mM).

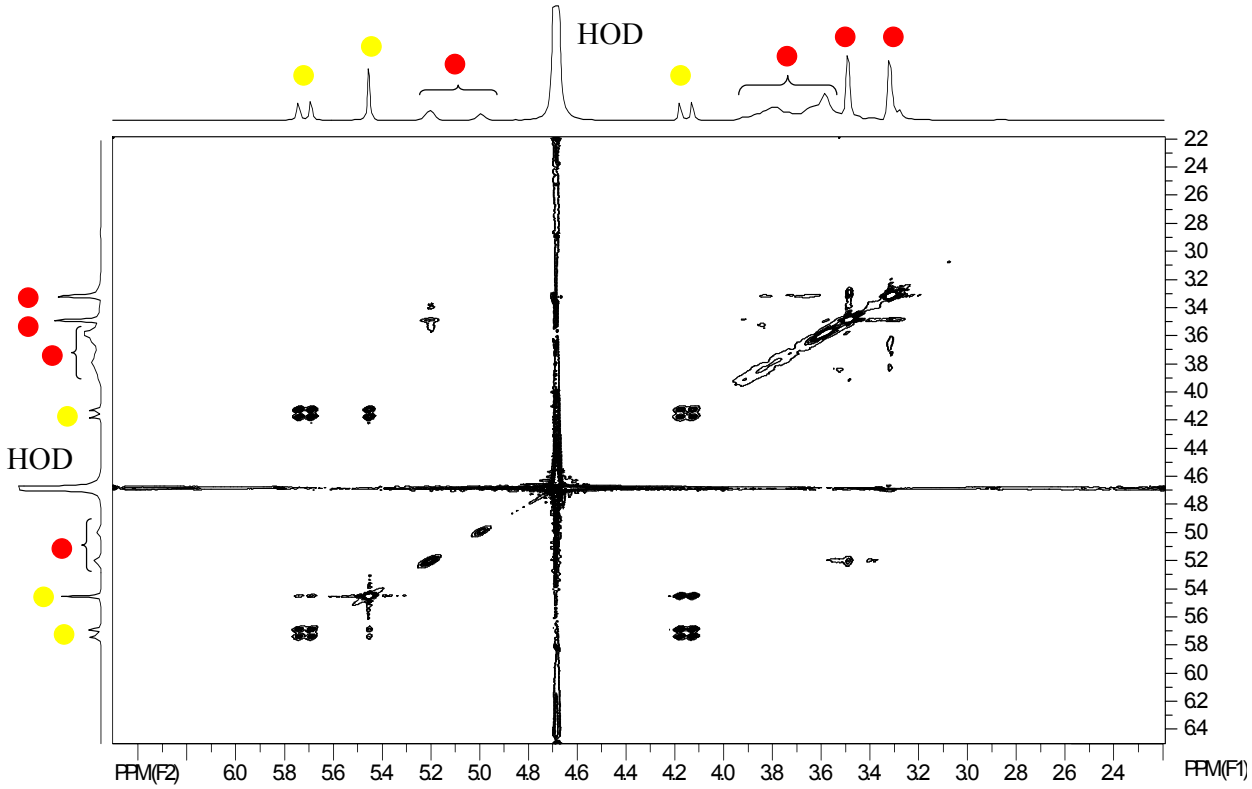


Partial 2D ROESY NMR spectra for an equimolar mixture of **CB[7]** and **β-DIME** in $D_2O$ at 298K (4mM).

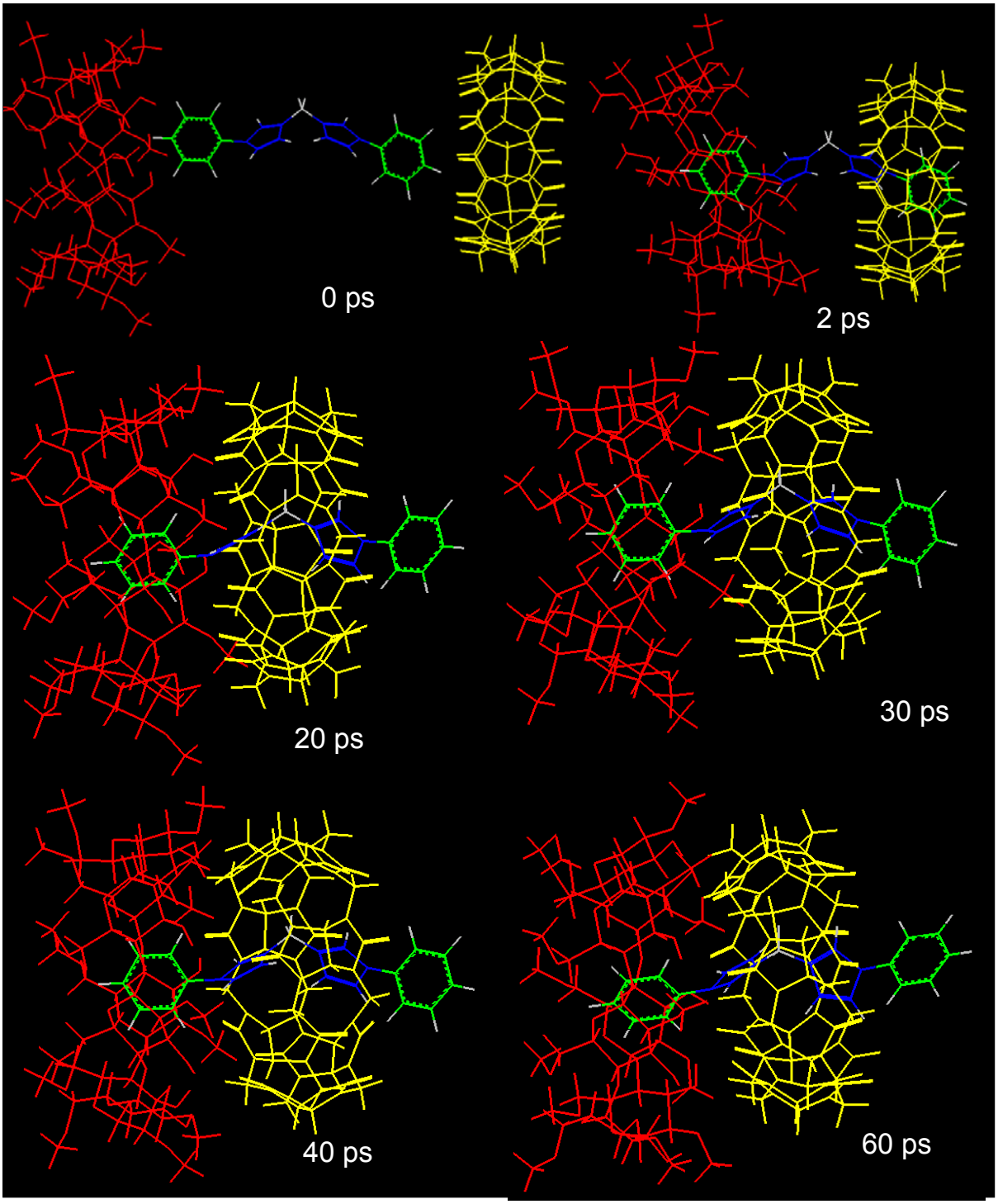


Snapshots of the MD simulation of **[2][Br]$_2$**, **CB[7]** and **β-DIME** in water. Water molecules have been removed in order to provide more visualization of the macrocycles position.

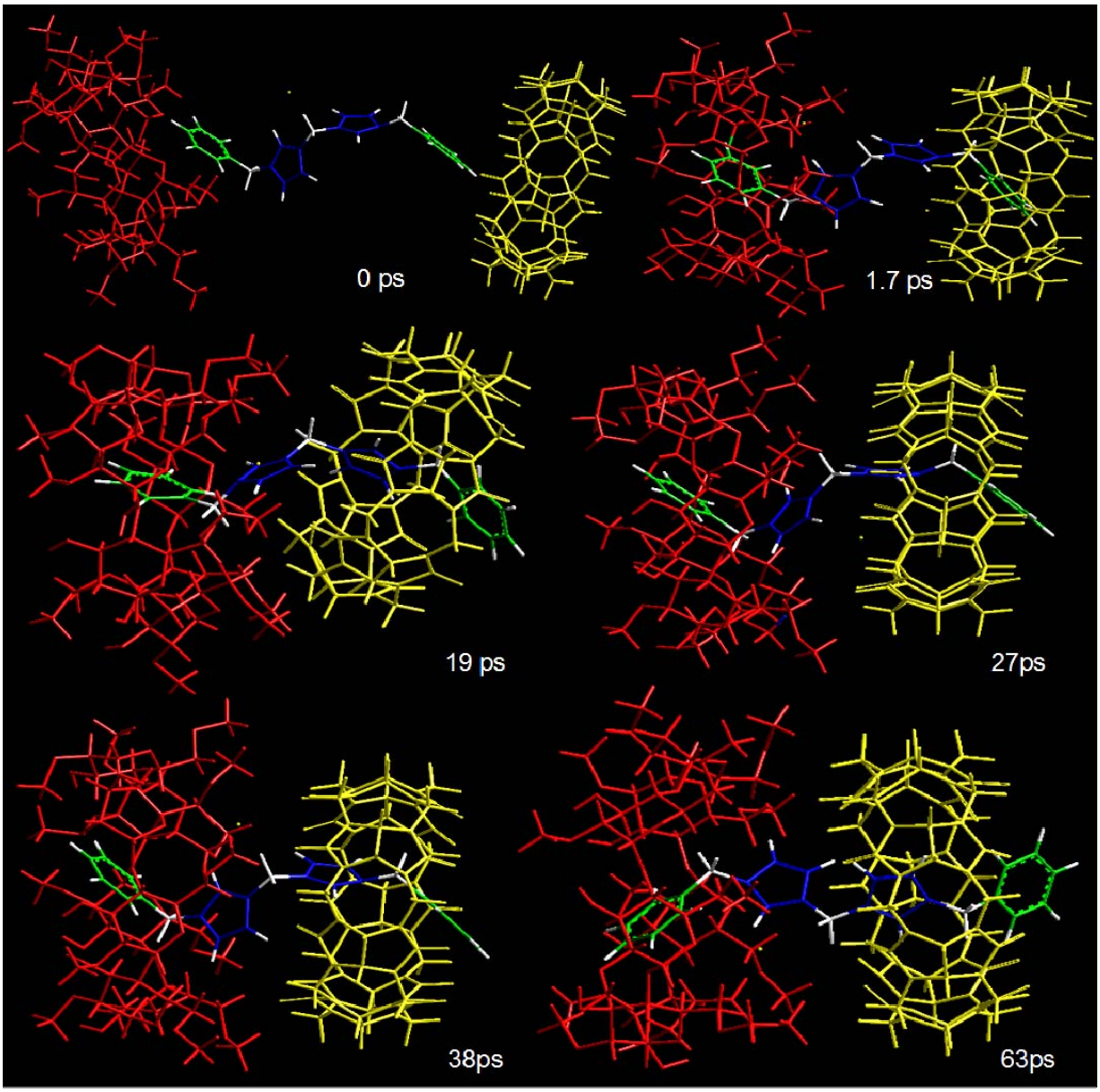


Snapshots of the MD simulation of **[3][Br]$_2$**, **CB[7]** and **β-DIME** in water. Water molecules have been removed in order to provide more visualization of the macrocycles position.

.

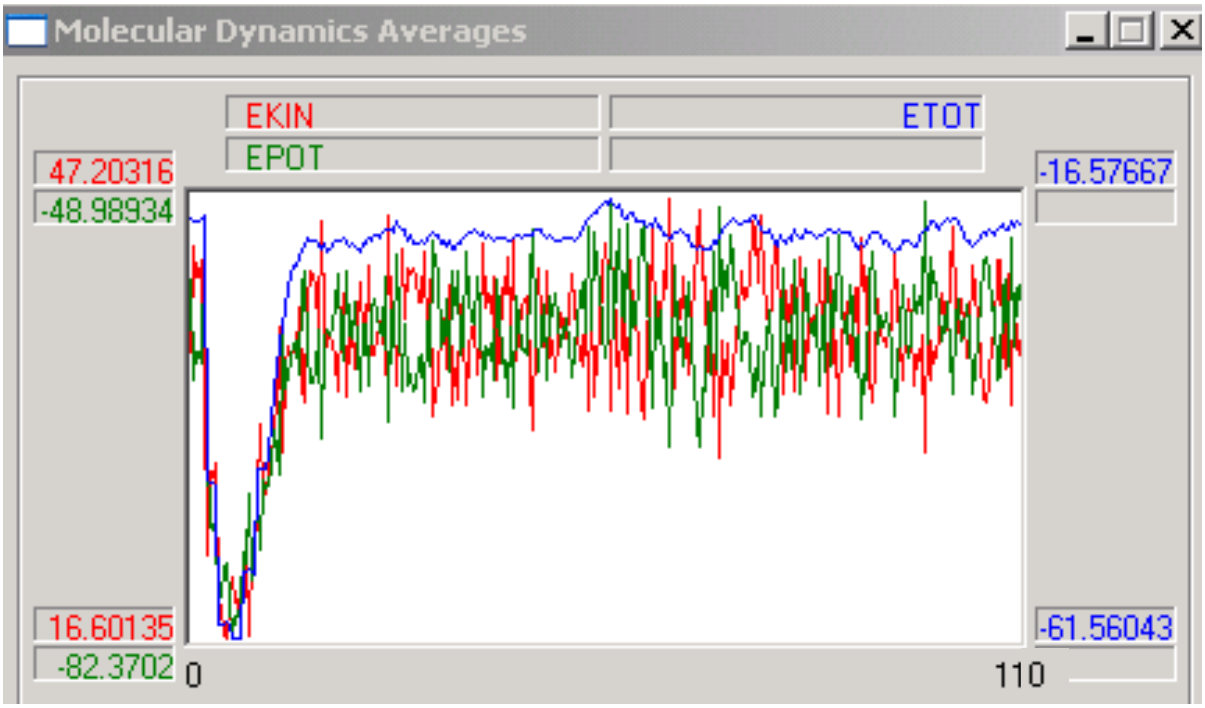


MD trajectory simulation of **[2][Br]$_2$**, **CB[7]** and **β-DIME** in water.

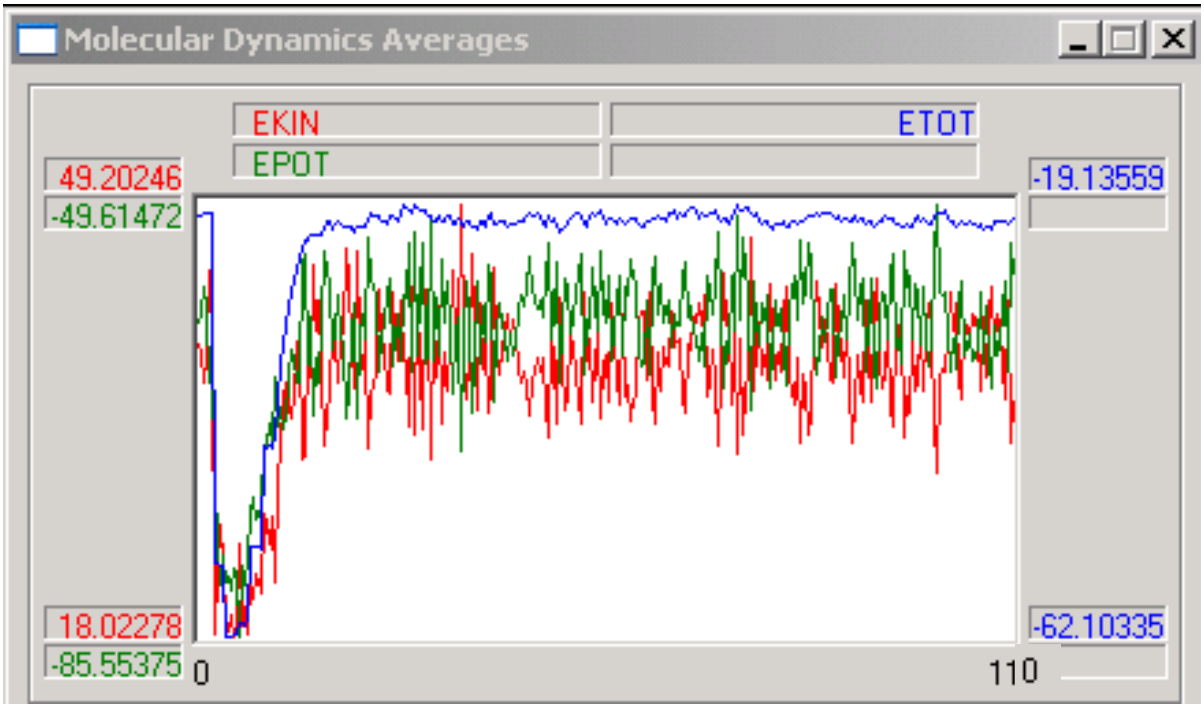


MD trajectory simulation of **[3][Br]$_2$**, **CB[7]** and **β-DIME** in water.

# Annexe 3 : « Supporting information » de l'article 3 : Formation of inclusion complexes between 1,1'-dialkyl-3,3'-(1,4-phenylene)bisimidazolium dibromide salts and cucurbit[7]uril

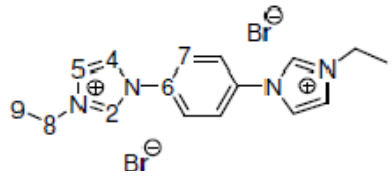


**DiimC$_2$ in D$_2$O**

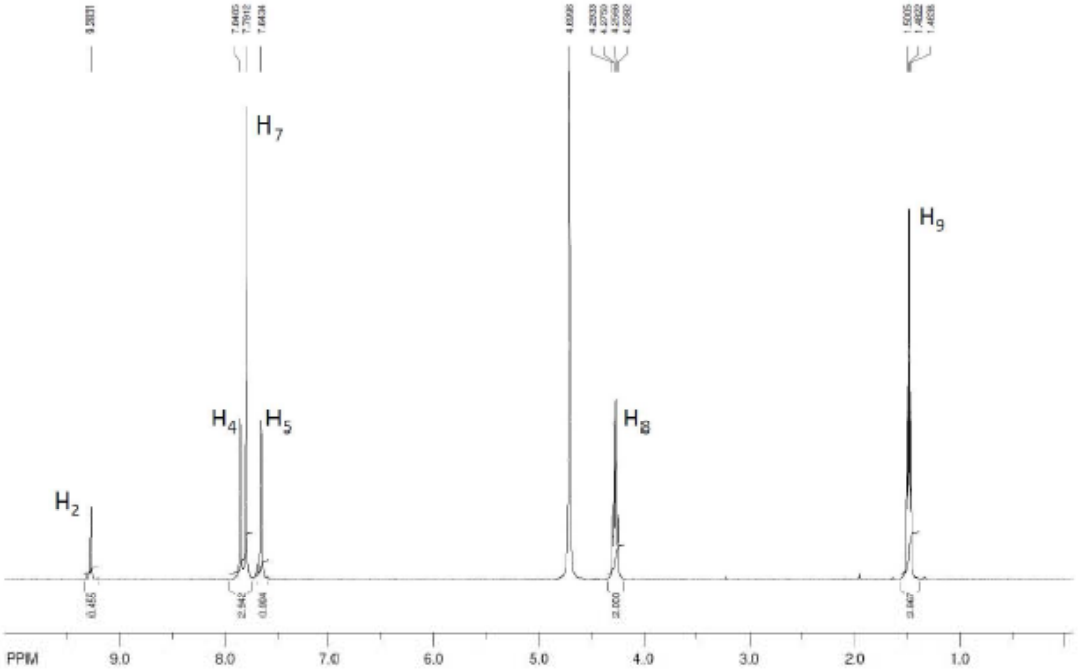


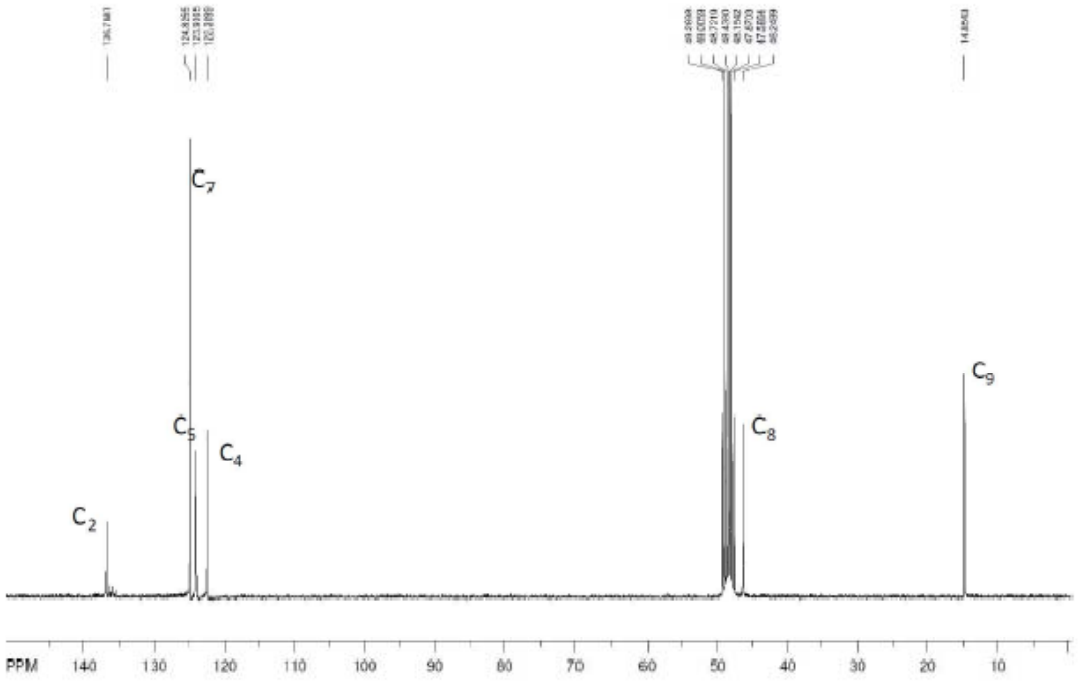

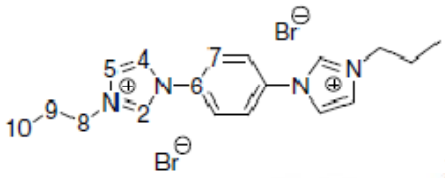


**DiimC$_3$ in CD$_3$OD**

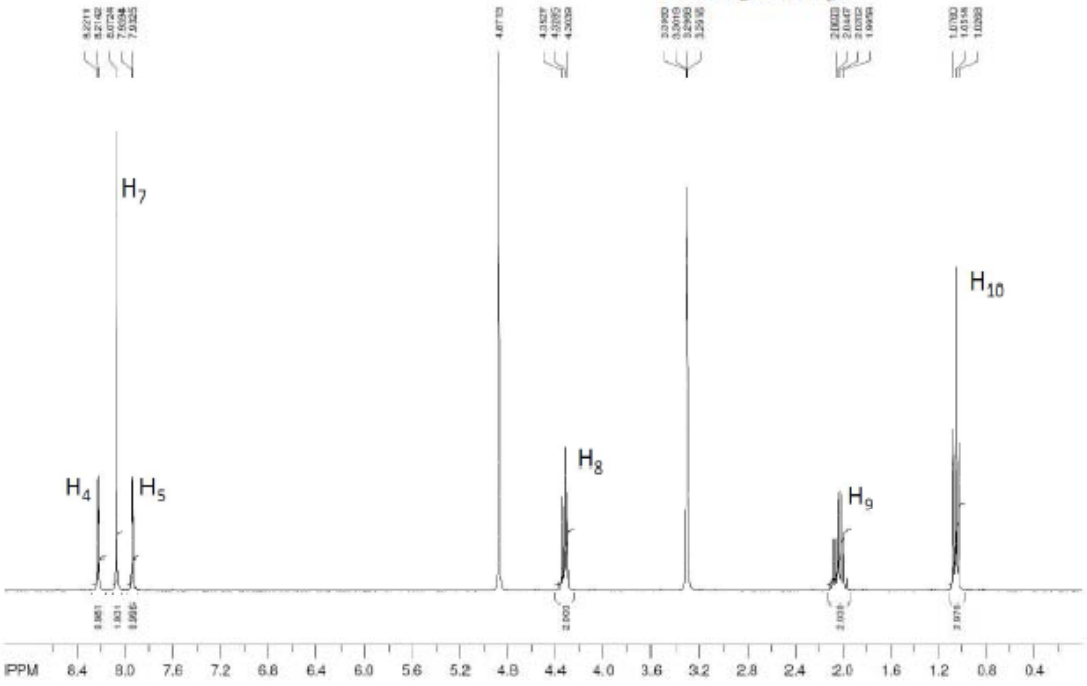


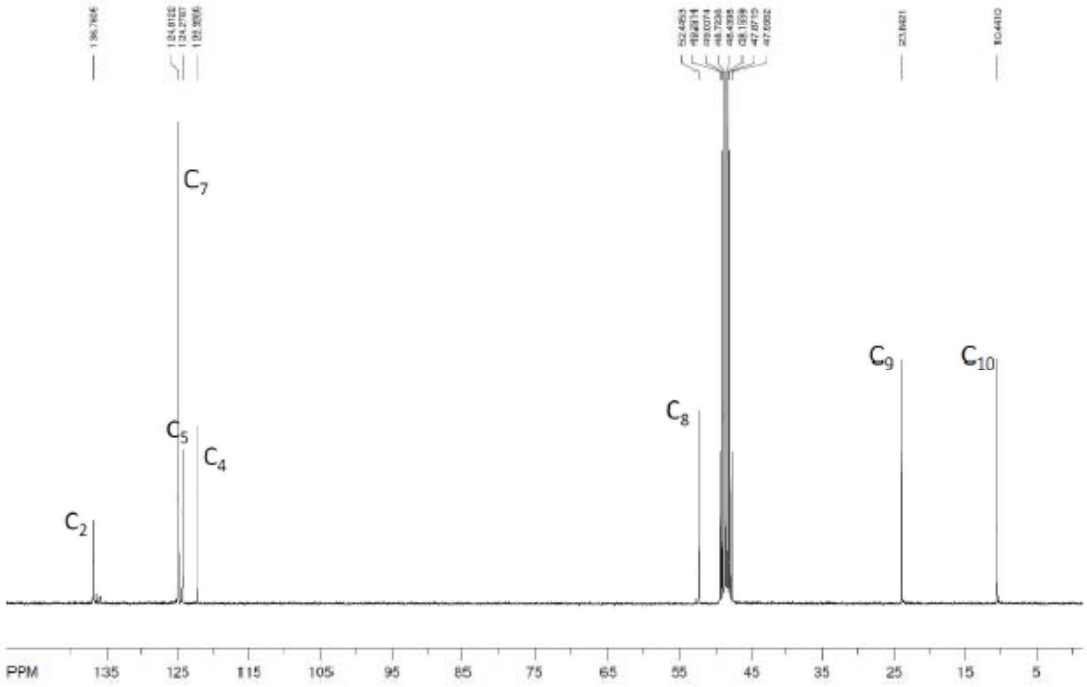

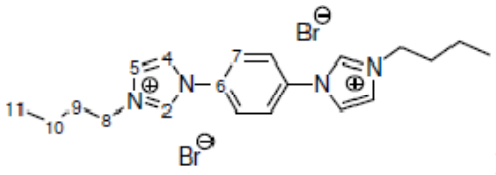


**DiimC$_4$ in CD$_3$OD**

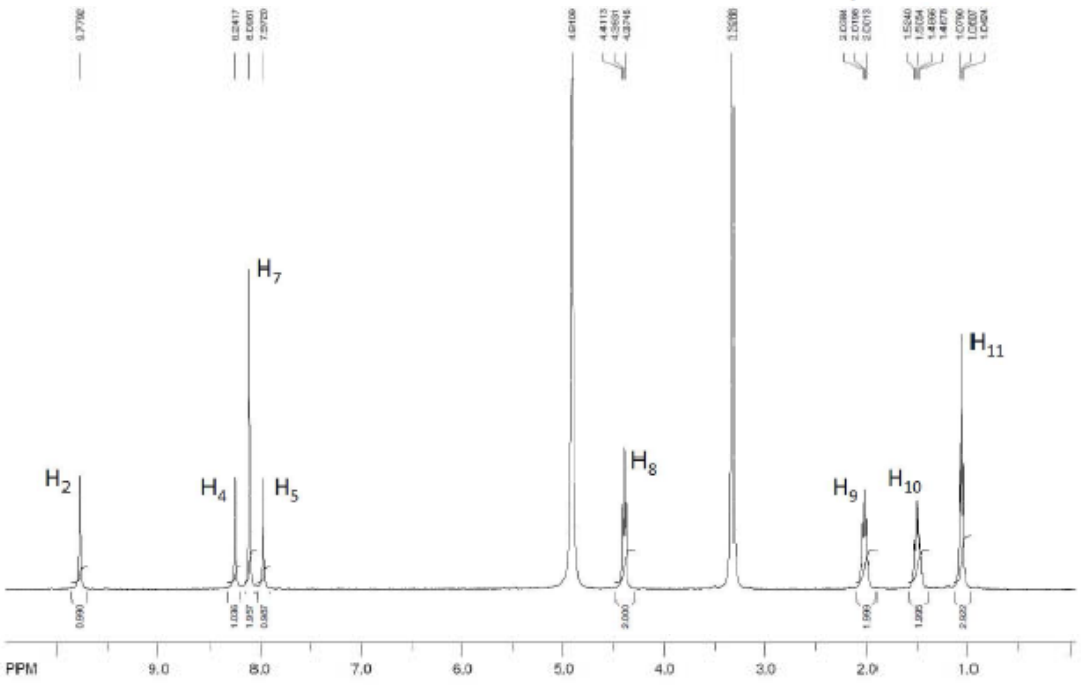


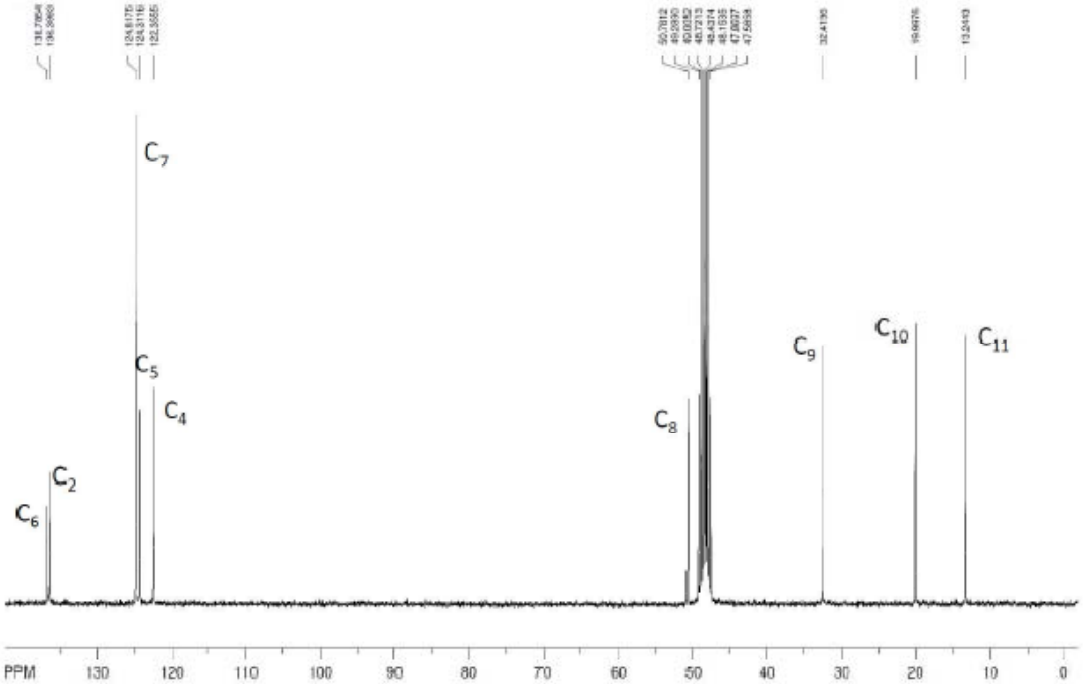

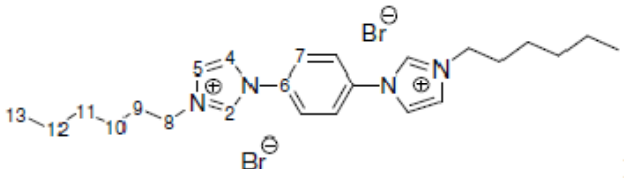


**DiimC$_6$ in CD$_3$OD**

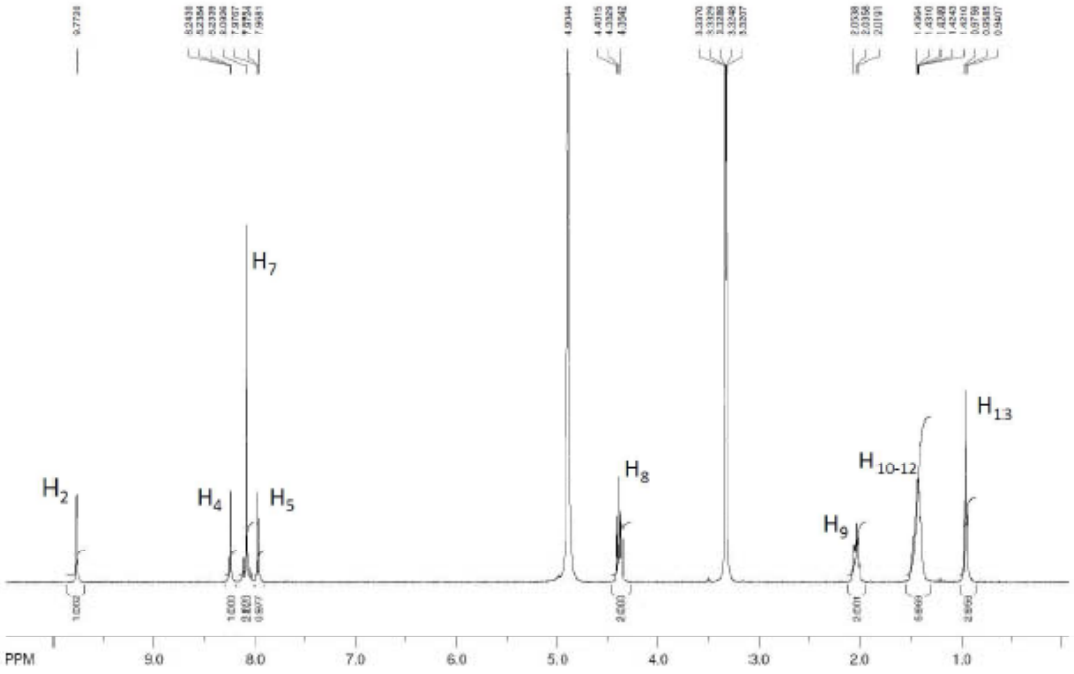


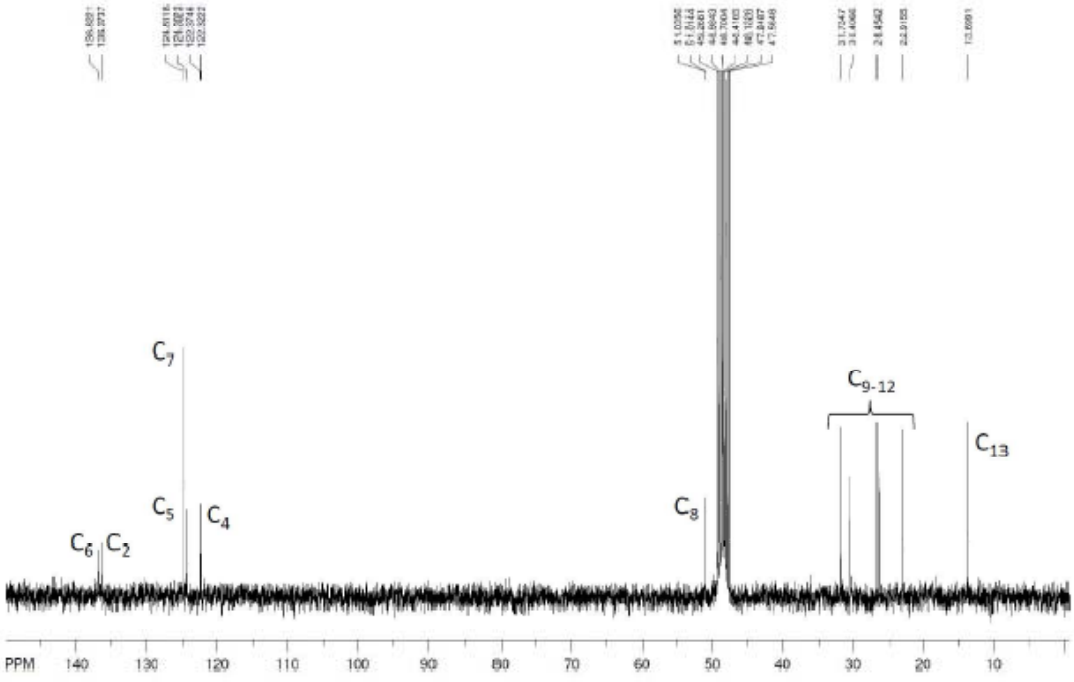

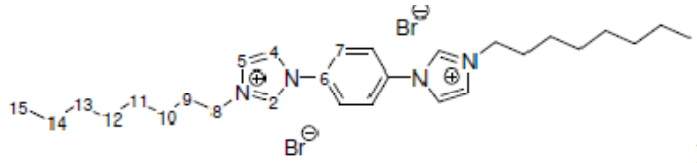


**DiimC$_8$ in D$_2$O**

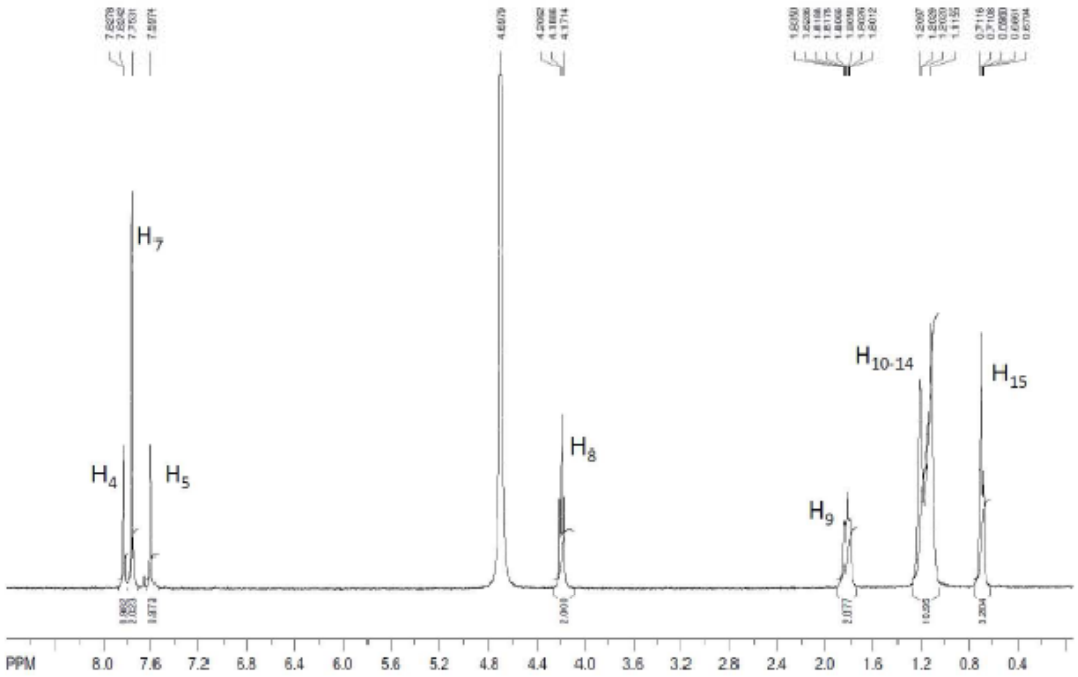


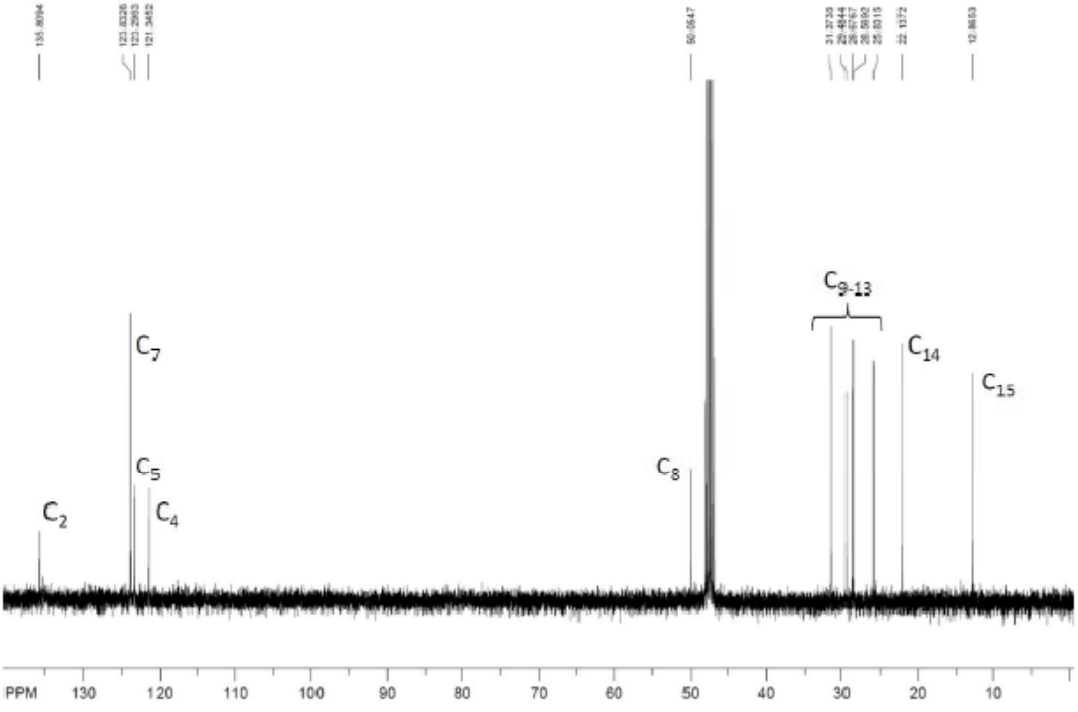

**Association constant for the formation of Diim$C_2$·CB[7] complex by UV titration:**

[I] is the concentration of free bisimidazolium dication

[C] is the concentration of free **CB[7]**

[I·C] is the concentration of 1:1 complex

$[I]_0$ is the initial concentration of bisimidazolium

$[C]_0$ is the initial concentration of **CB[7]**

$$I + C \rightleftharpoons I \cdot C \qquad K_{11} = \frac{[I \cdot C]}{[I][C]} \qquad (1)$$

$$[C]_0 = [C] + [I \cdot C] \qquad (2)$$

$$[I]_0 = [I] + [I \cdot C] \qquad (3)$$

By combining equations (1), (2) and (3), we get the following equation:

$$K_{11}[C]^2 + [C](1 + K_{11}[I]_0 - K_{11}[C]_0) - [C]_0 = 0 \qquad (4)$$

The use of Beer-Lambert law gives the absorbance in this solution:

$$\frac{A}{l} = \varepsilon_I[I] + \varepsilon_C[I] + \varepsilon_{IC}[I \cdot C] \qquad (5)$$

Since the **CB[7]** doesn't absorb at the wavelength where the complex is absorbing, its molar absorptivity is $\varepsilon_C = 0$.

With $$\Delta A = A - \varepsilon_I l[I]_0 \qquad (6)$$

And $$\Delta\varepsilon_{IC} = \varepsilon_{IC} - \varepsilon_I \qquad (7)$$

Equation (5) can be written as follows:

$$\frac{\Delta A}{l} = \Delta\varepsilon_{IC}[I \cdot C] = \Delta\varepsilon_{IC} K_{11}[I]_0 \frac{[C]}{1 + K_{11}[C]} \qquad (8)$$

Equation (4) can then be solved for each estimated value of $K_{11}$ (nonlinear regression algorithm) until the best fit to the experimental data is obtained.

The association constant $K_{11}$ was found to be 7.58 x $10^5$ $M^{-1}$ with an error of 10 %.

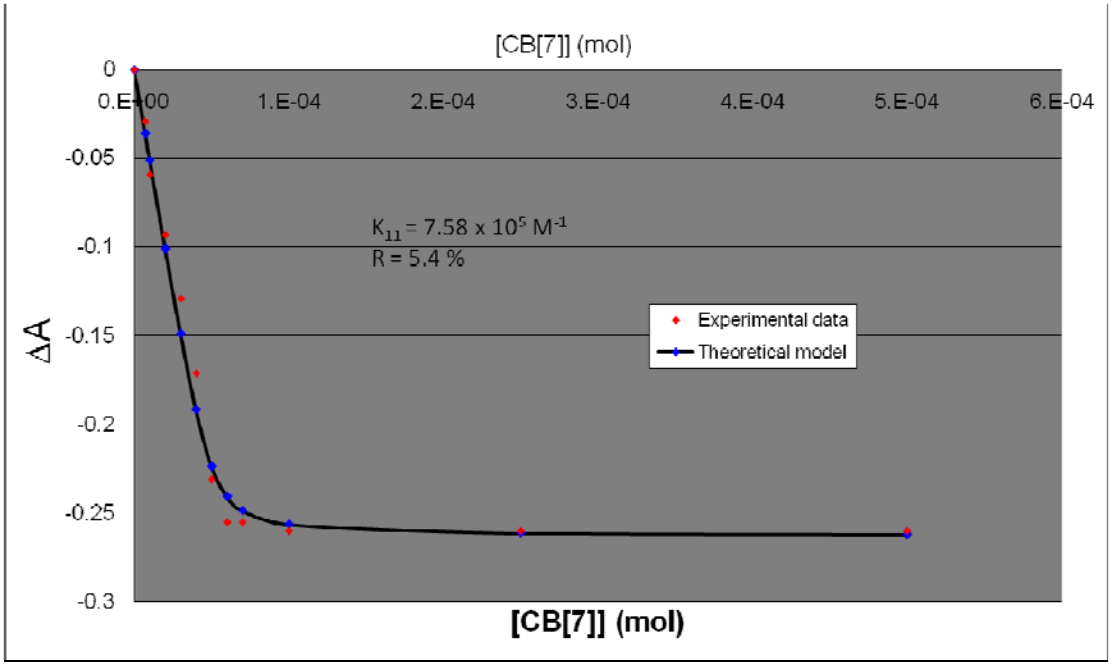


**Estimation of the association constants for the formation of complexes between DiimC$_3$ and CB[7] by UV titration:**

[I] is the concentration of free bisimidazolium

[C] is the concentration of free **CB[7]**

[I·C] is the concentration of the primary 1:1 complex

[I·C*] is the concentration of the secondary 1:1 complex

[I·$C_2$] is the concentration of the 1:2 complex

$[I]_0$ is the initial concentration of bisimidazolium

$[C]_0$ is the initial concentration of **CB[7]**

$K_{11}$ is kept constant to the previously obtained value on the **DiimC$_2$·CB[7]** complex

$$I + C \longleftrightarrow I \cdot C \qquad K_{11} = \frac{[I \cdot C]}{[I][C]} \qquad (1)$$

$$I \cdot C \longleftrightarrow I \cdot C^* \qquad K^* = \frac{[I \cdot C^*]}{[I \cdot C]} \qquad (2)$$

$$I \cdot C^* + C \longleftrightarrow I \cdot C_2 \qquad K_{12} = \frac{[I \cdot C_2]}{[I \cdot C^*][C]} \qquad (3)$$

$$[C]_0 = [C] + [I \cdot C] + [I \cdot C^*] + 2[I \cdot C_2] \qquad (4)$$

$$[I]_0 = [I] + [I \cdot C] + [I \cdot C^*] + [I \cdot C_2] \qquad (5)$$

By combining equations (1), (2), (3), (4) and (5), a third degree equation that can be numerically resolved for every estimate of the binding parameters K* and $K_{12}$ is obtained. The theoretical values of [C], [I·C], [I·C*] and [I·$C_2$] are obtained for each $[C]_0$ and the theoretical relative absorbance is plotted against the experimental plot.

Similarly to the **DiimC$_2$·CB[7]** complex, the relative UV-Vis absorbance can be derived:

$$\frac{\Delta A}{l} = \Delta\varepsilon_{IC}[I \cdot C] + \Delta\varepsilon_{IC^*}[I \cdot C^*] + \Delta\varepsilon_{IC2}[I \cdot C_2] \qquad (6)$$

With: $\Delta A = A - \varepsilon_I l[I]_0 \qquad (7)$

$$\Delta\varepsilon_{IC} = \varepsilon_{IC} - \varepsilon_I \qquad (8)$$

$$\Delta\varepsilon_{IC^*} = \varepsilon_{IC^*} - \varepsilon_I \qquad (9)$$

$$\Delta\varepsilon_{IC2} = \varepsilon_{IC2} - \varepsilon_I \qquad (10)$$

The quality of fit was estimated by using the "merit-function" shown in equation (11, see reference 22 in the manuscript) where *Wi* is the weight attributed to observation *i* (data points were assigned equal weights for this study):

$$R = 100\sqrt{\frac{\sum W_i(\Delta A_{obs} - \Delta A_{calc})^2}{\sum W_i(\Delta A_{obs})^2}} \qquad (11)$$

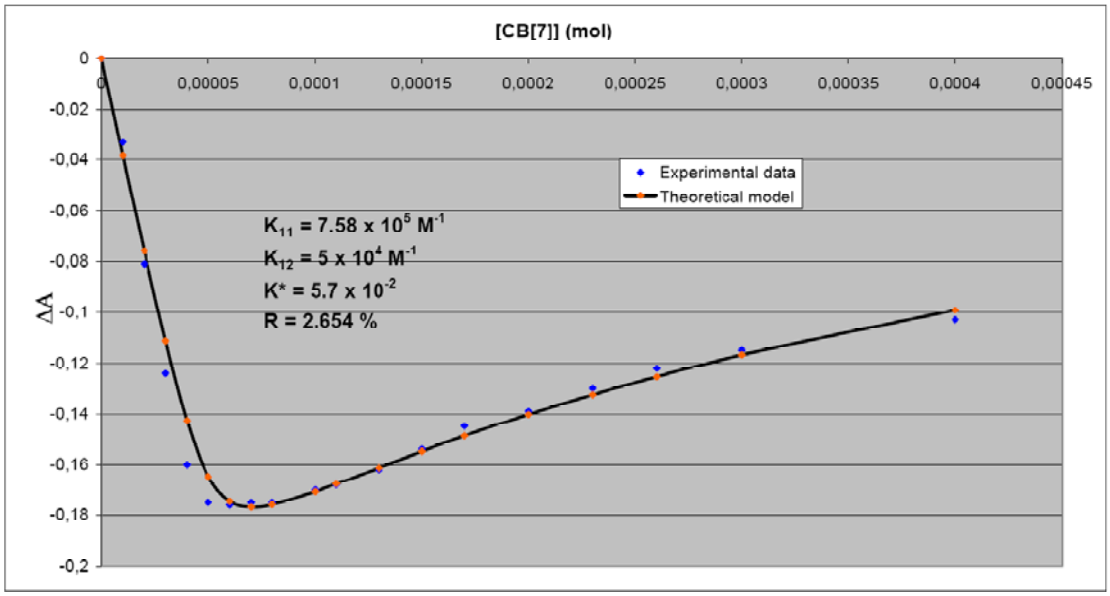


**Estimates of $K_{12}xK^*$ for $DiimC_4$, $DiimC_6$ and $DiimC_8$**

For these 3 guests, assuming a very high $K_{11}$ which we calculated to be $7.6x10^5$ $M^{-1}$, it is possible to extract the product $K_{12}xK^*$ by fitting the titration curve starting at 2 equivalents of CB[7] added. These values are only estimates to have a general trend and by no means actual measurements.

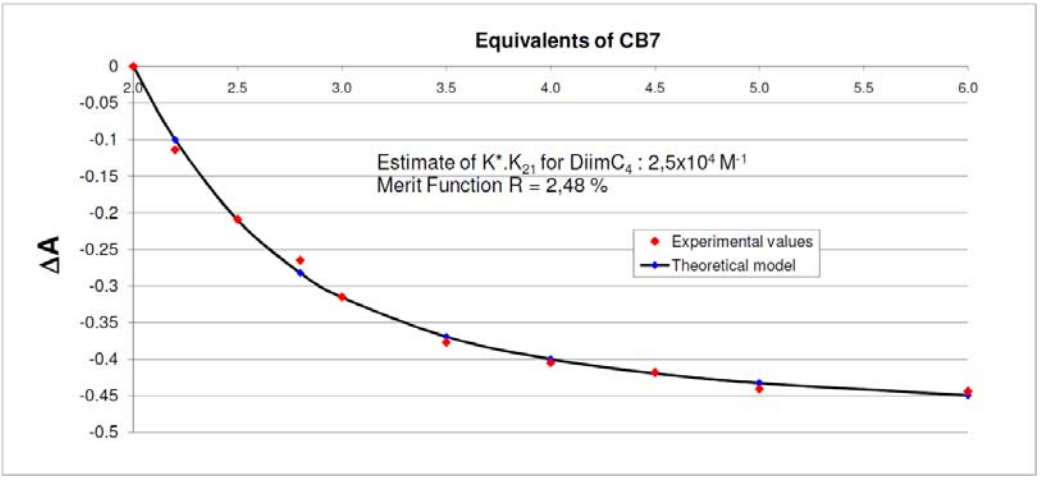

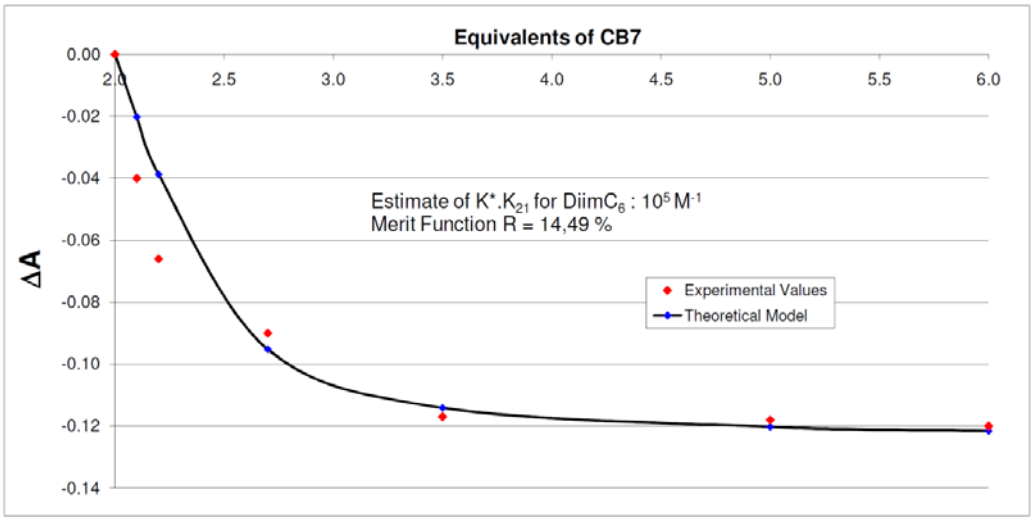
Equivalents of CB7
ΔA
Estimate of K*.K21 for DiimC6 : 10^5 M^-1
Merit Function R = 14,49 %
Experimental Values
Theoretical Model

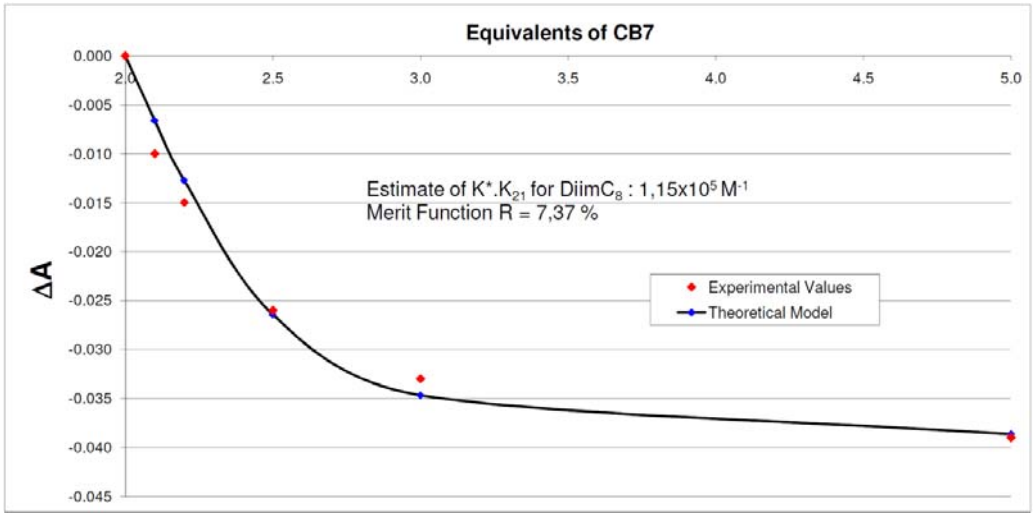
Equivalents of CB7
ΔA
Estimate of K*.K21 for DiimC8 : 1,15x10^5 M^-1
Merit Function R = 7,37 %
Experimental Values
Theoretical Model

## Mass Spectra of the observed complexes

### $DiimC_2$·CB[7]

$[M-2Br]^{2+}$ observed : $(C_{58}H_{62}N_{28}O_{14})^{2+}$

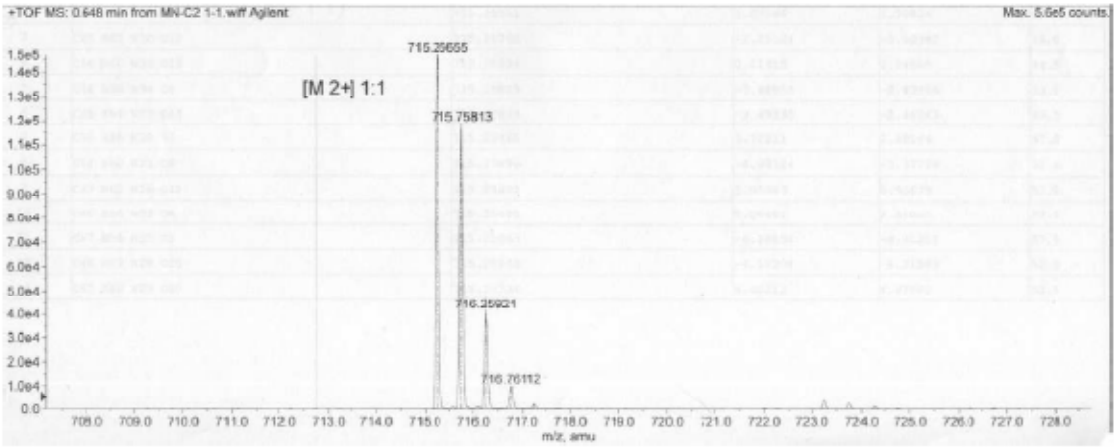


### $DiimC_3$·CB[7]

$[M-2Br]^{2+}$ observed : $(C_{60}H_{66}N_{32}O_{14})^{2+}$

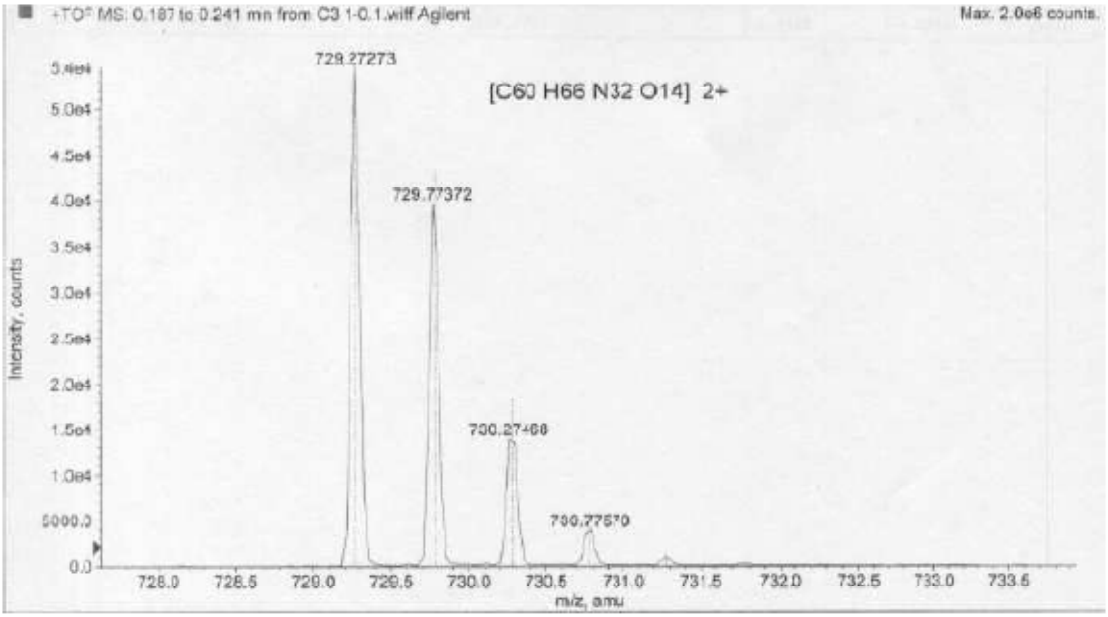

**DiimC$_3$·CB[7]$_2$**

$[M-2Br]^{2+}$ observed : $(C_{102}H_{108}N_{60}O_{28})^{2+}$

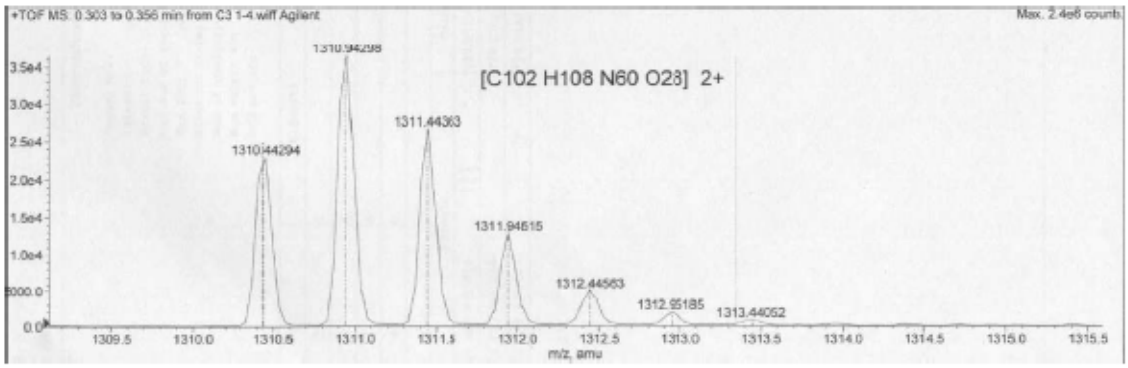


**(DiimC$_4$)$_2$·CB[7]**

$[M-2Br]^{2+}$ observed : $(C_{82}H_{98}Br_2N_{36}O_{14})^{2+}$

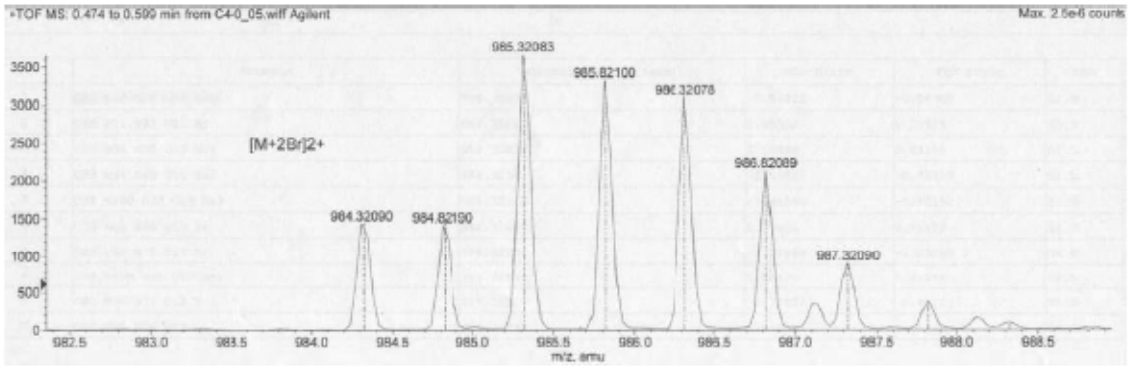


**DiimC$_4$·CB[7]**

$[M-2Br]^{2+}$ observed : $(C_{62}H_{70}N_{32}O_{14})^{2+}$

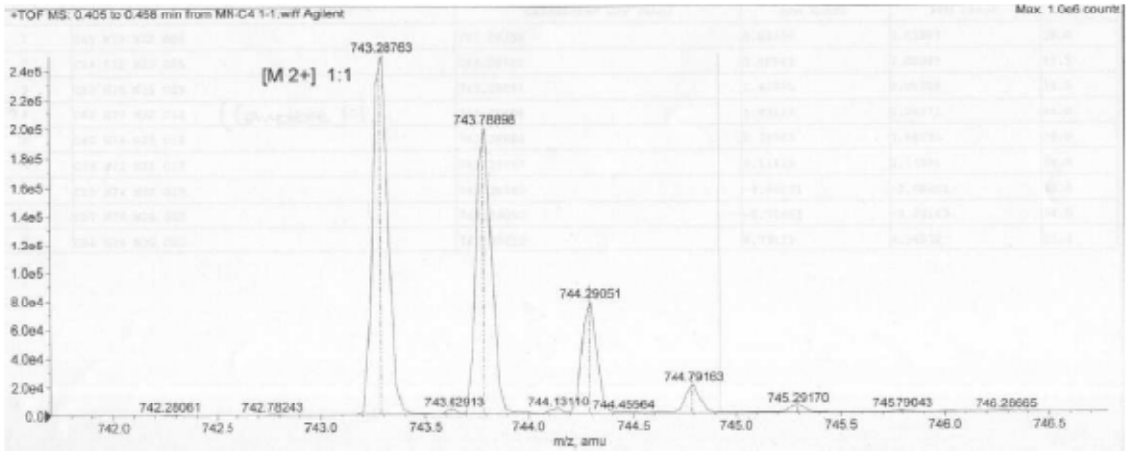

**$DiimC_4$·CB[7]$_2$**

$[M-2Br]^{2+}$ observed : $(C_{104}H_{112}N_{60}O_{28})^{2+}$

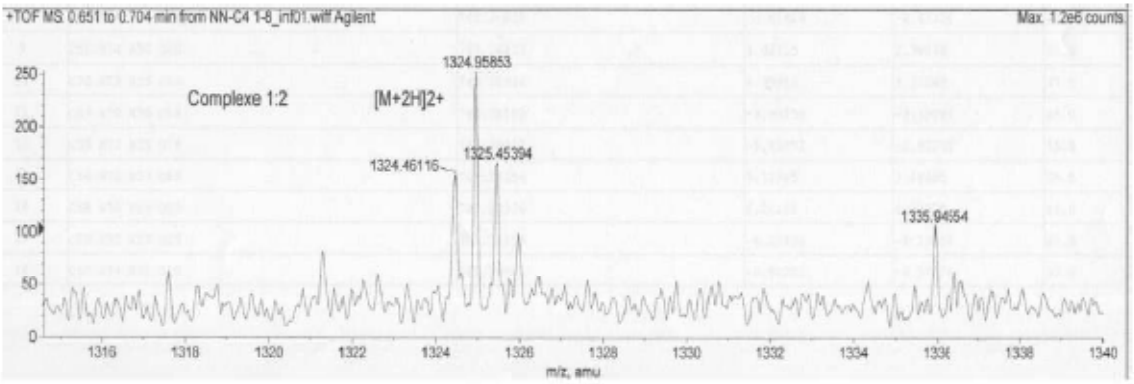


**$(DiimC_6)_2$·CB[7]**

$[M-2Br]^{2+}$ observed : $(C_{90}H_{114}Br_2N_{36}O_{14})^{2+}$

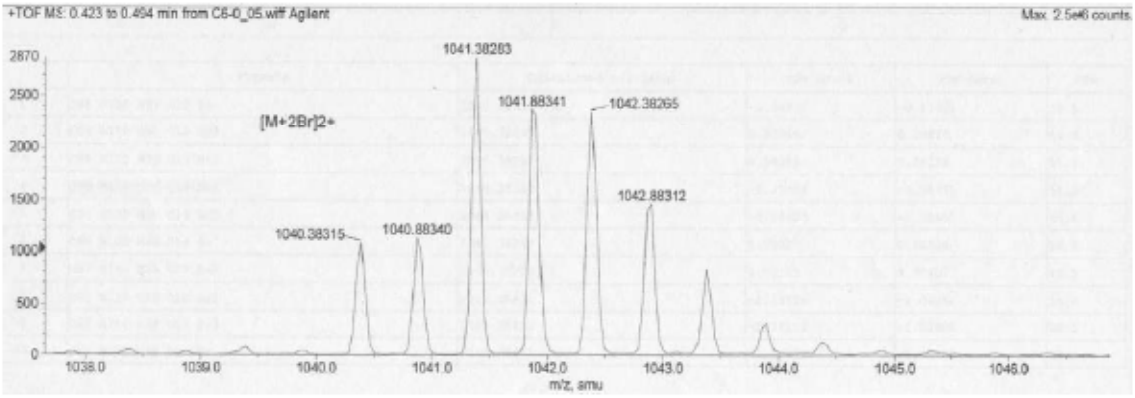


**$DiimC_6$·CB[7]$_2$**

$[M-2Br]^{2+}$ observed : $(C_{108}H_{120}N_{60}O_{28})^{2+}$

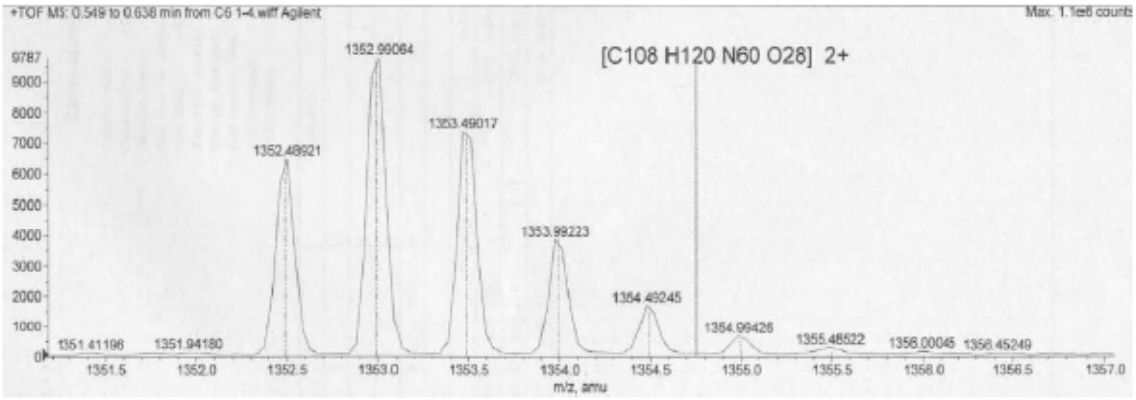

**DiimC$_6$·CB[7]**

[M 2Br]$^{2+}$ observed : $(C_{66}H_{78}N_{32}O_{14})^{2+}$

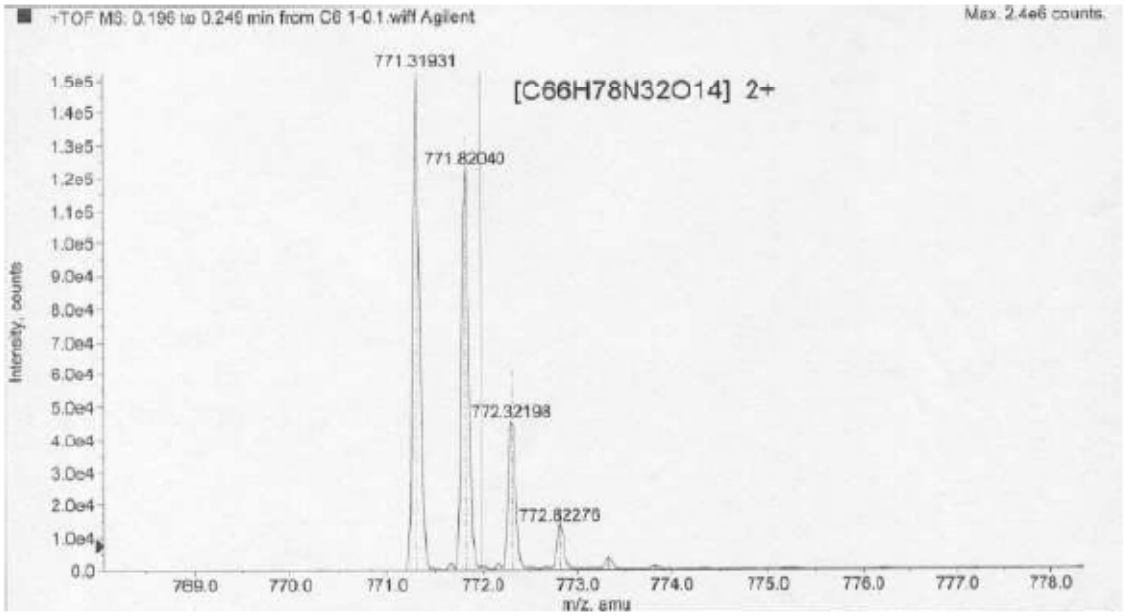


**DiimC$_8$·CB[7]**

[M-2Br]$^{2+}$ observed : $(C_{70}H_{86}N_{32}O_{14})^{2+}$

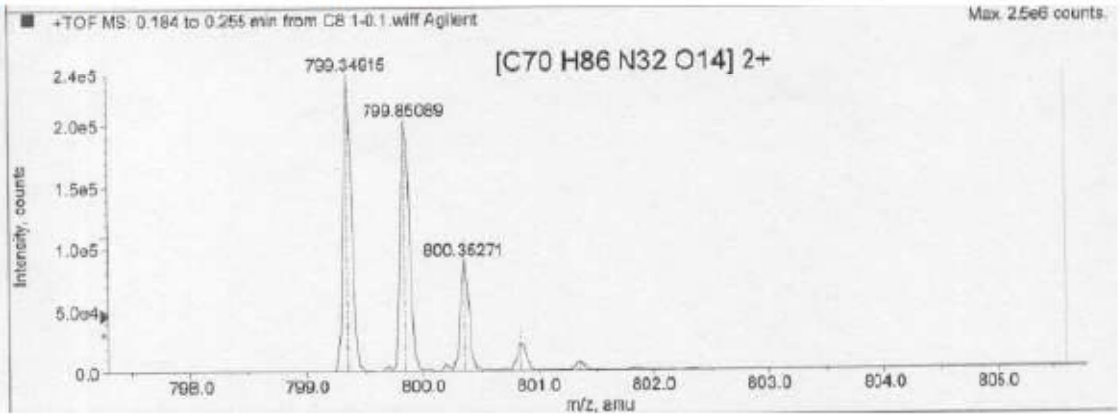

**$(DiimC_8)_2$·CB[7]**

$[M-4Br-2H]^{2+}$ observed : $(C_{98}H_{128}N_{36}O_{14})^{2+}$

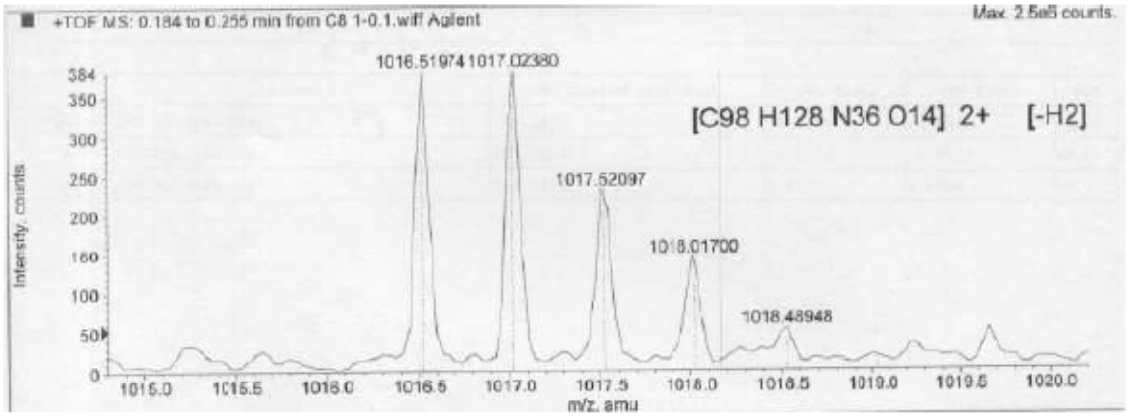


**$DiimC_8$·CB[7]$_2$**

$[M-2Br]^{2+}$ observed : $(C_{112}H_{128}N_{60}O_{28})^{2+}$

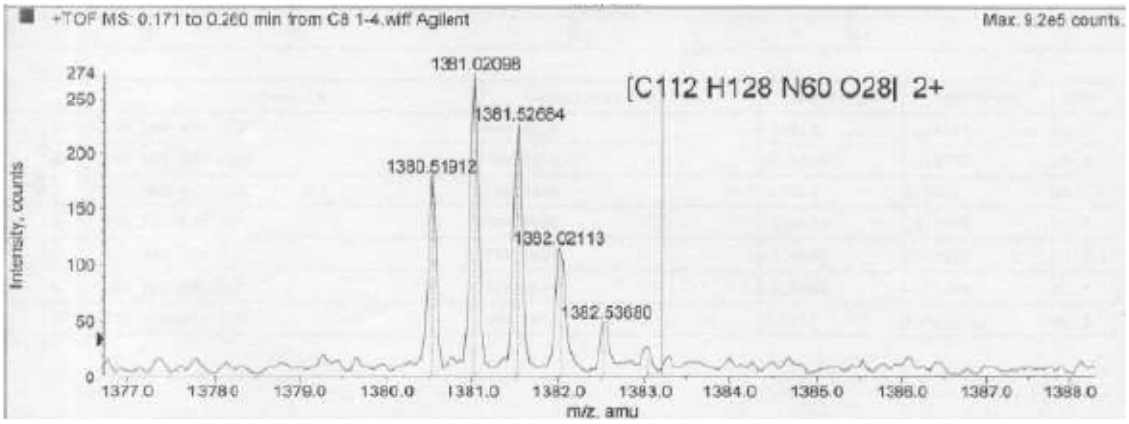

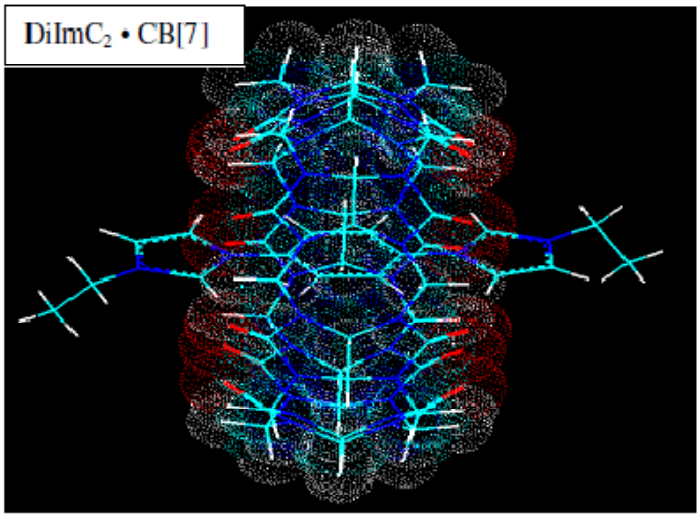
DiImC2 • CB[7]

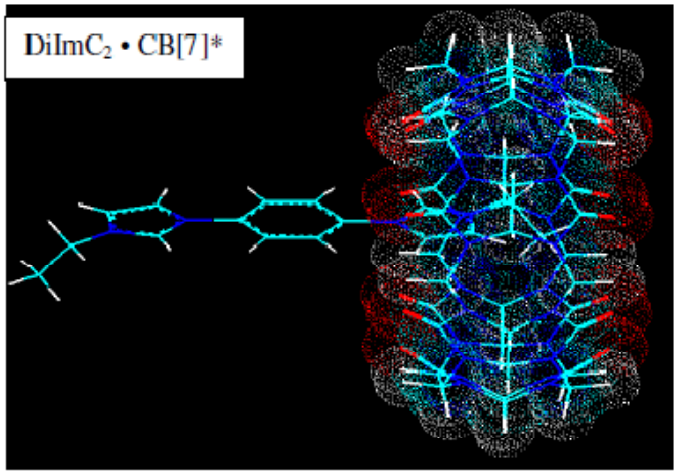
DiImC2 • CB[7]*

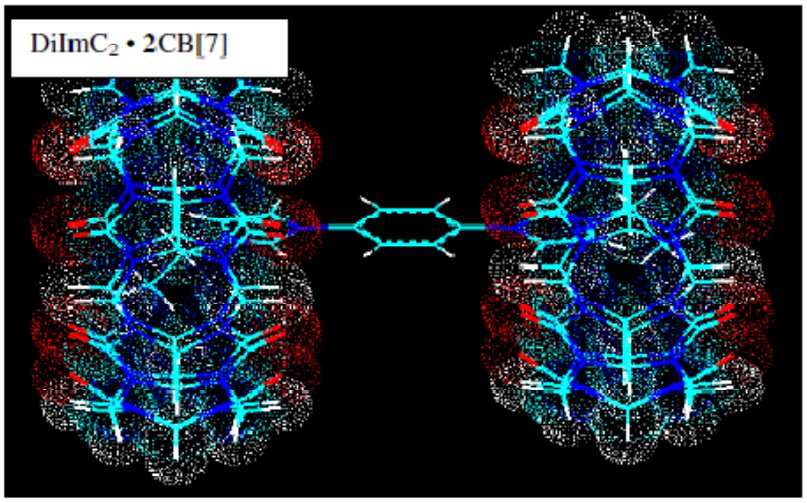
DiImC2 • 2CB[7]

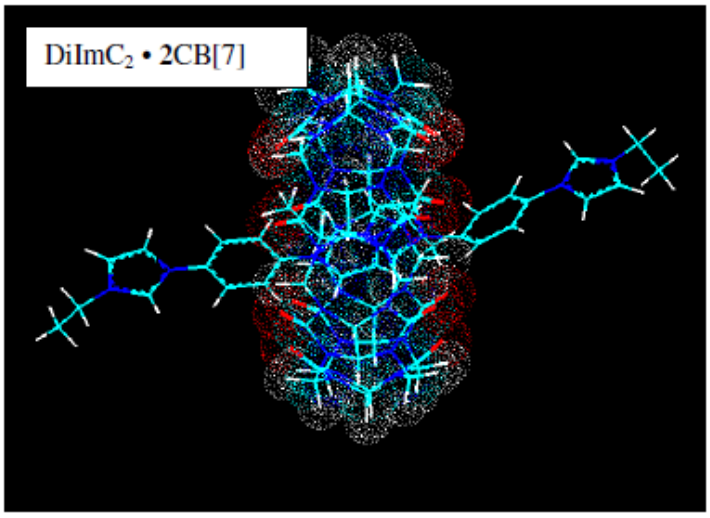


$DiImC_2$: -61.24 kcal·mol$^{-1}$

CB[7] : -251.41 kcal·mol$^{-1}$

$DiImC_2$ • CB[7] : -342.4 kcal·mol$^{-1}$

$DiImC_2$ • CB[7] *: -312.37 kcal·mol$^{-1}$

$DiImC_2$ • **2** CB[7] : -555.1 kcal·mol$^{-1}$

**2**$DiImC_2$ • CB[7] : -371.81 kcal·mol$^{-1}$

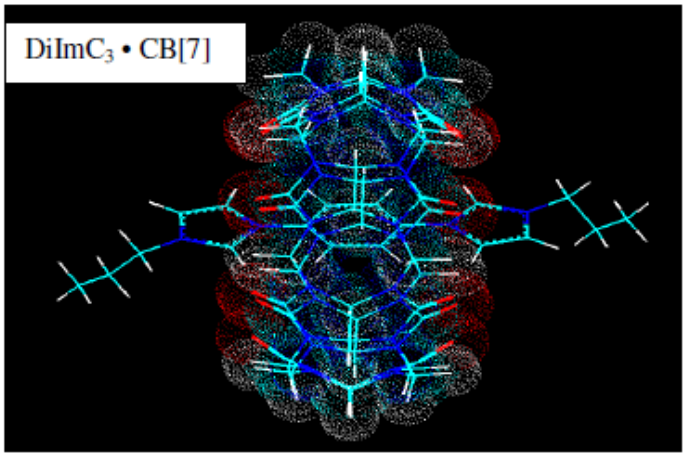

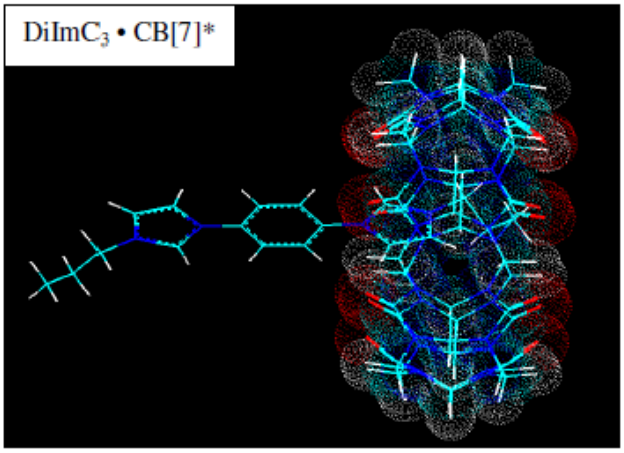


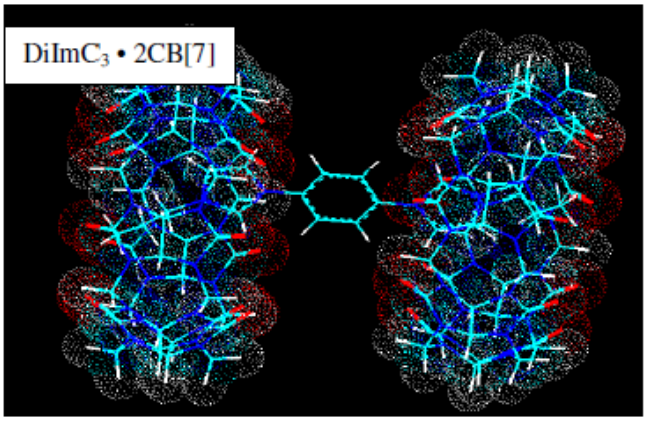


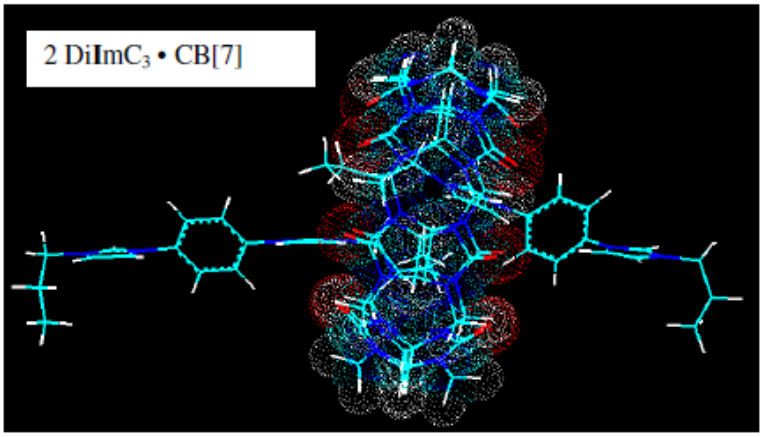


DiImC3: - 63.70 kcal·mol$^{-1}$

DiImC3 • CB[7] : -345.25 kcal·mol$^{-1}$

DiImC3 • CB[7] *: -331.62 kcal·mol$^{-1}$

DiImC3 • **2** CB[7] : -571.08 kcal·mol$^{-1}$

**2**DiImC3 • CB[7] : -376.45 kcal·mol$^{-1}$

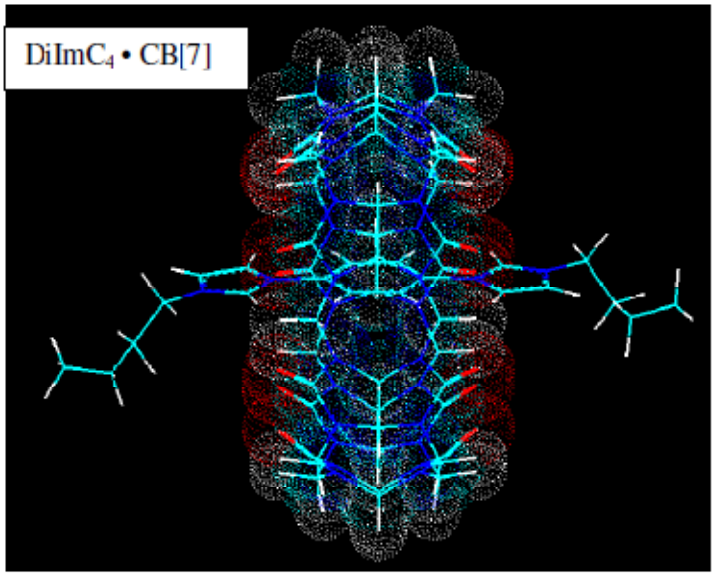
DiImC4 • CB[7]

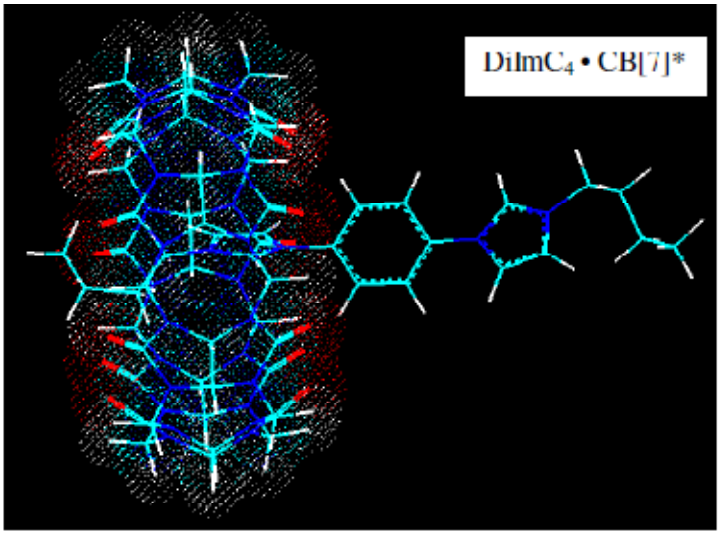
DiImC4 • CB[7]*

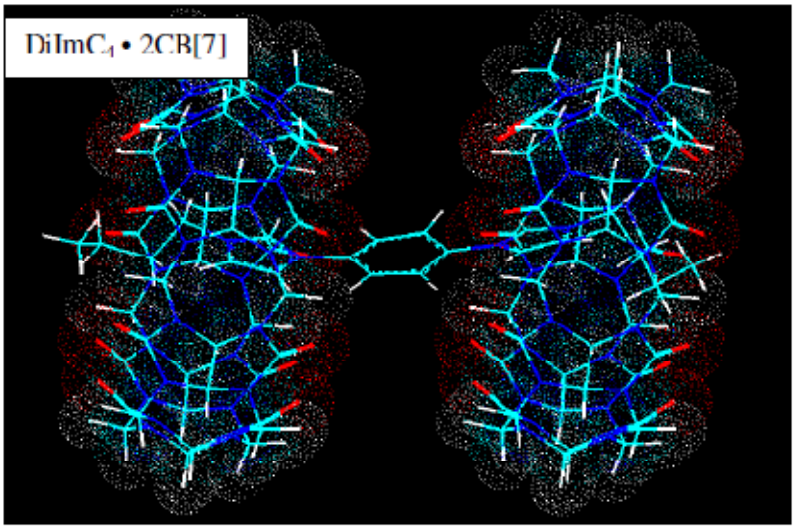
DiImC4 • 2CB[7]

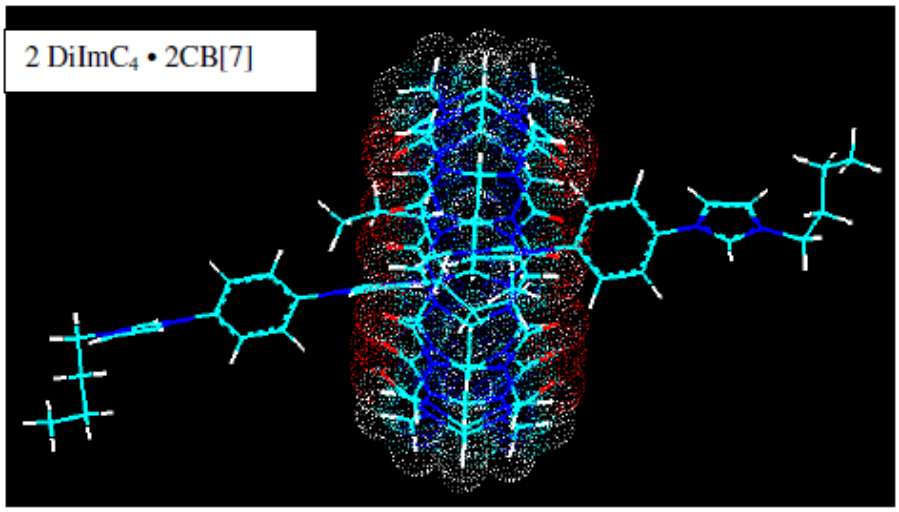


DiImC4: -68.54 kcal·mol$^{-1}$

DiImC4 • CB[7] : -345.12 kcal·mol$^{-1}$

DiImC4 • CB[7] *: -342.07 kcal·mol$^{-1}$

DiImC4 • **2** CB[7] : -624.91 kcal·mol$^{-1}$

**2**DiImC4 • CB[7] : -597.82 kcal·mol$^{-1}$

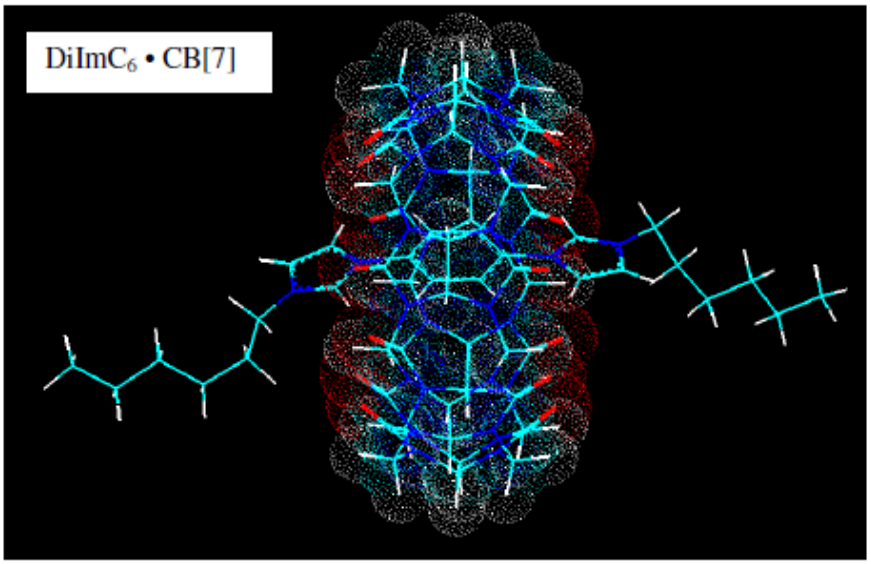

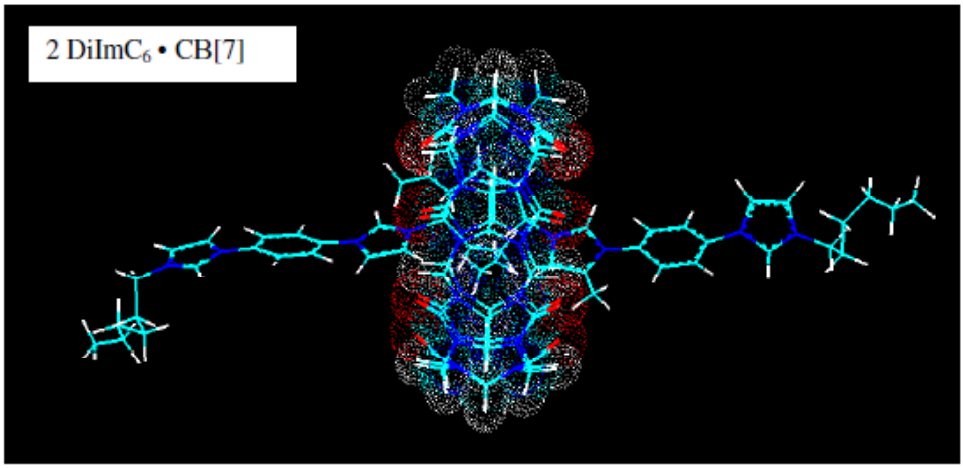
2 DiImC6 • CB[7]

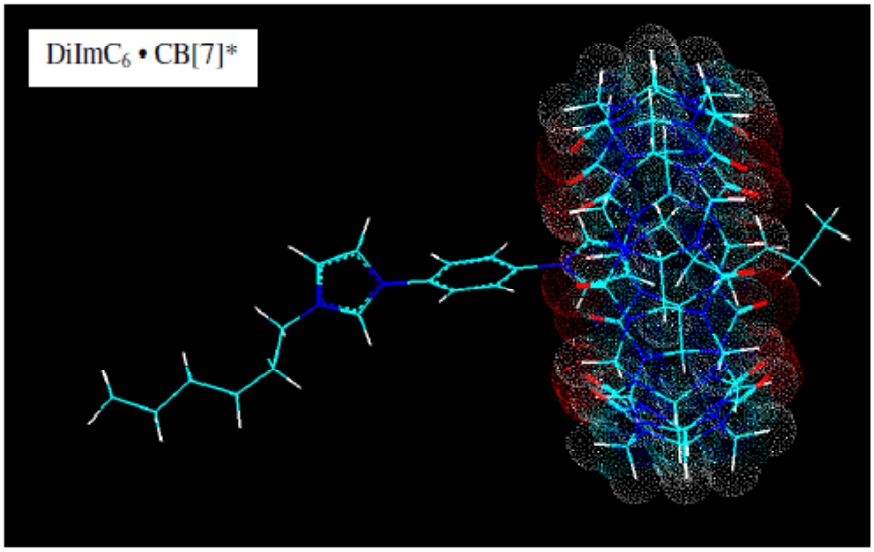
DiImC6 • CB[7]*

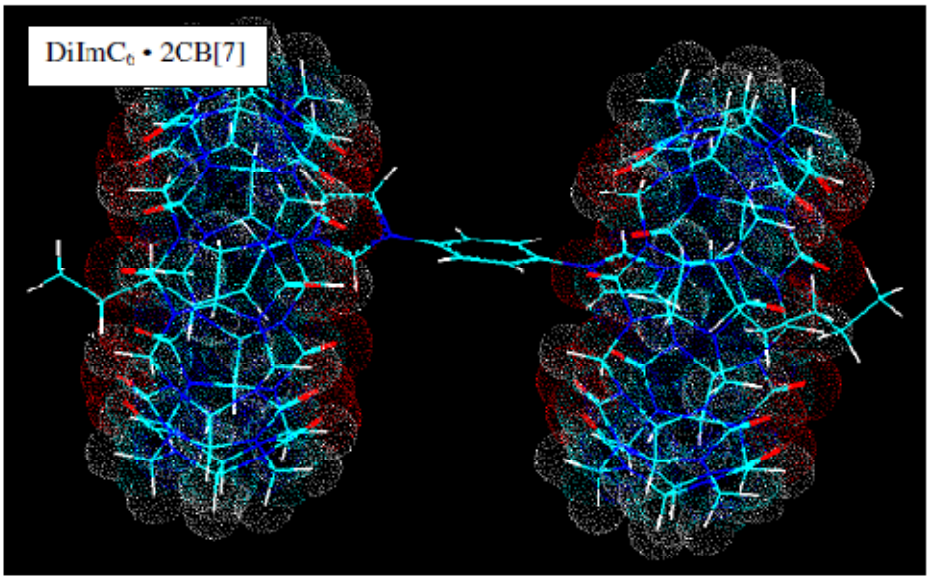


DiImC6: -73.82 kcal·mol-1

DiImC6 • CB[7] : 352.23 kcal·mol 1

DiImC6 • CB[7] *: -357.67 kcal·mol-1

DiImC6 • 2 CB[7] : -604.58 kcal·mol-1

2DiImC6 • CB[7] : -453.22 kcal·mol-1

# Annexe 4 : « Supporting information » de l'article 4 : Aromatic stacking: A new toolkit to obtain molecular channels with *N,N'*-diaromatic diimidazolium cations

**Materials and general methods**

$D_2O$ (99.95 % isotopic purity) and all other chemicals were purchased from Aldrich and used without further purification. All reactions were carried out in oven-dried glassware under nitrogen, using standard Schlenk and vacuum line techniques. "Distilled" solvents were obtained using a GlassContour system (Irvine, CA). NMR experiments were recorded on Advance 300 or 400 Brucker spectrometer (300 MHz or 400 MHz) with the samples nonspinning. Chemical shifts are given in ppm (δ) and measured relative to the HOD signal. ESI/HR-MS mass spectra were recorded with a Mass spectrometer TSQ Quantum Ultra (Thermo Scientific) with accurate mass options instrument (Université de Montréal Mass Spectrometry Facility). Calculations were performed on a Linux workstation with Ghemical 2.95 software that allows running MOPAC7. The initial configurations of diimidazolium cations have been obtained from AM1 semi empirical calculations in gas phase. For studying molecular structures and their energies in detail, we have calculated plots that show how energy is dependent on torsion angles. We get 2D plot depending on the both torsion angles studied.

**Synthesis**

The *N,N'*-disubstituted methylenediimidazolium salts were obtained by a double $S_N2$ reaction involving *N*-substituted imidazoles and dibromomethane. The methodology is already reported see: Noujeim, N.; Leclercq, L.; Schmitzer, A. R. *J. Org. Chem.* **2008**, *73*, 3784-3790.

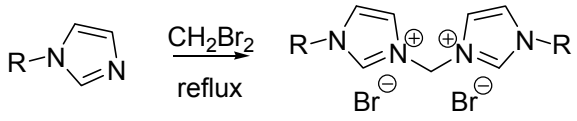


**R = Ph : $[PM][Br]_2$ ; 54 %**
**R = Bn : $[BM][Br]_2$ ; 78 %**

**1,1'-Diphenyl-3,3'-methylenediimidazolium bis(bromide) $[PM][Br]_2$**: $^1H$ NMR ($D_2O$, 400 MHz): δ (ppm) 8,02 (m, 4H), 7.64-7.70 (m, 10H), 6.96 (s, 2H). $^{13}C$ NMR ($D_2O$, 75

MHz): δ (ppm) 135.0, 131.6, 131.2, 124.2, 123.5, 123.5, 123.3, 60.3. HR-MS *m/z* found: 301.1439 $(M-H)^+$, calc: 301.1453. m.p. 270-272°C. (Yield 54%).

**1,1'-Dibenzyl-3,3'-methylenediimidazolium bis(bromide) [BM][Br]$_2$**: $^1$H NMR ($D_2O$, 400 MHz): δ (ppm) 7.79 (d, 2H, J = 2.2 Hz), 7.61 (d, 2H, J = 2.2 Hz), 7.46-7.47 (m, 10H), 6.67 (s, 2H), 5.44 (s, 4H). $^{13}$C NMR ($D_20$, 75 MHz): δ (ppm) 137.7, 133.4, 130.5, 130.3, 129.9, 124.6, 123.1, 59.8, 54.4. HR-MS *m/z* found: 329.1762 $(M-H)^+$, calc: 329.1766. m.p. 278-280 °C (Yield 78%).

A solution of phenylimidazole (500 mg, 3.47 mmol, 2 eq.) and α,α'-dibromo-*p*-xylene (458 mg, 1.73 mmol, 1 eq) in dry toluene (10 mL) is refluxed for 24 hours. After filtration, the white residue is washed with hexane (3 × 10 mL) and dried under vacuum. The 1,1'-diphenyl-3,3'-benzylenediimidazolium bis(bromide) (851 mg, 89 %) is obtained as a white powder. For the synthesis of 1,1'-dibenzyl-3,3'-benzylenediimidazolium bis(bromide) the same methodology is used with benzylimidazole as precursor.

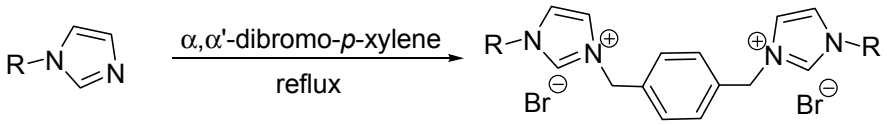


**R = Ph : [PB][Br]$_2$ ; 89 %**
**R = Bn : [BB][Br]$_2$ ; 86 %**

**1,1'-Diphenyl-3,3'-benzylenediimidazolium bis(bromide) [PB][Br]$_2$**: $^1$H NMR ($D_2O$, 400 MHz): δ (ppm) 9.78 (s, 0.1H/1.9D), 8.13 (d, 2H) 7.87 (d, 2H) 7.75-7.78 (m, 4H), 7.60-7.70 (m, 10H), 5.62 (s, 4H). $^{13}$C NMR (Acétone, 75 MHz): δ (ppm) 134.6, 134.5, 129.8, 129,7, 129.1, 122.7, 121.6, 52.2. HR-MS *m/z* found: 196.1003 $(M)^{2+}$, calc: 196.0995. m.p. > 350°C. (Yield 89%).

**1,1'-Dibenzyl-3,3'-benzylenediimidazolium bis(bromide) [BB][Br]$_2$**: $^1$H NMR ($D_2O$, 400 MHz): δ (ppm) 8.86 (s, 0.5H/1.5D), 7.44-7.51 (m, 9H), 7.41-7.44 (s, 4H), 7.34-7.41 (m, 5H), 5.40 (s, 4H), 5.38 (s, 4H). $^{13}$C NMR ($D_2O$, 75 MHz): δ (ppm) 137.6, 133.8, 130.2,

129.8, 129,6, 129.1, 128.1, 123.4, 122.5, 54.0, 51.0. HR-MS *m/z* found: 211.1522 $(M)^{2+}$, calc: 211.1235. m.p. 232°C (Yield 86%).

**Crystallization and X-ray diffraction**

All the crystallizations are performed in an open flask by dissolving the diimidazolium cation (33 wt.%) in 10 mL of hot water. After a week at room temperature, single crystals suitable for X-ray diffraction were obtained. All X-ray data were collected at $T = 150$ K and the structures were solved by the direct method with ShelxS-97. All non-H atoms were refined by full-matrix least-squares with anisotropic displacement parameters while hydrogen atoms were placed in idealized position. Hydrogen atoms from the water molecules were initially located from a difference Fourier map, then their locations were adjusted using restrains at idealized distances (0.84 Å) and angles (104.5°) in the direction of the hydrogen bonding acceptors, i.e. bromide anions.

X-ray crystallographic data for **[PB][Br]$_2$**, **[BM][Br]$_2$** and **[BB][Br]$_2$**, were collected from a single crystal sample, which was mounted on a loop fiber. Data were collected using a Bruker microstar diffractometer equipped with a Platinum 135 CCD Detector, Helios optics and Kappa goniometer. The crystal-to-detector distance was 4.0 cm, and the data collection was carried out in 512 × 512 pixel mode. The initial unit cell parameters were determined by a least-squares fit of the angular setting of strong reflections, collected by a 10.0° scan in 33 frames over three different parts of the reciprocal space (99 frames total). One complete sphere of data was collected.

X-ray crystallographic data for **[PM][Br]$_2$** were collected from a single crystal sample, which was mounted on a loop fiber. Data were collected using a Bruker Platform diffractometer, equipped with a Bruker SMART 4K Charged-Coupled Device (CCD) Area Detector using the program APEX II and a Nonius FR591 rotating anode equipped with Montel 200 optics. The crystal-to-detector distance was 5.0 cm, and the data collection was carried out in 512 × 512 pixel mode. The initial unit cell parameters were determined by the same procedure (see above). One complete sphere of data was collected, to better than 0.80 Å resolution.

In each case, the refinement was on $F^2$ using all reflections. The weighted *R*-factor (w*R*) and goodness-of-fit *S* are based on $F^2$, conventional *R*-factors (*R*) are based on *F*, with *F* set to zero for negative $F^2$. The threshold expression of $F^2 > 2\sigma(F^2)$ is used only for calculating *R*-factors (gt) etc. and is not relevant to the choice of reflections for refinement. All esds (except the eds in the dihedral angle between two l.s. planes) are estimated using the full covariance matrix.

# Annexe 5 : « Supporting information » de l'article 5 : Dialkyl(1,4-phenylene)diimidazolium salts: a new class of ionic liquid crystals

**Experimental details**

All commercially available chemicals were used without further purification. NMR experiments were done either on a Brüker Avance AV400 operating at 400 MHz for $^{1}H$ NMR experiments and at 100 MHz for $^{13}C$ NMR experiments or on a Brüker Avance AV300 operating at 75 MHz for $^{13}C$ NMR experiments. ESI mass spectra were recorded with a TSQ Quantum Ultra (Thermo Scientific) Mass Spectrometer with accurate mass options instrument (Université de Montréal Mass Spectrometry Facility). DSC analyses were carried out on a Q2000 TA instruments. XRD studies were carried out on a Brüker D8 Discover, equipped with a Hi-Star detector. XRD data was collected using GADDS 4.1.1.4 software and EVA 8.0.0.2 was used for data analysis. A custom made XYZ stage with a temperature control chamber and a Cu source ($K_{\alpha}$ energy of 8.04 KeV and $\lambda$ = 1.541838 Å) were used.

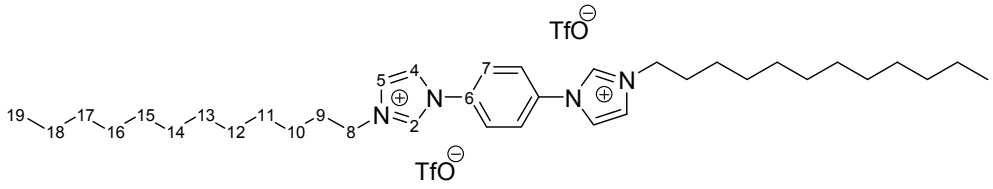
TfO⊖
TfO⊖

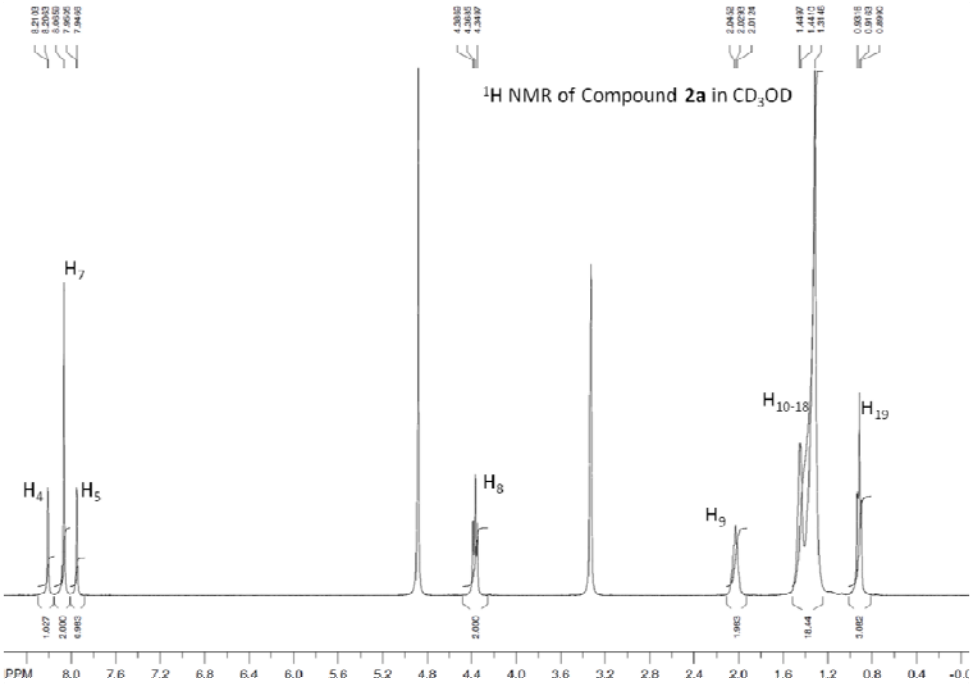
¹H NMR of Compound 2a in CD3OD
H7
H4
H5
H8
H9
H10-18
H19
PPM

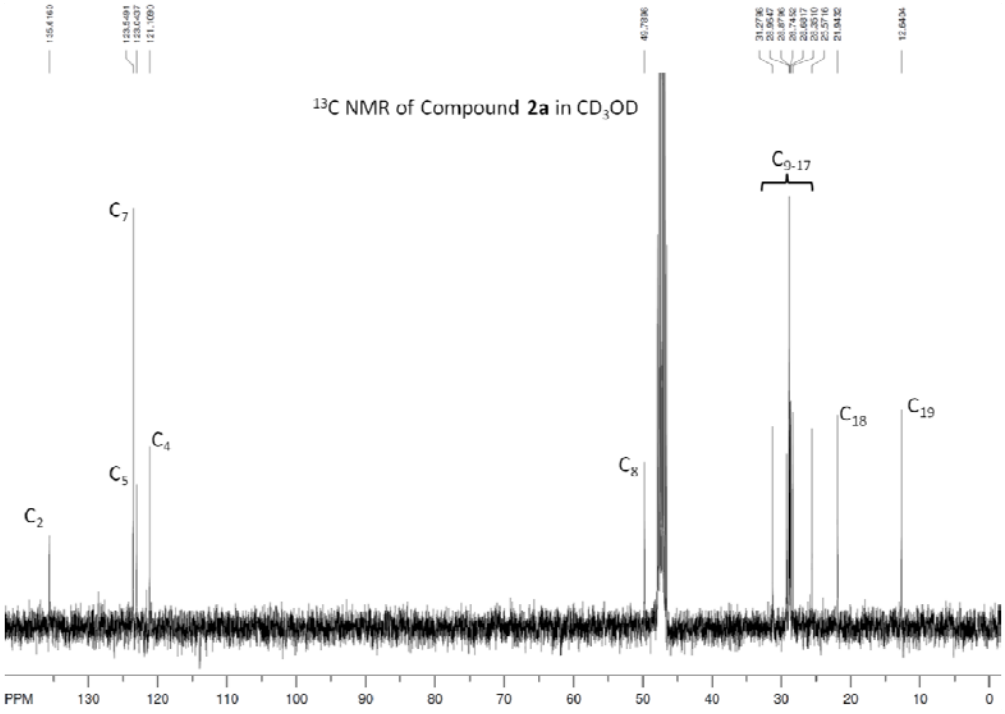
¹³C NMR of Compound 2a in CD3OD
C0-17
C7
C4
C5
C2
C8
C18
C19
PPM

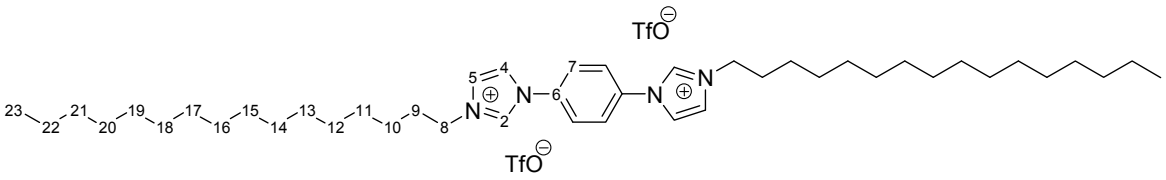
TfO
TfO
N
N
N
N
1
2
4
5
6
7
8
9
10
11
12
13
14
15
16
17
18
19
20
21
22
23

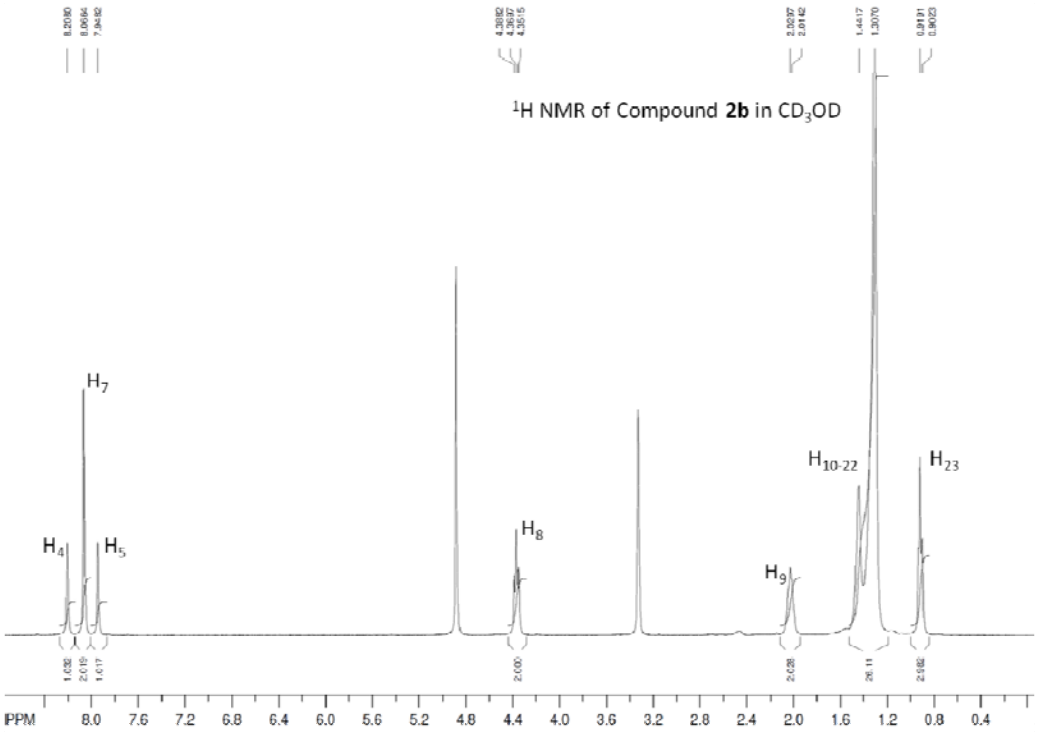
$^1$H NMR of Compound **2b** in $CD_3OD$
$H_4$
$H_7$
$H_5$
$H_8$
$H_9$
$H_{10-22}$
$H_{23}$
PPM
8.0
7.6
7.2
6.8
6.4
6.0
5.6
5.2
4.8
4.4
4.0
3.6
3.2
2.8
2.4
2.0
1.6
1.2
0.8
0.4

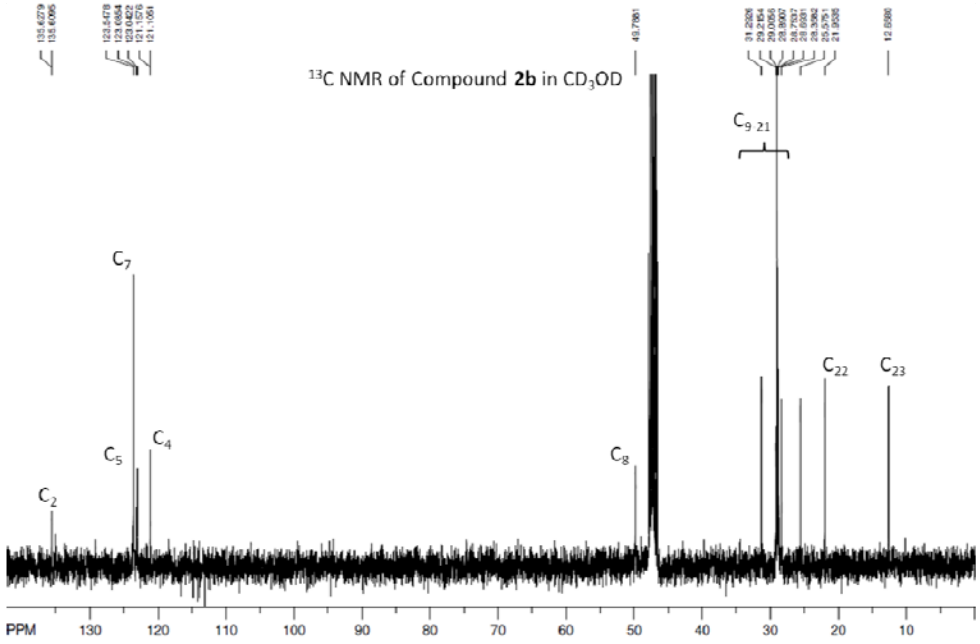
$^{13}$C NMR of Compound **2b** in $CD_3OD$
$C_{9\ 21}$
$C_7$
$C_5$
$C_4$
$C_2$
$C_8$
$C_{22}$
$C_{23}$
PPM
130
120
110
100
90
80
70
60
50
40
30
20
10

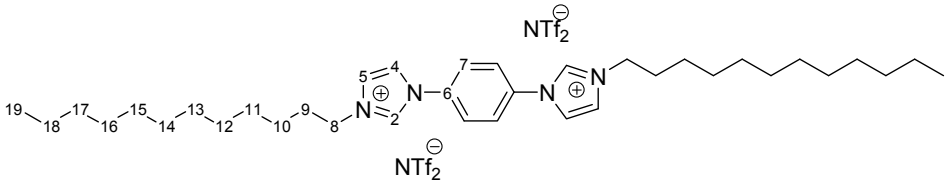
NTf2
NTf2

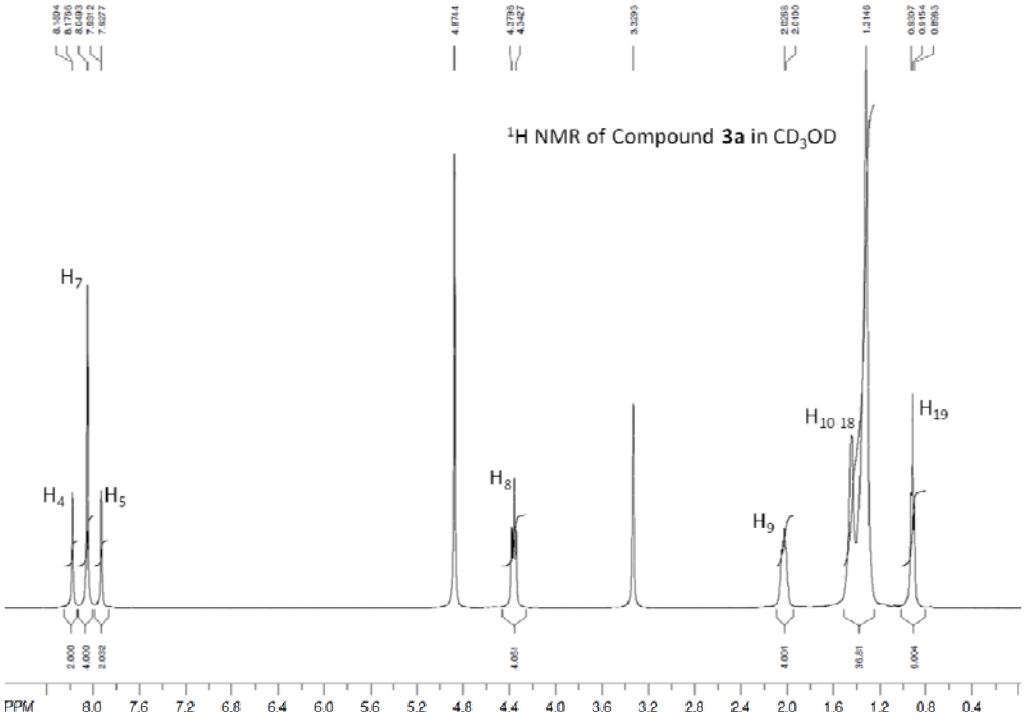
1H NMR of Compound 3a in CD3OD
H7
H4
H5
H8
H9
H10 18
H19
PPM

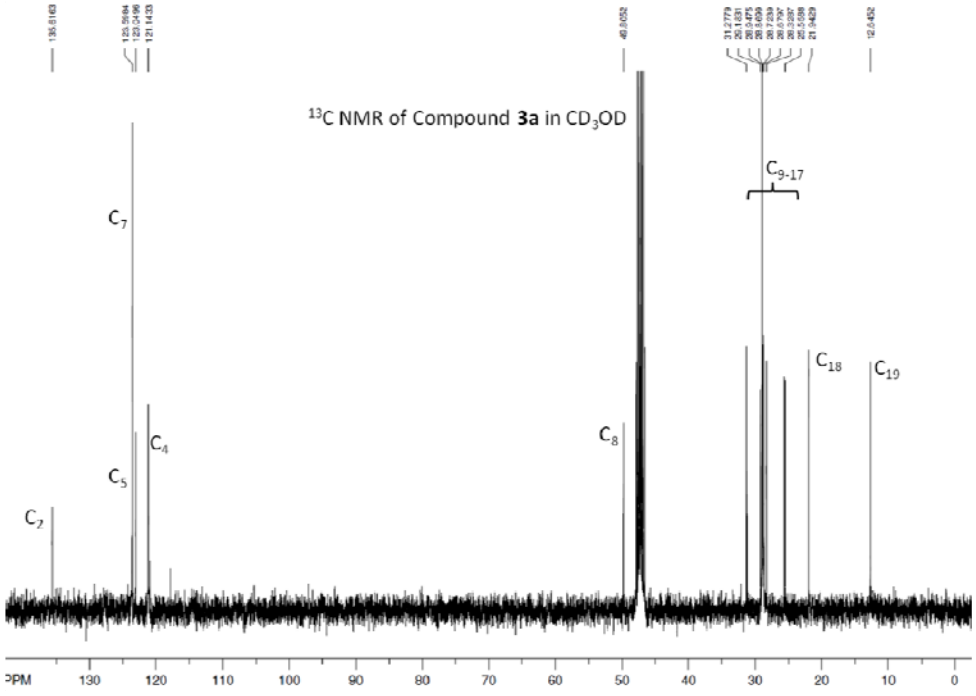
13C NMR of Compound 3a in CD3OD
C9-17
C7
C5
C4
C7
C8
C18
C19
PPM

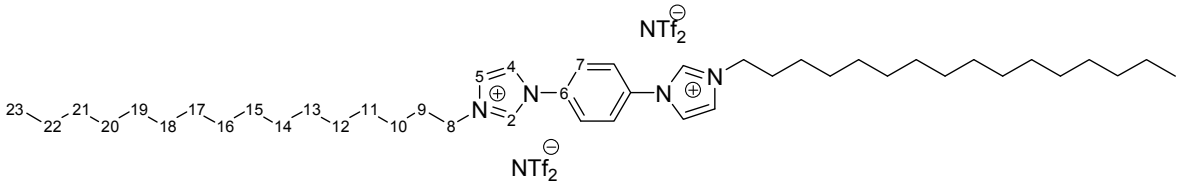
NTf2
NTf2

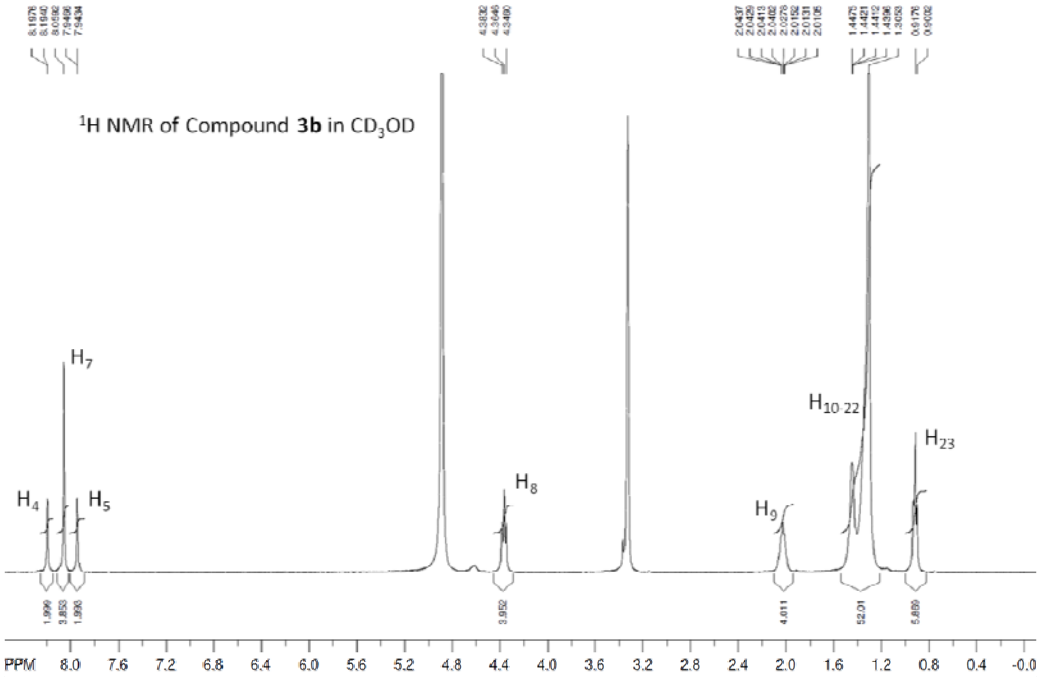
1H NMR of Compound 3b in CD3OD
H7
H4
H5
H8
H9
H10-22
H23
PPM

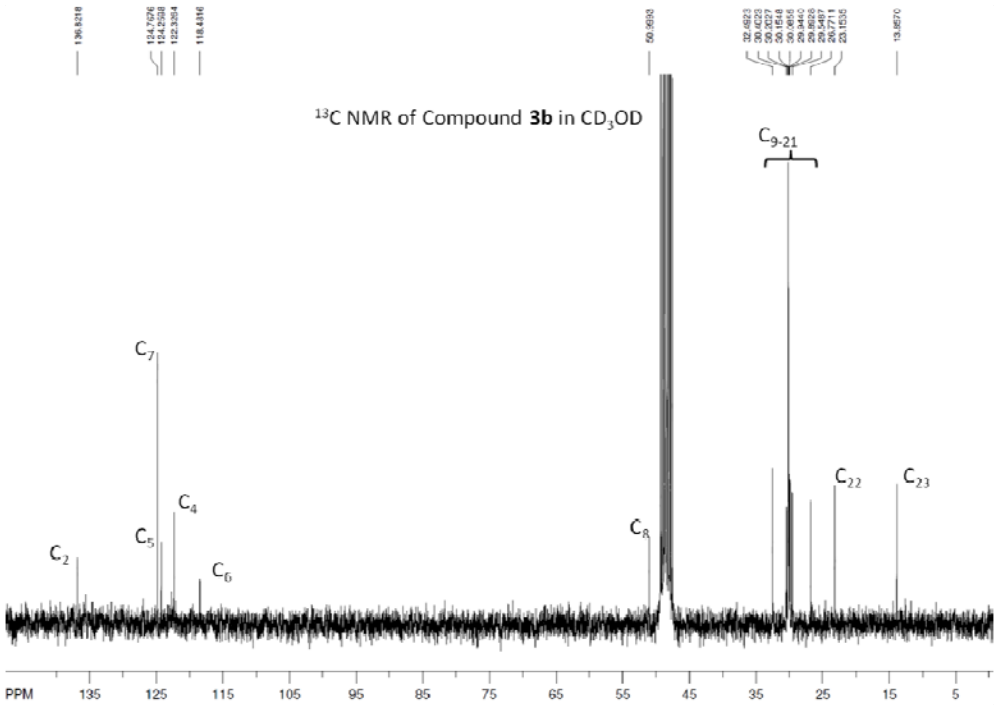
13C NMR of Compound 3b in CD3OD
C9-21
C7
C4
C5
C2
C6
C8
C22
C23
PPM

DSC of compound **2a:**

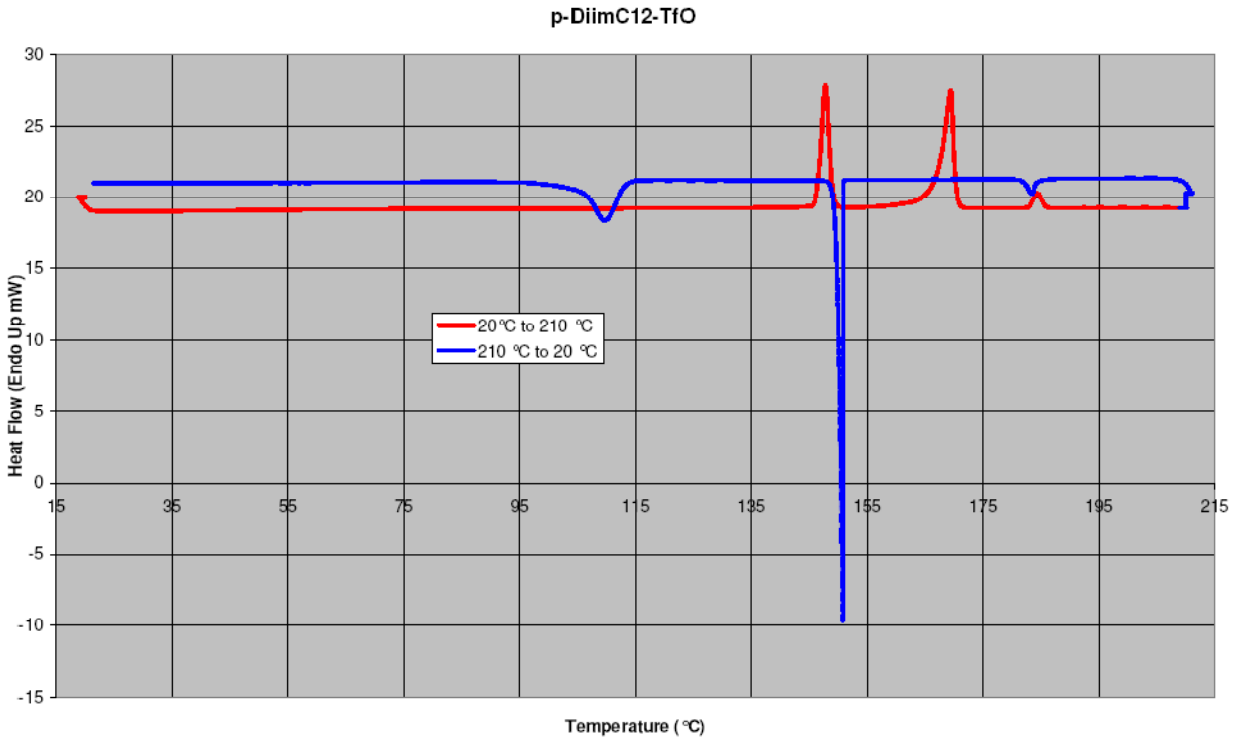


DSC of compound **2b:**

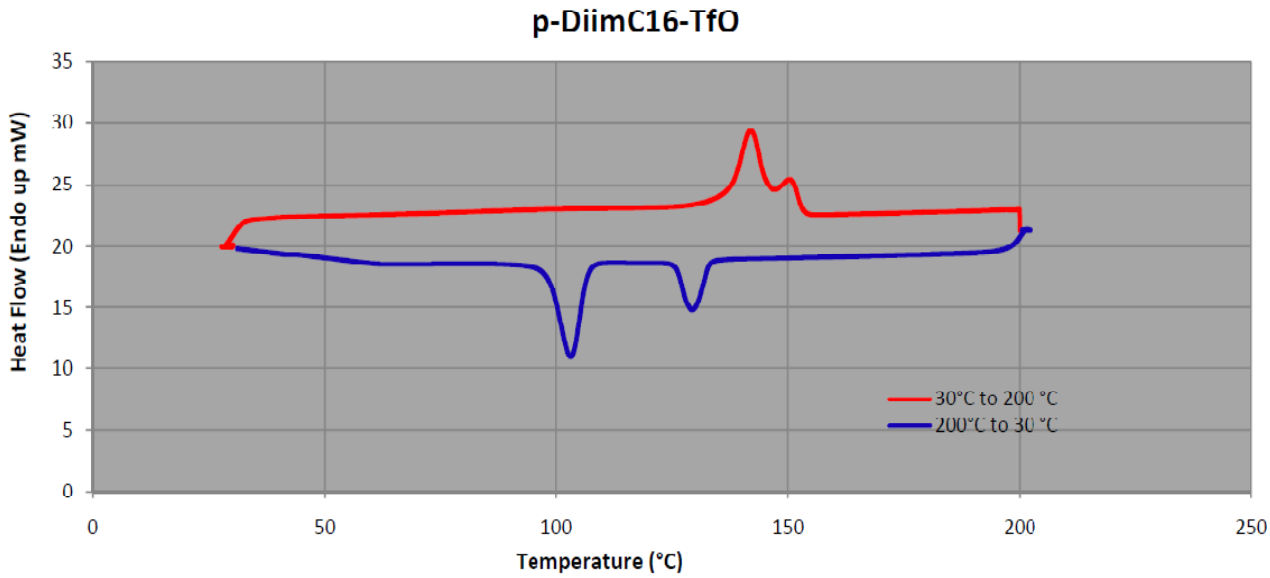

DSC of compound **3a:**

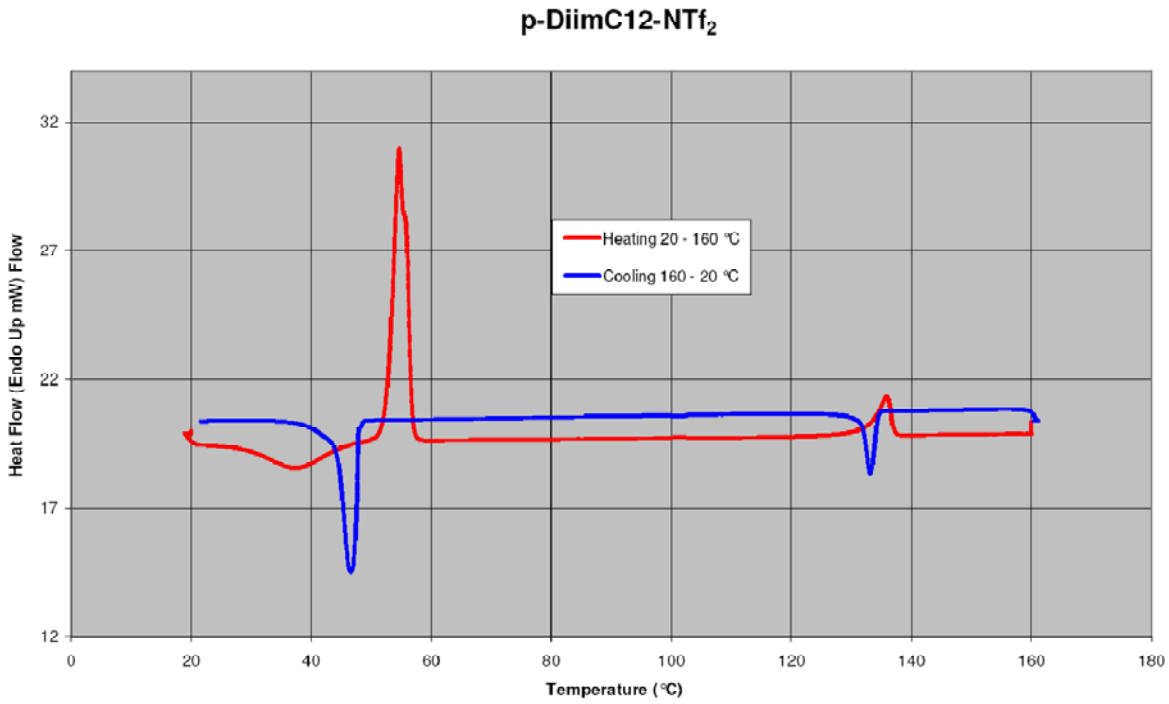


DSC of compound **3b:**